Development of a methodology for generating aggregated energy models to control the flexibility of the residential consumptionDéveloppement d'une méthodologie pour générer des modèles énergétiques agrégés pour piloter la flexibilité de la consommation résidentielle

Quynh Mai Nguyen

PSL UNIVERSITÉ PARIS

THÈSE DE DOCTORAT
DE L'UNIVERSITÉ PSL

Préparée à Mines Paris - PSL

Development of a methodology for generating aggregated energy models to control the flexibility of the residential consumption

Développement d'une méthodologie pour générer des modèles énergétiques agrégés pour piloter la flexibilité de la consommation résidentielle

Soutenue par
Mai Quynh NGUYEN
Le 12 Decembre 2023

Dirigée par
Xavier LE PIVERT
Gilles GUERASSIMOFF

École doctorale n° 84
STIC-Science et Technologies de l'information et de la Communication

Spécialité
Contrôle, optimisation, prospective

Composition du jury :

Erwin, FRANQUET Professeur, Université Côte d'Azur	*Président*
Marc, PETIT Professeur, CentraleSupélec	*Rapporteur*
Thai-phuong, DO Ingénieur de recherche, CEA-INES	*Examinatrice*
Bruno, DUPLESSIS Maître assistant , MINES Paris – PSL	*Examinateur*
Xavier, LE PIVERT Ingénieur de recherche, CEA-INES	*Examinateur*
Gilles, GUERASSIMOFF Professeur, MINES Paris – PSL/CMA	*Directeur de thèse*

MINES PARIS | PSL

Résumé

Dans un contexte d'intégration massive d'énergies renouvelables non pilotables, l'équilibre entre production et consommation d'électricité deviendra crucial à l'avenir. Pour relever les défis posés par les sources d'énergie renouvelables, un système électrique plus flexible est nécessaire. L'un des moyens de maintenir l'équilibre est de contrôler la consommation d'électricité afin de l'adapter à la production, ce que l'on appelle la flexibilité du côté de la demande. De nombreuses questions sont posées sur le potentiel réel de flexibilité de la consommation dans les réseaux intelligents, à la fois sur le plan géographique et en termes temporels. La gestion et l'évaluation de la flexibilité nécessitera différents modèles, en fonction de l'application (stabilité de la fréquence et de la tension du réseau, exploitation de la distribution, participation aux marchés d'équilibrage et SPOT) et du niveau d'agrégation considéré (individu, logement collectif, quartier, ville).

La thèse se concentre sur le développement de divers modèles, qui peuvent servir d'outils utiles aux différents acteurs du marché, qu'il s'agisse du Gestionnaire du Réseau de Transport (GRT), du gestionnaire de Réseau de Distribution (GDR), d'agrégateurs, d'utilisateurs finaux ou même de chercheurs. Notre idée est de construire un modèle qui peut donner une estimation de la consommation d'énergie pour différents types de charges résidentielles, mais sur une grande échelle spatiale. Cela permettra d'aborder et d'accéder à la consommation d'énergie de l'agrégation de nombreux ménages à différents niveaux nationaux, d'un petit quartier à une grande ville, voire à une région ou même à l'échelle d'un pays.

Dans notre recherche, nous développons des méthodologies pour générer des modèles agrégés pour les charges flexibles résidentielles : l'eau chaude domestique, le chauffage résidentiel et la recharge des véhicules électriques. L'objectif étant de transformer ces modèles en un outil efficace pour aider les différents acteurs du marché de l'énergie à quantifier la flexibilité de la consommation d'énergie.

Les résultats démontrent que les modèles agrégés développés sont capables de prédire efficacement la consommation d'énergie pour l'eau chaude domestique, la recharge des véhicules électriques et le chauffage dans les habitations. Une étude de cas a été réalisée pour montrer et explorer le potentiel et les avantages des modèles proposés pour l'aide à la décision des agrégateurs dans leur gestion de la charge pour différentes mailles.

Abstract

In a context of massive integration of non-controllable renewable energies, the balance between the electricity production and electricity consumption will be more and more important in the future. Coping with problems caused by renewable energy sources calls for a more flexible power system. One of the solutions to maintain the balance is to control the electricity consumption in order to match with electricity production, which is known as demand-side flexibility. Many questions arise about the real potential for flexibility in consumption in smart grid, and this depending on the geographical level but also the time range. The management of flexibilities as well as their valuation, will require various models, depending on the application (frequency and voltage stability of the network, operation of the distribution, participation in the balancing market and SPOT markets) and the level of aggregation considered (individual, collective housing, district, city).

The thesis focuses on developing various models, which can act as useful tool for different actors on the market, from TSO, DSO, aggregators, end users or even the researchers. Our idea is to build a model, which can give a power consumption estimation for various types of the residential load but in a large spatial scale. This will allow to tackle and access the power consumption of the aggregation of numerous households at different country levels, from a small quartier to a big city and then to a region and even at country scale.

In our research, we develop methodologies for generating aggregated models for residential flexible loads, including domestic hot water, heating in residential and electric vehicle charging, with the objective of turning these models into an effective tool in aiding different energy market participants to access the energy consumption flexibility.

The result demonstrate that the aggregated models is capable of predicting effectively the power consumption for domestic hot water, electric vehicle charging and heating in residential. A case study has been done to explore the potential and advantages of the proposed models in assisting the aggregators in their load management.

Acknowledgements

This thesis was written during my time as a Ph.D. student at The National Energy Solar Institute (CEA-INES) from November 2020 to November 2023. During these 3 years, I have learned so many things as well as faced so many challenges but at the end of the journey, what I got is so much more than I expected.

First, I would like to express my utmost and sincere gratitude to Mr. Xavier LE PIVERT and Professor Gilles GUERASSIMOFF for giving me the opportunity to pursue my Ph.D. studies at CEA-INES and Mines Paris. I came to the end successfully thanks to their support, guidance, orientation and of course, their patience with my French language ability. Even though the first 3 months were tough both for me and for them when trying to find the common sense of working and understanding each other, they were always there whenever I needed them and gave me the advice whenever I was stuck. Their contribution to this work is undeniable.

I would like to show my gratitude to all jury members for accepting to participate to my defense I also would like to give my appreciation to Mr. Antoine and Luca for useful discussions. They was willing to answer all my questions, my concerns and always help me with good scientific materials and information.

I would like to thank the Vietnamese team in INES for making my PhD life become easier. I would like to thank Kien for the love and affection that he gave me, thank him for his patience, his support and understanding and always by my side. I also thank my friend, Ninh, for the encouragement and support for philosophical discussions and a never-ending sharing of stories.

I am grateful to my family for their giant amount of support for my education. Although they live far away from me, I know they are always there and always welcome me. This was truly a great motivation and support, which no one can give except family. Thanks to them, I feel motivated to continue my career and do not have to worry much. Without them, nothing can happen.

Finally, I would like to thank myself for going to the end of this journey. I thank myself for not quitting and not giving up, for facing all challenges and difficulties and for making the right decision in pursuing a PhD and for doing a good job to complete another step of my life.

Quynh Mai NGUYEN
12/12/2023

Acronym

COP	Coefficient of performance
DHW	Domestic hot water
DSM	Demand side management
DSO	Distribution system operator
EDF	Electricité de France
EVC	Electric vehicle charging
EWH	Electric water heater
HP	Heat pump
HR	Heating in residential
LPG	Load Profile Generator
MAE	Mean absolute error
TSO	Transmission system operator
TWH	Thermodynamic water heater
EV	Electric vehicle
GA	Genetic Algorithm

Nomenclature

Chapter 1:

Q_{TWH}	Thermal power of the thermodynamic water heater (W)
A_n	Exchange surface area of n^{th} layer (m^2)
C_n	Thermal capacitance of a water tank at n^{th} layer (J/K)
c_p	Specific heat capacity of water (J/kgK)
d	Thickness of each layer (m)
H_{avg}	Average height of all EWHs (m)
k	Conductivity coefficient of water (W/mK)
m	Flow rate of hot water demand (m^3/s)
N	Number of water tank layers
n	Index of water tank layer ([1,N])
N_{EWH}	Number of EWHs
P_{agg}	Aggregated power (W)
P_{avg}	Average power rating of all EWHs (W)
P_{awh}	Power of the aggregated water heater (W)
P_{EWH}	Power rating of the electric water heater (W)
P_{TWH}	Power rating of compressor (W)
Q_{EWH}	Thermal power of the electric water heater (W)
Q_{heat}	Thermal capacity (W)
$Q_{loss,n}$	Power lost to the environment at n^{th} layer (W)
T_{air}	Air temperature (°C)
T_{amb}	Ambient temperature (°C)
$T_{deadband}$	Dead band temperature (°C)
T_{hb}	High bound temperature (°C)
T_{in}	Inlet water temperature (°C)
T_{lb}	Low bound temperature (°C)
T_{set}	Thermostat setting temperature (°C)
T_{sim}	Simulation period
T_w	Water temperature (°C)
$T_{w,n}$	Water temperature at n^{th} layer (°C)
U	Thermal transmittance coefficient (W/m^2K)
V_{avg}	Average volume of all EWHs (m^3)
V_{EWH}	Volume of the electric water heater (m^3)
V_n	Volume of n^{th} layer (m^3)

η	Conversion efficiency
ρ	Density of water (kg/m^3)

Chapter 2:

Q_{TWH}	Thermal power of the thermodynamic water heater (W)
A_n	Exchange surface area of n^{th} layer (m^2)
C_n	Thermal capacitance of a water tank at n^{th} layer (J/K)
c_p	Specific heat capacity of water (J/kgK)
d	Thickness of each layer (m)
H_{avg}	Average height of all EWHs (m)
k	Conductivity coefficient of water (W/mK)
m	Flow rate of hot water demand (m^3/s)
N	Number of water tank layers
n	Index of water tank layer ([1,N])
N_{EWH}	Number of EWHs
P_{agg}	Aggregated power (W)
P_{avg}	Average power rating of all EWHs (W)
P_{awh}	Power of the aggregated water heater (W)
P_{EWH}	Power rating of the electric water heater (W)
P_{TWH}	Power rating of compressor (W)
Q_{EWH}	Thermal power of the electric water heater (W)
Q_{heat}	Thermal capacity (W)
$Q_{loss,n}$	Power lost to the environment at n^{th} layer (W)
T_{air}	Air temperature (°C)
T_{amb}	Ambient temperature (°C)
$T_{deadband}$	Dead band temperature (°C)
T_{hb}	High bound temperature (°C)
T_{in}	Inlet water temperature (°C)
T_{lb}	Low bound temperature (°C)
T_{set}	Thermostat setting temperature (°C)
T_{sim}	Simulation period
T_w	Water temperature (°C)
$T_{w,n}$	Water temperature at n^{th} layer (°C)
U	Thermal transmittance coefficient (W/m^2K)
V_{avg}	Average volume of all EWHs (m^3)

V_{EWH}	Volume of the electric water heater (m^3)
V_n	Volume of n^{th} layer (m^3)
η	Conversion efficiency
ρ	Density of water (kg/m^3)

Chapter 3:

C_m	Thermal capacitance of the wall (J/K)
C_{m-avg}	Thermal capacitance of the wall (J/K) for the aggregated model
A_1, A_2 , A_3, A_4	The element of matrix A, regarding characteristics of the houses
$A_{1\text{-}avg}$, $A_{2\text{-}avg}$, $A_{3\text{-}avg}$, $A_{4\text{-}avg}$	The element of matrix A_{agg} , regarding characteristics of the houses for the aggregated model
B_1 to B_{12}	The element of matrix B, regarding characteristics of the houses
$B_{1\text{-}avg}$ to $B_{12\text{-}avg}$	The element of matrix B_{agg} , regarding characteristics of the houses for the aggregated model
C_{cloud}	Cloud coverage coefficient
C_{int}	Thermal capacitance inside the house (J/K)
$C_{int\text{-}avg}$	Thermal capacitance inside the house (J/K) for the aggregated model
c_p	Specific heat of air (J/kgK)
i	The i^{th} time step
$P_{avg\text{-}agg}$	Average thermal power of the aggregated model (W)
P_{heat}	Thermal power consumed for heating (W)
$P_{heating\text{-}avg}$	Average thermal power rating (W)
$P_{heat\text{-}residential}$	Electrical power consumed for heating in residential (W)
P_{TWH}	Power rating of the compressor in heat pump (W)
Q_{heater}	Maximal power rating of heating system (W)
$Q_{heat\text{-}heating}$	Thermal power from heating system at each time step (W)
R_{fi}	Thermal resistance associated to the heat transfer through low inertia elements (glazing, doors) (K/W)
$R_{fi\text{-}avg}$	Thermal resistance associated to the heat transfer through low inertia elements (glazing, doors) (K/W) for the aggregated model
R_m	Thermal resistance of the wall (K/W)
R_{m12}	Thermal resistance associated to the conduction heat transfer (K/W)
$R_{m12\text{-}avg}$	Thermal resistance associated to the conduction heat transfer (K/W) for the aggregated model
R_{m22}	Thermal resistance associated to the conduction heat transfer (K/W)

$R_{m22\text{-}avg}$	Thermal resistance associated to the conduction heat transfer (K/W) for the aggregated model
R_{se}	Thermal resistance associated to the convection heat transfer with outer side of the wall (K/W)
$R_{se\text{-}avg}$	Thermal resistance associated to the convection heat transfer with outer side of the wall (K/W) for the aggregated model
R_{si}	Thermal resistance associated to the convection heat transfer with inner side of the wall (K/W)
$R_{si\text{-}avg}$	Thermal resistance associated to the convection heat transfer with inner side of the wall (K/W) for the aggregated model
R_{sky}	Thermal resistance associated to heat exchange between sky and the wall (K/W)
$R_{sky\text{-}avg}$	Thermal resistance associated to heat exchange between sky and the wall (K/W) for the aggregated model
T_{ext}	External temperature (°C)
T_{int}	Air internal temperature (°C)
$T_{lb\text{-}heating}$	Low bound temperature (°C)
T_m	Wall temperature (°C)
$T_{out\text{-}avg}$	Average external temperature (°C)
T_{se}	Temperature of inner side of the wall (°C)
$T_{set\text{-}avg}$	Average setting temperature (°C)
T_{si}	Temperature of inner side of the wall (°C)
T_{sky}	Sky temperature (°C)
V	Volume of the house (m^3)
α	The absorption coefficient, which represent the proportion of the incident radiation absorbed by the wall
β	The absorption coefficient, which represent the proportion of the incident radiation absorbed by the window glass
Φ_{heater}	Heat flow emitted from heating system (W)
Φ_{int}	Heat flow to the internal house (W)
Φ_m	Heat flow injected inside the wall (W)
$\Phi_{occupant}$	Heat flow emitted from the occupants (W)
Φ_{se}	Heat flow injected into the outer surface of the house (W)
Φ_{si}	Heat flow injected into the inner surface of the house (W)
Φ_{wall}	Heat flow from solar radiation, received by the wall (W)
Φ_{window}	Heat flow from solar radiation, transmit through window (W)

ρ	Mass density of air (kg/ m^3)

Chapter 4:

S_i	The control signal at i^{th} time step
C_i	The electricity price at i^{th} time step (€/MWh)
D1	The day January 3rd 2023
D2	The day January 17st 2023
D3	The day January 21st 2023
N	Total of time steps per day
P_{DHW-i}	Domestic hot water power consumption at i^{th} time step (W)
P_{EVC-i}	Electric vehicle charging power consumption at i^{th} time step (W)
P_{HR-i}	Heating in residential power consumption at i^{th} time step (W)

List of figures

List of tables

I. Background and motivation

1. Energy context

Starting from the end of the 19th century with the first basic ideas, electric power systems have experienced a significant transformation as the influence of needs for innovations [1]. Their structure and properties have been changed continuously as the adaptation of new technologies for power production, transmission, storage, distribution and consumption. The most recent and radical changes are occurred due to the urgent necessity in declining the Greenhouse Gas (GHG) emissions, which acts as a catalyst for a paradigm shift in energy policy objectives and legislation to move towards low-carbon and sustainable energy solutions.

In "2030 Climate and Energy Policy Framework" adopted in 2014, Europe has committed to reach at least 32 percent for the share of renewable energy in its energy consumption in 2030 [2]. To achieve this target, it plans to produce 54% of its electricity consumption from renewable sources by 2030, which requires a significant increase in these production resources. In 2020, renewable sources accounted for 38 percent of Europe's electricity, for the first time, taking over fossil fuel, which decreased to 37 percent [3]. As a result, with the rapid development of renewable energy sources, energy system research has put lots of research effort into the transition towards a more renewables-pe

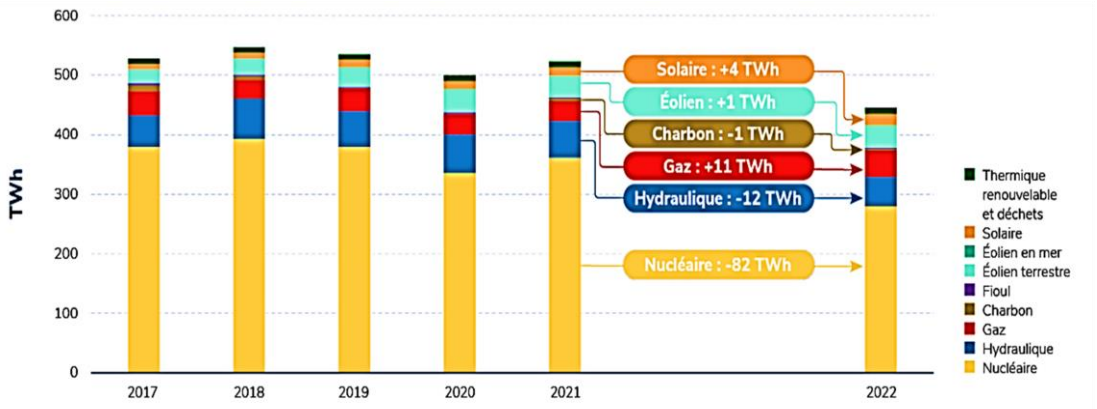

Figure 1: Electricity production by sector from 2015 to 2022 in France [4]

In 2022, the electricity production in France stayed at 445.2 TWh [4] (Figure 1). With this number, France witnessed a significant reduction in its electricity production, which is approximately 15.78% less when compared to the year 2021. This decline in the production of electricity had strong impact on the country's energy landscape. For France, nuclear power remains the dominant source in the generation of electricity, contributing approximately 280 TWh to the national grid, accounting for 65% in 2022. However, this figure illustrates a decrease compared to the previous year, where nuclear

power played an even more substantial role, providing over 360 TWH of electricity. Hydropower is the second-largest energy source for electricity production within France in 2022, with the share of 9%, which is following by wind energy with almost 9% [4].

The reduction in energy production observed in 2022 can be primarily attributed to several factors. The main factor is the availability of nuclear power decreased, affecting its contribution to the national grid. Additionally, France experienced severe drought conditions that adversely affected hydropower production. These combined difficulties bring some challenges in maintaining a stable and sustainable energy supply.

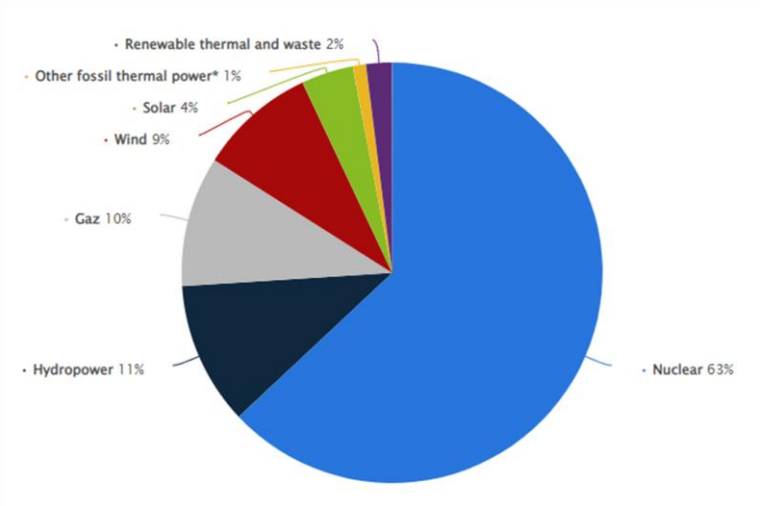

Figure 2: The electricity consumption by sector in 2022 in France [4]

3. Evolution of electricity consumption

Over the past 10 year, France has experienced various events that have greatly affected its electricity consumption trends. In the year 2021, annual electricity consumption in France amounted to around 470 TWh. However, in 2022, there was a decrease in electricity consumption. Total electricity consumption declined by 3.6% compared to 2021 with 459 TWh. This drop was even more pronounced when compared to the average electricity consumption recorded over the period from 2012 to 2021 with 9.9% reduction. The electricity consumed by residential sector account for 37 % in 2022 with 166 TWh [4].

.

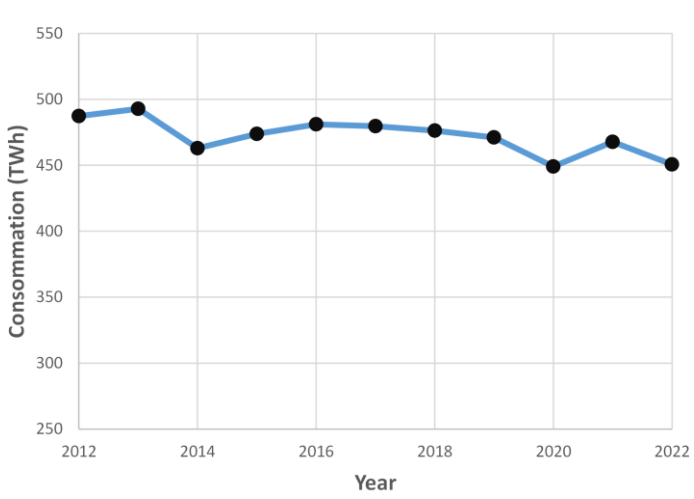

Figure 3: The electricity consumption from 2012 to 2022 in France [4]

One of the reasons that leads to the reduction in electricity consumption is the ongoing conflict between Ukraine and Russia. This international problem has led to a significant rise in the cost of energy sources, influencing energy markets not only in Europe but also worldwide. Figure 4 illustrates the evolution of electricity prices on the SPOT market.

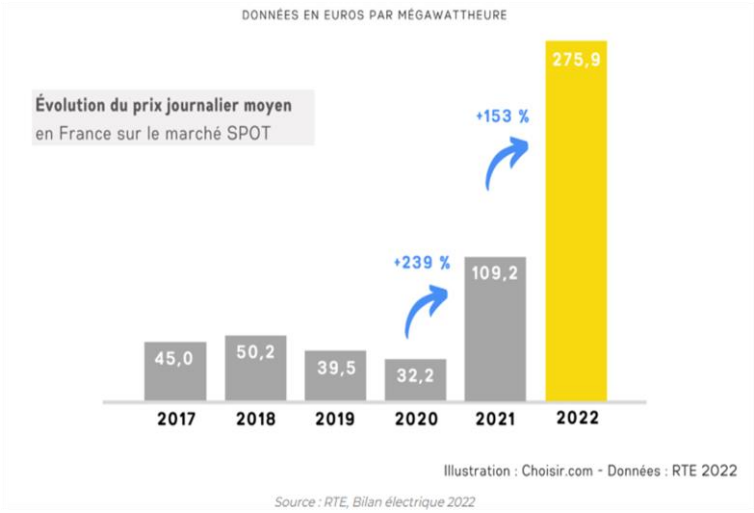

Figure 4: The evolution of electricity price on SPOT market [5]

It is observable that in 2021, the electricity price surged, increasing by 239% compared to the previous year, 2020. This upward trend in electricity prices continued into 2022, with prices increasing by an additional 153% compared to 2021 [5]. Consequently, the rise in electricity prices provides an

obvious explanation for the decrease in electricity consumption in France during 2022, with the residential sector also witnessing a reduction in electricity usage, 4TWh less than the year 2021.

4. The current energy situation of France

It can be said that the year 2022 was unforgettable to France. After being an electricity exporter for 43 years, France was becoming a net import for first time. In 2022, France needed to import 15TWh to balance the energy consumption. Even though France are in the situation that the consumption of electricity was decreasing, the electricity production also experienced a decline. This lead to the fact that the amount of electricity production was not enough to balance the electricity consumption in 2022, as depicted in Figure 5.

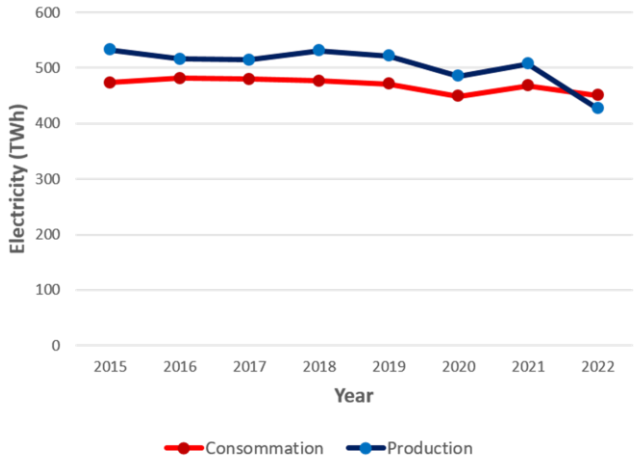

Figure 5: The electricity production and consumption from 2015 to 2022 in France [4]

The primary reason lied in the notable decrease in nuclear power generation. In 2021, nuclear power production was 22% lower than in previous years, particularly experiencing a stark decline of 26.2% compared to the average from 2015 to 2021. It is inevitable that France's nuclear power plants are aging, with 29 of the country's 56 nuclear reactors shut down [6]. Besides, due to the COVID pandemic, the maintenance of the nuclear reactors was interrupted and postponed. Additionally, the drop in hydropower also affects to the current energy situation in France.

In order to address the problem that France are facing, it is essential that France is in need of a significant increase in renewable energy sources integrated to electrical power system. This step toward renewables is not only necessary but also indispensable to ensure a reliable and stable power system.

5. The challenge of renewable energy

Besides the advantages that renewable energy sources bring, it is undeniable that they are intermittent and uncontrollable like wind and solar energy. Wind energy is dependent strongly on the season; weather conditions and the time of day and solar energy can be only generated during daylight hours, which is also affected by the season and weather. Thus, the basic challenge associated with the integration of these sources lies in the fact that the power system was constructed around the concept of controllable electricity generation. The intermittence and fluctuation of these renewables is becoming problematic when finding the solutions for the balance between electricity production and consumption. The responsibility of the power system operator is to ensure the balance between electricity supply and demand at any given time; otherwise, a black-out is unavoidable. The equilibrium point in the European network is at 50 Hertz and it always needs to stabilize 24 hours a day, 7 days a week [7].

6. Demand-side flexibility

Coping with problems caused by renewable energy sources calls for a more flexible power system. One of the solutions to maintain the balance is to control the electricity consumption in order to match with electricity production, which is known as demand-side flexibility. One of the definitions of demand-side flexibility is the ability of a prosumer to deviate from its normal energy consumption, in response to price signals or market incentives, in other words, changing the load feed-in the systems. The change of the demand can be either reduced, either increased or shifted within a specific time. It helps to compensate for the variation in energy generation by controlling flexible loads by modifying customers' demand. Recent studies have concentrated on evaluating the potential of demand response for load shaving and load shifting, e.g., by decreasing the load peak in the winter or by electricity sharing among final consumers [8], [9].

There are two types of demand-side flexibility: Implicit and explicit demand-side flexibility [10]

Implicit demand-side flexibility, known as "price-based" demand-side flexibility, is determined as the consumers' reaction to time-varying electricity prices, which reflects the change in electricity price during the day. The consumers have the choices of using electricity, which is suitable to their behavior. For instance, they can shift their electricity demand from high-price hours to low-price hours in order to get the savings on the electricity bills.

Explicit demand-side flexibility, so-called "incentive-based", is defined as the committed and dispatchable energy flexibility which can be traded on electricity markets, including wholesale, balancing and reserves markets… Consumers will receive an incentive for changing electricity consumption according to the request. Explicit demand-side flexibility is usually facilitated and managed by an aggregator, who acts as flexibility providers to the network.

The flexibility to the power systems can be obtained via different power demand sources, including power-to-heat, power-to-hydrogen, electric vehicles, smart appliances and industrial processes [11].

	Industrial	Commercial	Residential
Power-to-heat	○	○	○
Power-to-hydrogen	○	●	●
Electric vehicles	●	○	○
Smart appliances	●	○	○
Industrial processes	○	●	●

Table 1: The demand-side flexibility technologies, which is mapped with different end-user sectors. The light blue dots represent the technologies, which are suitable and the dark ones represent the technologies, which are unsuitable. [8]

Table 1 illustrates the demand-side flexibility technologies, which is mapped with different end-user sectors including industrial, commercial and residential sectors [12]. Power-to-heat technologies, electric-vehicle technologies and smart appliances technologies are the solutions which are competitive and suitable for the residential sector [12]. Domestic hot water (DHW) and heating in residential (HR) in the power-to-heat technologies and electric-vehicle charging (EVC) in electric-vehicle technologies are considered as flexible loads in the residential sector. There are various studies on the flexibility of energy consumption with different objectives. Some of them study the effect on the end-user's comfort when launching demand response programs [13]. Some focus on a specific type of load and study the control strategies needed to obtain the desired flexibility [14]–[16].

7. Objective

In the context of the energy sector in France, we aim to develop various models, which can act as useful tool for different actors on the market, from TSO, DSO, aggregators, end users or even the researchers. Our idea is to build a model, which can give a power consumption estimation for various types of the residential load but in a large spatial scale. This will allow to tackle and access the power consumption of the aggregation of numerous households at different country levels, from a small quartier to a big city and then to a region and even at country scale. Besides, we expect these models will be different from existing models, which can only give the prediction of residential power consumption and cannot react to the external control signals like electricity price control signals.

Our research focuses mainly on developing aggregated models for residential flexible loads, including domestic hot water, heating in residential and electric vehicle charging, with the objective of turning these models into an effective tool in aiding different energy market participants to access the energy consumption flexibility.

In this thesis, there are several questions need to be answered:

- How to build theses aggregated models if there is not enough information concerning the characteristic of households as well as the specifications of the DHW, EVC and HR systems?
- What are the advantages of using these models?
- How do these aggregated models allow accessing the energy flexibility of residential sector at large spatial scale?

The process and the organization of the thesis:

Chapter 1: Aggregated model for domestic hot water

In this chapter, we build the physical model of the electric water heater and thermodynamic water heater, detailed enough to provide a realistic power consumption of a water heater unit. We then simulate numerous water heater systems in the considered region, so-called unit model. Using the unit as the premise, the methodology for the aggregated model for both electric water heater and thermodynamic water heater, representing a large spatial area is proposed. To evaluate the model, we also studying the comparison between the power consumption obtained from aggregated model and that of the unit model.

Chapter 2: Aggregated model for electric vehicle charging.

Chapter 2 is about building the model to generate the usage profiles of EV users, taking into account the charging behavior of users as well as the schedule of using EV during the day. The same process as the chapter 1, we simulate the power consumption consumed by numerous EVs, so-called unit model. Then we propose the methodology for the aggregated model for electric vehicle charging without and with control signals. The final section is to study the comparison between the power consumption obtained from aggregated model and that of the unit model.

Chapter 3: Aggregated model for heating in residential

In this chapter, the thermal model which can represent the thermal behavior of a house to obtain the internal temperature in time series is presented and be used to simulate the power consumption consumed by numerous houses. The methodology for the aggregated model for heating residential, taking into account the weather factors as well as the users' behavior factor is proposed and a study about the comparison between the power consumption obtained from aggregated model and that of the unit model is executed.

Chapter 4: Investigation the case study, which demonstrate the utile of the aggregated models

Within this chapter, we integrate all three aggregated models for domestic hot water, electric vehicle charging and heating in residential and use the optimization method to find the optimal control strategy which gives the minimum electricity cost. We investigate different scenarios, considering the objective of minimizing the electricity cost.

There are several objectives need to be obtained in this thesis and constitute our contributions in the domain:

- Constructing diverse models designed to comprehensively quantify energy flexibility for distinct load types.
- These models will cater to various levels of aggregation, ranging from the microcosm of individual units to the macroscopic scope of districts and cities, enhancing their applicability across different spatial scales.
- Pioneering innovative methodologies for the development of aggregated models tailored specifically to each load type, ensuring that these models not only exhibit robust computational efficiency but also manifest versatile functionality in accurately estimating energy flexibility.

II. Chapter 1: Domestic hot water

La contribution de ce chapitre réside dans le développement d'une méthodologie pour la construction d'un modèle agrégé pour la demande d'eau chaude sanitaire utilisant des chauffe-eaux électriques, qui est équivalent à de nombreux modèles d'unités de chauffe-eau avec une approche plus détaillée et une meilleure précision tout en réduisant le temps de calcul. Tout d'abord, nous construisons un modèle de réservoir d'eau à température stratifiée multicouche. Ensuite, nous développons la méthodologie mentionnée pour construire un modèle agrégé. Enfin, le modèle agrégé est appliqué avec différentes options de signaux de contrôle pour quantifier et évaluer la flexibilité de la consommation d'énergie. Les résultats obtenus sont présentés, ils montrent la pertinence du comportement du modèle agrégé pour un grand nombre de chauffe-eau électriques.

---

1. Introduction

Domestic hot water (DHW), which is known as a thermal controlled load, has been considered to provide a useful source of flexibility to power systems, due to its correlation with thermal energy storage. In the residential sector, the volume of energy used for heating water ranks second, after energy used for space heating, and accounts for 15.1 percent of residential energy consumption in Europe [17]. According to the French Environment and Energy Management Agency (ADEME), around 11 million electric water heater systems are installed in France [18]. DHW demand constitutes a flexible load since it can be turned off without compromising consumers' comfort.

In France, a tariff scheme is in place known as the "peak and off-peak hours tariff", in which the electricity price at peak hours is higher than at off-peak hours [19]. Consumers are encouraged to use electric water heaters to produce hot water during off-peak hours and to try to avoid heating water during peak hours. By doing this, consumers can make savings in their electricity bills, while power system operators can prevent some unwanted problems that might occur during peak hours, such as a blackout. Recently, France has focused investments on thermodynamic water heaters - a type of water heater using a heat pump – because of their higher energy efficiency [20]. However, currently, the majority of domestic hot water systems in residential areas are still standard electric water heaters because of their relatively low capital costs. A single residential household using a standalone water heater unit only makes a negligible contribution to demand-side flexibility services. However, when these individual loads are combined and aggregated, they collectively represent a significant portion of energy consumption. Harnessing this flexibility potential on a larger scale can offer valuable opportunities to enhance the overall efficiency and responsiveness of the energy system.

To fully tap into this flexibility potential at a broader level, it becomes crucial to assess and manage the collective electric load of numerous water heater units. This involves coordinating the control of

these small units to optimize their operation and contribute to the flexibility of the entire system. However, as the scale increases, especially on a national level, the task of individually modeling each water heater unit becomes cumbersome and time-consuming.

This is where the concept of an aggregated model comes into play. An aggregated model allows representing numerous water heater units as a single entity, streamlining the modeling process and avoiding the need to consider each unit separately. The aggregated model serves as a tool for different market actors in the energy market. It offers several advantages, including the ability to assess and quantify the potential energy flexibility achievable by aggregating multiple water heater units and testing various control strategies.

The aggregated model facilitates the evaluation of how different control signal strategies affects domestic hot water energy consumption. Moreover, its versatility allows it to be applied across different spatial scales, ranging from local districts to entire cities or regions. By employing an aggregated model, the computational calculation time are reduced significantly, assessing energy flexibility more efficient and less time-consuming. This, in turn, empowers decision-makers and energy planners to make informed choices and implement effective strategies for demand-side management and optimization.

2. Literature review

Using domestic hot water in providing demand-side flexibility has been studied in various research papers [5–9]. Reference [22] works on the characterization of parameters for the flexibility of electric water heaters and their impact on the system operator. Reference [14] focuses on the direct control of electric water heaters to adjust their energy consumption for providing regulation services. Reference [16] tests the responses of residential electric water heaters with different control signals to provide balancing services. Reference [23] proposes a model for quantifying the flexibility potential of multiple residential heat pump water heaters for the provision of a secondary reserve. One thing that these references have in common is that they propose models on a large scale involving a population of water heaters. In other words, they all need to utilize aggregated models. However, their aggregated models are built by considering every physical model of each water heater unit, which leads to computationally intensive simulations. Besides, many references consider water tanks with well-mixed temperatures [24]–[26]. Normally, when considering a simulation for an aggregated model of many water heaters, this type of model is chosen for its simplicity and faster computation.

The contribution of this chapter lies in the development of a methodology for building an aggregated model for domestic hot water demand using electric water heaters, which is equivalent to numerous models of water heater units with a more detailed approach and a better accuracy while reducing the computation time. First, we construct a multi-layer stratified temperature water tank model. Second, we develop the mentioned methodology to build an aggregated model. Finally, the aggregated model

is applied with different control signal options to quantify and assess the energy consumption flexibility. The results obtained are presented, they show the relevance of the aggregated model behavior for a large amount of electric water heaters (EWHs).

3. Water heater models

3.1. Electric water heater

Electric water heaters employ an electric resistance element to heat water. At the bottom of the water tank, cold water is injected through a dip tube and then heated by the electric resistance. At the top of the tank, the hot water is then flown through the heat-out pipe. Each electric water heater has a specific volume V_{EWH} and a corresponding nominal power P_{EWH} which is supplied to the electric resistance heating element. The thermal power Q_{EWH} generated from these heaters is transferred to the cold water. An electric water heater is modelled using a conversion efficiency η, which gives:

$$Q_{EWH} = \eta P_{EWH} \text{ (Watt)}$$

3.2. Thermodynamic water heater

Thermodynamic water heaters also use electricity as their power source. Each individual has a hot water tank with a heat pump, which harnesses energy from the surrounding air to heat the water inside the tank. The amount of thermal power Q_{TWH} used to heat hot water depends on the capacity of the heat pump's compressor P_{TWH} and its coefficient of performance (COP). The value of COP fluctuates based on the temperature of the heat sink and air source.

In fact, the COP of TWHs is influenced by the temperature difference between air sources and heat sinks. [27] presents the COP as a function of the temperature difference between the air temperature and the water outlet temperature (ΔT). However, due to limited technical information available for TWHs, hence, in this chapter, we assume a linear relationship between the COP and ΔT.

$$COP = c_0 + c_1 \Delta T$$

The coefficients c_i are calculated by using heat pump data from manufacturers [30]–[32].

ΔT is obtained using: $\Delta T = T_w - T_{air}$

The thermal capacity Q_{TWH} provided by heat pump is then calculated by:

$$Q_{TWH} = P_{TWH}\, COP \quad \text{(Watt)}$$

3.3. Multi-layer water tank model

In reality, the water temperature inside the tank is never uniform, but is subject to stratified phenomena [33] [34]. This corresponds with demand from users: the hot water comes out at the top of the tank, the cold water is injected near the tank's bottom, and the hot water inside the tank flows upwards. Hence, the temperature of the coldest water displaces to the lower layers of the tank, while the warmest water is at the higher layers. In this case, we commonly use a multi-layer water tank

model considering the stratified water tank with N layers, to accurately obtain the water temperature dynamics inside the tank (Figure 6).

There are several assumptions applied to it:

- A uniform temperature in each layer
- Thermal losses are defined for each layer
- All layers have the same thickness

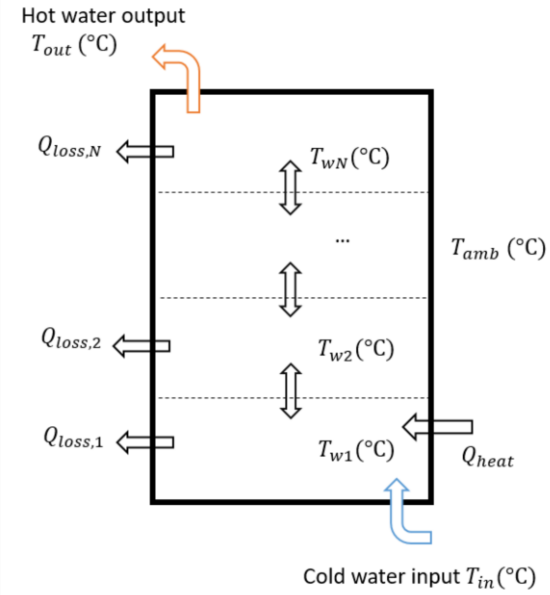

Figure 6: Multi-layer water tank model

The energy balance equation for determining the water temperature for each layer is shown as follows:

- Layer 1:

$$C_1 \frac{dT_{w1}}{dt} = Q_{heat} + m\rho c_p(T_{in} - T_{w1}) + A_1 U(T_{amb} - T_{w1}) + k\frac{V_1}{d^2}(T_{w2} - T_{w1})$$

- Layer 2 to layer N-1:

$$C_n \frac{dT_{w,n}}{dt} = m\rho c_p(T_{w,n-1} - T_{w,n}) + A_n U(T_{amb} - T_{w,n}) + k\frac{V_n}{d^2}(T_{w,n+1} + T_{w,n-1} - 2T_{w,n})$$

- Layer N:

$$C_N \frac{dT_{w,N}}{dt} = m\rho c_p(T_{w,N-1} - T_{w,N}) + A_N U(T_{amb} - T_{w,N}) + k\frac{V_N}{d^2}(T_{w,N-1} - T_{w,N})$$

When considering thermal stratified water heaters, when relying solely on the thermal diffusion to distribute the heat injected by the electrical resistance, it is impossible to physically model the water tank with accuracy. Several non-physical artifacts can be seen in the simulation results, for example the higher layers might experience lower temperatures than the bottom layer. One of the explanations for this is the presence of turbulence and mixing caused by natural convection when injecting heat from the thermal source into the water column: the so-called buoyancy effect [35]. Several methods have been introduced by Lago et al. [36] in order to model buoyancy effects accurately. In this chapter, we have opted to apply the method describing buoyancy effects via a maximum function to simulate the stratified temperature inside the water tank. Then, the water temperature of each layer is calculated at any given time. According to Kizilors et al., [37], the position of the thermostat at the bottom of the water tank shows a better performance than other positions inside the tank. Hence, the water temperature at the bottom layer (layer 1) of the water tank is chosen to control the switching actions. They can be designed as follows:

If $T_{w,1} <= T_{set} - T_{deadband}$ then turn on the water heater

If $T_{w,1} >= T_{set}$ then turn off the water heater

If $T_{set} - T_{deadband} < T_{w,1} < T_{set}$ then do the same action as in the previous time step.

Where $T_{w,1}$ is the water temperature of layer 1 (°C). T_{set} is the thermostat setting temperature (°C) and $T_{deadband}$ is the dead-band temperature (°C).

We have simulated the multi-layer water tank model with different number of layers. We realize that there is not much different in water temperature at the bottom layer inside the water tank – which is used to regulate the thermostat. Additionally, in this chapter, we consider a large amount of water heater units, therefore, to reduce the computational calculation, N = 4 is chosen as the number of layers in the multi-layer water tank model

3.4. Unit model of water heaters

In this chapter, the assumption is made that each household possesses only one EWH. Prior to transitioning to the aggregated model, a model is constructed by repetitively simulating a physical model featuring multiple water heater units. This iterative simulation is carried out to acquire the power consumption pattern for DHW. The obtained power consumption curve serves as a fundamental basis for evaluating the aggregated model. Consequently, each individual EWH is simulated to obtain the DHW power consumption profile for each household. To differentiate it from the forthcoming aggregated model, this collection of simulations for each EWH using the physical model is referred to as a **unit model**, as illustrated in Figure 7.

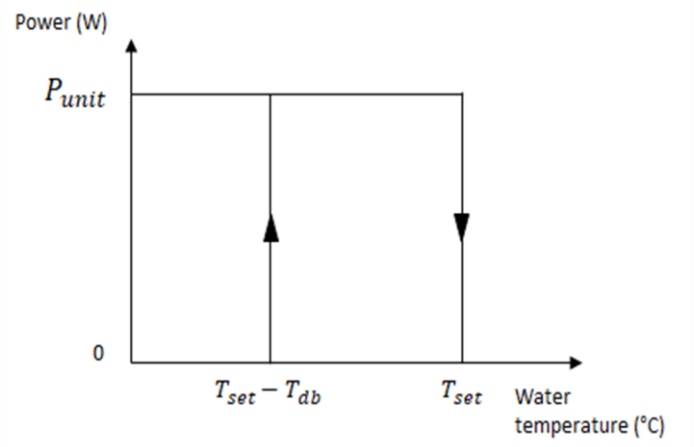

Figure 7: The relation between the power and the water temperature of a water heater model

Each individual water heater possesses a specific power rating, which provide heat to the water tank for heating purpose. In the absence of any demand for hot water, the water temperature keeps rising until it reaches the designated thermostat setting temperature, denoted as T_{set}. Once this temperature is reached, the thermostat takes over and tells the water heater to switch off, resulting in a zero thermal power supply ($Q_{heat} = 0$). However, due to the energy lost to the surrounding environment, the water temperature subsequently decreases. If it falls to a value lower than or equal to $T_{set} - T_{deadband}$, the thermostat triggers the water heater once again to turn on. In this scenario, Q_{heat} corresponds to the thermal power supplied by an electric water heater Q_{EWH}, while Q_{TWH} represents the thermal power supplied by a thermodynamic water heater equipped with a heat pump.

3.5. Aggregated model of water heaters

When dealing with large spatial scales, such as regions, acquiring relevant data becomes a significant challenge. Specifically, obtaining information about a region's characteristics for determining DHW power consumption is often difficult. To overcome this obstacle and streamline the process, the methodology proposed in this chapter introduces an aggregated model. This model enables the estimation of DHW power consumption without relying on detailed data for each individual EWH.

The requirements for this aggregated model include average values pertaining to EWH characteristics within the specific region. These average values encompass the thermostat setting temperature T_{set}, average power rating of all EWH P_{avg}, average volume of all EWH V_{avg} and average height of all EWH H_{avg}. These values can be accessible based on the number of households and the population of the considered region.

For example, in 2020 the population of Grenoble was reported 746,358 with 341,005 households [38]. This indicates an average of approximately 2.2 residents per household. According to EDF [39], an individual residing in a two-room house typically opts for a water heater with a capacity of 75 liters.

Therefore, the average volume of EWHs (V_{avg}) is estimated to be 165 liters. Taking into account data from manufacturers ([28], [29]), it is observed that for a volume of 165 liters, the corresponding power rating is around 1980W, and the height of the water tank is approximately 1.33m. Hence, depending on the usages of the aggregated model as well as the characteristics of different district, cities, or regions, we can establish distinct sets of values for P_{avg}, V_{avg}, H_{avg} and T_{set}.

The aggregated model of EWHs operates on the premise of having all households equipped with individual electric water heaters.

This aggregated water heater is characterized by several parameters, including:

- The maximum power rating, which is determined by summing up the power ratings of all individual EWHs.
- The volume, which is calculated by adding up the volumes of all individual EWHs.
- The height, which is obtained by averaging the heights of all individual EWHs.
- The insulation characteristics, which are identical to those of the individual EWHs.

The inputs to the aggregated model are the time-series data of DHW demand. The model takes this demand into account and calculates the power consumption utilized by the aggregated electric water heater across all households. Additionally, the model tracks the water temperature at each layer, updating it at each time step.

In summary, the aggregated model simplifies the simulation process by considering a single, representative water heater that encapsulates the collective characteristics of multiple individual EWHs. It considers DHW demand and provides outputs such as the power consumption of the aggregated water heater and the water temperature at each layer, which is dynamically updated over time.

4. Methodology

4.1. Domestic hot water demand

First, we have to generate DHW demand profiles. To proceed we have used a tool called Load Profile Generator (LPG) [40]. LPG is a useful tool capable of synthesizing the hot water consumption patterns of individual households by considering the "psychological" dimension of its residents. It incorporates human behaviors and activities, such as cooking, eating, sleeping, and the timing of leaving for work.

The goal of using LPG is to generate realistic scenarios for users' profile based on their specific database, which is provided to the tool. By utilizing LPG, a database of DHW demand profiles is generated for various households, representing different spatial scales. The profiles are created at a time interval of 1 minute over the span of 1 year. In essence, LPG enables the generation of dynamic and realistic DHW demand profiles by considering the psychological and behavioral aspects of

residents. This allows for a more realistic representation of the actual hot water consumption patterns at different spatial scales.

Figure 8 a and b describe some examples of the DHW consumption profile during 1 day (1,440 minutes) for two different households, with an interval of 1 minute.

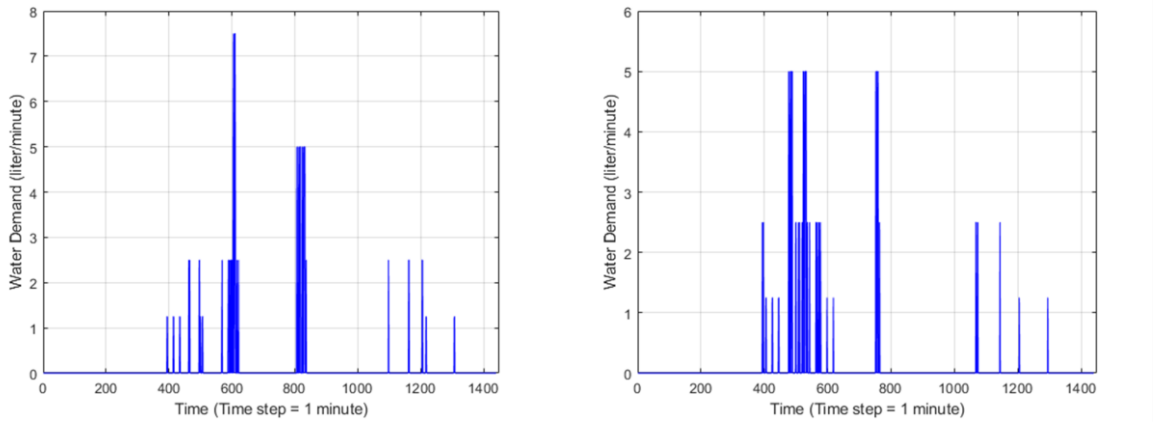

a b

Figure 8: (a), (b) The water consumption data obtained from LPG in 1 day (1440 minutes) of 2 different households

4.2. Control signal options

The control signal strategies play a role in accessing the energy flexibility. Depend on the user's behavior, these strategies are designed to optimize the operation of the model. The control signal options employed in this chapter are defined as commands that govern the regulation of water heaters, incorporating the concept of load shifting. Load shifting refers to adjust energy consumption timing to preferable and optimal periods while considering several factors like electricity pricing or grid stability. One of the control signal options is the "off-peak hour". This describes that the water heaters are turned off during peak hours when there is high electricity consumption. Instead, they are activated during off-peak hours when electricity demand is low.

In this chapter, it is assumed that water heaters receive the same control signal simultaneously. By taking into account load-shifting strategies, the control signals employed in this research enables the management of energy consumption, taking advantage of periods with lower electricity demand to minimize costs. Hence, in this chapter, we use electricity price signal as examples to prove the capabilities of our model.

4.2.1. Electricity price control signal

The electricity price control signal used in this study is derived from data obtained on 2nd May 2023 [41]. This dataset provides information on the cost of electricity on the SPOT market at an hourly frequency, measured in €/MWh (Euros per megawatt-hour).

Figure 9 displays the electricity price data for a selected day from the SPOT market. Upon examining the data, it is observable that the electricity price is higher during specific periods, from 7h to 10h and 18h to 22h. Consequently, the price control signal is selected to be activated during these time periods. This implies that the reduction energy usage for DHW purposes will occur between 7h to 10h and 18h to 22h. By utilizing this price control signal strategy, we aim to take advantage of lower-cost electricity periods and curtail electricity consumption during the time of higher electricity prices.

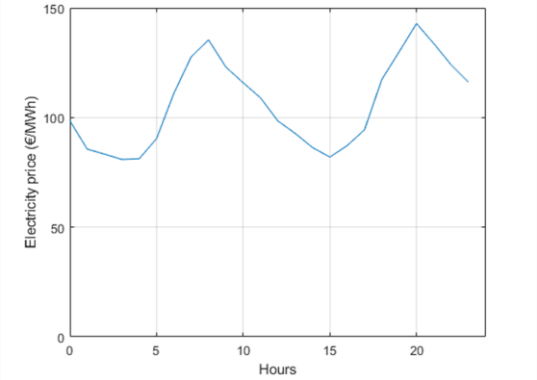

Figure 9: The electricity price in the spot market on 2nd May 2023

4.2.2. Peak and off-peak hour control signal

In France, various tariff systems exist for electricity, one of which is known “s "peak hours/off-peak ho”rs" [19]. This system entails different electricity prices for consumers depending on the time of the day. During off-peak hours, electricity costs is often lower than during peak hours. The electricity distribution system operator ENEDIS sets the number of off-peak hours at 8 hours per day, with the remaining hours considered as peak hours. However, certain time slots are mandatory peak hours, from 8:00 h to 12:00 h and from 17:00 h to 20:00 h. Service providers have the flexibility to allocate the remaining 8 off-peak hours within the periods of 12:00 h to 17:00 h and 20:00 h to 8:00 h. It is important to note that the schedules for peak and off-peak hours are different by region. For instance, to ensure equitable national distribution, Paris has only 2 options for off-peak hours, while Marseille offers up to 5 options [19]. In this chapter, the off-peak hour control signal applied is specific to Chambery, as indicated in Table 2.

Off-peak hours options in Chambery	
Option 1	2H30-7H30;13H30-16H30
Option 2	23h00 - 07h00
Option 3	1H30-7H30;12H30-14H30
Option 4	2H00-6H00;12H30-14H30;20H00-22H00

Table 2: Four options of off-peak hours in Chambery

4.3. Methodology for generating aggregated water heaters

To begin, as we are dealing with residential sector, a period of one week is chosen to include weekdays and week-ends. So a simulation of the unit model is conducted for these 7 days (10,080 minutes) with a time step of 1 minute, considering a total of 5,000 households. In order to assign a specific type of EWH to each household, data regarding the characteristics of different EWH types is sourced from a manufacturer [42]. The selection of EWH types for households is based on a uniform distribution. Hence, each household is assumed to be equipped a particular type of EWH featuring a specific power rating, volume and height of the water tank as described in details in ANNEX ***A***. Furthermore, the initial water temperature for each household is also determined using a uniform distribution, with values ranging between 58°C and 60°C. Table 3 outlines the parameters employed in the simulation of the unit model.

Through this simulation, the unit model enables the evaluation of power consumption patterns for individual households, considering the diverse characteristics and variations in EWH types and initial water temperatures.

Parameter	Value	Unit	Parameter	Value	Unit
T_{set}	60	°C	c_p	4186	J/kgK
T_{in}	15	°C	ρ	997	kg/m^3
T_{amb}	20	°C	k	0.6	W/mK
$T_{deadband}$	2	°C	U	0.5265	W/m^2K
η	1	_	T_{sim}	7	days
N	4	_			

Table 3: The parameters for simulation of the unit model

The unit model simulation involves the implementation of two different control approaches:

1. Case 1: Only thermostat regulation. In this case, the water heater switch is solely controlled by the thermostat. The thermostat regulates the water heater to turn on when the water temperature drops below a specific threshold and turns it off when the temperature reaches the thermostat temperature setting.
2. Case 2: Peak and off-peak hour signals in addition to thermostat control. This case uses peak and off-peak hour signals alongside the thermostat control. During peak hours, all EWHs are turned off, and they can only be activated during off-peak hours.

Within these simulations, each individual household performs its own power consumption profile for DHW. As a result, at each time step, the total power consumed and average water temperature at each layer of the water tank are calculated for all 5,000 households.

It needs to mention that the water temperature at the bottom layer (layer 1) of the water tank is opted to control the switching actions of the EWHs. Figure 10 depicts the relationship between the total power consumed and the average water temperature at the bottom layers of the 5,000 EWHs at each time step, obtained from the simulation of the unit model for both control cases. Figure 10 illustrates that the total power consumed and average water temperature at the bottom layer follow a quadratic equation-like relationship. Based on this curve displayed in the figure, it can be observed that the total power consumed never exceeds the summation of the maximum power ratings of all EWHs. Additionally, the total power consumed equals zero when the average temperature is higher than or equal to the thermostat setting temperature. This analysis of the power consumption and temperature relationship allows understanding the power consumption patterns and acts as a premise for the generation of the aggregated model

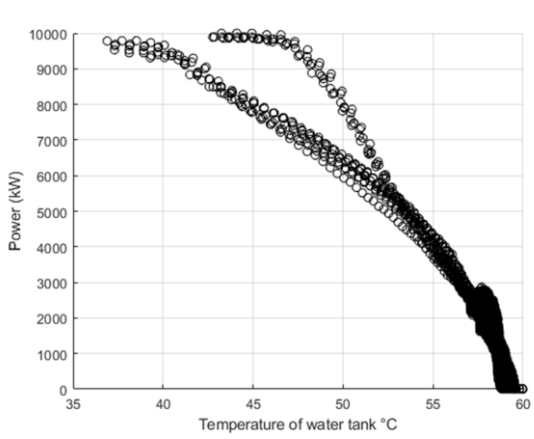

Figure 10: The relationship between the total power consumed (kW) and average water temperature at the bottom layer of 5000 households in each time step

Hence, the idea for generating the aggregated model is to define the relationship curve between total power consumed and average water temperature as a quadratic function with some additional constraints. This function is described by the curve in Figure 11, where the aggregated power P_{agg} is the sum of the maximum power of all EWHs, the point M is the maxima of the curve and the lower bound temperature T_{lb} and higher bound temperature T_{hb} act as the constraints for the relation curve. It can be seen that the water temperature is set by a thermostat setting temperature, hence, T_{hb} is defined as the setting temperature of the aggregated water tank. T_{lb} is the threshold decision point for whether the total power consumed is equal to the aggregated power P_{agg}.

By incorporating these constraints and considering the quadratic function, the aggregated model aims to capture the relationship between power consumption and water temperature. It allows effectively modeling the behavior of the water heating system at a larger scale, facilitating analysis of power consumption patterns.

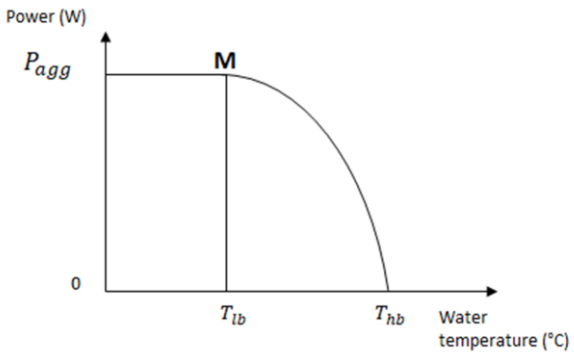

Figure 11 : The relation curve between the power and the temperature of the water tank for the aggregated model

From the simulation result of the unit model (ANNEX B), we can always obtain a set of values for P_{agg}, T_{lb} and T_{hb} and now the question is how to calculate them from the shortage of information concerning the detailed characteristics of each EWH. An approach is proposed using average parameters related to EWH characteristics, including T_{set}, P_{avg}, V_{avg}, and the number of EWHs (N_{EWH}).

1. P_{agg} (aggregated power) is determined by multiplying the average power rating P_{avg} (in watts) by the number of EWHs (N_{EWH}):

$$P_{agg} = P_{avg}\, N_{EWH}$$

T_{hb} (higher bound temperature) is defined by the temperature setting of the water tank, T_{set} (in °C):

$$T_{hb} = T_{set}$$

T_{lb} (lower bound temperature) is calculated using a linear function that incorporates the average power rating P_{avg}, average volume V_{avg}, and temperature setting of the water tank T_{set}:

$$T_{lb} = \text{function}(P_{avg}, V_{avg}, T_{set})$$

To obtain the coefficients for the T_{lb} function, simulations are conducted for the unit model considering different numbers of households and varying values of P_{avg}, V_{avg}, and T_{set}. This allows for the derivation of different T_{lb} values. We investigate five cases corresponding to different numbers of households, as presented in Table 4. Since each house is equipped with a specific EWH type (ANNEX A), the values of P_{avg} and V_{avg} vary accordingly. Additionally, for each case, the value of T_{set} ranges from 55 to 64 °C with a 1-degree increment (Table 4).

By conducting simulations and analyzing the results, the coefficients for the T_{lb} function can be determined.

Number of households	P_{avg} (W)	V_{avg} (liter)	T_{set} (°C)
2000	2002	154.6	From 55 to 64 °C with 1 degree step.
3000	2091	167.2	
5000	2174	178.5	
7000	2541	217.2	
10000	2498	216.1	

Table 4: The value of P_{avg}, V_{avg} and T_{set} for different numbers of households

From the simulations conducted for the 5 cases, along with the variation of T_{set} across 10 different values, a total of 50 T_{lb} values are obtained. These T_{lb} values reflect the lower bound temperature calculated from the unit model simulations, considering various combinations of P_{avg}, V_{avg}, and T_{set}. To establish a relationship between T_{lb} and the parameters (P_{avg}, V_{avg}, and T_{set}), a linear regression model is fitted to the obtained data. This regression model helps identify the coefficients that govern the relationship between the variables.

Figure 12 visualizes the 50 T_{lb} values obtained from the unit model simulations. The black line represents these values, reflecting the lower bound temperature determined through the simulations. Additionally, the red line represents the results obtained from the fitted linear regression model, illustrating the regression line that best approximates the relationship between T_{lb} and the parameters (P_{avg}, V_{avg}, and T_{set}). The regression line provides a mathematical representation of the relationship, allowing for the estimation of T_{lb} based on the given parameters.

By employing the linear regression model, the coefficients for the relationship between T_{lb} and the parameters (P_{avg}, V_{avg}, and T_{set}) can be determined, enabling the calculation of T_{lb} values for the aggregated model based on the average EWH characteristics and the desired water temperature setting.

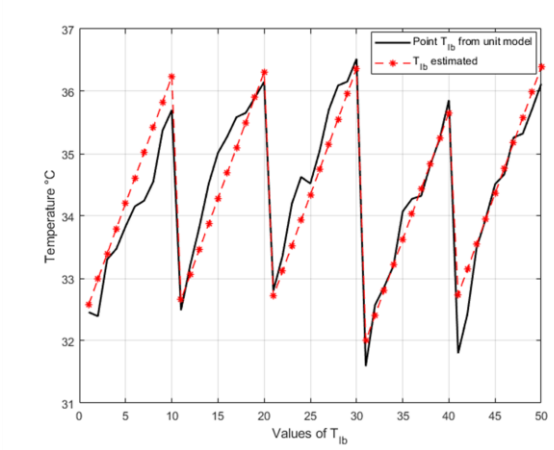

Figure 12 : The value of T_{lb} when changing the values of P_{avg}, V_{avg} and T_{set}

After determining the coefficients for P_{avg}, V_{avg} and T_{set}, the final equation for T_{lb} can be established as a linear function of P_{avg} (in watts), V_{avg} (in liters), and T_{set} (in °C) as follow:

$$T_{lb} = 18.937 - 0.011P_{avg} + 0.0856V_{avg} + 0.4059T_{set}$$

With the coefficients in place, the values for P_{agg}, T_{hb} and T_{lb} can be calculated based on the given parameters of P_{avg}, V_{avg} and T_{set}. Additionally, a hypothesis is made regarding the relationship curve between the total power consumed and the water temperature. It is assumed that “the maximum point

M on Figure 11 represents the peak of the quadratic function that characterizes the relationship between power and water temperature in the water tank."

To summarize, with P_{agg}, T_{hb}, and T_{lb} defined, and point M representing the maximum of the quadratic curve, the calculation of the power of the aggregated water heater (P_{awh}) becomes dependent on the following equation:

$$P_{awh} = a_1 T_{w,1}{}^2 + a_2 T_{w,1} + a_3$$

With the following conditions:

- The point M is the maximum of the quadratic equation
- $T_{in} <= T_{w,1} <= T_{set}$
- If $T_{w,1} <= T_{lb}$ then $P_{awh} = P_{agg}$
- If $T_{w,1} >= T_{hb}$ then $P_{awh} = 0$

a_1, a_2, a_3 are the coefficients, which are calculated by using 3 values of P_{agg}, T_{hb} and T_{lb}:

$$a_1 = \frac{-P_{agg}}{(T_{lb} - T_{hb})^2}$$

$$a_2 = \frac{-2\,P_{agg}\,T_{lb}}{(T_{lb} - T_{hb})^2}$$

$$a_3 = \frac{P_{agg}(T_{hb}{}^2 - 2T_{lb}T_{hb})}{(T_{lb} - T_{hb})^2}$$

With all the elements defined, the control logic of the aggregated water heater model is then designed as follows:

If $T_{lb} < T_{w,1} < T_{set}$ then $P_{awh} = a_1 T_{w,1}{}^2 + a_2 T_{w,1} + a_3$ under the mentioned conditions

If $T_{w,1} >= T_{set}$ then $P_{awh} = 0$

If $T_{w,1} <=$ Tlb then $P_{awh} = P_{agg}$

5. Simulation settings of the aggregated electric water heater model

Unlike the unit model, the power P_{heat} of the aggregated model functions in a different way. Table 5 below illustrates the comparison between the unit model and the aggregated model.

The unit model	The aggregated model
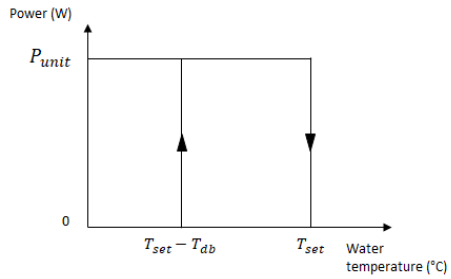 The power P_{heat} of the unit model functions as a piecewise function including 2 linear functions	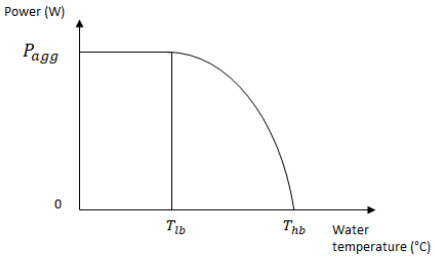 The power P_{agg} of aggregated model functions as a piecewise function including 1 linear function and 1 quadratic function
To obtain the energy consumption curve, there is a need for running a simulation for each water heater.	Run only 1 simulation of aggregated model
Need to have detailed parameters of each water heater. Each water heater has a different set of parameters.	Just need the temperature setting T_{set}, the average power rating P_{avg} ,average volume V_{avg} and average height $H_{avg}$of all water heater tanks in that region.

Table 5: A comparison between the unit model and the proposed aggregated model

The model is implemented using MATLAB R2019b with a sampling time of one minute. The outcomes of the aggregated model are then compared to those of the unit model. At beginning, we conducted a 7-day simulation to comprehensively understand the aggregated model's behavior compared to the unit model in terms of performance and computation time. However, in this chapter, we present the results over a 3-day period (4,320 minutes) as it effectively demonstrates the aggregated model's behavior. As mentioned in many studies, the range of inlet water temperature is from 15°C to 25° C [43]–[45]. In the simulation, the inlet water temperature is set to 15°C. The ambient temperature is assumed to be 20°C as it is also the value that used in many research [43], [45]. These values of inlet water temperature and ambient temperature can be changed to adapt to a specific scenario. The temperature setting of the thermostat is defined as 60°C. To represent the aggregated model, the water demand utilized is the summation of all water demand profiles from the chosen number of houses. This aggregated water demand captures the overall water consumption pattern for the entire system. Table 6 provides the parameters necessary for simulating the EWH multi-layer aggregated model. Specifically, it states that the water tanks in this chapter are considered

to have four layers. By employing these parameters and conducting the simulation, the model can simulate the behavior of the multi-layer EWH system over a simulation process.

Parameter	Value	Unit	Parameter	Value	Unit
T_{set}	60	°C	c_p	4186	J/kgK
T_{in}	15	°C	ρ	997	kg/m^3
T_{amb}	20	°C	k	0.6	W/mK
N	4	_	U	0.5265	W/m^2K
η	1	_	T_{sim}	7	days

Table 6: The parameters for simulation of the aggregated model

Table 7 provides the specific values of P_{avg}, V_{avg}, H_{avg} and T_{set} for two distinct scenarios with different spatial scales the simulation of the aggregated model. The scenario 1 is for 5,000 households and the scenario 2 is for 10,000 households. Leveraging the comprehensive data found in ANNEX A, which outlines the technical particulars of different EWH types, we undertake a process of modifying the probability distribution associated with each individual EWH type. By executing this alteration within each scenario, we are able to procure distinct sets of values for P_{avg}, V_{avg} and H_{avg} for each scenario.

	Scenario 1	Scenario 2
Number of households	5000	10000
P_{avg} (W)	2492	2004
V_{avg}(liter)	216	155.1
H_{avg}(m)	1.48	1.18
T_{set}(°C)	60	60

Table 7: The values of P_{avg}, V_{avg} , H_{avg} and T_{set} for 2 scenarios of 5,000 and 10,000 households, respectively

The determination of P_{avg} and V_{avg} values for two scenarios comes from the assignment each EWH for each households. P_{avg} values is then calculated by taking the average power rating of all the EWH for the number of households considered. In the case of V_{avg}, it is defined by taking the average of all EWHs' volumes.

In the context of the aggregated model, the input parameter is the collective demand for domestic hot water (DHW) depicted as a time series. This dataset can be acquired through diverse methodologies. One such approach involves leveraging a tool known as the Load Profile Generator, which help to generate the water usage for different types of households. An alternative technique encompasses the application of models established in various research works. For example, in reference [46], an model is constructed, enabling the creation of hot water profiles as a function of the number of occupants. Similarly, the employment of a probabilistic model outlined in reference [47] facilitates the derivation of hot water usage profiles.

The output of the aggregated model is the power consumption utilized by all the EWHs also in time series.

6. Simulation results of the aggregated electric water heater model

This section illustrates the simulation of the aggregated model for two scenarios of 5,000 and 10000 houses, representing different spatial scale. The values of average parameters, including P_{avg}, V_{avg} , and T_{set} are defined in Table 7 . Two different control methods are applied in the simulation of the aggregated model. The first method involves solely thermostat control and is referred to as the "aggregated model without control signals." The second method incorporates an electricity price control signal (section 4.2.1) in addition to the thermostat control and is known as the "aggregated model with control signals."

The simulation results are presented in Figure 13. This figure illustrates the power consumption for DHW by varying numbers of households over the course of 3 days, with a time interval of 1 minute. The blue and red curves in Figure 13 represent the power usage generated by the unit model and the aggregated model, respectively. Specifically, Figure 13 a and b depict the simulation results of the unit models and aggregated models applied to scenario 1 with and without the electricity price control signal, respectively. On the other hand, Figure 13c and d present the same simulation results for scenario 2.

These figures provide visual representations of the power consumption patterns of the DHW systems for different numbers of households, comparing the unit model results with those of the aggregated model, with and without the additional control signals. These results allow for a comparative analysis of the effectiveness and efficiency of the aggregated model with control signals in managing power consumption for DHW and in curtailing the calculation time, all while using a simple collection of average parameters associated with EWH in large-scale scenarios.

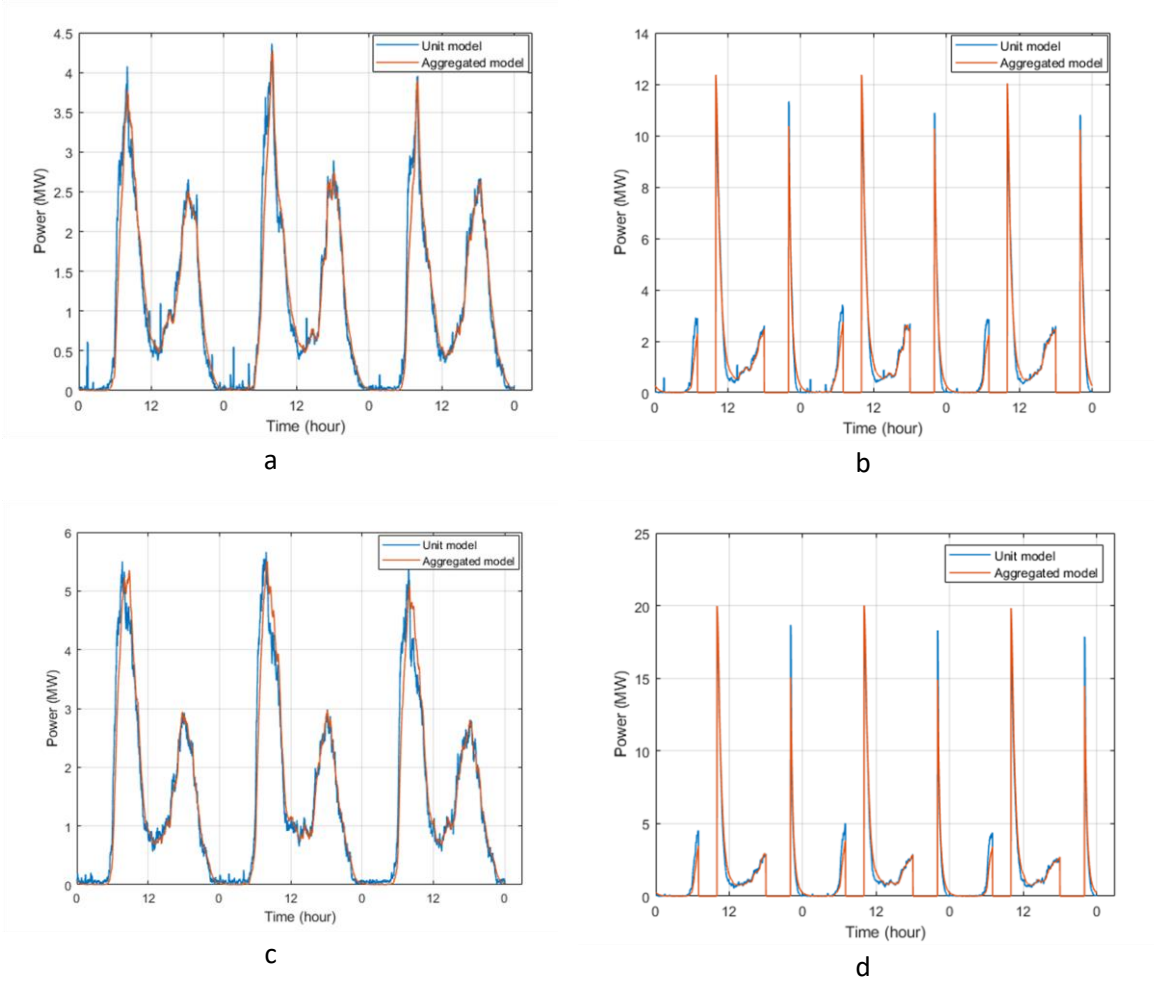

Figure 13: The electrical power consumption for DHW of EWH in 3 days (kW). [a] and [b] describe the simulation of the aggregated models without and with the electricity price control signal applied for scenario 1, respectively while [c] and [d] present those for scenario 2.

The figures presented illustrate that the aggregated model effectively captures the power usage behavior for DHW, both with and without the application of control signals. This demonstrates the relevance of the aggregated model's behavior in representing the power consumption patterns of a large number of EWHs. The simulation time for this aggregated model is only 2.621 seconds, a staggering 2622 times faster compared to the unit model's simulation time of 6872 seconds (about 1,9 hour) for the scenario 2 of 10,000 houses. These computation times were recorded using MATLAB R2019b on a Dell PC with an Intel(R) Core (TM) i5-8265U CPU running at 1.60GHz.

To further evaluate the accuracy of the aggregated model, Table 8 provides the normalized absolute mean error between the aggregated model and the unit model.

Normalized Mean Absolute Error (NMAE) between aggregated model and unit model without and with control signal is calculated for different numbers of households:

$$\text{MAE} = \frac{\sum_{i=1}^{N}(P_{agg}(i) - P_{unit}(i))}{N}$$

NMAE = MAE / Average power consumption

N : Number of data points

P_{agg} : Power consumed in the aggregated model

P_{unit} : Power consumed in the unit model

This error is calculated by taking the absolute difference between the power consumption values obtained from the aggregated model and the unit model, and then normalizing it by dividing by the average power consumption of the unit model.

Table 8 provides a measure of the deviation between the aggregated model and the unit model in describing the power consumption behavior for DHW. This allows for an assessment of the accuracy and reliability of the aggregated model in capturing the overall power usage trends compared to the more detailed unit model.

Model type	**Scenario 1 (%)**	**Scenario 2 (%)**
The aggregated model without control signals	12.68	13.09
The aggregated model with control signals	15.32	16.26

Table 8: Normalized Absolute Mean Error (NMAE) (percentage) of the aggregated model with multilayer model, compared to the unit model for two scenarios.

There is a slight difference in the values of NMAE of aggregated model for two scenarios both in 2 cases without and with control signal. Notably, the parameter sets used for the aggregated models in these two scenarios exhibit significant differences (refer to Table 7), reflecting the diverse characteristics of the considered region. This represents the robust of the aggregated model in simulating the DHW power consumption across varying spatial scales. The consistent performance of the aggregated model in estimating power consumption for both 5,000-household and 10,000-household scenarios further highlights its reliability.

The subsequent figures, Figure 9 (a1, a2, a3, b1, b2, b3), demonstrate the sensitivity of the NMAE with respect to the aggregated power consumption when varying the value of one of the parameters (P_{avg}, V_{avg}, or T_{set}) while keeping the values of the other two parameters constant. These figures illustrate the impact of modifying a specific parameter on the accuracy of the aggregated model, as

indicated by the NMAE. By varying one parameter at a time and observing its influence on the NMAE, these figures provide insights into the sensitivity and understanding the effects of parameter variations on the performance of the aggregated model.

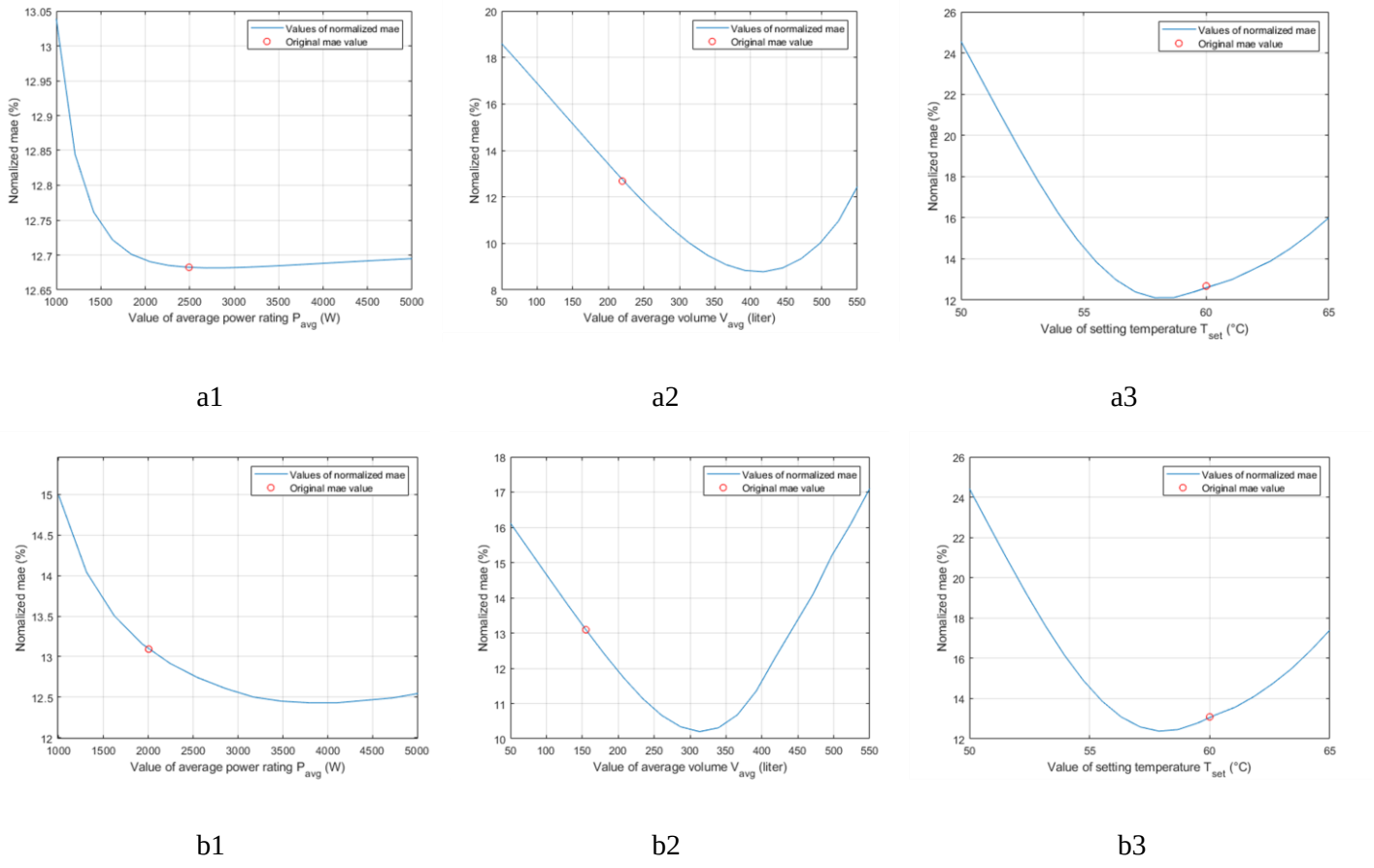

Figure 14: (a1, a2, a3, b1, b2, b3,) Normalized mae when varying the value of P_{avg}, V_{avg} and T_{set} respectively. a, b represent scenario 1 and scenario 2, respectively.

The aim of this sensitivity analysis is to quantify the impact of a lack of precise knowledge about the average characteristics of the DHW stock on the output of the aggregated model. The sensitivity analysis conducted in Figure 14 (a1, a2, a3, b1, b2, b3) involves the plotting of the NMAE as the blue line, while the red dot represents the original value of the parameter being varied. By examining the relationship between the variations in parameter values and the resulting NMAE, insights can be gained into the sensitivity and importance of each parameter in influencing the accuracy of the aggregated model's predictions.

To do so, we employ an approach where the aggregated model is subjected to simulation while altering each parameter within a defined range. The output of this varied aggregated model is then compared with the output of the unit model, which maintains a consistent set of initial parameters (P_{avg}, V_{avg} and T_{set}). For example, when considering the scenario 2 involving 10,000 EWHs. The initial

parameter values (P_{avg}, V_{avg} and T_{set}) are set to (2004, 155.1, 60). Consequently, if we want to test the sensitivity of parameter T_{set} on the aggregated model, we introduce variations in T_{set} values in range between 55°C and 65°C while keeping values of P_{avg} and V_{avg} constant. For each value of T_{set}, we perform simulations and compare the output of the aggregated model to that of the unit model. The NMAE and of the aggregated model using the initial set of parameter chosen will play a role in defining if the aggregated model is sensitive to the parameter T_{set}. Similarity, we execute the same process for other parameters.

The analysis of Figure 14 a3 and b3 reveals the sensitivity of the aggregated model to the parameter T_{set}, representing the setting temperature. By varying T_{set} from 50°C to 65°C, the NMAE values exhibited as a curve. Notably, the curve reaches its minimum point at around 58°C, where the values of NMAE are observed to be 12.01% and 12.43% for both scenario 1 and 2, respectively. These minimum NMAEs signify the point at which the aggregated model achieves its highest accuracy in estimating power consumption. The NMAE values gradually increase as T_{set} deviates from this optimal value. The maximum NMAEs of 24.5% and 24.4% occurred at 50°C for 5,000-household and 10,000-household scenario, respectively. This finding underscores the sensitivity of the aggregated model to the T_{set} parameter and emphasizes the criticality of selecting the appropriate value to achieve the best possible performance.

Additionally, a similar trend is observed when analyzing the sensitivity of the aggregated model to the parameter V_{avg} (average volume). By varying V_{avg} within the range of 50 liters to 550 liters, a corresponding variation in NMAE is observed. This indicates that the aggregated model is sensitive to changes in the V_{avg} parameter. Similar to the findings for T_{set}, the NMAE values form a curve, and the minimum NMAE is observed at the point of 410 liters and 320 liters for scenario 1 and 2, respectively. This minimum NMAE value signifies the value for V_{avg}, at which the aggregated model achieves the highest accuracy in power consumption estimation.

On the other hand, when examining the parameter P_{avg} (average power rating), a slightly different trend is observed. The NMAE values increase insignificantly as the value of P_{avg} deviates from the optimal point, which is observed at around 2700W and 3750W for scenario 1 and 2, respectively. This suggests that the aggregated model is relatively less sensitive to changes in the P_{avg} parameter compared to T_{set} and V_{avg}. However, we can still conclude that the aggregated model remains reasonably robust and maintains its performance in estimating power consumption even with marginal deterioration in accuracy observed.

7. Simulation results of the aggregated thermodynamic water heater model

Different from electric water heaters, thermodynamic water heaters are powered by a heat pump and the capacity of the heat pump depends on the coefficient of performance COP. However, the idea for the aggregated model methodology is similar to that of the electric water heater model. We also consider 2 parts. The first part will take into account the simulation of a physical model of thermodynamic water heater. Here, the detailed model of the heat pump is not considered for the simplification. Also using the data provided by the manufacturer, each household is randomized with a particular type of thermodynamic water heater with a specific heat pump's capacity and COP, volume and height of the water tank by using the uniform distribution. However, COP varies according to the air source temperature and the temperature of the water inside the tank. The second part is about simulation results of the aggregated model using proposed methodology.

7.1. Parameters of the aggregated TWH model

We applied the same approach as we use for electric water heater to build the aggregated model.

Hence, P_{agg} is calculated by the average power rating P_{avg} (W) multiplied by the number of TWHs (N_{TWH}):

$$P_{agg} = P_{avg}\, N_{TWH}$$

T_{hb} is defined by the temperature setting of the water tank T_{set} (°C):

$$T_{hb} = T_{set}$$

T_{lb} is given by the linear function of the average power rating P_{avg} (W), the average volume V_{avg} (m^3), and temperature setting of the water tank T_{set} (°C):

$$T_{lb} = 27.9394 - 0.0172\, P_{avg} - 0.0508\, V_{avg} + 0.5505\, T_{set}$$

A glance at the the equations for T_{lb} for TWH, when we alter the value of P_{avg} within the range of 300W to 800W, the corresponding portion of the equation, 0.0172 * P_{avg}, results in a range of values between 5.16 and 13.76. This indicates that changes in P_{avg} have a noticeable but relatively moderate effect on T_{lb}. Similarly, when we adjust V_{avg} within the range of 100 liters to 400 liters, the associated part of the equation, 0.0508 * V_{avg}, varies between 5.08 and 20.32. Like P_{avg}, changes in average volume show an effect on T_{lb}, although it remains in a moderate range. In contrast, the part of the equation linked to 0.5505 * T_{set} demonstrates a substantial variation. When T_{set} is varied between 55°C and 65°C, this component fluctuates significantly, ranging from 30.28 to 35.78. This demonstrates that T_{set} plays a dominant and prominent role in influencing T_{lb} for TWH. And for the case of EWH, the same trend is also observed that when vary value of T_{set}, the part of the equation linked to 0.4059 *T_{set} is in range of 22.32 and 26.38 when changing value of T_{set} between 55°C and 65°C. Furthermore, looking at the constant term within the T_{lb} equation, the constant is higher in the case of TWH compared to EWH. This divergence arises from the distinct range of T_{lb} values obtained

from unit models: TWH exhibits a range of 36 to 44°C, whereas EWH's range is slightly lower, spanning from 32 to 37°C.

7.2. Simulation of aggregated model for thermodynamic water heater

The simulation of the aggregated model is done with the time step of 1 minute for different numbers of households (5,000 and 10,000 houses).

As obtained from the uniform distribution for choosing types of thermodynamic water heater for each household, some parameters of the aggregated model are determined including the average power rating P_{avg}, average volume V_{avg} and average height H_{avg} for different numbers of households (Table 9). The value of COP for aggregated model is also defined by a function:

$$COP_{agg} = c_{0_{avg}} + c_{1_{avg}} \Delta T$$

$c_{0_{avg}}$, $c_{1_{avg}}$is calculated by taking the average value of all corresponding coefficients from all thermodynamic water heaters.

Number of households	**5000**	**10000**
P_{avg} (W)	488	501.9
V_{avg}(liter)	254.5	258.1
H_{avg}(m)	1.7	1.77
T_{set}(°C)	60	60
$c_{0_{avg}}$	5.149	5.317
$c_{1_{avg}}$	-0.045	-0.049

Table 9: The values of the average power rating P_{avg} ,average volume V_{avg} , average height H_{avg} , setting temperature T_{set} and 2 average coefficient values of the COP's equation 5,000 and 10,000 households, respectively.

Figure 15 shows the simulation results between unit model and aggregated model for TWH

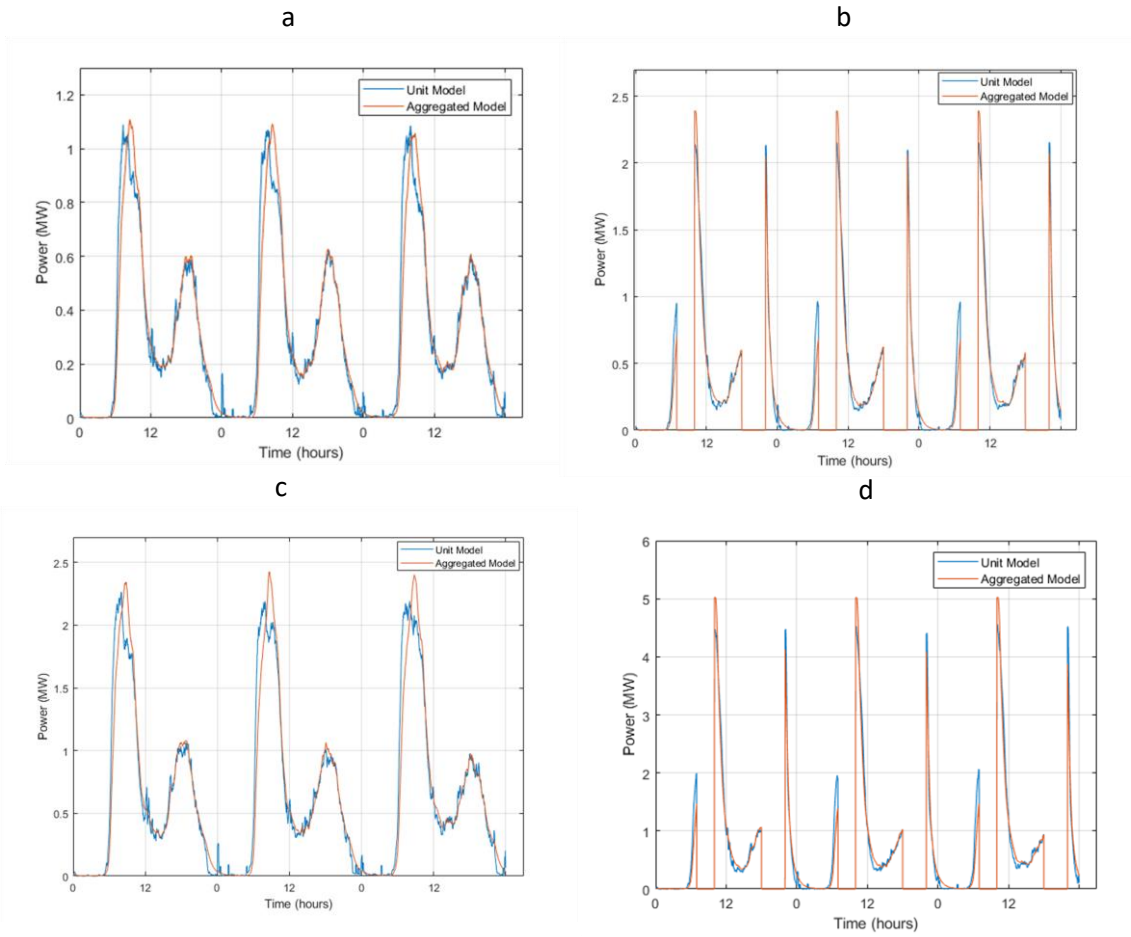

Figure 15: The electrical power consumption for domestic hot water for TWH in 3 days (kW). [a] and [b] describe the simulation of the aggregated models without and with the electricity price control signal applied for 5,000 households, respectively while [c] and [d] present those for 10,000 households.

Model type	**5,000 households (%)**	**10,000 households (%)**
The aggregated model without control signals	13.89	14.11
The aggregated model with control signals	14.30	15.01

Table 10: Normalized Absolute Mean Error (NMAE) (percentage) of the TWH aggregated model, compared to the unit model for 5,000 and 10,000 households, respectively.

Table 10 shows NMAE of the aggregated model compared to the unit model in different spatial scales (5,000 houses and 10,000 houses).

The development of the aggregated model for thermodynamic water heaters brings an enhancement in capturing the power consumption dynamics of DHW systems. In fact, we can incorporate both EWH and TWH in effectively creating a comprehensive representation of power consumption for DHW by estimating the distribution of each type and run model in parallel. By doing so, we can achieve a more presentative model that reflexes the power consumption for DHW in real-world scenarios.

By developing aggregated models for both EWHs and TWHs, we have expanded our analytical toolkit to gain a deeper understanding of energy flexibility in domestic hot water systems. These models play a role in connecting theoretical concepts and practical applications, aligning with the ongoing shift towards optimizing energy usage and demand-side management.

8. An application of the aggregated model

As mentioned in the introduction, the demand-side flexibility brings benefits to power system operation services such as frequency control, voltage control or power call from the grid. In order to exploit the full range of consumers in the demand-side flexibility, a new market actor, so called "aggregator", is introduced with the role of promoting and offering flexible products on the electricity market meanwhile incentivizing consumers' participation. The assessment of the flexibility energy can assist aggregators to determine the possible demand that can be flexible with less time-consuming and more efficient computation by using the proposed aggregated model.

In this part, we only consider the aggregated model for EWH. Here, we define 6 cases to facilitate visualization (Table 11).

Case	Description
S0	The aggregated model without control signal
S1 to S4	The aggregated model with the off-peak hours control signal using option 1 to option 4 (Table 2)
S5	The aggregated model with the electricity price control signal

Table 11 : Six different cases, in which the aggregated model is applied with different control signals

With the electricity price control signal applied to the aggregated model, the logic of the control is as follows: during high-price hours, the aggregated water heater is turned off and it is only turned on

during low-price hours. Hence, high-price control signals are defined from 7h to 10h and from 18h to 22h. When the off-peak hours control signal is applied to the aggregated model, during peak hours, the aggregated water heater is turned off and it is only turned on during off-peak hours. In this section, it is assumed that during peak hours and high price hours, all EWHs are turned off at the same time.

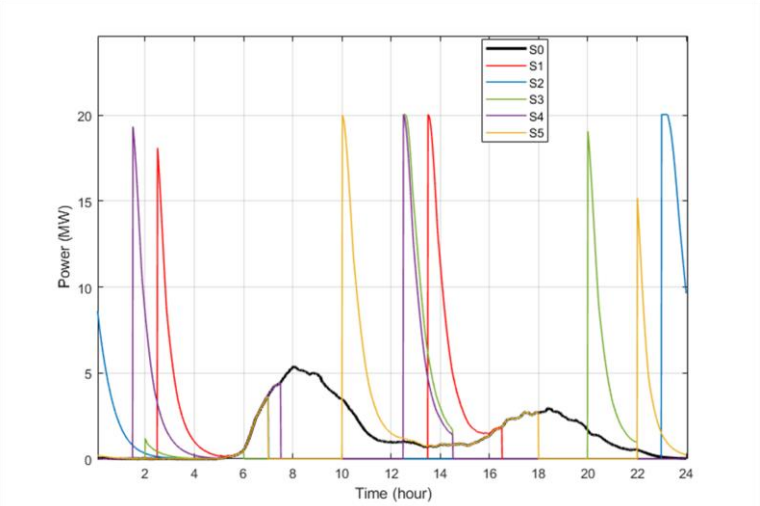

Figure 16: The simulation results of the power consumption for the electric water heater of 10,000 households using the aggregated model with price control signal applied.

Figure 16 demonstrates the simulation results of power. The results show that for each control signal option, a certain amount of power is cut off during peak hours and high-price electricity hours which lead to the power demand rises significantly during off-peak and low-price electricity hours. However, we can still determine energy flexibility,

We investigate several indicators to assess the flexibility for 6 cases.

- Indicator 1: The percentage of energy shifted during peak hours (the total energy shifted from peak to off-peak hours is divided by the total energy consumed in the simulation time).
- Indicator 2: The time during which user comfort is compromised (when the water temperature is lower than 40°C).
- Indicator 3: The cost of electricity can be reduced.

Indicators	Case 0	Case 1	Case 2	Case 3	Case 4	Case 5
Shifted average energy /house/day (%)	0	80.89	92.92	89.38	82.50	58.16
The time in which comfort is sacrificed /house/ day (minutes)	0	0	0	0	0	0
The reduction in electricity cost /house/day (%)	0	33.62	33.60	19.27	32.45	13.81

Table 12 : Results of three mentioned indicators for 6 cases

It is essential to emphasize that the control signal of the case S1 to S4 encompass an off-peak control signal spanning a total of 8 hours daily (as detailed in Table 2). In practical terms, this implies that the EWHs are exclusively activated during these 8 designated off-peak hours, remaining inactive for the remaining 16 hours. In contrast, for the case S5, there are 7 hours characterized by elevated electricity prices during the day, from 7h to 10h and from 18h to 22h. Consequently, the EWHs remain switched off throughout these 7 hours, while they are operational during the other periods. This explains the lower energy shift observed during a day of the case S5 in comparison to cases S1 to S4. Examining case S3, it is apparent that the reduction in electricity costs is notably less compared to cases S1, S2, and S4. This can be attributed to the fact that in case S3, an off-peak interval from 20h to 22h coincides with peak electricity prices (as depicted in Figure 9). It is also observable that the percentage of energy cost reduction in case S5 is the lowest with 13.81%, given that it involves merely 7 hours of power reduction. Additionally, the timeframe during which the average water temperature falls below 40°C is negligible, amounting to zero. This observation signifies that there is no compromise on user comfort within this context. Nevertheless, it is worth noting that the aggregated model only provides an average perspective on domestic hot water power consumption, thus a more comprehensive examination of user comfort would require further research. In the scope of this chapter, our focus centers on elaborating the methodology for constructing the aggregated model for DHW and evaluating energy flexibility using this model. In summary, the use of the aggregated model enables estimation and calculation of energy flexibility for domestic hot water, while also facilitating the assessment of diverse control strategies to aid decision-making for users of the model.

9. Conclusion

The aggregated model, representing multiple EWHs, proves to be an effective tool for featuring the power usage behavior of DHW, regardless of whether control signals are applied or not. Its versatility allows for various applications and benefits in different contexts. One notable application of the aggregated model is the assessment and quantification of flexibility achieved through the aggregation

of multiple water heater units. By testing different control strategies on the model, the impact of these strategies on DHW power consumption can be measured and evaluated. This provides insights into the effectiveness and efficiency of different control approaches at various spatial scales, ranging from districts to cities to entire regions. The aggregated model enables faster and more efficient computation, allowing for scalable analysis of DHW. The simulation time for this aggregated model is 2622 times faster compared to the unit model's simulation for 10,000 houses. These computation times were recorded using MATLAB R2019b on a Dell PC with an Intel(R) Core(TM) i5-8265U CPU running at 1.60GHz. Furthermore, the application of the aggregated model can contribute to the development of smart buildings and smart cities. As demand-side flexibility becomes increasingly important in optimizing energy management, the aggregated model could be a useful tool, which helps for integrating and coordinating multiple energy sources within a smart grid framework. By considering the aggregated behavior of EWHs, the model enables the assessment of the overall impact of demand-side flexibility, facilitating the optimization of energy usage and enhancing the development of smart and sustainable urban environments.

10. Limitation of the aggregated model

While the aggregated model for EWHs provides insights and benefits, it also has certain limitations that need to be acknowledged. These limitations include:

1. Errors in power consumption estimation: The methodology used in the aggregated model assumes a quadratic relationship between power consumption and water temperature for the aggregated water heater. However, this assumption, along with the determination of the higher bound and lower bound temperatures, may introduce errors. In fact, the water temperature of the aggregated water heater represents the average temperature of all individual EWHs. When the water temperature is lower than the lower bound, the aggregated model assumes maximum power consumption. However, in practice, not all individual EWHs may operate at their maximum power. This discrepancy can lead to inaccuracies in the power consumption estimation by the aggregated model.
2. The model's primary objective is to provide an overall understanding of power consumption behavior and optimize energy management. However, it does not account for the potential loss of comfort experienced by specific users who may be affected by the aggregated control strategies implemented. Therefore, there is possibility that several households so not having the desired water temperature at any given time during the day.

11. Proposed research

In future research, a possible next step could involve the enhancement of the precision and accuracy in measuring the parameters employed during the construction of the aggregated model for domestic hot water, with the aim of refining their accuracy and reducing potential sources of uncertainty.

ANNEX A: Data regarding characteristics of EWHs and TWHs

ANNEX A1: The data concerning the characteristics of EWHs is collected from the manufacturer [42]

Type	Capacity (liters)	Power rating (W)	Height (m)
1	50	1500	0.575
2	75	1200	0.76
3	100	1200	0.89
4	150	1800	1.21
5	150	2200	1.25
6	200	2400	1.57
7	250	3000	1.69
8	300	3000	1.78

Table 13: The data concerning the characteristics of EWHs.

There are eight different types of EWH as described in Table 13.

ANNEX A2: The data concerning the characteristics of TWHs is collected from the manufacturer

Type	Volume (litre)	Power rating (W)	Height (m)	COP_1	COP_2	T_air_1 °C	T_air_2 °C	T_water °C
1	190	423	1.83	3.22	3.66	7	15	55
2	220	597	1.5	2.68	3.55	7	20	55
3	251	425	1.75	2.88	3.26	7	20	55
4	254	425	1.75	2.88	3.26	7	20	55
5	291	582	1.9	2.75	3.51	7	20	55
6	300	496	1.93	3.66	4.04	7	15	55
7	302	573	1.8	2.79	3.51	7	20	55

Table 14: The data concerning the characteristics of TWHs.

There are seven different types of TWH as shown in Table 14

ANNEX B: Finding the relation between power consumption and water temperature.

Starting with the electric water heater, the unit model is obtained by repeating the simulation for the physical model of the electric water heater. The simulation for 7 days (10,080 minutes) with the time step of 1 minute is done for 5,000 households. The initial water temperature is a decided using a uniform distribution with the values vary between 58°C and 60°C. Using the data provided by a manufacturer, which features different types of electric water heater, each household is randomized

with a particular type of electric water heater with a specific power rating, volume and height of the water tank using uniform distribution. Electric water heaters are at OFF state.

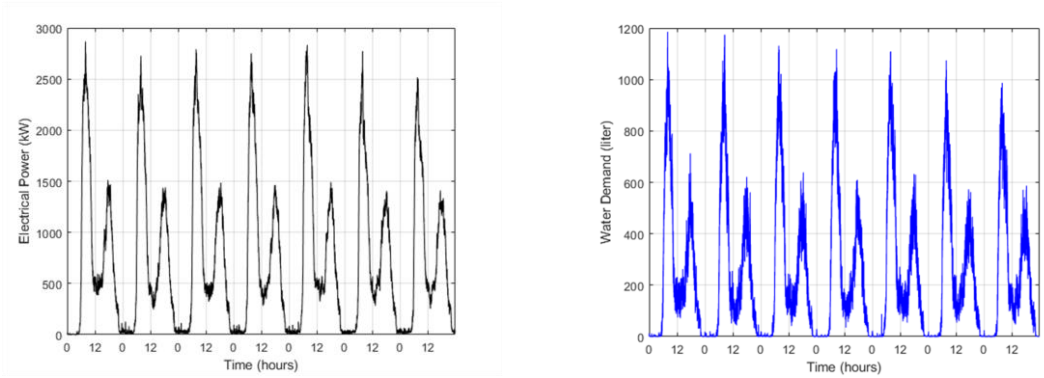

a *b*

Figure 17: (a,b), describe the power consumption (kW) and hot water demand (liter) of for 5,000 households

For the case above, there is no control signal applied to the water heaters, only the thermostat regulates the switches of the water heaters. Look at Figure 17, the highest power total of 5,000 households at each time step does not exceed 3,000kW, while the maximum total power of 5,000 households can reach to over 10,000kW (Figure 18) when off-peak period is considered. Hence, to obtain characteristics for full-range total power of 5,000 households, we use off-peak hours control signals in addition to the control from the thermostat. Along with thermostat control, when in the peak hours, all water heaters are turned off and only turned on in off-peak hours.

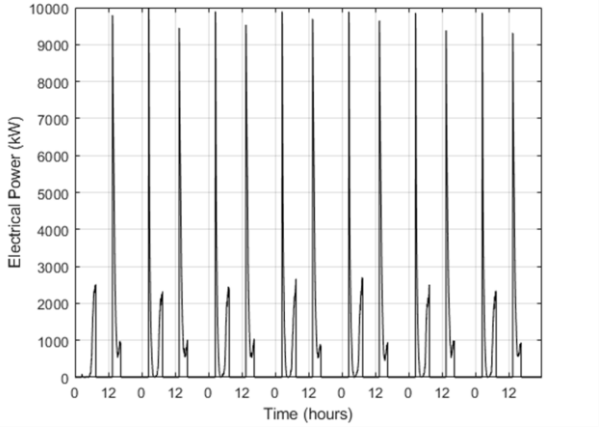

Figure 18: Power consumption (kW) of domestic hot water for 5000 households using EWH unit model with the off-peak signal applied

Within the unit model with and without off-peak hours control signal, each household has its own power consumption profile for domestic hot water. Hence, for each electric water heater at each time step, we have one value of electrical power along with one value of water temperature. Figure 19 illustrates the relation between the total power consumed and average water temperature of 5,000 electric water heater units at each time step. The black dots represent the total power and average water temperature obtained from the simulation of the unit model.

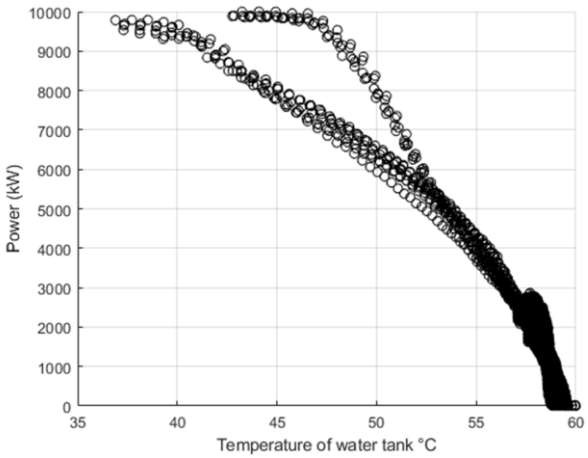

Figure 19: The relation between the total power consumed (kW) and average water temperature of 5000 houses in each time step

Figure 19 shows that the total power and average water temperature has a relation that follows a form of a quadratic equation. Based on this curve, the total power consumed never exceeds the sum of maximum power of all water heaters and the total power equals zero if the average temperature is higher than the thermostat setting temperature. For other cases, total power consumed seems to have a quadratic relationship with average water temperature.

ANNEX C: Finding the functions of P_{agg}, T_{lb} and T_{hb} for EWH

From the result obtained in ANNEX B**,** the total power consumed never exceeds the sum of maximum power of all water heaters and the total power equals zero if the average temperature is higher than the thermostat setting temperature. For other cases, total power consumed seems to have a quadratic relationship with average water temperature. Hence, the idea for the aggregated model is to define the relationship curve between total power and the water temperature as a quadratic function with some constraints accompanied.

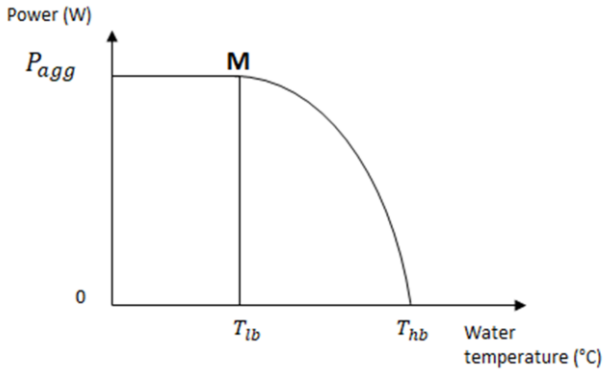

Figure 20: The relation curve between the power and the temperature of the water tank defined in the methodology for the aggregated model

The figure is represented from Figure 20, with the aggregated power P_{agg} is the sum of maximum power of all electric water heaters, the lower bound temperature T_{lb} and the higher bound temperature T_{hb} act as the constraints for the relation curve. It can be seen that the water temperature is set by thermostat setting temperature, hence, T_{hb} is defined as the set temperature of the water tank. T_{lb} is the threshold where decides whether the total power consumed is equal to the aggregated power P_{agg}.

From the simulation result of the unit model in ANNEX B, we can always get a set of values for P_{agg}, T_{lb} and T_{hb} and now the question is how to calculate them with a shortage of the information concerning detailed characteristics of each electric water heater. One of the solutions is to calculate them from some parameters regarding the water heater systems in the region considered including: the temperature setting T_{set}, the average power rating P_{avg} ,average volume V_{avg} of all water heater tanks in that region and the number of electric water heaters considered. With that idea, we propose our approach for the aggregated model accompanied by these hypotheses:

P_{agg} is is calculated by the average power rating P_{avg} (W) multiplies the number of households considered (Nbhouse).

$$P_{agg} = P_{avg} Nbhouse$$

T_{hb} is defined by the temperature setting of the water tank T_{set} (°C).

$$T_{hb} = T_{set}$$

T_{lb} is given by the linear function of the average power rating P_{avg} (W), the average volume V_{avg} (m^3) and temperature setting of the water tank T_{set} (°C) as the outcome of the proposed approach.

$$T_{lb} = function(P_{avg}, V_{avg}, T_{set})$$

In order to find the coefficients for the function of T_{lb}, the simulations of the unit model for different numbers of households, different values of P_{avg} , V_{avg} and T_{set} are done so as to get the different values of T_{lb}. There are 5 cases corresponding to 2000, 3000, 5000, 7000 and 10000 households. Values for P_{avg} and V_{avg} vary regarding the number of households. For each case, the value of T_{set} is varied from 55 to 64 °C with 10 values (Table 15).

The choice of T_{lb} is determined as follows (Figure 21): For each point representing the relationship between total power consumption and average water temperature, we take the average of all points, which are inside the range (T_w-ΔT, T_w+ΔT). In this study, we set ΔT equals 0.2. After having modified curve, the value of T_{lb} takes the value of the point, which have the second largest power consumption and the lowest average water temperature. To achieve this, we carried out several trials and tests during the work for this thesis to find a preferable point that can represent T_{lb}.

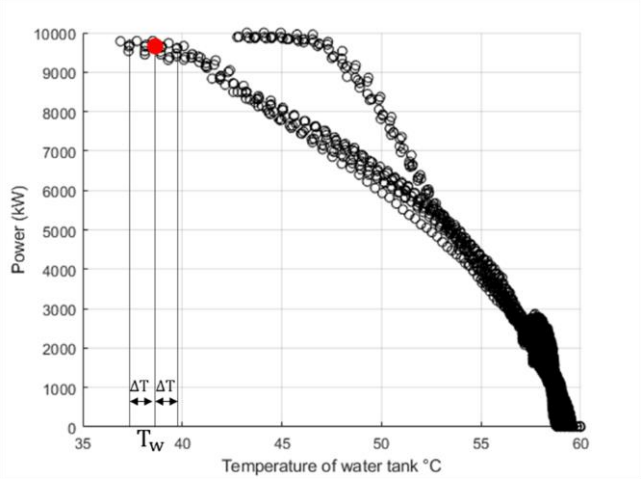

Figure 21: The relation between the total power consumed (kW) and average water temperature of 5000 houses in each time step

The value of T_{lb} are obtained following a simulation with the unit model for 1 given scenario. It is not the T_{lb} of the aggregate model. Then, via the numerous scenarios simulated with the unit model and linear regression, we have an equation for the T_{lb} of the aggregate model, expressed as a function of average parameters (P_{avg}, V_{avg} and T_{set}).

Number of households	P_{avg} (W)	V_{avg} (liter)	T_{set} (°C)
2000	2002	154.6	From 55 to 64 °C with 1 degree step.
3000	2091	167.2	
5000	2174	178.5	
7000	2541	217.2	
10000	2498	216.1	

Table 15: The values of P_{avg}, V_{avg} and T_{set} of different numbers of households for EWH

Hence, from the simulations of 10 cases along with the variation of T_{set} (10 values) 50 values of T_{lb} are obtained. A fitted linear regression model is used to identify the coefficients for the relationship between T_{lb} and P_{avg}, V_{avg} , T_{set}. Figure 22 demonstrates 50 values of T_{lb} . The black line shows 50 values of T_{lb} obtained from simulations of the unit model while the red line represents the results obtained from a fitted linear regression model.

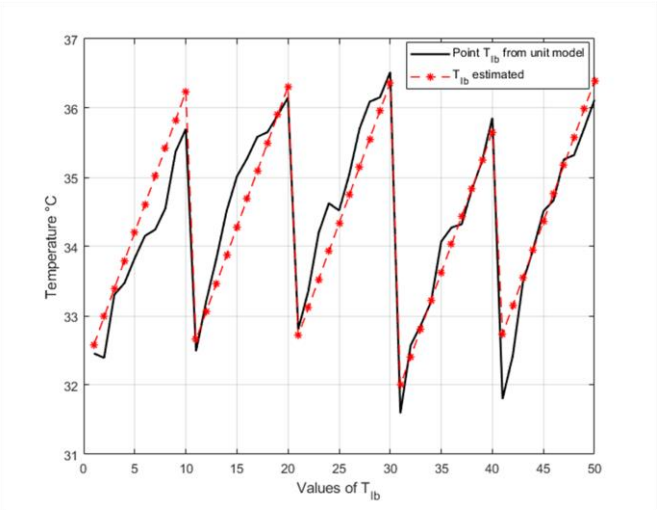

Figure 22: The value of T_{lb} when changing the value of P_{avg}, V_{avg} and T_{set} for EWH

Hence, the coefficients for P_{avg} (W), V_{avg} (liter), T_{set} (°C) are found and the final equation of T_{lb} is then shown as follow:

$$T_{lb} = 18.937 - 0.011P_{avg} + 0.0856V_{avg} + 0.4059T_{set}$$

ANNEX D: Finding the functions of P_{agg}, T_{lb} and T_{hb} for TWH

The same process in Annex B to find the final equation of T_{lb} is done for thermodynamic water heaters. There are 5 cases corresponding to 2000, 3000, 5000, 7000 and 10000 households. Values for P_{avg} and V_{avg} vary regarding the number of households. For each case, the value of T_{set} is varied from 55 to 64 °C with 10 values (Table 16).

Number of households	P_{avg} (W)	V_{avg}(liter)	T_{set}(°C)
2000	508.2	260.2	[55,64]
3000	477.1	254.2	[55,64]
5000	488.9	264.9	[55,64]
7000	493.3	214.1	[55,64]
10000	484.1	265.8	[55,64]

Table 16: The values of P_{avg}, V_{avg} and T_{set} of different numbers of households for thermodynamic water heater

In Table 16, it can be observed that for 7,000 households, the value of P_{avg} and V_{avg} are 493.3W and 214.1 liter, respectively while those values of 10,000 households are 484.1W and 265.8 liter. An explanation for this inconsistency is from the specifications data from the manufacturers. There are some types of TWH have high power rating but low volume, which leads to the situation that the average value of power rating for 7,000 households are high, but the average value of volume is low.

Figure 23 demonstrates 50 values of T_{lb} . The black line shows 50 values of T_{lb} obtained from

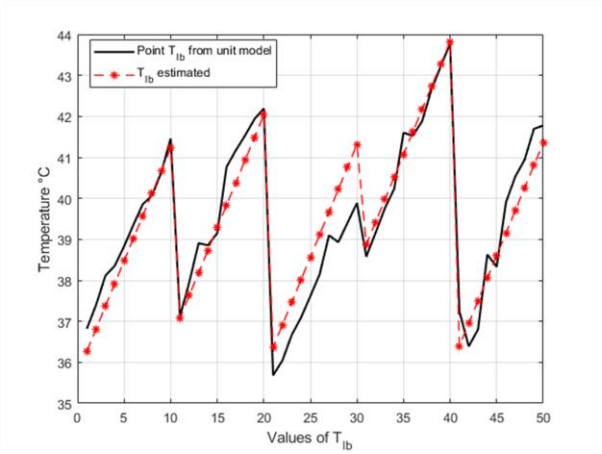

Figure 23: The value of T_{lb} when changing the value of P_{avg} , V_{avg} , T_{set} for the thermodynamic water heater

simulations of the unit model while the red line represents the results obtained from a fitted linear regression model.

The final equation of T_{lb} as function of P_{avg} (W), V_{avg} (liter), T_{set} (°C) for TWH is then shown as follow:

$$\mathrm{T_{lb}} = 27.9394 - 0.0172\,\mathrm{P_{avg}} - 0.0508\,\mathrm{V_{avg}} + 0.5505\,\mathrm{T_{set}}$$

III. Chapter 2: Electric vehicle charging

Le chapitre 2 porte sur la construction du modèle permettant de générer les profils d'utilisation de VE, en tenant compte du comportement de recharge des utilisateurs ainsi que de l'horaire d'utilisation des VE au cours de la journée. De la même manière qu'au chapitre 1, nous simulons la consommation d'énergie de plusieurs VE, ce que l'on appelle le modèle unitaire. Ensuite, nous proposons une méthodologie pour le modèle agrégé pour la charge des véhicules électriques sans et avec signaux de contrôle. La dernière section est consacrée à l'étude de la comparaison entre la consommation d'énergie obtenue à partir du modèle agrégé et celle du modèle unitaire.

---

1. Introduction

Recently, there has been a significant rise in the number of plug-in electric vehicles [48], which apparently contributes to the mission of electrification and decarbonization in the world. The transformation caused by renewable energy integration in the power systems creates a major movement in the transportation sector towards more sustainable mobility facilities. The idea of using electricity as an energy source to power the car brings independence from gasoline and petroleum and benefits also in the evolution towards a green power system in the future. In 2018, the report from International Renewable Energy Agency for the European Commission raised the importance in electrifying the transport sector in order to boost the growth in the power generation from renewable sources and reduce the greenhouse gas emissions [49].

Nowadays, more and more countries have put more attention on the e-mobility industry. According to the International Energy Agency (IEA), in 2021, there were more than 16.5 million electric vehicles on the road all over the world [48]. Several European countries have shown good development in the rate of electric vehicles on the mobility market. For example, in Norway, electric cars accounted for approximately 75 percent in 2020, compared to 56 percent in 2019 [48]. This is due to the suitable incentives for the electric car drivers, which is implemented by the government to boost electric vehicle uptake. As Europe's second largest auto market, France witnessed a percentage of 21.4% market share in the number of electric vehicles while Germany saw 24.3 percent of that in 2022 [48].

Beside the advantages in lowering fuel consumption, cost and reducing carbon dioxide emissions, the plug-in electric vehicles offer versatility and flexibility by being charged from the electric grid, where users can benefit from low-cost charging at home. Hence, the flexible recharge demand of electric vehicles, resulting in not having to be charged every day, could be useful to participate in demand-side flexibility programs and at the same time, boosts the utilization of electricity generated by renewable sources for electric vehicle charging.

Several studies have been carried out on the potential of electric vehicle charging in providing demand-side flexibility services [14], [50], [51]. However, when it comes to the topic of domestic EV charging, most studies obtain total charging load by taking into account the consumption of each household. In other words, one load model is needed for one EV. Consequently, when considering the load consumption of thousands of EVs, it will take a lot of time in computation calculation.
The contribution of this chapter, similar to the objective of domestic hot water models, is to develop an aggregated model for EV charging demand, which is equivalent to many individual models of one EV. First, the EV profile model is built to create the usage profile for each EV. Second, the methodology for creating an aggregated model is proposed.

2. Literature review

The common thing between studies which research about EV charging is about the objective of adapting to the evolution in the power system, resulting in integrating more renewable energy sources, and finding solutions to mitigate impact of these stochastic and intermittent sources on the system operation. Reference [52] demonstrates a model for primary frequency control by using plug-in electric vehicles, in order to improve the frequency response of the system. In reference [53], the authors build an aggregated model for a fleet of electric cars using an vehicle-to-grid technology to provide ancillary services to the power system. All plug-in EVs can be both charged and discharged. Normally, for estimating domestic EV charging, especially for thousands of EVs, it is challenging because of the need for large quantity of data, resulting in a complex data treatment. Reference [54] uses advanced deep learning to predict the residential EV charge. Their model is required to have the actual historical dataset of numerous EVs in the east of the USA. In some studies [55]–[57], when considering a big amount of EVs, each EV needs its own charging model, which can take a lot of time in computation. In this study, the management of aggregation of electric vehicles is presented. One thing that needs to be mentioned is that most studies do not focus on the aggregation of domestic EV charging. They care more about aggregated electricity demand at charging stations or at parking while charging at home is also a matter when it comes to a city or a country.

The remainder of this chapter presents the model of generating a profile for each electric vehicle usage. Then a physical model for charging an electric vehicle is built, in order to build the unit model for EV charging. The result from the unit model is then used to be a premise for building the aggregated model for at-home power charging when there is no control signals applied. Finally, using this aggregated model to build another model which can represent the power consumption when applying the control signal.

3. Electric vehicle charging profile

The primary objective of this study is to create an aggregated model for EV charging. The underlying idea of the model is as follows: The aggregated model is provided with specific parameters and the input data represented as a series over the time. Then, the model produces a corresponding time series of power consumption for charging as the output. The input data for this model is derived from statistical model Figure 24

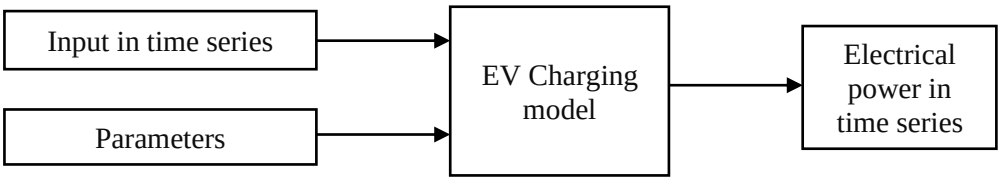

Figure 24: Idea for the aggregated model for EV charging

.

The rest of this section presents how the input is created and then a methodology for generating the aggregated model for EVC.

3.1. Charging level of electric vehicles

Electric vehicles can be charged at different locations: at home, at public stations or at workplaces. In this study, only level 1 and level 2 charging are used for charging the vehicles at home. Level 1 charging, also known as slow charging, refers to connecting an electric vehicle's cable to the domestic socket. A standard household socket can only deliver 2.3 kW (10 A), hence this way of charging the car is slowest. To fulfill the battery of 50kWh, it will take around 21 hours. Level 2 charging, on the other hand, involves charging the vehicle at a station or through the electrical box which can be installed at home. Level 2 chargers can be found in both commercial and residential locations. Compared to level 1, level 2 charging is significantly faster as it can deliver up to 22 kW. However, for charging at home, the common output power of 3.7 kW is typically used for level 2 charging.

3.2. Monte Carlo method

Monte Carlo simulation, so called Monte Carlo method, is **a mathematical technique, which creates random variables of an uncertain event** [58]. It involves generating random inputs using probability distributions such as a Gaussian distribution, log normal distribution…

In the context of this study, to represent the diversity of the household's behavior regarding their habits for charging their EV at home, the Monte Carlo method is employed to generate data that is utilized to construct the electric vehicle charging profile. By using probability distributions, random inputs are generated to simulate various charging scenarios.

3.3. Data used to generate electric vehicle charging profile

The data used to generate EV charging load profiles is adapted from the reference [59] and German mobility survey Mobilität in Deutschland (Mobility in Germany) [60]. The German mobility survey was done with the participation of 155000 households between May 2016 to September 2017 by the Federal Ministry for Digital and Transport. This extensive survey aimed to collect comprehensive mobility data across the residential population of Germany. It involves different regions in Germany, different types of households and diverse vehicles. For more in-depth information regarding the data obtained from the German mobility survey, it is recommended to refer to ANNEX E, which contains a detailed description and analysis of the data used in the study. We chose this source of data since it is the most comprehensive one that we could find, which allows us to have better representation of our model. This data source gives a better grasp of reality even if some bias may exist when combing to our model. For the other part of our model in this chapter, we tailored for the French context.

3.4. EV profile charging load model

Electricity demand for charging EVs is largely influenced by user behavior, emphasizing the need for a precise understanding of users' charging behavior. There are several factors, predominantly driven by users' decisions, play a crucial role in this regard, such as "range anxiety" [61] and charging time. 'Range anxiety' refers to the limitation of the state of charge of the battery at which users feel safe enough to reach the next destination. In other words, 'range anxiety' is the concern individuals have of running out of battery capacity while driving. This leads to the fact that users tend to charge their vehicles to a level that can cover the amount of electricity needed for next trips plus the 'range anxiety'.

Charging time is another decision that users can make, and it depends on the charging options available. They can either charge at home via domestic socket, at the workplace or at the public station. Each option will require different charging times since the power ratings delivered are different. In this research, users are assumed to charge only via level 1 and level 2 charging with the maximum power rating is 22 kW [62].

To simplify understanding, the EV charging model is divided into 3 particular parts, which are **tracking EV location model, EV physical model** and **plug-in decision model**.

- **The tracking EV location model** utilizes the data generated by Monte Carlo approach and the data from reference source [59].
- **EV physical model** allows monitoring the state of charge of the EVs
- **The plug-in decision mode**l decides whether the car should be charged or not. This model is affected significantly by users' behaviors.

These three models, are discussed and presented in detail in subsequent sections of the research, providing a comprehensive understanding of the EV charging model.

3.4.1. Tracking EV location model

The tracking EV location model plays a role in generating the location profile of each electric vehicle every day. It creates a one-minute-frequency time series that provides full information about the car's location, whether the EV is on the road, at home, at the workplace or in the public. This model utilizes an approach described in reference [59] to generate the electric vehicle charging load profile.

The tracking EV location model employs a time step of 1 minute to capture detailed information about the vehicle's location. Using the data obtained from the German Institute for Economic Research, the input of the tracking EV location model is described on Table 17. This table describes the list of inputs used for tracking EV location model. In ANNEX E1, we will find a comprehensive breakdown of each input used in the tracking EV location model, shedding light on the specifics of the data used for generating the location profile of electric vehicles. Additionally, ANNEX E2 provides an in-depth explanation of how the tracking EV location model operates, further elucidating the methodology employed in this research.

	List of inputs for tracking EV location model
1	Type of driver
2	Number of trips per day
3	Distance of the trip
4	Duration of the trip
5	Time departure of each trip
6	Destination of the trip
7	Time limitation of one trip regarding the location
8	Total time limitation of one location for one day

Table 17: List of inputs for tracking EV location model

This statistical information pertaining to the inputs for the tracking EV location model could be accessed through the sociological research studies. For example "Mobility in France: Panorama from the national survey transports et travel 2008", conducted by Ministry of Ecological Transition [63]. This particular research provides data on various aspects, including mobility patterns, transportation behaviors, and travel habits in France. By referring to this study, researchers can access the necessary statistical information required for constructing the inputs of the tracking EV location model. However, because the survey data has not yet been consolidated and requires filtering to select the suitable parameters for the input of the EV location tracking model. Moreover, the primary focus of this chapter is to create the aggregated model for Electric Vehicle Charging (EVC). Therefore, the decision has been made to utilize the data source from reference [59], which provides comprehensive information concerning users' behaviors.

3.4.2. EV physical model

EV physical model allows to monitoring the SOC of the EV. The principle of charge or discharge of an electric vehicle is simple. The EV discharges when it is used by users. The decision of charging the EV is defined by using the plug-in decision model. The energy loss when the EV parks is ignored in this study. Then, the energy consumption when driving is defined as below.

$$Q_{discharge} = D \cdot d_{trip}$$

$Q_{discharge}$	Energy discharge (kWh)
D	Driving energy consumption per km (kWh/km)
d_{trip}	Distance travel of the car (km)

Opposite to discharge the energy, the charging energy to the EV is calculated as follows.

$$Q_{charge} = P_{rating} \cdot t$$

Q_{charge}	Energy charge (kWh)
P_{rating}	Power rating (kW)
t	Charging time (h)

The state of charge of an electric car when the car is charged is determined as below.

$$SOC = SOC_{int} + \frac{Q_{charge}}{B}$$

SOC	State of charge
SOC_{int}	Initial state of charge
Q_{charge}	Energy charge (kWh)
B	Battery capacity (kWh)

The state of charge of an EV when it is discharged is defined as follows.

$$SOC = SOC_{int} - \frac{Q_{charge}}{B}$$

SOC	State of charge
SOC_{int}	Initial state of charge
$Q_{discharge}$	Energy discharge (kWh)
B	Battery capacity (kWh)

3.4.3. Plug-in decision model

The plug-in decision model has an objective of deciding whether the users will charge their vehicle. As previously highlighted, users' behavior plays a pivotal role in influencing the electricity demand for EV charging. Consequently, to generate the EV charging profile, it is essential to consider multiple factors that contribute to building a model for the generation of the EV charging load profile. These factors includes

- **Required state of charge**: define the SOC in need for the upcoming trip $SOC_{required}$
- **Charging location**: define where to charge the EVs
- **Users' charging behavior**: define the users' charging behavior coefficient U and then the plug-in probability P_{plug} is determined, representing the users' preferences to charge their EVs

Each of these factors is discussed in detail in following sectors.

3.4.3.1. Required state of charge

The required state of charge is the SOC needed for the next trip to get to the next destination. This amount of energy is affected by the distance between two destinations and also the 'range anxiety'. The 'range anxiety' is presented using the 'range anxiety factor' in this study.

The required SOC ($SOC_{required}$) for the next trip is determined as below:

$$SOC_{required} = \frac{d_{next\_trip}.\ D.R}{B}$$

d_{next_trip}: Distance for the next trip (km)

D : Driving energy consumption per kilometer (kWh/km)

R : Range anxiety factor

B: Battery capacity (kWh)

3.4.3.2. Charging location

Depending on the location of the EV, users can have different options to charge their cars. However, in this study, the focus is on the charging power available at home, and certain assumptions are made regarding the power ratings at different locations. Specifically, the power ratings considered are 11 kW for the workplace and 22 kW for public stations. For charging at home, the maximum power rating is set at 3.7 kW. The selection of power ratings for home charging is based on a probability distribution for charging level 1 and level 2 in reference [64], which indicates that BEV owners utilize level 2 chargers at home is about 2.5 times higher than using level 1 charger. Hence, we assume that 70% users have level 2 charger at home and 30% users use level 1 to charge their EVs.

3.4.3.3. Users' charging behavior

Users' charging behavior is captured through the parameter U which is studied in the reference [65]. This parameter, U, represents users' preferences and their inclination to charge their EVs. To delve into further detail, each user ensures that their EV has sufficient State of Charge (SOC) to cover the upcoming trip as well as their "anxiety range"- the additional SOC needed to alleviate any concerns about running out of battery power. This amount of SOC required is called $SOC_{required}$. When the EV arrives at a charging destination, if the vehicle' SOC at arrival is lower than the $SOC_{required}$, it is certain that the user will charge their cars. However, if the SOC at arrival is equal or higher than the SOC required, this is where the parameter U does its role. It assists in deciding whether the user wants to charge their EV or not, taking into account their personal charging preferences and behavior. The parameter U serves as a determinant, influencing the decision-making process for users regarding whether they choose to initiate charging for their EVs based on their specific circumstances and preferences.

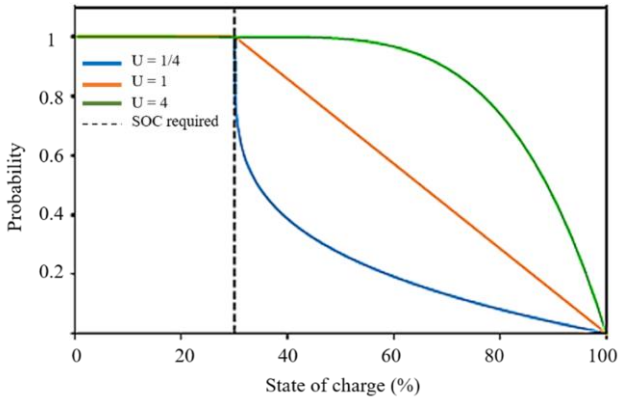

Figure 25 : Plug-in probability curves with different values of U.

The required SOC for next trip is 30%

U is used to calculate the plug-in probability of the user at any value of SOC at arrival. Different values of U result in different behavior of different users. For example, when U values are close to zero, the EV is typically charged only when users need to ensure sufficient energy for their next trip. In contrast, higher values of U, approaching one, indicate a significantly higher likelihood that users will charge their EVs regularly, potentially on a daily basis. Figure 25 provides illustrative examples of plug-in probability curves depicting various values of the parameter U. These curves show how different values of U influence the probability of users initiating charging at different SOC levels.

Finally, the plug-in probability (P_{plug}) at any SOC is defined as follow:

$$P_{plug} = \begin{cases} 1 & \text{if } SOC < SOC_{required} \\ 1 - \dfrac{SOC - SOC_{required}}{(1 - SOC_{required})^{U}} \end{cases}$$

P_{plug} : The plug-in probability

U : Users' charging behavior coefficient

Because each user will have different behavior, hence each user has its own value of parameter U to represent. In this study, a range of values of U from 0.89 to 1.31 is chosen [65].

3.5. Parameters for EV charging load model

In this sector, we synthesize all the parameters needed for building the EV charging load model, including:

1. Power rating for charging (P_{rating}): Our assumption is made for power rating for charging at home, at public and workplace, and the probability distribution of charging level 1 and level 2 at home.

2. Battery capacity (B): Depending on EVs' characteristics

3. Driving energy consumption per kilometer (D): Depending on EVs' characteristics

4. Range anxiety factor (R): Affecting users' charging decision, mentioned in [61]

5. Charging behavior coefficient (U): Representing for users' charging behavior, which is studied in the reference [65]

Each parameter is discussed further as follows:

3.5.1. Power rating for charging (P_{rating})

When charging at home, charging level 1 and level 2 are chosen. Hence, in this study, an assumption is made regarding the power ratings for home charging. Specifically, the power rating for level 1 charging at home is set at 2.3 kW, while the power rating for level 2 charging at home is set at 3.7 kW. Among the total number of electric vehicles (EVs) considered, it is assumed that 70% of them will use level 2 charging, while the other 30% will use level 1 charging [64]. For charging at the workplace and at public stations, the power ratings are assumed to be 11 kW and 22 kW, respectively. When users are in public locations, such as shopping areas, running errands, accompanying others, or engaging in leisure activities, they have the opportunity to charge their EVs at public stations, as

outlined in Table 24. These assumptions regarding power ratings at different charging locations enable the study to analyze and model the EV charging load profile accurately. By considering the various charging options and power ratings available, the study captures the diversity of charging behaviors in different settings and provides valuable insights into the overall EV charging dynamics.

3.5.2. Battery capacity (B)

Battery capacity of each EV considered in this study falls within the range of 17.6 kWh to 100 kWh [66]. We assume that the distribution of the battery capacity follows a Gaussian distribution with average battery capacity is 50 kWh and the standard deviation is 20 kWh [67]. This Gaussian distribution allows for the representation of the battery capacities of EVs in a probabilistic manner. By considering the average and standard deviation values, the study takes into account the variability in battery capacities among different EVs.

3.5.3. Driving energy consumption per kilometer (D)

Each EV possesses its own driving energy consumption per kilometer. In general, EVs have the driving energy consumption per km in the range between 0.12 to 0.20 kWh/km [68]. In this study, we also assume that the driving energy consumption per km follows the Gaussian distribution with average value is 0.16 and the standard deviation is 0.04.

3.5.4. Range anxiety factor (R)

Because range anxiety factor is affected mostly by users' behavior, which means that different users will have different values of range anxiety factor. Hence, in this research, the range anxiety factor is also assumed to have a Gaussian distribution with average value is 1.5, as in [61] and the standard deviation is 0.2**.**

3.5.5. Charging behavior coefficient (U)

As mentioned earlier, each user has its own value of charging behavior coefficient – parameter U to represent. From the reference [65], author used the real data to study the plug-in behavior of 601 users with various EVs and various battery capacity. This study highlight that EV users do not necessarily charge their vehicles daily and aim to quantitatively assess the influence of irregular plug-in behavior. To achieve that the author has developed a module considering a probabilistic plug-in decision, which is affected by the charging behavior coefficient U. The outcomes indicate that the module correctly captures the diverse charging preferences of users, making it suitable for generating load profiles across a wide spectrum of EV scenarios. This encompasses various battery capacities and driving patterns. Authors used the approach as mentioned in session 3.4.2.2 and conclude that a range of values of U varies from 0.89 to 1.31. In this chapter, we use this range of value for the parameter U

and then use the Gaussian distribution to distribute values of U to all the users considered. The average value of U and the standard deviation are 1.1 and 0.1, respectively.

3.6. The unit model of electric vehicle charging

Similar to the approach used for Domestic Hot Water modeling, the same process is applied to EV charging. In this case, before discussing the aggregated model, an individual model is constructed by repeatedly simulating the physical model for multiple EVs. This simulation aims to generate the charging power curve, which serves as a basis for evaluating the aggregated model. Using the EV charging profile, the charging power for each household can be estimated.

In this chapter, the set of simulations performed for each EV using the physical model is referred to as **the unit model**. The unit model is developed in MATLAB with a sampling time of one minute. A three-day simulation period is selected, considering a population of 5000 EVs. The input for the unit model consists of the time series data for the tracking location profile of the EVs. The output of the unit model is the total power consumption for charging activities at home, the workplace, and public charging stations.

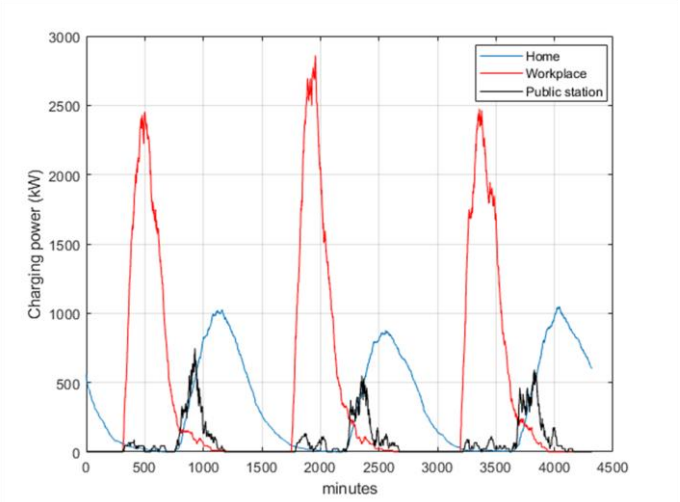

Figure 26 : The total charging power at home, at the workplace and at public stations of 5,000 EVs for 3 days

Figure 26 illustrates the results of the unit model for 5,000 EVs within 3 days. It shows different power consumption curves corresponding to different charging locations. It is observable that users exhibit a higher tendency to charge their EVs predominantly at their workplaces. This inclination can be attributed to the fact that individuals spend a significant portion of their day at work, thereby creating opportunities for EV charging. By the end of the day, users engage in various activities, often utilizing public charging stations for their EVs. Additionally, the pattern logically indicates that during nighttime hours, users opt for charging their EVs at home. This distinct pattern underscores

the efficacy of the EV charging load model in effectively illustrating the distribution of charging power across diverse locations.

3.7. Aggregated model of electric vehicle charging

The aggregated model for EV charging is developed to estimate the power consumption for home charging without requiring detailed information about the characteristics of individual households as well as the technical specifications of EVs. By utilizing this aggregated model, the need for simulating the charging power consumption of each individual EV is eliminated, saving computational time and resources.

In this chapter, we propose two aggregated models: one without any control signals applied and the other with control signals implemented. These models can determine the home-charging power consumption of all considered EVs, whether control signals are applied or not. They allow to quickly quantify the impact of different control strategies and access easily the energy flexibility. Besides, these models exhibit an efficient performance in saving computational time, which is thousands times faster than the performance of the unit model.

The input requirements for these aggregated models include the number of EVs considered, as well as the average values of certain parameters used in the simulation of the unit model. The parameters for which average values are needed are as follows:

1. Average battery capacity ($\mathbf{B_{avg}}$) in kilowatt-hour (kWh).
2. Average range anxiety factor ($\mathbf{R_{avg}}$).
3. Average driving energy consumption per kilometer ($\mathbf{D_{avg}}$) in kilowatt-hours per kilometer (kWh/km).
4. Average behavior coefficient ($\mathbf{U_{avg}}$).
5. Average distance traveled per day ($\mathbf{K_{avg}}$) in kilometer (km).

To obtain the average battery capacity (B_{avg}) and average driving energy consumption (D_{avg}), various sources can be accessed, such as the document "Evolution du parc roulant automobile depuis janvier 2010" from Avere-France [69] and "Fiches techniques voitures électriques" from [70]. The average distance traveled per day (K_{avg}) can be gathered from the document "Getting around by car: alone, or carpooling?" [71], which is compiled by the Ministry of Ecological Transition. The average range anxiety factor (R_{avg}) and behavior coefficient (U_{avg}) can be found in references [65] and [61], respectively.

By utilizing these average values for the parameters, the aggregated models can provide estimates of the power consumption for home charging for the entire population of EVs under consideration. This approach eliminates the need for detailed household information and facilitates a more efficient

analysis of EV charging dynamics. However, the aggregated models requires having the time series of the number of EVs presenting at home as an input.

3.7.1. The aggregated model without control signals applied

In the absence of control signals, which means there are no external demands influencing users' charging decisions, the aggregated model focuses on estimating the home-charging power consumption. Only the electric vehicles (EVs) that are present at home are considered to determine the total power consumption for charging at home. Since, at any given time, some EVs may be actively charging, while others may already be fully charged or not charging at all, therefore, instead of considering the total charging power consumption of all EVs at each time step, the average charging power consumption of all EVs at home is taken into account. We execute the simulation of the unit model for 7 days with the input is a time series of the number of EVs presenting at home, which is derived from the EV charging load model. Initially, the same approach used for the aggregated model for domestic hot water is employed. The objective is to establish a relationship between the average power charging consumption and the average SOC of all EVs. Figure 27 shows the relation between the average power charging consumption and the average SOC of all EVs and as we can see no obvious and apparent connection between them.

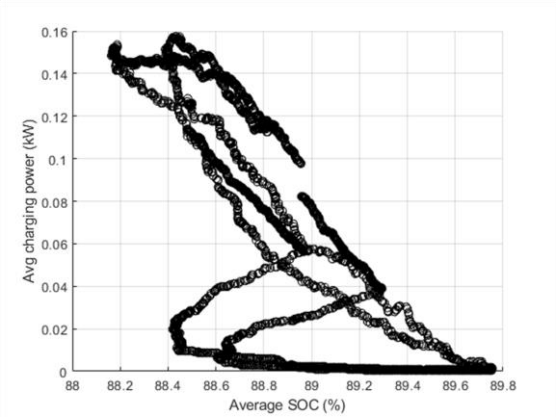

Figure 27 : Relation between average power charging and average SOC of 5,000 EVs

Consequently, an alternative approach is pursued to obtain a better understanding. We plotted the figure, which features the relation between the average power charging consumption of all EVs at home and number of EVs at home. Figure 28 displays the average home-charging power consumption of EVs that are present at home, as well as the corresponding number of vehicles at home, considering a population of 5,000 EVs. The figure is analyzed from right to left, representing the progression of time throughout the day. At midnight, the number of vehicles at home is at its maximum. As time progresses, the vehicles gradually leave home as users commute to work. The number of vehicles at

home will then reach its minimum at a specific time, referred to as T_{min-ev}. Subsequently, users begin returning home, leading to an increase in the number of EVs at home.

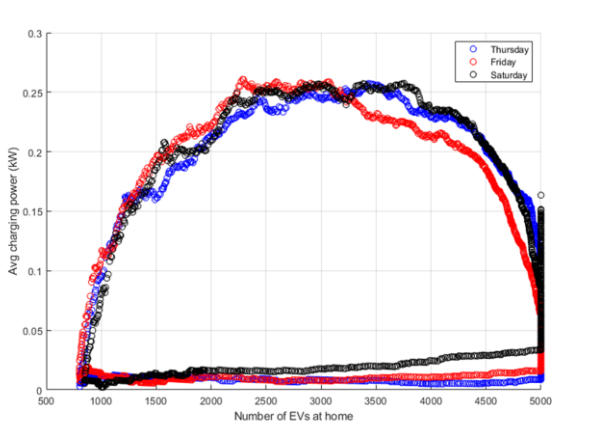

Figure 28 : The relation between the average power charging consumption of all EVs at home and number of EVs at home for 5,000EVs

Based on this observation, two conclusions can be drawn from the figure. Firstly, before the time T_{min-ev}, there is a linear relationship between the average home-charging power consumption of EVs at home and the number of EVs at home. Secondly, after the time T_{min-ev}, the relationship between the average home-charging power consumption and the number of EVs at home follows a form resembling half of an ellipse.

These conclusions serve as the foundation for developing the methodology for generating the aggregated model for home-charging power consumption of EVs. Based on this premise, the following hypotheses are formulated:

1. The average home-charging power is determined as a function of the number of the EVs which present at home. The relation between them is described by the black line in Figure 29. ANNEX **F** provides detailed information on how this relationship line is derived and established.

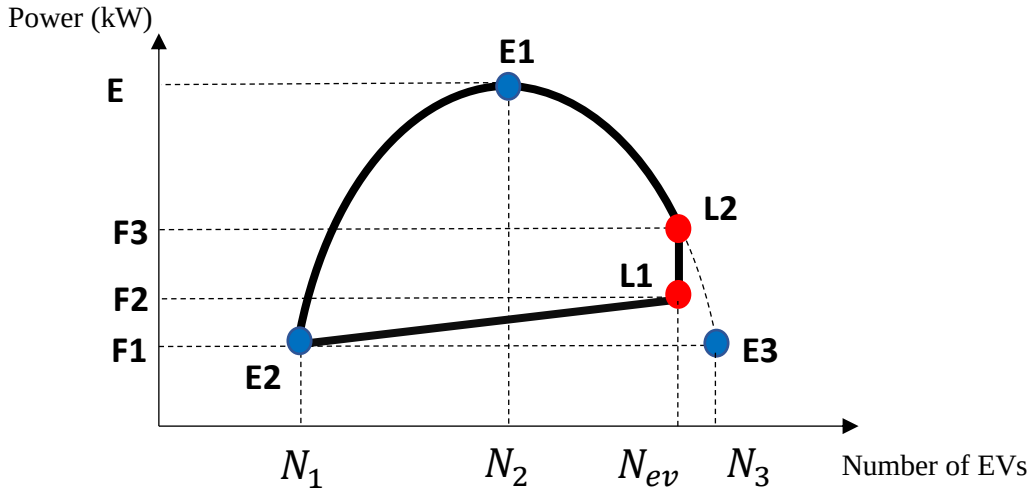

Figure 29: The relation curve between the average home-charging power and the number of the EVs, which present at home for the aggregated model without control signals applied

2. We assume this relation line is presented by using a half of an ellipse and linear functions. The ellipse curve here is defined from 3 points: E1, E2 and E3. The linears are defined from E2 and L1, and from L1 and L2. The point F2 and F3 are used to define the point L1 and L2, respectively. F1 and N1 are used to determine the point E2. F1 and N3 are used to determine the point E3. E and N2 are used to determine the point E1. In other words, to find the relation line, it is necessary to find 5 points: E1, E2, E3, L1 and L2.
3. The point E1 is determined as the maxima of the ellipse curve and in order to define E1, it is necessary to define the values of point E.

   Figure 30 is a representation of the relationship curve between the average home-charging power and the number of EVs present at home. In this figure, the points N_1, N_2, and N_3 are replaced with N_{min}, N_{mid}, and N_{max}, respectively.

   Within the methodology, N_1 represents the minimum number of vehicles at home (N_{min}) observed at the time $T_{min\text{-}ev}$. N_3 (N_{max}) is used solely for defining the ellipse curve. N_2 (N_{mid}) corresponds to the number of vehicles in the middle of N_{max} and N_{min}. F3 denotes the power consumed at around midnight, when all EVs (N_{ev}) are at home and at this moment, most of EVs are fully charged. Hence, from this time, the charging power consumption progressively decreases as time passes, following the indicated arrows in Figure 30. F2 signifies the power consumption all EVs at home (N_{ev}) and at this point, users start leaving home. F1 represents the power consumed when the number of EVs at home is at its minimum, typically occurring

when individuals go to work and in the afternoon. Following this point, people begin returning home and charging their EVs. E denotes the maximum charging power consumption observed. The evolution of time is depicted through the arrows in Figure 30, highlighting the changes in the number of EVs at home and the corresponding power consumption patterns.

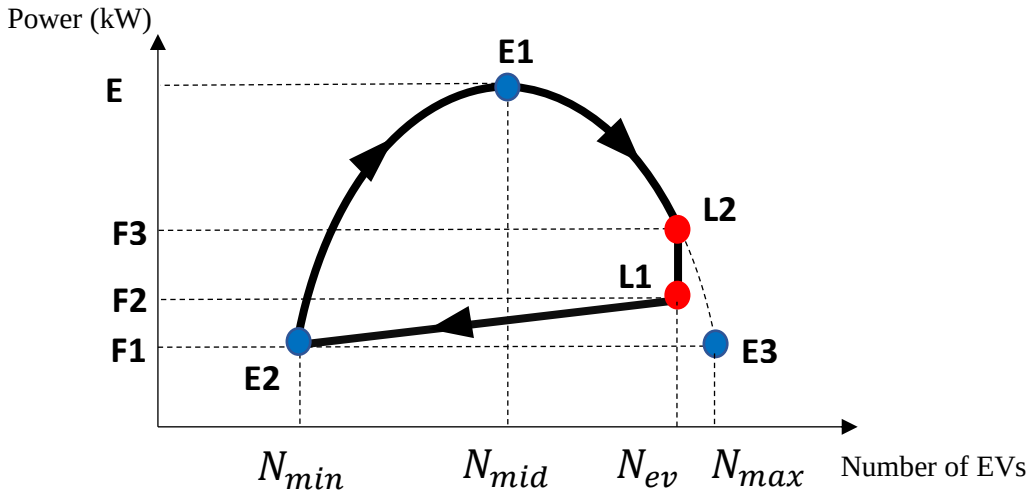

Figure 30: The relation curve between the average home-charging power and the number of the EVs at home (recreated from Figure 29)

4. The values of E, F1, F2, F3, N_{min} and N_{max} are defined based on the number of EVs (N_{ev}) and the average values of parameters including average battery capacity, average range anxiety factor, average driving energy consumption per kilometer, average behavior coefficient and average distance travelled per day . A specific study is done in ANNEX G2, which presents how six values of E, F1, F2, F3, N_{min} and N_{max} are obtained.

5. In short, we divide into two parts: "**after the time T_{min-ev} to midnight"** and **"before the time T_{min-ev}"**

   The time T_{min-ev} is defined using the input of the aggregated model which is the time series of number of EVs at home.

   - **Part 1: after the time T_{min-ev} to midnight (**Define E **,** N_{min} and N_{max}**)**
     - E is given by the linear function of B_{avg} (kWh), R_{avg}, D_{avg} (kWh/km), U_{avg} and K_{avg}(km).

   E = function (B_{avg}, R_{avg} , D_{avg}, U_{avg}, K_{avg})

As mentioned in ANNEX G2, by using multiple linear regression, the coefficients are found and the final equation of E is then shown as follow:

$$E = -0.6375 - 0.0053\, B_{avg} + 4.1829\, D_{avg} + 0.0132\, U_{avg} + 0.1685\, R_{avg} + 0.0172\, K_{avg}$$

- The value of N_{min}, representing the minimum number of EVs at home, is determined by extracting the minimum value from the time series of the number of EVs at home, which serves as the input to the aggregated model. The time series data provides information on the variation of the number of EVs present at home during the day.
- N_{max} is defined as follow:

$$N_{max} = \gamma N_{ev}$$

γ is defined by using the hypothesis of ellipse relation between average home-charging power consumption of EVs at home and the number of EVs at home after the time T_{min-ev}. γ then is described as a function of average battery capacity B_{avg} (kWh), average range anxiety factor R_{avg}, average driving energy consumption per kilometer D_{avg} (kWh/km), average behavior coefficient U_{avg} and average distance travelled per day K_{avg} (km).

ANNEX G2 presents how γ is obtained and then γ is determined:

$$\gamma = 0.9533 + 0.00065\, B_{avg} + 0.1714\, D_{avg} - 0.009\, U_{avg} + 0.0009\, R_{avg} + 0.0007\, K_{avg}$$

In general, the idea of all hypothesis is to determine the functions of the relation curve between the average home-charging power $P_{avg-agg}$ and the number of the EVs which present at home $N_{ev-home}$, which is defined by 4 values of E, N_{min}, N_{mid} and N_{max}. The calculation for the average home-charging power for EVs at home of the aggregated model ($P_{avg-agg}$) then depends on the equations below:

$$\frac{P_{avg-agg}{}^2}{a_1{}^2} + \frac{N_{ev-home}{}^2}{a_2{}^2} = 1$$

$P_{avg-agg}$: Average home-charging power consumption of the aggregated model without signal

$N_{ev-home}$: The number of the EVs, which present at home

With following conditions: The point E1 is the maxima of the ellipse equation and $P_{avg-agg} >= 0$

a_1 and a_2 are the coefficients, which are calculated by using 6 values of B_{avg}, R_{avg} , D_{avg}, U_{avg}, K_{avg} and Nbhouse.

a_1 = E = -0.6375 -0.0053 B_{avg} +4.1829 D_{avg}+0.0132 U_{avg}+0.1685 R_{avg} +0.0172 K_{avg}

a_2= $N_{mid} - N_{min}$

Hence,

$$P_{avg-agg} = \sqrt{|E|^2 - \frac{|E|^2}{(N_{mid} - N_{min})^2} N_{ev-home}{}^2}$$

- **Part 2: before the time T_{min-ev} (Define F1, F2 and F3)**
  - The value of F1 and F2 are defined by the linear function of B_{avg} (kWh), R_{avg}, D_{avg} (kWh/km), U_{avg} and a K_{avg} (km). Use the same method for finding E, multiple linear regression is used to find the coefficients (ANNEX G2)

    F1 = -0.0077 -0.00003 B_{avg} +0.0585 D_{avg}+0.0008 U_{avg}+0.0009 R_{avg} +0.0006 K_{avg}

    F2 = -0.1928 +0.0015 B_{avg} +0.697 D_{avg}-0.015 U_{avg}+0.0012 R_{avg} +0.0025 K_{avg}

  - With the ellipse function built in part 1, the value of F3 is also calculated by replacing number of EVs (N_{ev}) to the function.

$$F3 = \sqrt{|E|^2 - \frac{|E|^2}{(N_{mid} - N_{min})^2} N_{ev}{}^2}$$

Before the time T_{min-ev}, the average home-charging power $P_{avg-agg}$ is defined using 2 linear functions: One is generated from E2 and L1 and the other is generated from L1 and L2 with E2 (N_{min}, F1), L1(N_{ev}, F2) and L2(N_{ev}, F3). Hence, we have:

If $N_{ev-home} < N_{ev}$ then

$$P_{avg-agg} = b_1 + b_2 N_{ev-home}$$

$$b_1 = F1 - \frac{(F2 - F1)N_{min}}{N_{ev} - N_{min}}$$

$$b_2 = \frac{F2 - F1}{N_{ev} - N_{min}}$$

If $N_{ev-home} = N_{ev}$ then $P_{avg-agg} = F2 + \frac{F3-F2}{\tau}$

τ is the number of time steps at which $N_{ev-home}$ equals N_{ev}

With all the elements defined, the total home-charging power consumption in each time step can be found by taking the average home-charging power $P_{avg-agg}$ multiplies the number of the EVs which present at home $N_{ev-home}$ of each time step:

$$P_{ev-agg} = P_{avg-agg} . N_{ev-home}$$

3.7.2. The aggregated model with control signals applied

With control signals, in other words, means that users' decisions in charging the electric vehicles are affected by external demands, for example, the peak and off-peak hours during the day or the price signal. This concept, known as load shifting, implies that during periods when control signals are applied, EVs that are at home and currently charging will pause their charging process, resuming only when the signals are no longer in effect.

The objective of the aggregated model with control signals remains the same as the model without control signals, which is to estimate the home-charging power consumption of EVs that are present at home. However, in this case, the model considers the average charging power consumption of all EVs at home instead of the total charging power consumption. This average charging power consumption is referred to as $P_{avg-agg-2}$.

In this study, the control signal period is defined by two time points, T1 (in minutes) and T2 (in minutes), where T2 is greater than T1. The total number of time steps in a day, denoted as T_{end}, is calculated based on the chosen time interval of 1 minute, resulting in T_{end} = 1440. The difference between T2 and T1 represents the duration during which users do not charge their vehicles, leading to an average home-charging power consumption $P_{avg-agg-2}$ of zero during this period.

In the process of find the idea for the aggregated model with control signals, we make a comparison between average home-charging power consumption of the unit model without and with control signals, as shown in the Figure 31. We simulate the unit model without and with control signals in 2 days for 5,000 EVs. The control signal is limited by T1 = 18h and T2 = 20h.

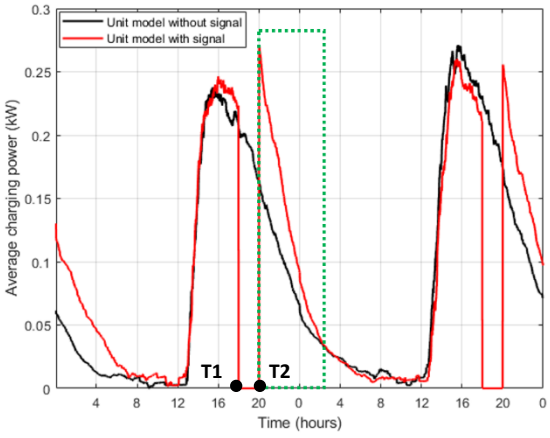

Figure 31: The average home-charging power consumption of the unit model without and with control signals from 18 h to 20 h for 2 days

Looking at Figure 31, we realize that we could rely on the power difference between these two models to develop the aggregated model. As after the cutting-power period from 18h to 20h, we can see that

there is a rebound effect of the power consumption, and it lengthens until the morning of the following day.

We then plot the power difference (the green rectangle in Figure 31) after the power-cutting period (defined by T2 = 20h) of the current day plus to a part of the following day at which the power difference equals zero as depicted in the Figure 32 and we realize that this follows a trend as a linear function.

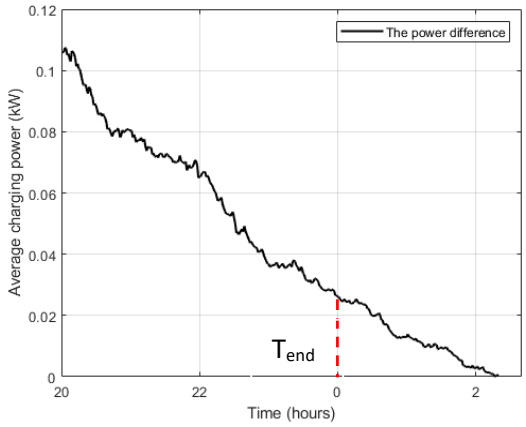

Figure 32: The power difference between average home-charging power consumption of unit model with and without the control signals (after the time T2=20h)

Hence, we come up with the idea of considering the power different between average home-charging power consumption of all EVs at home of models with and without control signals is determined **as a linear function** (Figure 33).

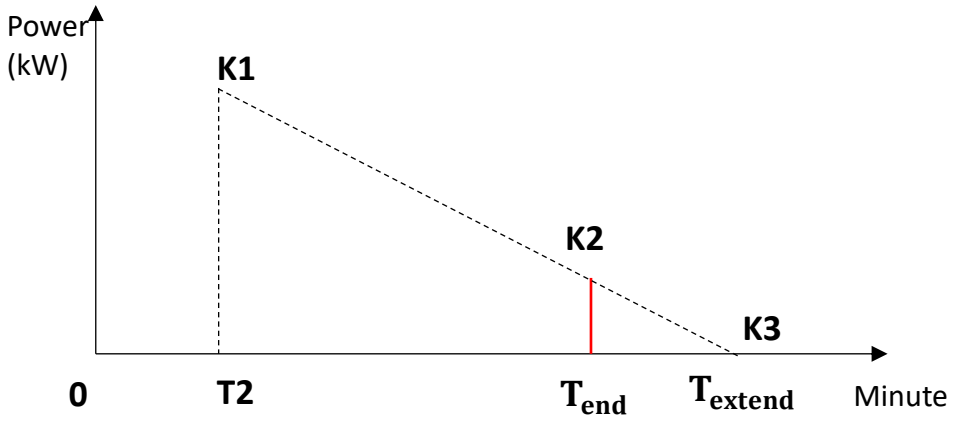

Figure 33: The linear line represents the power difference between average home-charging power of the models with and without control signals

This linear function is defined by K1 at the time T2 and K2 at the time T_{end} of the current day and it lengthens to the time T_{extend} of the following day at which power difference equals zero.

To summarize, T is the time step during the day ($0 < T <= T_{end}$), the methodology for the aggregated model with control signals is developed using the hypothesis listed below:

- Hypothesis 1: After the time T2, **the power difference** between average home-charging power consumption of all EVs at home of models with and without control signals is determined **as a linear function** shown in Figure 33.
- Hypothesis 2: The home-charging power consumption for the time before T1 is determined using Hypothesis 1 with the assumption about **the power difference** as **a linear function.** It is discussed further below.

The idea now is to determine this linear function in Figure 33, which is determined by K1 and K2. For the determination of K1 and K2, we can consider them as functions of T1 and T2. We use **Hypothesis 1** in addition to the determination of K1 and K2 to find the linear function which represents the power difference between average home-charging power consumption of all EVs at home of models with and without control signals.

First, we have, as following, the values of K1 and K2 as functions of T1 and T2

$$K1 = \text{Function}(T1, T2)$$

$$K2 = \text{Function}(T1, T2)$$

As mentioned in ANNEX H, by using multiple linear regression, the coefficients are found, and the final equations of K1 and K2 are then shown as follow:

$$K1 = 0.1072 - 0.00081\ T1 + 0.00073\ T2$$

$$K2 = 0.204 - 0.00033\ T1 + 0.00049\ T2$$

We denote D_{power} as the power consumption difference between the average home-charging power consumption of all vehicles at home in the aggregated model with and without control signals. The linear function for the power consumption difference has a formula

$$D_{power} = d_1 T + d_2$$

T: Time step ($T2 < T <= T_{end}$)

Using **Hypothesis 1**, the coefficients d_1, d_2 are defined. ANNEX H2 presents the method to find these coefficients.

$$d_1 = \frac{K2 - K1}{T_{end} - T2}$$

$$d_2 = K1 - T2 d_1$$

With d_1, d_2 defined, the linear function representing the power consumption difference between the average home-charging power consumption of all vehicles at home in the aggregated model with and without control signals is completed. We now can define the value T_{extend}. At the time T_{extend}, the power difference equals 0, hence:

$$T_{extend} = -\frac{d_2}{d_1}$$

Using the defined linear function for the power difference, the calculated power difference from the time T_{end} to the time T_{extend} will be added to the power consumption at the beginning of the following day. In another words, which means that the power consumption at the beginning of the current day is defined using the power difference of the previous day. Let's say the power difference of the previous day denotes as $D_{power-previous}$. Hence, $D_{power-previous}$ is determined as:

$$D_{power-previous} = d_{1-previous} T + d_{2-previous}$$

With $d_{1-previous}$ and $d_{2-previous}$ are the coefficient of the linear K1K3 of the previous day. $T_{extend-previous}$ is the time that $D_{power-previous}$ equals zero. Hence,

$$T_{extend-previous} = -\frac{d_{2-previous}}{d_{1-previous}}$$

Hence, the power difference of the previous day, which is added to the power consumption of the current day, is defined as:

$$D_{power-previous} = d_{1-previous}T + d_{2-previous}$$

With T: Time step ($T_{end-previous} < T <= T_{extend-previous}$)

$T_{end-previous}$ presents the end of the previous day.

In the case $(T_{extend-previous} - T_{end-previous}) < T1$, then the power consumption from $(T_{extend-previous} - T_{end} + 1)$ to T1 will equal to power consumption of the aggregated model without control signals.

With all elements defined, the average home-charging power consumption is determined as follows:

If $T <= T_{extend-previous} - T_{end-previous}$ $P_{avg-agg-2} = P_{avg-agg} + d_{1-previous}T + d_{2-previous}$

If $T_{extend-previous} - T_{end} < T < T1$ $P_{avg-agg-2} = P_{avg-agg}$

If $T1 <= T <= T2$ $P_{avg-agg-2} = 0$

If $T > T2$ $P_{avg-agg-2} = P_{avg-agg} + d_1T + d_2$

If T2 < the time where there are minimum vehicles at home, then:

$$P_{avg-agg-2} = P_{avg-agg}$$

In the case of having two control signal periods from T1 to T2 and from T3 to T4, the same approach used for the first period (from T1 to T2) is applied.

4. Simulation settings

We present here the inputs that are needed of our aggregated models to produce the desired output (the time series of the home charging power) for the two cases chosen (with and without tariff signal considered).

4.1. Simulation settings of the aggregated model without signal

The simulation of the aggregated model without control signals is built in MATLAB and has a one-minute sampling time. The time series of tracking location used for the aggregated model is generated

for 5000 households. This data represents the movement and location profiles of the electric vehicles throughout the day. Once the tracking location data is available, the simulation proceeds by calculating the number of EVs at home for each time step, which is a key input of the aggregated model.

The inputs of the model are shown as follow:

- The number of electric vehicles (N_{ev}) chosen for simulation
- The number of EVs present at home in time series N_{ev-agg} (inferred from EV charging profile model)
- The average battery capacity B_{avg} of all electric vehicles of all households (kWh)
- The average driving energy consumption per kilometer D_{avg} of all EVs of all households (kWh/km)
- The average behavior coefficient U_{avg} of all households
- The average range anxiety factor R_{avg} of all households
- Average distance travelled per day K_{avg} (km).

The output is the average power consumption of all EVs in time series

4.2. Simulation settings of the aggregated model with signal

The inputs of the model are shown as follow:

- Inputs from the model without control signals
- $P_{avg-agg}$ Average home-power consumption obtain from the aggregated model without control signals
- N_{ev-agg} Number of electric vehicles, which are present at home in time series
- The starting time of control signals T1 (Minute)
- The ending time of control signals T2 (Minute)

The output is the average power consumption of all EVs in time series

5. Simulation results

5.1. The simulation of the aggregated model without control signal

The simulation of the aggregated model is conducted for a duration of one day, equivalent to 1440 minutes, with the time step of one minute. The simulation is performed involving 5,000 EVs.
The parameters of the aggregated mode without control signals are determined, including average battery capacity B_{avg} (kWh), average range anxiety factor R_{avg}, average driving energy consumption per kilometer D_{avg} (kWh/km), average behavior coefficient U_{avg} and average distance travelled per day K_{avg} (km). See Table 18 for the scenario of 5000 EVs.

Number of EVs	5000
B_{avg} (kWh)	45
D_{avg} (kWh/km)	0.15
R_{avg}	1.5
U_{avg}	1.25
K_{avg} (km)	15

Table 18: Values of average battery capacity B_{avg} (kWh), average range anxiety factor R_{avg}, average driving energy consumption per kilometer D_{avg} (kWh/km), average behavior coefficient U_{avg} and average distance travelled per day K_{avg} (km) for 5,000 EVs.

The aggregated model without control signal for EV charging is then built and the simulation result is presented at the Figure 34

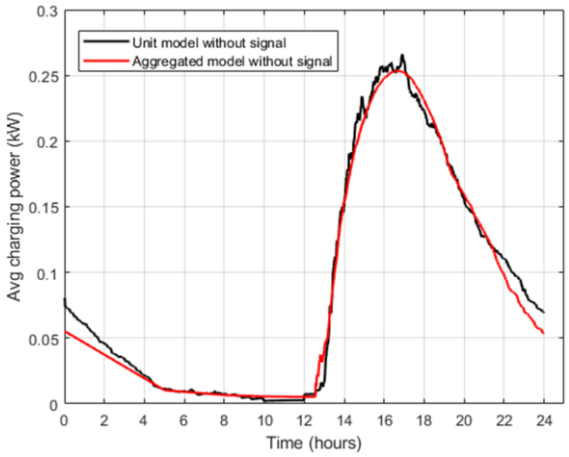

Figure 34: The average home-charging power consumption of EVs at home (without signals applied)

Figure 34 provides an illustration of the average home-charging power consumption of EVs at home over a period of 1 day, with a time interval of 1 minute. The power consumption generated by both the unit model and the aggregated model is depicted by the black and red curves, respectively. This figure demonstrates that the aggregated model without control signals can effectively describe the behavior of average home-charging power consumption observed in the unit model. At the beginning of the day, there is a power consumption gap observed between the unit model and the aggregated model. This discrepancy arises due to the assumptions made in the generation of the aggregated model. In Figure 30, the point L1 represents the time at the beginning of the day, and its determination is based on the value of F3. F3 is calculated using the ellipse curve described in section 3.8.1. This difference in power consumption at the start of the day is expected, as the unit model considers the usage of EVs on the previous day, while the aggregated model relies on the assumptions and simplifications made in its construction. Consequently, the average power consumption from the unit model may be either higher or lower than the average power consumption from the aggregated model during this initial period. The simulation time for this aggregated model is only 0.21 seconds, 11,680 times faster compared to the unit model's simulation time of 2453 seconds (about 41 minutes) for

Number of EVs	**5,000 EVs (%)**
NMAE	6.66

Table 19: NMAE between the aggregated and unit model without control signals for 5,000 households

5,000 houses. These computation times were recorded using MATLAB R2019b on a Dell PC with an Intel(R) Core(TM) i5-8265U CPU running at 1.60GHz.

Table 19 shows Normalized Mean Absolute Error (NMAE) of the aggregated model without signal applied compared to the unit model of 5,000 houses. The absolute mean error is normalized over the average power consumption of the unit model.

As mentioned, the relation curve between average charging power consumption and the number of EVs at home depends on the parameters including B_{avg} (kWh), R_{avg}, D_{avg} (kWh/km), U_{avg} and K_{avg} (km).

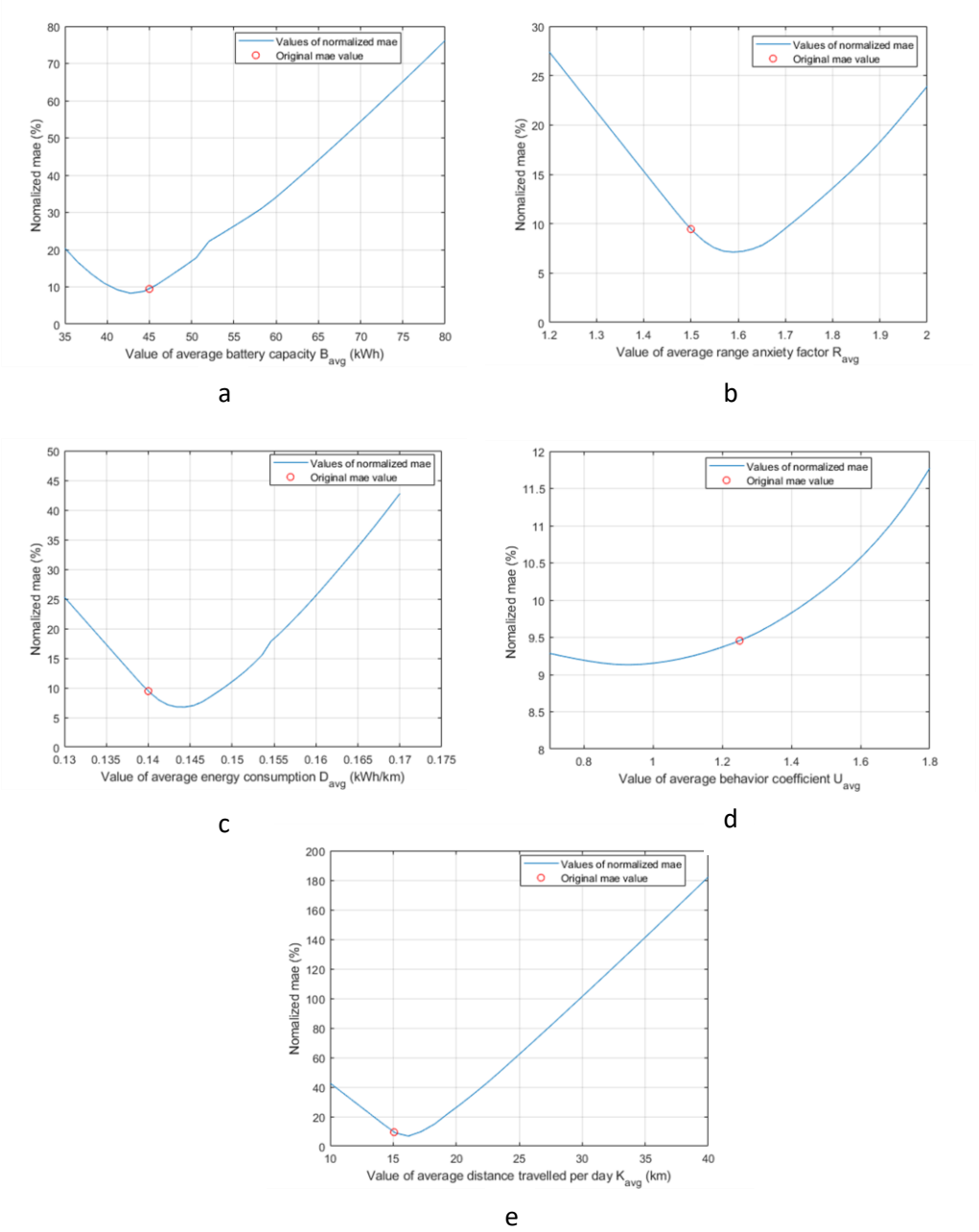

Figure 35: The sensibility of NMAE when we vary the value of 1 value in B_{avg}, R_{avg}, D_{avg} , U_{avg} and K_{avg} and keep the values of the other four for 5,000 EVs.

The next figures (Figure 35 a, b, c, d, e) show the sensitivity analysis of NMAE concerning the aggregated power consumption, achieved by altering the value of a singular parameter in B_{avg} (kWh), R_{avg}, D_{avg} (kWh/km), U_{avg} and K_{avg} while maintaining the values of the remaining four parameters constant.

The sensitivity analysis conducted aims to assess the impact of imprecise knowledge regarding the average parameters: B_{avg} (kWh), R_{avg}, D_{avg} (kWh/km), U_{avg} and K_{avg} on the output of the aggregated model. It provides the insights into the impact of variations in parameter values on the accuracy of the aggregated model's predictions for power consumption estimation. The normalized mae is used as a metric to quantify the accuracy of the aggregated model, with the blue line representing the NMAE values and the red dot indicating the original value of the parameter being varied.

Analyzing Figure 35 a, which focuses on the sensitivity of the aggregated model to the B_{avg} parameter (representing the average battery capacity), it is observed that the NMAE values form a curve with the minimum NMAE of 8.3% are achieved at approximately 43 kWh for 5,000 EVs. Deviations from this optimal value result in increasing NMAE values, reaching maximum NMAE of 75 % at 80 kWh. These findings shows the sensitivity of the aggregated model to the B_{avg} parameter. This also emphasize the importance of selecting the appropriate value of B_{avg} to ensure optimal performance in power consumption estimation.

Similarly, when analyzing the sensitivity of the aggregated model for EVC to the R_{avg} parameter (representing range anxiety factor), it can be seen that variations in R_{avg} results in changes in NMAE (Figure 35 b). The NMAE values form a curve, with the minimum NMAE occurring at a R_{avg} value of approximately 1.58. This optimal value signifies the point at which the aggregated model achieves the highest accuracy in power consumption estimation. The results indicate the sensitivity of the aggregated model to changes in the R_{avg} parameter, highlighting the need to select the appropriate value for accurate estimation of power consumption. The same trend is also observed in the NMAE results for D_{avg} and K_{avg} (Figure 35 c, e), indicating that the aggregated model is sensitive to the chosen values for D_{avg} and K_{avg}..

Nevertheless, the sensitivity analysis of the U_{avg} parameter (representing average behavior coefficient) reveals a slightly different trend (Figure 35 d). The NMAE values show a marginal increase as U_{avg} deviates from the optimal point, which is observed at U_{avg} equals 0.92. This suggests that the aggregated model for EVC is less sensitive to variations in the U_{avg} parameter compared to B_{avg} , R_{avg}, D_{avg} and K_{avg}.

Overall, the sensitivity analysis provides insights into the critical parameters affecting the accuracy of the aggregated model's power consumption estimation. It underscores the importance of selecting

appropriate values for B_{avg} , R_{avg}, D_{avg} and K_{avg}, while also highlighting the robustness of the aggregated model to variations in U_{avg}.

5.2. The simulation of the aggregated model with control signal applied

The simulation of the aggregated model is done for 1 day (1440 minutes) with the time step of 1 minute for different numbers of households (5,000 and 10,000 houses). The control signals are defined by T1 and T2. The value of T1, T2 is shown below:

T1 (minute)	**T2 (minute)**
1080 (18 o'clock)	1200 (20 o'clock)

Table 20 : The values of T1 and T2

The aggregated model with control signals for EV charging is then built and the simulation result is presented at the Figure 36

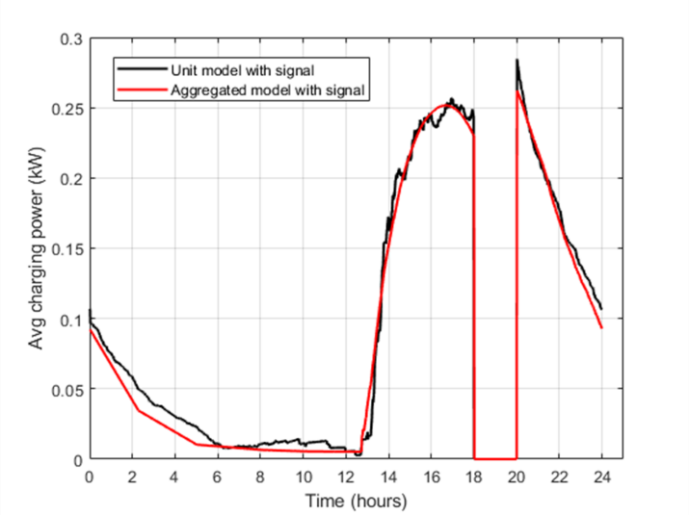

Figure 36: The average home-charging power consumption of vehicles at home for 5,000 EVs

In Figure 36, the black curve represents the average home-charging power consumption generated by the unit model, while the red curve represents the average power consumption of the aggregated model with control signals. It can be observed that the aggregated model is able to capture the general behavior of the average power consumption observed in the unit model. However, there is a mismatch between the two models at the beginning of the day. This discrepancy arises due to the hypothesis

made before the control signals start. As we simulate the aggregated model with control signals for several days and show the results of 1 day, hence, by the end of the previous day, due to the power cut during the control signal period, the power consumption in the unit model is already higher compared to that of the aggregated model without control signals at the same time. As a result, when transitioning to the following day, the unit model starts with a higher power consumption due to the carry-over effect from the previous day's power cut. Besides, the hypothesis for defining the power consumption before the time T1 for current day is defined by taking the sum of the power difference from the previous day and the power consumption before T1 of the model without signal. This allows the aggregated model to represent the power consumption before the time T1 as close as possible but is not be able to demonstrate precisely. This leads to the observed mismatch between the aggregated model and the unit model at the beginning of the day.

Number of EVs	**5,000 EVs**
Normalized mae **(%)**	7.99

Table 21 : NMAE between the aggregated model and unit model of 5,000 households with control signal

6. Conclusion

The aggregated models, representing multiple EVs, proves to be an effective tool for characterizing power consumption in the realm of home-charging EVs without and with control signals. Its adaptability offers a multitude of applications and advantages across diverse contexts. An usage of these aggregated models are their capability to quantify flexibility harnessed through the aggregation of numerous EVs by subjecting the model to various control strategies. This provides understanding the effectiveness and efficiency of different control strategies at different spatial scales, spanning from local districts to expansive regions. The aggregated model's efficiency is a standout feature, enabling rapid and streamlined computations that facilitate scalable EVC analyses. The simulation time for this aggregated model is 11,680 times faster than the unit model's simulation for 5,000 houses. These computation times were recorded using MATLAB R2019b on a Dell PC with an Intel(R) Core(TM) i5-8265U CPU running at 1.60GHz. Moreover, the aggregated model's potential extends to the advancement of smart buildings and smart cities. As demand-side flexibility assumes a role in optimizing energy management, the aggregated model can serve as a bridge in the integration of diverse energy sources within a smart grid framework. By embracing the collective behavior of EVs, the model enables a comprehensive evaluation of demand-side flexibility’s impact. This, in turn,

fosters energy utilization optimization and bolsters the evolution of intelligent and sustainable urban landscapes.

7. The methodology still has a few limitations:

The development of an aggregated model for home-charging power consumption using electric vehicles has its own limitations and considerations:

1. The aggregated model requires the generation of the number of electric vehicles (EVs) at home in time series. This information can be obtained through statistical models or by having access to statistical data on the average departure and arrival times of EVs. Having accurate data on the number of EVs at home is crucial for estimating the power consumption accurately.

2. Despite efforts to construct an aggregated model, errors are inevitable when estimating home-charging power consumption. This is primarily due to the assumption made regarding the relationship between average charging power consumption and the number of vehicles at home. The model assumes a certain correlation between these variables, but individual variations and specific charging patterns may lead to discrepancies between the aggregated model and the actual power consumption.

3. The aggregated model for EVC does not require detailed information about each household or individual electric vehicle. While this simplifies the modeling process, it also means that the aggregated model does not account for the specific preferences of individual users. The aggregated model takes an aggregated view, potentially overlooking variations in EV charging behavior and potential impacts on user habits.

8. Proposed future improvements

For the future research, minimizing the errors associated with aggregated models for home-charging power consumption would be a valuable direction. By refining and enhancing the model, researchers can work towards reducing the discrepancies between the aggregated model and the actual power consumption of individual households.

ANNEX E: Data for the EV charging profile model taken from [59]

ANNEX E1: Data for the EV charging profile

As mentioned above, there are several factors that affect the EV charging profile (Table 17).

- Type of driver

In this research, we target commuters who have a job, and always go to work on normal days. For this type of commuter, they will have the possibility to charge at the workplace.

- Number of trips per day

The number of trips per day is generated using the data from the table below:

Number of trips	Normal days	Weekend
0	35.4	50.7
1	0	0
2	29.9	27.5
3	8.3	4.4
4	12.5	10.2
5	13.9	7.2

Table 22: Probability distribution (%) for the number of trips per day.

This table represents the probability distributions for the number of trips for working days and weekend days. The Monte Carlo method is used to generate the number of trips per day for each household. Data is obtained from [59].

- Distance and duration of each trip

Distance (km)	Duration of a trip (minute)						
	10	10-15	15-20	20-30	30-45	45-60	60-185
1	2.9	0.3	0	0	0	0	0
1-2	3.5	4.8	0.8	0	0	0	0
2-5	8.4	10.2	5.7	0	1.2	0.4	0
5-10	1.3	12.2	14.4	0	2.4	0.6	0.7
10-20	0	0.9	6.3	0	4.7	1.3	0.5
20-50	0	0	0	0	8.6	2.1	1.6
50-100	0	0	0	0	0	0.6	2.1
100-400	0	0	0	0	0	0	1.5

Table 23 : Joint probability distribution (%) for the duration of a trip and distance travelled of that trip.

The distance and duration of each trip is defined using the data in the table. This table demonstrates the joint probability distribution for the distance traveled and the duration. The distance traveled refers to the distance of driving from this destination to the next destination and the duration of the trip refers to the time needed to drive between 2 destinations. Data is obtained from [59].

- Time departure and destination of the trip

Normal day	Work place	Shopping	Errands	Escort	Leisure	Home
05:00–07:00	11.1	0.5	0.5	1.1	0.5	0.8
07:00–10:00	3.1	1.8	1.4	0.8	1.4	1.8
10:00–13:00	1.3	2.5	2.3	0.7	3.2	5.5
13:00–16:00	1.1	2.3	2.2	1.8	3.8	8.9
16:00–19:00	0.3	3	2.2	1.4	4.9	14
19:00–22:00	0.3	0.4	0.6	0.4	2.4	6.1
22:00–05:00	0.6	0	0.1	0.1	0.4	2.4
Saturday						
05:00–07:00	0.7	1.2	0.3	0.2	0.8	0.8
08:00–10:00	0.5	4.8	1.9	0.7	2.7	3
10:00–13:00	0.4	7.1	3.5	1.4	5.2	9.1
13:00–16:00	0.2	3.4	2.5	1.2	7	7.6
16:00–19:00	0.1	2.3	1.7	1.1	6	9.5
19:00–22:00	0.1	0.4	0.5	0.4	2.5	4.9
22:00–05:00	0.2	0	0.1	0.2	0.8	3
Sunday						
05:00–07:00	0.6	0.3	0.2	0.1	0.8	0.4
08:00–10:00	0.4	1.5	1.4	0.6	4.8	2
10:00–13:00	0.3	0.7	2.8	1.3	11.7	7.2
13:00–16:00	0.3	0.5	2.6	1.4	13.7	8.8
16:00–19:00	0.2	0.2	1.8	1	6.8	13.3
19:00–22:00	0.2	0.1	0.5	0.4	2	6.4
22:00–05:00	0.1	0	0.1	0.1	0.4	2

Table 24 : Joint probability distribution (%) for the destination of each trip and the departure time of each trip.

There are six destinations which are mentioned in this study, including workplace, home, shopping, errands, escort and leisure. The departure time and the destination of the trip are determined using the data on the table. Table shows the joint probability distribution for the trip destinations and departure time. Data is obtained from [59].

- Time limitation of one trip regarding the location

Time limitation of one trip regarding the location describes the minimum and maximum time when vehicle reaches one destination. This definition is used as a rule to apply to the generation of the tracking EV profile, to make the profile as close as possible to reality. For example, for each trip, the minimum time at the workplace is 3.5 hours and 3 hours for normal days and weekend days, respectively. Besides, for other locations, the minimum time is 0.5 hour.

- Total time limitation of one location for one day

Total time limitation of one location for one day refers to the minimum and the maximum total time the vehicle spends at one location. For example, user can go to work multiple times per day, but the total time at work needs to be at least 7 hours and cannot exceed 8 hours per day. Except on the weekend days, the maximum time at work is 4 hours and minimum time is 3 hours. At home, the minimum time is 9 hours and there is no maximum time to stay at home.

Rule		Normal day	Weekend
Minimum time at (hours)	Workplace	3.5	3
	Home	0.5	0.5
	Others	0.5	0.5
Minimum time per day at (hours)	Workplace	7	3
	Home	9	6
	Others	_	_
Maximum time per day at (hours)	Workplace	8	4
	Home	_	_
	Others	_	_
At least one trip to	Workplace	Yes	No
	Home	yes	yes

Table 25 : Rules used to generate an EV profile for one day.

Besides, at least 1 trip to the workplace and the final destination is always at home. As mentioned before, in order to generate EV tracking profile, the approach in reference [59] is used. The output of the tracking location model for each vehicle is a time series of the location of the electric car during

the day, which means that the location of the electric car at each time step is defined. Data is obtained from [59].

ANNEX E2: Tracking EV location model

The tracking EV location model provides the information regarding the location of the EV. We have simulated the location profile for each vehicles. In this research, we target commuter who have an occupation. The first and final destination are assumed to always be home. Hence, each user either does not go anywhere or execute at least two travels a day. Using the probability distribution for number of trips per day in Table 22, we can decide how many travels that the user makes during the day. Next, the distance and the duration of the trip is defined using the statistical data in Table 23. And using the data in Table 24 to generate the departure time of for each destination.

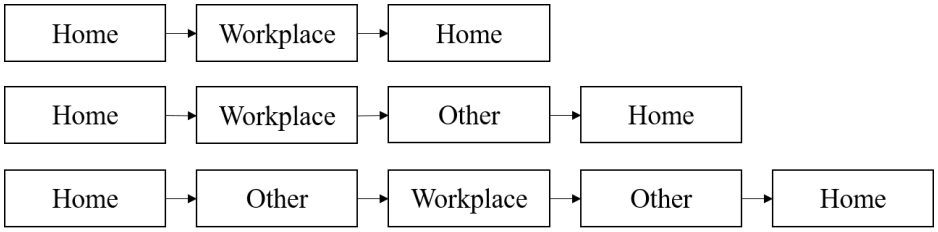

Figure 37: Trip schedule possibilities during a normal day

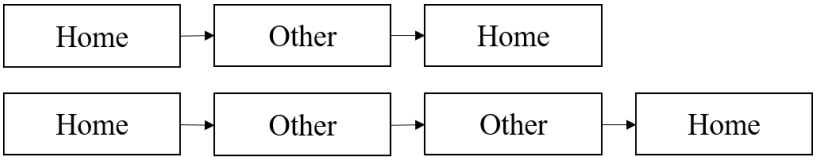

Figure 38: Trip schedule possibilities during a weekend day

Figure 37 and Figure 38 show the possible sequences of different trips during the day at normal day and at the weekend. "Other" represents for different destination from "home" and "workplace", for example "shopping", "Errands", "Escort" and "Leisure". In general, different users have different trip schedules for normal day and weekend day. Table 25 refers to minimum and maximum total time the vehicle spends at one location. For example, user can go to work multiple times per day, but the total time at work needs to be at least 7 hours and cannot exceed 8 hours per day. Except on the weekend days, there is still a possibility that the user goes to work but the working time will be limited. The maximum time at work in weekend is 4 hours and minimum time is 3 hours. At home, the minimum

time is 9 hours and there is no maximum time to stay at home. And for other location the minimum time duration is half of an hour.

Indeed, to build an EV location profile, the related characteristics are defined randomly according to the predetermined probability distribution, which is accessible on sociological data. These characteristics includes:

- Total number of trips per day
- Type of day (normal day or weekend day)
- Distance for each trip
- Time departure for each trip
- Time duration spent at a location

We run the simulation defines the location of each EV at each time step. From this tracking EV location model, for each time step, we deduce the number of EVs present at home (whose location is equal to the "home" value).

ANNEX F: Finding relation between average home-charging power and number of EVs at home

As mentioned earlier, the unit model for electric vehicle charging is obtained by repeating the simulation for the physical model of each electric vehicle. The simulation for 3 days (4320 minutes) with the time step of 1 minute is done for 5000 EVs. The battery capacity, the driving energy consumption per kilometer, range anxiety factor and behavior coefficient are chosen for each household using the Monte Carlo approach. By using the EV tracking profile model, the location of the vehicle is defined for each time step.

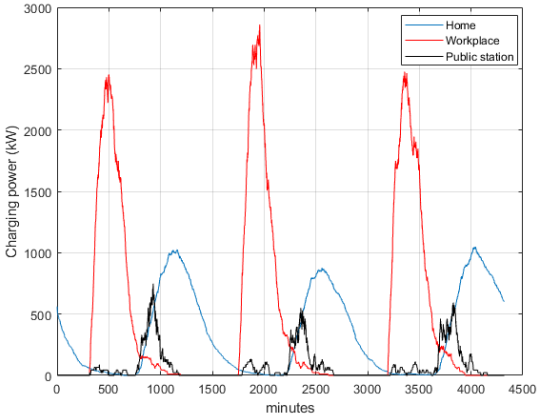

Figure 39: The charging power consumption (kW) for 5000 households at 3 locations: home, workplace and public station

In this study, only home-charging power consumption is taken into account. For each day (1440 time steps), we calculate the average home-charging power consumption of all vehicles, which are present at home

Figure 40 illustrates the relation between average home-charging power consumption and the number of vehicles at home for 5,000 EVs over the period of 3-day simulation. The figure shows that the average home-charging power consumption of EVs, which are present at home and the number of EVs at home has a relation that follows a form of half of an ellipse. Based on this curve from the figure, the maximum number of vehicles, of course, never exceeds the total number of vehicles considered. This discovery is a premise for the methodology for generating the aggregated model for home-charging power consumption for electric vehicles.

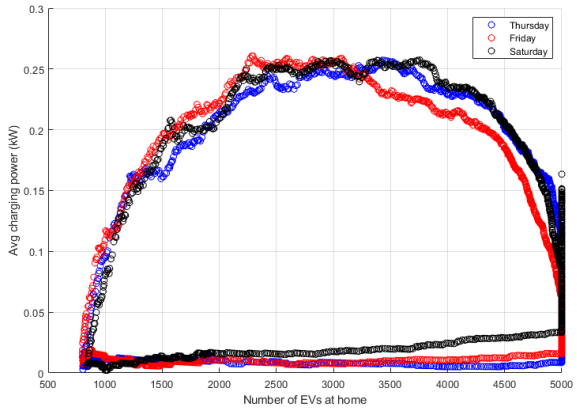

Figure 40: The average home-charging power consumption of EVs at home and the number of EVs at home for 5000 households

Besides, to support the discovery about this relationship, we did other simulations of the unit model by changing value of the average battery capacity. The range chosen is in the set 45kWh, 60kWh and 85kWh.

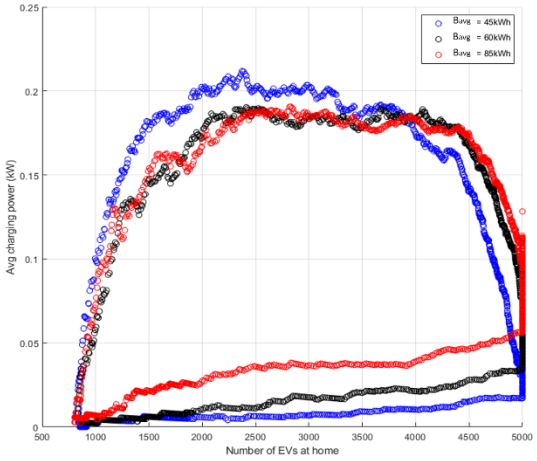

Figure 41: The average home-charging power consumption of EVs at home and the number of EVs at home for 5000 households with different values of average battery capacity

Look at the figure, the relationship between average home-charging power and the number of EVs at home still form a half of ellipse, but there appears a diagonal line which affect the form of the ellipse. For this reason, we come up with the idea for the aggregated model for home-charging, as shown in Figure 42

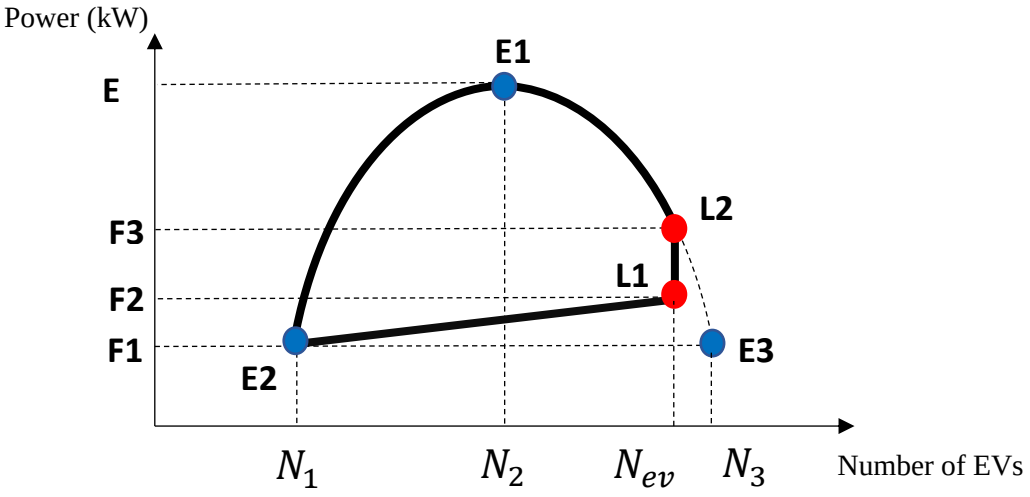

Figure 42: The relation curve between the average home-charging power and the number of the EVs, which present at home for the aggregated model without control signals applied

ANNEX G: Define the power relation curve using B_{avg}, D_{avg}, U_{avg}, R_{avg}, K_{avg}

ANNEX G1

From the unit model simulation, before the time T_{min-ev}, the average home-charging power consumption of EVs at home and the number of EVs at home follows linear functions while after the time T_{min-ev}, their relation follows a form of half of an ellipse. Hence, the idea for the aggregated model without control signals is to define these relationships between the average home-charging power consumption of vehicles at home and the number of vehicles at home as linear functions and an ellipse function with some constraints accompanied.

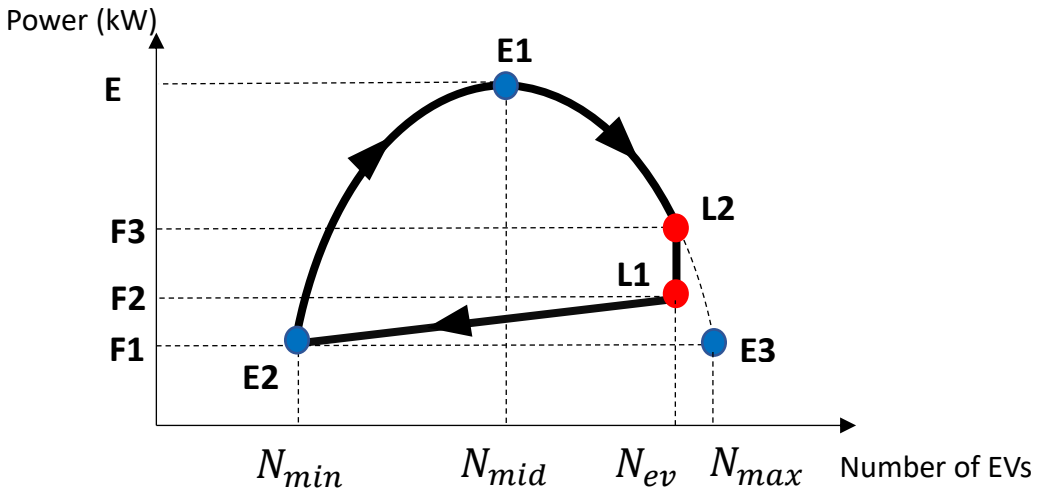

Figure 43: The relation curve between the average home-charging power and the number of the EVs at home of the aggregated model without control signals applied

The idea now is to define E, F1, F2, F3, N_{min} , N_{max}

From the simulation result of the unit model, we can always get a set of values for E, F1, F2, N_{min} and N_{max} and now the question is how to calculate them. We apply the same approach that we did for the domestic hot water part. We calculate them from some parameters regarding the electric vehicle characteristics and the behavior of users in the region considered, including: average battery capacity B_{avg} (kWh), average range anxiety factor R_{avg}, average driving energy consumption per kilometer D_{avg} (kWh/km), average behavior coefficient U_{avg} and average distance travelled per day K_{avg} (km) of all households in that region and the number of electric vehicles considered.

ANNEX G2

Part 1: After the time T_{min-ev} (Finding E, N_{min}, N_{max})

- E is given by the linear function of B_{avg}, R_{avg} , D_{avg} ,U_{avg} and K_{avg}

$$E = \text{function } (B_{avg}, R_{avg} , D_{avg} ,U_{avg}, K_{avg})$$

In order to find E, we consider E as described as a function of average battery capacity B_{avg} (kWh), average range anxiety factor R_{avg}, average driving energy consumption per kilometer D_{avg} (kWh/km), average behavior coefficient U_{avg} and average distance travelled per day K_{avg} (km). The variation of the parameters is describe in Table 26.

Number of households	B_{avg}(kWh)	D_{avg}(kWh/km)	R_{avg}	U_{avg}	K_{avg}
3000	[40,50,60]	[0.14,0.15,0.16]	[1.4,1.5,1.6]	[1.1,1.2,1.3]	[15, 40, 60]
5000	[40,50,60]	[0.14,0.15,0.16]	[1.4,1.5,1.6]	[1.1,1.2,1.3]	[15, 40, 60]
7000	[40,50,60]	[0.14,0.15,0.16]	[1.4,1.5,1.6]	[1.1,1.2,1.3]	[15, 40, 60]
10000	[40,50,60]	[0.14,0.15,0.16]	[1.4,1.5,1.6]	[1.1,1.2,1.3]	[15, 40, 60]

Table 26: Different values of B_{avg}, R_{avg} , D_{avg} , U_{avg} and K_{avg}

In order to find the coefficients for the function of E, the simulations of the unit model for different numbers of households, different values of B_{avg}, R_{avg} , D_{avg} and U_{avg} are done so as to get the different values of E. There are 4 cases corresponding to 3000, 5000, 7000 and 10000 households. Values for B_{avg} vary from 40 to 60 kWh. Values for R_{avg} vary from 1.4 to 1.6. Values for D_{avg} vary from 0.14 to 0.16 kWh/km. Values for U_{avg} vary from 1.1 to 1.3. Values for K_{avg} vary from 15 to 60 km (Table 26).

For each unit simulation, we decide the value of E as the maximum average power consumption. Hence, with the variation of the parameters, 972 values of E are obtained. A fitted linear regression model is used to identify the coefficients for the relationship between B_{avg}, R_{avg} , D_{avg} ,U_{avg} and

K_{avg} . Figure 44 demonstrates 972 values of E. The black line shows 972 values of E obtained from simulations of the unit model while the red line represents the results obtained from a fitted linear regression model.

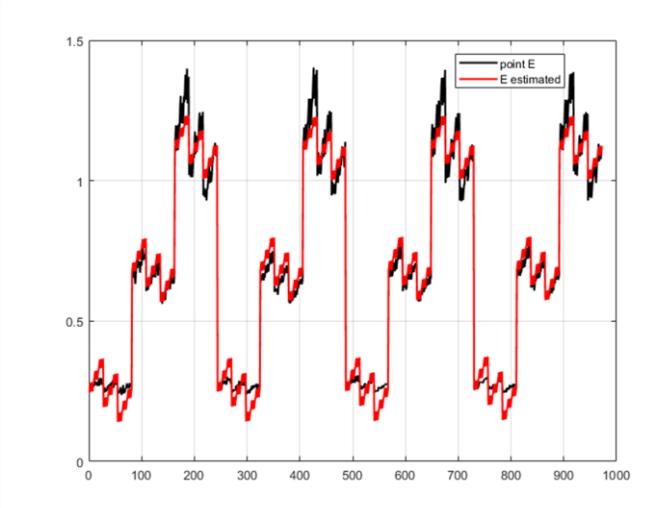

Figure 44: The values of E when changing the value of between B_{avg}, R_{avg} , D_{avg} ,U_{avg} and K_{avg}

Hence, the coefficients for B_{avg}, R_{avg} , D_{avg} ,U_{avg} and K_{avg} are found and the final equation of is then shown as follow:

$$E = -0.6375 - 0.0053\, B_{avg} + 4.1829\, D_{avg} + 0.0132\, U_{avg} + 0.1685\, R_{avg} + 0.0172\, K_{avg}$$

- N_{min}: The minimum number of EVs at home.

  One thing need to be mentioned here is that N_{min} is the minimum number of EVs at home, which can be obtained from the EV profile model. Because the input for the aggregated model is the time series of number of EVs at home. Hence, N_{min} is chosen by using the input of the aggregated model

- N_{max} is defined as follow:

$$N_{max} = \gamma N_{ev}$$

γ is also described as a function of average battery capacity B_{avg} (kWh), average range anxiety factor R_{avg}, average driving energy consumption per kilometer D_{avg} (kWh/km), average behavior coefficient U_{avg} and average distance travelled per day K_{avg} (km).

We do the same approach to find γ as finding for E. We also use Table 26 as the range for each average parameter. However, for each unit simulation, in order to find γ, we need to decide value of N_{max}. Each value of N_{max} from each unit simulation is determined by N_{min} and N_{mid}. Using the value of N_{min} as the minimum number of EVs at home and N_{mid} is corresponded to the position of E (the maximum average power consumption). The value of N_{max} is defined as: $N_{max} = N_{min} + (N_{mid} - N_{min}) * 2$

As a result, for each unit simulation, we obtain one the value N_{max}, from that value of $\gamma = N_{max} / N_{ev}$. Hence, 972 values of γ are obtained by varying the average parameters. A fitted linear regression model is used to identify the coefficients for the relationship between B_{avg}, R_{avg} , D_{avg} ,U_{avg} and K_{avg} . Figure 45 demonstrates 972 values of γ. The black line shows 972 values of γ obtained from simulations of the unit model while the red line represents the results obtained from a fitted linear regression model.

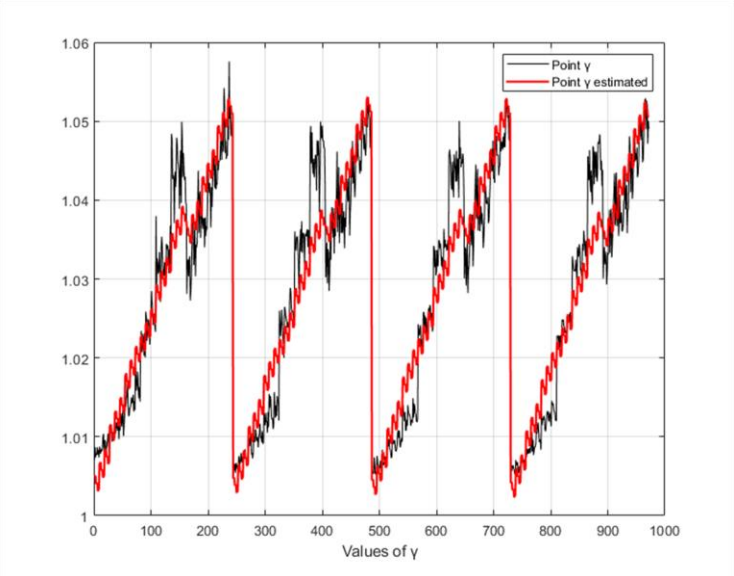

Figure 45: Different values of γ

Hence, the coefficients forB_{avg}, R_{avg} , D_{avg} ,U_{avg} and K_{avg} are found and the final equation of γ is then shown as follow:

$$\gamma = 0.9533 + 0.00065\, B_{avg} + 0.1714\, D_{avg} - 0.009\, U_{avg} + 0.0009\, R_{avg} + 0.0007\, K_{avg}$$

Part 2: Before the time T_{min-ev}

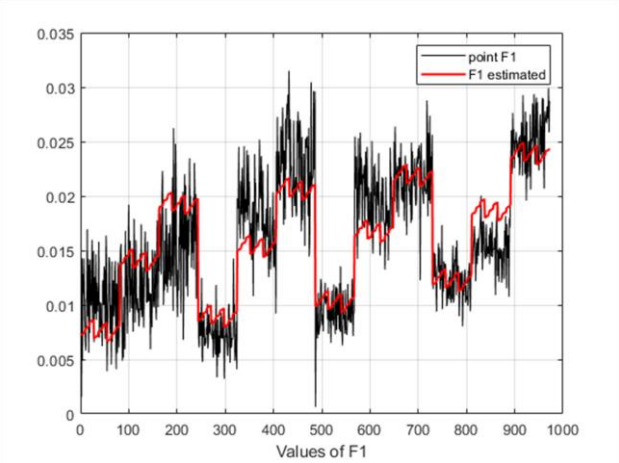

Figure 46 : The values of F1 when changing the value of between B_{avg}, R_{avg} , D_{avg} ,U_{avg} and K_{avg}

F1 and F2 are defined using the same method for E and γ

The chosen value of F1 in the unit simulation is taking the value of minimum average power consumption. F1 is given by the linear function of B_{avg}, R_{avg} , D_{avg} ,U_{avg} and K_{avg} (Figure 46)

$$F1 = -0.0077 - 0.00003\, B_{avg} + 0.0585\, D_{avg} + 0.0008\, U_{avg} + 0.0009\, R_{avg} + 0.0006\, K_{avg}$$

From the unit model simulation, F2 is chosen by taking the minimum power consumption when all EVs are at home. Then F2 is given by the linear function of B_{avg}, R_{avg} , D_{avg} ,U_{avg} and K_{avg} (Figure 47)

$$F2 = -0.1928 + 0.0015\, B_{avg} + 0.697\, D_{avg} - 0.015\, U_{avg} + 0.0012\, R_{avg} + 0.0025\, K_{avg}$$

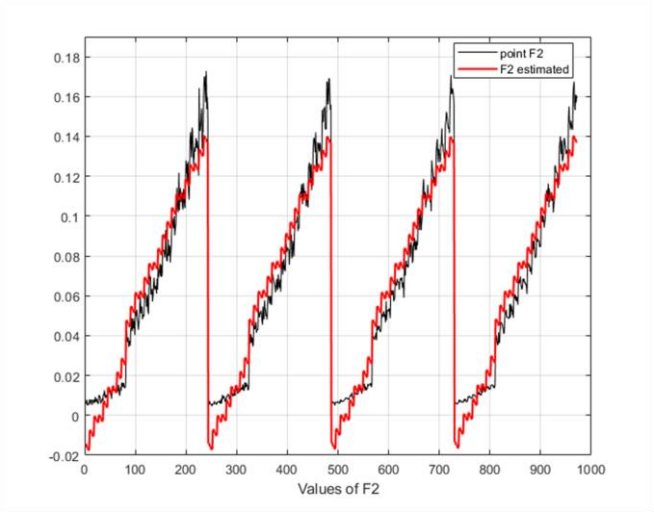

Figure 47: The values of F2 when changing the value of between B_{avg}, R_{avg} , D_{avg} ,U_{avg} and K_{avg}

With the ellipse function built, the value of F3 is also calculated by replacing number of vehicles considered N_{ev} to the function.

$$F3 = \sqrt{|E|^2 - \frac{|E|^2}{(N_{mid} - N_{min})^2} {N_{ev}}^2}$$

Before the time T_{min-ev}, the average home-charging power $P_{avg-agg}$ is defined using 2 linear functions: One is generated from E2 and L1 and the other is generated from L1 and L2 with E2(N_{min}, F1), L1(N_{ev}, F2) and L2(N_{ev}, F3). Hence, we have:

If $N_{ev-home} < N_{ev}$ then

$$P_{avg-agg} = b_1 + b_2 N_{ev-home}$$

With:

$$b_1 = F1 - \frac{(F2 - F1)N_{min}}{N_{ev} - N_{min}}$$

$$b_2 = \frac{F2 - F1}{N_{ev} - N_{min}}$$

If $N_{ev-home} = N_{ev}$ then $P_{avg-agg} = F2 + \frac{F3-F2}{\tau}$

τ is the number of time steps at which $N_{ev-home}$ equals N_{ev}

ANNEX H: Define the linear function for the power difference (The aggregated model with control signals)

ANNEX H1: Finding values for K1 and K2

We assume that the power difference between average home-charging power consumption with and without the control signals can be represented by a linear function, as shown in Figure 48

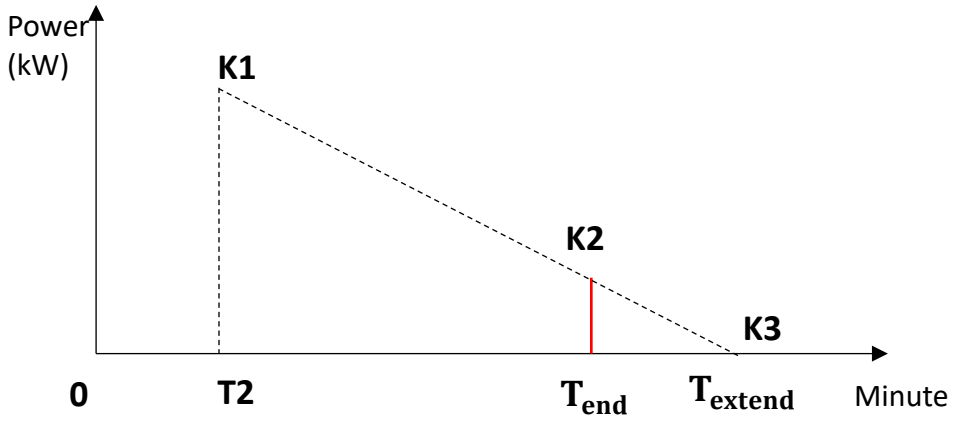

Figure 48: The linear line represents the power difference between average home-charging power of the models with and without control signals

In order to find the linear function for the difference in the average home-charging power consumption between with and without the control signals, it is necessary to find the values of the point K2

In order to find the values for the point K1 and K2, the aggregated model with signals is simulated using different control signal period of time (Table 27)

T1 (hours)	T2 (hours)
15	17
17	19
16	18
16	20
17	19
17	21
18	20
18	22
19	21
19	23
20	22

Table 27: The different values of T1 and T2

The values of K1 and K2 are defined as a linear function of T1 and T2 .

The value of K1 and K2 are presented as follow:

$$K1 = b_1 + b_2 T1 + b_3 T2$$

$$K2 = b'_1 + b'_2 T1 + b'_3 T2$$

By using regression model to find the coefficients for b1, b2 and b3, the final equation of K1 is:

$$K1 = 0.1072 - 0.00081\ T1 + 0.00073\ T2$$

Doing the same way for K2, we have:

$$K2 = 0.204 - 0.00033\ T1 + 0.00049\ T2$$

ANNEX H2: Define the linear function of the power difference.

With two values of K1 and K2 found in **ANNEX H1**, we assume the linear equation of the difference in the mean of average home-charging power consumption between with and without the control signals is:

$D_{power} = d_1 T + d_2$

T: Time step (T>=T2)

D_{power}: The difference **in the average home-charging power consumption between with and without the control signals**

Now, it is necessary to find d_1 and d_2

We have 2 equations that help to find d_1 and d_2:

1. K1 is defined (ANNEX H1) and K1 is the power difference at time step T2. Hence,

$$d_1 T2 + d_2 = K1$$

2. K2 is defined (ANNEX H1) and K2 is the power difference at time step T_{end}. Hence,

$$d_1 T_{end} + d_2 = K2$$

Solving the equations, d_1 and d_2 are found:

$$d_1 = \frac{K2 - K1}{T_{end} - T2}$$

$$d_2 = K1 - T2 d_1$$

T_{extend} is defined when $D_{power} = 0$ hence, $T_{extend} = -d_2/d_1$

IV. Chapter 3: Heating in residential

Notre contribution dans ce chapitre est de construire un modèle agrégé pour le chauffage électrique, qui permet d'accéder à la consommation d'énergie pour le chauffage des locaux de nombreux systèmes de chauffage en peu de temps, mais qui est également suffisamment précis pour fournir des informations sur la consommation d'énergie pour le chauffage dans les habitations. Ce chapitre relève le défi que nous avons proposé dans les deux chapitres précédents. La méthodologie que nous proposons, basée sur le "modèle RC" simplifié pour le comportement thermique et la simulation du modèle d'unité pour les ménages individuels, aborde les défis et les complexités liés à l'agrégation des données sur la consommation d'énergie pour le chauffage. Par conséquent, nous présentons tout d'abord le "modèle RC" simplifié pour le comportement thermique de la maison et toutes les données d'entrée nécessaires. Ensuite, nous construisons la simulation du modèle unitaire pour trouver la consommation d'énergie de chauffage pour chaque ménage. Enfin, nous proposons une méthodologie pour générer le modèle agrégé du système de chauffage dans le secteur résidentiel.

---

1. Introduction

Electric heating systems are considered as one possible promising group in providing demand side flexibility [11] . Their flexibility is proved by their ability to modify their electrical consumption pattern without affecting the final thermal energy services. In France, heating represents a significant portion of the final energy consumption in the residential sector, making it an important area to explore for flexibility options. According to Eurostat, space heating accounts for 68.7 % of the final energy consumption in residential sector in 2021 [72]. In order to exploit the potential of heating systems for flexibility, it is necessary to have an accurate thermal model.

Developing a highly accurate thermal model for a home is not an easy task. In most cases, building energy model for heating is complex and have nonlinear parameters that are strongly influenced by multiple variables such as, weather conditions, operating hours, building materials and occupant behavior [73]. This brings several challenges when finding the energy consumption for heating of a large number of heating systems. It will ask for the simulation of each electric heating system of each household. Moreover, the diversity in the characteristics of each house, including total heated area, wall material, house direction, and window area, poses additional difficulties in creating a unified model that can accurately represent all heating systems.

In residential dwellings, the occupants according to their comfort preferences typically decide the set point temperature. Heating control systems, often equipped with smart thermostats, play a crucial role in maintaining the indoor temperature close to the user-defined set point. Today, majority of the heating systems are installed with a thermostat that allow the users to program in advance and

remotely the temperature set points in the different rooms in the house, and most recent electric heating systems also include this feature. This smart thermostat control then becomes a bridge to exploit the potential flexibility, such as load shifting, load shedding, and demand response, offered by residential heating system.

Indeed, exploiting the flexibility of electric heating systems comes with its own set of challenges and complexities. When dealing with control signals like off-peak hours from the grid, the ability to anticipate and respond quickly to changes in demand becomes crucial. However, individually considering each household's heating system can be time-consuming, especially when dealing with a large number of systems, such as over 10,000 heating systems. Additionally, reducing heating-related consumption can lead to a rebound effect, where consumption increases beyond its usual values during the period following the reduction. This rebound effect needs to be carefully managed to ensure that the overall energy-saving benefits are not compromised.

In our research, we deal with electric heating systems using heat pump as a source of flexibility. Our contribution in this domain is to build an aggregated model for electric heating, which allows to access the power consumption for space heating of numerous heating systems within a short time but also accurate enough to provide the insights about heating power consumption at residential. This chapter addresses the challenge that we proposed in the two previous chapters. The methodology we propose, based on the simplified "RC model" for thermal behavior and the unit model simulation for individual households, addresses the challenges and complexities involved in aggregating heating power consumption data. Hence, firstly, we present the simplified “RC model” for the thermal behavior of the house and all the necessary inputs. Secondly, the unit model simulation to find heating power consumption for each household is constructed. Finally, the methodology for generating the aggregated model for heating system in dwellings is proposed.

2. Thermal model of a house

To access the power consumption of residential heating systems, an appropriate thermal model is essential. Two types of models can serve this purpose. The first one is the detailed physical model, which considers various thermal zones within a house and requires precise information about the house's geometry, wall materials, doors, windows, internal thermal sources (furniture, occupants), and heating systems. Additionally, meteorological conditions such as sunshine, atmospheric pressure, and external temperature also influence the model's accuracy. However, detailed physical models are complex to use in the research studies since they require many precise structural information about the house. As an alternative, a simpler model called the reduced thermal model can be employed. This model reduces the complexity to a single thermal zone and a single interface with the external environment. It employs a thermo-electrical analogy to establish connections between temperature

changes at various points and external/internal factors through a system of linear differential equations.

This thermal model should replicate the dynamics of the heat transfer within a house and ascertain its internal temperature. The reduced thermal model is explored in various studies [74]–[77]. For the purposes of this chapter, the selected model to portray building thermal behavior is the 6R2C model, as depicted in Figure 49 [7]. The work of Berthou et al [78] have shown the relevance of this model for describing the thermal behavior of the houses. Besides, the decision to adopt this particular reduced model is influenced by its usage in a prior study [7], where the author employed it to investigate the thermal behavior of the INCAS house – the one that we use as a base for establishing diverse house characteristics for our analysis. Subsequent sections will delve into the details of the house INCAS.

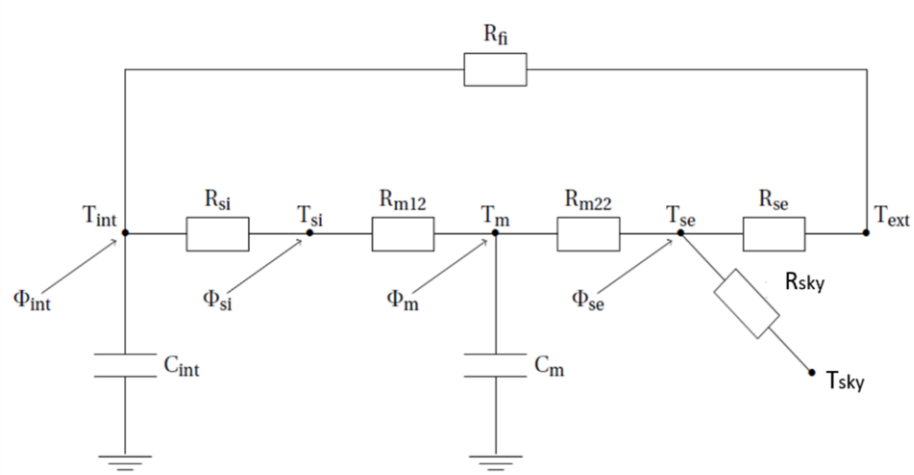

Figure 49: Thermal reduced model 6R2C

- All walls are assumed to be only one wall with equivalent thermal capacitance and thermal resistance C_m, R_m.
- The wall is represented by two thermal resistances, which are R_{m12} and R_{m22}. These thermal resistances are associated to the conduction heat transfer between both sides of the wall capacity.
- Absorbed solar radiations for the outer surface of the walls are integrated in the heat flow Φ_{se}.
- R_{fi} represents the heat transfer through low inertia elements (glazing, doors, and windows).

- Φ_{int} represents the heat flow from inside the house and also take into account proportion of solar radiation through glazing.
- Φ_{si} describes the heat flow injected into the inner side of the house. It comprises the solar radiation transmitted through glazing and be absorbed by inner surface of the wall as well as the radiative part of the internal loads.
- Φ_m is a heat flow injected inside the wall. In this chapter, it is equal to zero.
- R_{si} is thermal resistance associated to the convective heat transfer between internal air and inner side of the wall.
- R_{se} is thermal resistance associated to the convective heat transfer between external air and outer side of the wall.
- R_{sky} presents infrared radiation between outer wall and environment.

The thermo-electric analogy of the R6C2 type is parameterized by six resistors and two capacitors. The electrical diagram of this model is given in Figure 49. Within this model, the building is symbolized through two thermal nodes: the interior volume of the house and its wall. These thermal nodes are defined by their temperature, which is expressed as functions of the external factors, such as outside air temperature and incident solar radiation on the walls. Additionally, internal influences like thermal power emitted by occupants or heating systems contribute to these temperatures. Subsequently, energy balance equations are formulated for each temperature node.

$$C_{int}\frac{dT_{int}}{dt} = \frac{T_{ext} - T_{int}}{R_{fi}} + \frac{T_{si} - T_{int}}{R_{si}} + \Phi_{int}$$

$$0 = \frac{T_{int} - T_{si}}{R_{si}} + \frac{T_m - T_{si}}{R_{m12}} + \Phi_{si}$$

$$C_m\frac{dT_m}{dt} = \frac{T_{si} - T_m}{R_{m12}} + \frac{T_{se} - T_m}{R_{m22}} + \Phi_m$$

$$0 = \frac{T_m - T_{se}}{R_{m22}} + \frac{T_{ext} - T_{se}}{R_{se}} + \frac{T_{sky} - T_{se}}{R_{sky}} + \Phi_{se}$$

These above differential equations can be represented in a matrix form as:

$$\begin{vmatrix} T_{int}(t) \\ T_m(t) \end{vmatrix} = \begin{vmatrix} A_1 & A_2 \\ A_3 & A_4 \end{vmatrix} \cdot \begin{vmatrix} T_{int}(t-1) \\ T_m(t-1) \end{vmatrix} + \begin{vmatrix} B_1 & B_2 & B_3 & B_4 & B_5 & B_6 \\ B_7 & B_8 & B_9 & B_{10} & B_{11} & B_{12} \end{vmatrix} \cdot \begin{vmatrix} T_{ext}(t-1) \\ T_{sky}(t-1) \\ \Phi_{int}(t-1) \\ \Phi_{si}(t-1) \\ \Phi_m(t-1) \\ \Phi_{se}(t-1) \end{vmatrix}$$

With A_1, A_2, A_3 and A_4 are the values related to state vectors, B_1 to B_{12} are the coefficients related to solicitations matrix. The function of these values is described in detail in ANNEX I. Hence, for each house, depending on its characteristics, values of A_1, A_2, A_3, A_4 and values of B_1 to B_{12} will be different.

3. Characteristics of the house

The reduced thermal model offers the advantage of not requiring precise knowledge about the specific characteristics of a house. In the reference [77], the author uses the reduced thermal model using 6 resistances and 2 capacitors in order to derive various sets of coefficient A_1, A_2, A_3, A_4 and B_1 to B_{12} for different houses. The author used the model of the experimental house "INCAS" built on the INES site at le Bourget du Lac, France. The "INCAS" house comprises two floors and encompasses seven thermal zones. The first floor has a living room and a kitchen, while the second floor contains three bedrooms and a bathroom [79], [80]. The experimental houses have a ceiling height of 2.4m on the upper floor and 2.7m on the first floor with suspended ceilings. The interior dimensions of the house measure 7.5 meters in length and 6.5 meters in width, yielding a total living area of 89 square meters. These houses are built on a crawl space that is 0.80 meters high, encompassing two habitable levels topped by attic space, which remains independent of the heated volume.

Notably, the north facades are oriented at a 15.3-degree angle from the north/south axis in a counter-clockwise direction. The roof design is with a north/south orientation, complemented by a 0.60-meter overhang on the east, west, and north sides. The south facade is equipped with bay windows shielded from the summer sun by a 1.3-meter-long balcony and a 1-meter-long roof overhang. Conversely, the north facade features two small openings fitted with triple-glazed joinery to minimize heat loss during winter. Glazed surfaces account for 12% of the total surface area of external vertical walls. The distribution of glazing for the four orientations corresponds to 28% to the south, 10% to the west, 5% to the east and 2.5% to the north.

The author utilizes ENERGY PLUS, a building simulation software [81], to create detailed physical models of the "INCAS" house. These models served as a foundation for establishing the coefficients for the R6C2 reduced thermal model. The identification of these coefficients are achieved through particle swarm optimization, a technique employed to optimize parameters based on historical data [82]. In her study, the author aimed to derive various sets of coefficients for the R6C2 model. To achieve this, she employed the "INCAS" experimental house model as a baseline and generated different houses with distinct characteristics and thermal power from the heating systems. This process yielded 18 different house models, each accompanied by its own set of coefficients denoted as A1, A2, A3, A4, and B1 to B12. The volumes and thermal performances of these house models were adjusted to better represent the characteristics of the existing housing stock [77]. Within each of

the heated thermal zones of the models, an air-to-air heat pump is incorporated. This heat pump is designed with a convective power of 50W/m^2 and is regulated by a thermostat.

4. Generation of different house characteristics

The primary objective of this chapter is to construct an aggregated model capable of assessing the heating power consumption across a significant number of households within a specific region. To achieve this, it is imperative to possess data that accurately reflects the characteristics of the targeted area. In this context, the focus is on a cluster of households situated within the same geographical region. Consequently, all these households are subject to identical weather conditions and solar irradiance patterns specific to that location. In line with the findings presented in the reference [77], the "INCAS" house, an experimental building dedicated to energy efficiency research, is employed as a fundamental component. This structure is characterized by its high thermal inertia and boasts a simple yet compact architectural design. The dimensions of the "INCAS" house are detailed in Section 3. As mentioned earlier, the building used is the single-family home INCAS at INES in Chambéry [79], [80]. This building is chosen because it is well known to the French modelling community, and because model comparison and calibration tests have been carried out in various studies [83]–[85], making it a reliable candidate for energy modeling.

However, when extending the analysis to encompass a larger number of households, a diverse and representative database becomes essential. This necessity arises due to the inherent variability in characteristics across individual households. To address this diversity requirement, the study leverages the 18 typologies (Table 28) outlined in the reference [77]. These 18 typologies effectively encapsulate various house configurations with differing surface areas, thereby offering a representative sample of residential scales.

House	Surface area (m^2)	Thermal power (W)
1	89	8600
2	94	9100
3	78	7600
4	88	8500
5	73	7100
6	103	10000
7	134	13000
8	99	9600
9	87	8400
10	121	11700
11	82	7900
12	89	8600
13	114	11100
14	90	8700
15	86	8300
16	71	6900
17	149	14500
18	86	8300

Table 28: Surface area and thermal power from a heating system for 18 typologies

Table 29 illustrates 18 distinct coefficient sets, as detailed in the reference [77]. It is important to note that these 18 typologies are derived from the foundational "INCAS" house, signifying a common high thermal inertia characteristic across all houses. These coefficients, originating from [77], have been subject to certain modifications in order to render them applicable to the real. The specific adjustments made to these 18 coefficient sets are outlined in the attached ANNEX J.

House	Matrix A	Matrix B
1	$\begin{vmatrix} 0.835 & 0.165 \\ 2.98.10^{-5} & 1 \end{vmatrix}$	$\begin{vmatrix} 2.17.10^{-4} & 1.31.10^{-8} & 1.05.10^{-4} & -2.90.10^{-5} & 0 & 1.80.10^{-11} \\ 6.31.10^{-6} & 1.54.10^{-7} & 1.76.10^{-9} & 2.60.10^{-8} & 0 & 2.15.10^{-10} \end{vmatrix}$
2	$\begin{vmatrix} 0.835 & 0.165 \\ 3.87.10^{-5} & 1 \end{vmatrix}$	$\begin{vmatrix} 1.55.10^{-4} & 2.08.10^{-8} & 1.00.10^{-4} & 9.05.10^{-6} & 0 & 1.85.10^{-11} \\ 1.05.10^{-5} & 2.45.10^{-7} & 2.18.10^{-9} & 2.36.10^{-8} & 0 & 2.18.10^{-10} \end{vmatrix}$
3	$\begin{vmatrix} 0.831 & 0.169 \\ 5.69.10^{-5} & 1 \end{vmatrix}$	$\begin{vmatrix} 2.06.10^{-4} & 6.80.10^{-8} & 1.22.10^{-4} & 5.85.10^{-6} & 0 & 3.88.10^{-11} \\ 1.48.10^{-5} & 7.81.10^{-7} & 3.91.10^{-9} & 4.30.10^{-8} & 0 & 4.46.10^{-10} \end{vmatrix}$
4	$\begin{vmatrix} 0.828 & 0.171 \\ 3.09.10^{-5} & 1 \end{vmatrix}$	$\begin{vmatrix} 2.50.10^{-4} & 5.48.10^{-8} & 1.05.10^{-4} & 2.80.10^{-5} & 0 & 2.37.10^{-11} \\ 7.07.10^{-6} & 6.20.10^{-7} & 1.85.10^{-9} & 1.59.10^{-8} & 0 & 2.68.10^{-10} \end{vmatrix}$
5	$\begin{vmatrix} 0.816 & 0.184 \\ 4.53.10^{-5} & 1 \end{vmatrix}$	$\begin{vmatrix} 2.73.10^{-4} & 5.69.10^{-8} & 1.30.10^{-4} & 2.69.10^{-6} & 0 & 3.30.10^{-11} \\ 1.02.10^{-5} & 5.99.10^{-7} & 3.36.10^{-9} & 3.47.10^{-8} & 0 & 3.47.10^{-10} \end{vmatrix}$
6	$\begin{vmatrix} 0.823 & 0.176 \\ 5.51.10^{-5} & 1 \end{vmatrix}$	$\begin{vmatrix} 1.34.10^{-4} & 2.89.10^{-8} & 9.16.10^{-5} & 7.39.10^{-6} & 0 & 2.14.10^{-11} \\ 1.15.10^{-5} & 3.17.10^{-7} & 2.87.10^{-9} & 2.92.10^{-8} & 0 & 2.35.10^{-10} \end{vmatrix}$
7	$\begin{vmatrix} 0.841 & 0.159 \\ 7.79.10^{-5} & 1 \end{vmatrix}$	$\begin{vmatrix} 1.12.10^{-4} & 3.24.10^{-9} & 7.07.10^{-5} & 7.40.10^{-6} & 0 & 7.63.10^{-13} \\ 1.76.10^{-6} & 3.97.10^{-8} & 3.09.10^{-10} & 3.42.10^{-9} & 0 & 9.35.10^{-12} \end{vmatrix}$
8	$\begin{vmatrix} 0.901 & 0.099 \\ 1.20.10^{-5} & 1 \end{vmatrix}$	$\begin{vmatrix} 2.05.10^{-4} & 4.34.10^{-9} & 9.09.10^{-5} & 5.80.10^{-6} & 0 & 3.09.10^{-12} \\ 4.97.10^{-6} & 8.66.10^{-8} & 5.82.10^{-10} & 1.09.10^{-8} & 0 & 6.16.10^{-11} \end{vmatrix}$
9	$\begin{vmatrix} 0.822 & 0.177 \\ 4.16.10^{-5} & 1 \end{vmatrix}$	$\begin{vmatrix} 2.76.10^{-4} & 2.53.10^{-8} & 1.03.10^{-4} & 1.51.10^{-6} & 0 & 1.53.10^{-11} \\ 8.67.10^{-6} & 2.76.10^{-7} & 2.44.10^{-9} & 2.63.10^{-8} & 0 & 1.67.10^{-10} \end{vmatrix}$
10	$\begin{vmatrix} 0.831 & 0.169 \\ 2.98.10^{-5} & 1 \end{vmatrix}$	$\begin{vmatrix} 1.37.10^{-4} & 1.55.10^{-8} & 7.70.10^{-5} & 1.24.10^{-5} & 0 & 8.34.10^{-12} \\ 6.45.10^{-6} & 1.78.10^{-7} & 1.29.10^{-9} & 1.26.10^{-8} & 0 & 9.58.10^{-11} \end{vmatrix}$
11	$\begin{vmatrix} 0.827 & 0.173 \\ 2.98.10^{-5} & 1 \end{vmatrix}$	$\begin{vmatrix} 2.84.10^{-4} & 4.50.10^{-8} & 1.16.10^{-4} & -4.65.10^{-6} & 0 & 1.26.10^{-11} \\ 8.33.10^{-6} & 5.06.10^{-7} & 2.57.10^{-9} & 2.99.10^{-8} & 0 & 1.41.10^{-10} \end{vmatrix}$
12	$\begin{vmatrix} 0.829 & 0.170 \\ 2.98.10^{-5} & 1 \end{vmatrix}$	$\begin{vmatrix} 2.22.10^{-4} & 1.31.10^{-8} & 1.02.10^{-4} & 7.55.10^{-6} & 0 & 2.82.10^{-11} \\ 8.16.10^{-6} & 1.50.10^{-7} & 1.81.10^{-9} & 1.93.10^{-8} & 0 & 3.21.10^{-10} \end{vmatrix}$
13	$\begin{vmatrix} 0.861 & 0.139 \\ 2.98.10^{-5} & 1 \end{vmatrix}$	$\begin{vmatrix} 1.77.10^{-4} & 3.46.10^{-8} & 8.08.10^{-5} & 1.46.10^{-5} & 0 & 1.80.10^{-11} \\ 1.29.10^{-5} & 4.84.10^{-7} & 2.26.10^{-9} & 2.64.10^{-8} & 0 & 2.53.10^{-10} \end{vmatrix}$
14	$\begin{vmatrix} 0.842 & 0.158 \\ 2.98.10^{-5} & 1 \end{vmatrix}$	$\begin{vmatrix} 1.77.10^{-4} & 4.58.10^{-9} & 1.04.10^{-4} & 1.11.10^{-5} & 0 & 1.69.10^{-11} \\ 8.27.10^{-6} & 5.63.10^{-8} & 1.93.10^{-9} & 2.14.10^{-8} & 0 & 2.08.10^{-10} \end{vmatrix}$
15	$\begin{vmatrix} 0.828 & 0.172 \\ 2.98.10^{-5} & 1 \end{vmatrix}$	$\begin{vmatrix} 2.72.10^{-4} & 3.31.10^{-8} & 1.07.10^{-4} & 9.46.10^{-6} & 0 & 2.49.10^{-11} \\ 9.80.10^{-6} & 3.74.10^{-7} & 2.68.10^{-9} & 2.79.10^{-8} & 0 & 2.82.10^{-10} \end{vmatrix}$
16	$\begin{vmatrix} 0.825 & 0.174 \\ 2.98.10^{-5} & 1 \end{vmatrix}$	$\begin{vmatrix} 1.56.10^{-4} & 6.50.10^{-9} & 1.24.10^{-4} & 1.46.10^{-5} & 0 & 5.65.10^{-12} \\ 3.36.10^{-6} & 7.22.10^{-8} & 1.02.10^{-9} & 1.01.10^{-8} & 0 & 6.27.10^{-11} \end{vmatrix}$
17	$\begin{vmatrix} 0.839 & 0.161 \\ 2.98.10^{-5} & 1 \end{vmatrix}$	$\begin{vmatrix} 9.11.10^{-4} & 7.41.10^{-9} & 6.38.10^{-5} & -1.30.10^{-5} & 0 & 4.35.10^{-12} \\ 5.25.10^{-6} & 8.92.10^{-8} & 8.08.10^{-10} & 1.15.10^{-8} & 0 & 5.23.10^{-11} \end{vmatrix}$
18	$\begin{vmatrix} 0.832 & 0.168 \\ 2.98.10^{-5} & 1 \end{vmatrix}$	$\begin{vmatrix} 2.67.10^{-4} & 8.83.10^{-9} & 1.05.10^{-4} & 1.35.10^{-5} & 0 & 6.15.10^{-12} \\ 5.14.10^{-6} & 1.02.10^{-7} & 1.06.10^{-9} & 1.08.10^{-8} & 0 & 7.11.10^{-11} \end{vmatrix}$

Table 29: 18 sets of coefficient of A1 to A4 and B1 to B12

The objective is to create a comprehensive database that can represent a region in reality. To achieve this, the 18 reference parameter sets are employed as a starting point, originating from the "INCAS" building. This initial set is then expanded to encompass thousands of distinct houses, possessing distinct characteristics. These numerous houses, each defined by a different set of attributes, serve as the basis for simulating the unit model for heating in dwellings. The process of generating these diverse house characteristics involves the utilization of a uniform distribution to introduce randomness into the number of households under consideration. This procedural step holds particular importance due to the inherent variation in house characteristics could give a better representation across different geographical zones. By introducing randomness into the characteristic parameters, the resulting set of houses is representative of the diverse houses within the considered region.

5. Occupant presence profile

As emphasized by the International Energy Agency IEA, the energy performance of a building is affected by a multitude of factors encompassing technical, physical and human factors [86]. Human factor holds particular significance in numerous research studies as it contributes significantly to comprehending a building's energy utilization. This signifies that occupants' presence substantially influences internal heat gains and the utilization patterns of appliances and equipment within a building. In this chapter, the model AMAPOLA is harnessed to generate the different occupant profiles in the buildings. This model is built by Eric Vorger using probabilistic models based on collected data through the measurement campaigns, sociological surveys conducted by INSEE in France [87]. It can generate different profiles of occupants' behavior. AMAPOLA is incorporated as a module within the Pléiades software, serving the purpose of generating housing occupancy scenarios and facilitating sensitivity analyses on these scenarios. The module, created by Izuba and based on Eric Vorger's thesis, permits the creation of household profiles, parameterized according to socio-economic attributes (such as age, employment status, standard of living), with people's routines influenced by these parameters based on INSEE time-use surveys and other sources. The user has the flexibility to input specific parameters while non-specified ones are randomly determined using INSEE statistics. To generate the different occupant profile for each household, , the model requires various parameters relating to occupant details (e.g., household composition, number of adults and children, ages, income) as well as information regarding the house's characteristics (e.g., room count, equipment distribution). We create three scenarios: a two-person family, a three-person family, and a four-person family. The configuration includes two adults for the two-person family, two adults and one child for the three-person family, and two adults and two children for the four-person family. All households are classified as actively occupied; implying that at least one member of the family is engaged in typical work activities on a regular day. Each house is equipped with a minimum of one bathroom, one bedroom, and one living room. Consequently, time series data reflecting the presence of occupants at home, with a time interval of 10 minutes, is obtained. In this chapter, the thermal

power that an occupant can produce is 80W [88]. The heat flux emitted by the occupants in the house is referred to as Φ_{occupant}.

6. Outdoor temperature

The model employs outdoor temperature data from the Rhone Alpes climate zones, which are representative of cold winters characterized by average temperatures ranging between 0°C and 6°C [89]. The 18 sets of coefficients (Table 29), employed for generating various houses' characteristics, are also established using temperature data specific to the Rhone Alpes region [77]. Consequently, a location within the Rhone Alpes region is selected to carry out simulations for both the unit and aggregated models. The decision to select the year 2016 for the simulations is attributed to its relatively absence of extreme weather conditions [90]. In contrast, the winters of the years 2015, 2018, and 2019 experienced relatively warmer temperatures [91]–[93] while the winters of the year 2017 was colder than normal [94], emphasizing the year 2016 as a suitable choice for conducting simulations that provide a representative outlook on typical weather conditions

The outdoor temperature values are sourced from The Integrated Surface Dataset (ISD), which compiles data collected in Grenoble, Auvergne Rhone Alpes, throughout the year 2016 [95]

7. Sky temperature

The sky temperature is determined from the outside temperature, we have chosen to use the model that is largely used in the literature: the Swinbank model [96].

$$T_{sky} = 0.0552\, T_{ext}^{1.5}$$

8. Solar radiation

Solar radiation as known as a kind of thermal radiation is a major issue which affects the internal temperature of the buildings since glazed windows are more popular in the building architecture. The influence of solar radiation on buildings has been extensively explored in various research studies [97], [98]. Measuring the heat gain resulting from solar radiation poses a challenge due to its intricate nature. When solar radiation infiltrates a building, the direct incident radiation strikes the floor, while the reflected incident radiation interacts with the walls and ceiling. This interplay is contingent on the materials' absorbance and transmittance properties. In our modeling approach, we calculate solar radiation under clear sky conditions at specific locations and times using a clear-sky model, which is developed by Rigollier et al. [99]. This model enables the computation of solar radiation on surfaces for a given location and time when the sky is unobstructed. However, it is important to acknowledge that real-world conditions involve variations in sky clarity due to cloud cover. To account for this

variability, we introduce a coefficient denoted as C_{cloud}, which quantifies cloud coverage. Consequently, this coefficient introduces an element of variability to the solar radiation calculation. The solar power resulting from solar radiation that enters through windows and interacts with walls is respectively referred to as Φ_{window} and Φ_{wall}, respectively.

9. Heating systems using heat pumps

In our model, we assume that all heating systems are equipped with a heat pump to supply the heat to the houses. The thermal power delivered by these heat pumps varies from one house to another, contingent upon the specific characteristics of each house. Utilizing data from [77], each house is already assigned a heating system with a specific thermal power output. This thermal power from the heating system is denoted as Φ_{heater}.

The thermal power generated by the heating systems is influenced by the capacity of the heat pump's compressor, denoted as P_{TWH} and its coefficient of performance (COP). The value of COP varies according to the temperature of the heat sink and air source.

In fact, the COP is affected by the difference of temperature between air sources and heat sinks [100]. Research reference [100] presents the COP as a function of the temperature difference between the outdoor temperature and internal temperature (ΔT). However, due to limited technical information available for heating systems, hence, in this chapter, the COP is modelled as a linear function of the difference of temperature between outdoor temperature and internal temperature [100] (ΔT) .

$$COP = c_0 + c_1 \Delta T$$

The coefficients c_i are calculated by using heat pump data from manufacturers [28], [29]. These manufacturers are chosen as they produce the heating system which are preferable to the French residential and they are available and easy to access on the internet.

ΔT is obtained using: $\Delta T = T_{int} - T_{out}$

Then the electrical power consumed for heating is then calculated by

$$P_{heat-residential} = P_{heat} / COP \quad \text{(Watt)}$$

With P_{heat} is thermal power consumed for heating in residential.

10. Heat sources

The heat flows Φ_{int}, Φ_{si} and Φ_{se} represent respectively internal loads and a part of solar radiations through glazing, radiative heat gain received by internal walls and radiative heat gains received by external walls. These heat flows are estimated as follows:

$$\Phi_{int} = \Phi_{heater} + \Phi_{occupant} + \beta \Phi_{window}$$

$$\Phi_{si} = (1 - \beta).\Phi_{window}$$

$$\Phi_{se} = \alpha.\Phi_{wall}$$

With α is the absorption coefficient, which represent the proportion of the incident radiation absorbed by the wall and β the absorption coefficient, which represent the proportion of the incident radiation absorbed by the window glass. These 2 coefficients are also identified for each house in [77] (Table 30) and we have decided to use them in our model.

House	α	β
1	0.689	0.371
2	0679	0.119
3	0.931	0.757
4	0.787	0.124
5	0.620	0.200
6	0.750	0.172
7	0.837	0.160
8	0.612	0.184
9	0.651	0.124
10	0.960	0.145
11	0.599	0.454
12	0.657	0.590
13	0.785	0.542
14	0.909	0.200
15	0.835	0.112
16	0.798	0.210
17	0.758	0.339
18	0.659	0.227

Table 30: 18 sets of coefficient α and β

11. Methodology

In this section, we outline the methodology employed for constructing the aggregated model, mirroring the approach previously utilized for domestic hot water. Our process commences with the simulation of the unit model, which involves executing the physical model's simulation for each individual household. Subsequently, we harness the outcomes derived from the unit model as a foundational basis for constructing the aggregated model.

11.1. The unit model of heating in residential

Our methodology initiates with an assumption that each dwelling is equipped with a single heating system. Each individual dwelling possesses unique attributes, including distinct characteristics and a specific thermal power output from its associated heating system. To establish the unit model, we implement a MATLAB-based framework with a time step of one minute. A simulation period of 7 days, comprising 10,080 minutes, is selected for an ensemble of 5,000 heating systems. The unit model incorporates inputs such as outdoor temperature, sky temperature, solar radiation, and

occupants' presence at home in time series. The resulting output represents the cumulative thermal power consumption for heating over a time series.

It is essential to emphasize that our focus during both unit model and aggregated model simulations is on thermal power consumption, rather than electrical power. The calculation of electrical power will be addressed in later in this chapter.

The heating system control strategy is straightforward: during occupants' presence, internal temperature decreases due to heat dissipation to the surroundings. Once the internal temperature falls to a level at or below the thermostat setting T_{set}, the heating system activates, and it deactivates only when the internal temperature surpasses T_{set}. Consequently, when the heating system is operational, the thermal power provided by the heating system at each time step $Q_{heat-heating}$ is equal to Q_{heater} with Q_{heater} is the maximal thermal power provided by the heating system and this value is pre-established for each dwelling based on data from Table 28. Conversely, when the heating system is inactive, $Q_{heat-heating}$ remains at zero. This straightforward control approach ensures a representation of heating system behavior in our simulations.

11.2. Aggregated model for heating in residential description

The purpose of constructing the aggregated model for residential heating is to estimate power consumption for heating without necessitating intricate details about individual house characteristics. Similar to the approaches taken for domestic hot water and electric vehicle charging, utilizing this aggregated model eliminates the need for simulating power consumption for each individual heating system, thereby significantly reducing computational time.

In this section, we introduce an aggregated model designed to evaluate heating power within households, both with and without the application of control signals. Through this methodology, the necessary input parameters consist of the total count of heating systems, along with the average values of parameters employed in the unit model simulation. These average parameters encompass average outdoor temperature $T_{out-avg}$, average setting temperature $T_{set-avg}$, cloud cover coefficient C_{cloud} and average heating system thermal power $P_{heating-avg}$.

11.3. Methodology for generating an aggregated model

As emphasized earlier, the aggregated model for heating systems necessitates the inputs: the quantity of heating systems involved and the average parameter values including average outdoor temperature $T_{out-avg}$, average setting temperature $T_{set-avg}$, cloud cover coefficient C_{cloud} and average heating system thermal power $P_{heating-avg}$. It is important to note that the aggregated model assumes the utilization of heat pump technology in the heating systems. In addition to the inputs required for the unit model,

the aggregated model also requires time series inputs for outdoor temperature, sky temperature, and solar irradiation. The outcome generated by the aggregated model is the time series of thermal power consumption.

For reminding, the control signal is already mentioned in the chapter 1. In this chapter, we use the control signals, which have the peak hours from 10 to 12 o'clock and from 18 to 22 o'clock.

Initially, we followed a similar approach to the one employed in developing the aggregated model for domestic hot water. However, we deviated from this approach when constructing the aggregated model for heating systems. Our focus shifted towards establishing a correlation between the average thermal power consumption and the collective average internal temperature across all households. This endeavor aimed to uncover the interdependence between these two factors. To illustrate this relationship, we created a graph, depicted as Figure 50, which portrays a quadratic linkage between the average thermal power consumption and the average internal temperature. For a more detailed elucidation of the methodology utilized to derive this relationship, a comprehensive breakdown is provided in ANNEX M. This insight provides a foundational premise for constructing the aggregated model for residential heating.

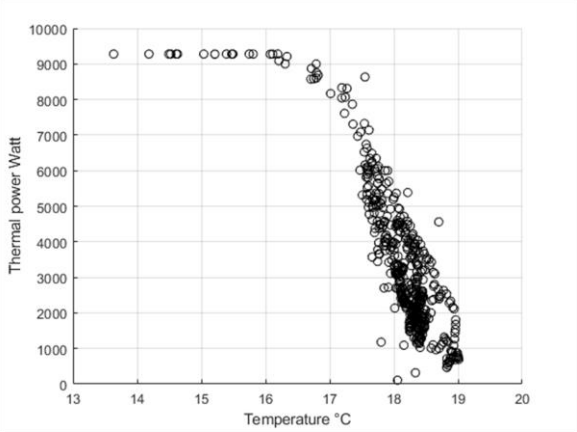

Figure 50 : The relationship between the average thermal power consumed (W) and average internal temperature of 5000 heating systems

Indeed, our strategy for formulating the aggregated model for heating entails an approach that mimics the behavior of a unit model dedicated to a single house with a singular heating system. However, in the context of the aggregated model, this house symbolizes an average vision of all houses, incorporating their average thermal attributes. This implies that we take the average values of the various sets of coefficients concerning the thermal characteristics of all individual houses. Besides, the thermal power consumption for this aggregated model house is subsequently determined using the quadratic relationship elucidated earlier. As a result, our approach for constructing the aggregated

model revolves around defining the relationship curve between the average thermal power consumption and the average internal temperature. This relationship is formulated as a quadratic function, subject to specific additional constraints. The visual representation of this function is depicted Figure 51, wherein $P_{avg\text{-}agg}$ signifies the average thermal power of all heating systems. Notably, the apex of the curve is marked by point H, while the lower bound temperature $T_{lb\text{-}heating}$ and higher bound temperature $T_{hb\text{-}heating}$ serve as the critical constraints governing the behavior of this relation curve.

It can be seen that the internal temperature of the house is affected by the setting temperature. Consequently, $T_{hb\text{-}heating}$ is designated as the collective average setting temperature for all heating systems. Meanwhile, $T_{lb\text{-}heatung}$ functions as a pivotal threshold, determining whether the average thermal power consumed equals the mean thermal power rating $P_{avg\text{-}agg}$.

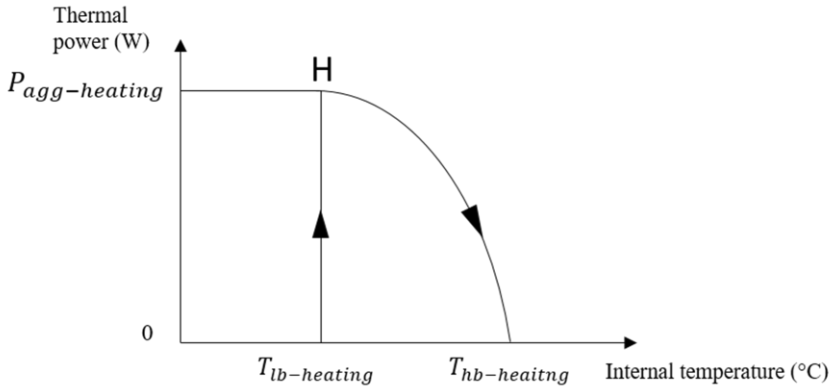

Figure 51 : The relation curve between the average thermal power (W) and the internal temperature for the aggregated model

Derived from the outcomes of the unit model simulation (as illustrated in Figure 50), a distinct set of values for $P_{avg\text{-}agg}$, $T_{lb\text{-}heating}$ and $T_{hb\text{-}heating}$ can be consistently extracted. The objective now is to express these values as functions of specific average parameters, encompassing aspects related to heating system attributes and weather conditions. These parameters comprise the average outdoor temperature $T_{out\text{-}avg}$, average setting temperature $T_{set\text{-}avg}$, cloud cover coefficient C_{cloud} and average heating system thermal power $P_{heating\text{-}avg}$

Following this idea, $P_{avg\text{-}agg}$ is chosen as the average heating system thermal power $P_{heating\text{-}avg}$

$$P_{avg\text{-}agg} = P_{heating\text{-}avg}$$

$T_{hb\text{-}heating}$ is defined by the linear function of $P_{heating\text{-}avg}$, $T_{set\text{-}avg,}$ $T_{out\text{-}avg}$,C_{cloud}

$$T_{hb\text{-}heating} = \text{function } (P_{heating\text{-}avg}, T_{set\text{-}avg,} T_{out\text{-}avg},C_{cloud})$$

$T_{lb\text{-}heating}$ is given by the linear function of $P_{heating\text{-}avg}$, $T_{set\text{-}avg,}$ $T_{out\text{-}avg}$,C_{cloud}

$$T_{lb\text{-}heating} = \text{function } (P_{heating\text{-}avg}, T_{set\text{-}avg,} T_{out\text{-}avg},C_{cloud})$$

To determine the coefficients for the functions of $T_{hb\text{-}heating}$ and $T_{lb\text{-}heating}$, a simulation of the unit model is undertaken, considering diverse scenarios involving varying numbers of heating systems and different parameter values of $P_{avg\text{-}heating}$, $T_{set\text{-}heating,}$ $T_{avg\text{-}out}$, C_{cloud} to obtain the different values of $T_{lb\text{-}heating}$. This approach is employed to derive an understanding of the relationships between these coefficients and the specified parameters.

The simulation of the unit model encompasses different scales, examining scenarios with 3000, 5000, 7000, and 10,000 houses, thereby representing various spatial scales, as detailed in Table 31. To ensure the robustness of our analysis, it is imperative to incorporate a broad range of parameter values for $P_{avg\text{-}heating}$, $T_{set\text{-}heating,}$ $T_{avg\text{-}out}$, $C_{cloud.}$. As mentioned on Table 28, the thermal power of the heating system is decided by considering the surface area of the household. If we use the uniform distribution to assign a heating system with a corresponding thermal power to a house, it can inadvertently lead to relatively similar average values of $P_{avg\text{-}heating}$ will be close to each other. This similarity diminishes the meaningful dependence of $T_{hb\text{-}heating}$ and $T_{lb\text{-}heating}$ on $P_{avg\text{-}heating}$.

To address this limitation and enhance the parameter variation, the distribution strategy is modified for each scenario involving a specific number of houses. This approach is pivotal in generating diverse of $P_{avg\text{-}heating}$. Values of $T_{set\text{-}avg,}$ $T_{out\text{-}avg}$ and C_{cloud} are also subject to variation, following the specifications outlined in Table 31. Specifically, $T_{set\text{-}avg}$ spans a range from 18°C to 21°C with increments of 1°C, which encompasses different user behaviors in terms of setting the indoor temperature within the residential premises. Given that the normal average winter temperature in France hovers around 5.4°C [101], we judiciously select a specific time frame for simulation input. Consequently, we utilize weather data spanning from January 2nd, 2016, to January 8th, 2016, for these simulations. This time period is chosen as it closely mirrors the average outdoor temperature during winter, approximating 5.6°C. Additionally, to determine the coefficient of $T_{out\text{-}avg}$ within the functions characterizing $T_{hb\text{-}heating}$ and $T_{lb\text{-}heating}$, it is essential to account for various weather scenarios. As a result, we systematically fluctuate the parameter $T_{out\text{-}avg}$ within a range of ±5°C from the real weather data. Specifically, $T_{out\text{-}avg}$ is modulated across the range of 0.6°C, 5.6°C, and 10.6°C, effectively encompassing scenarios of both colder and milder conditions. This approach ensures that the functional relationships are robustly calibrated to different weather conditions, enhancing the accuracy and reliability of the aggregated model for heating in residential. Meanwhile, C_{cloud} values encompass the set (0, 0.5, 1), corresponding to days characterized by no clouds, partial cloud coverage, and complete cloud coverage.

Number of heating systems	$P_{heating\text{-}avg}$ (W)	$T_{out\text{-}avg}$ (°C)	$T_{set\text{-}avg}$ (°C)	C_{cloud}
3,000	14,500	[0.6, 5.6, 10.6]	[18,19,20,21]	[0, 0.5, 1]
5,000	14,149			
7,000	11,321			
10,000	13,292			

Table 31: The value of $P_{heating\text{-}avg}$, $T_{set\text{-}avg}$, $T_{out\text{-}avg}$ and C_{cloud} for different numbers of heating systems

Through the unit model simulations conducted across four distinct scenarios, each characterized by varying numbers of houses, $T_{set\text{-}avg}$ (with 4 specific values), $T_{out\text{-}avg}$ (with 3 specific values), and C_{cloud} (with 3 specific values), a total of 144 data points for $T_{hb\text{-}heating}$ and $T_{lb\text{-}heating}$ are derived. The detailed methodology for establishing these values is outlined in the attached ANNEX N. Employing a fitted linear regression model, the coefficients governing the functions of $T_{hb\text{-}heating}$ and $T_{lb\text{-}heating}$ are ascertained. The graphical representations in Figure 52 and Figure 54 illustrate the outcomes. Here, the black line corresponds to values obtained from the unit model simulations, while the red line delineates the results derived from the fitted linear regression model.

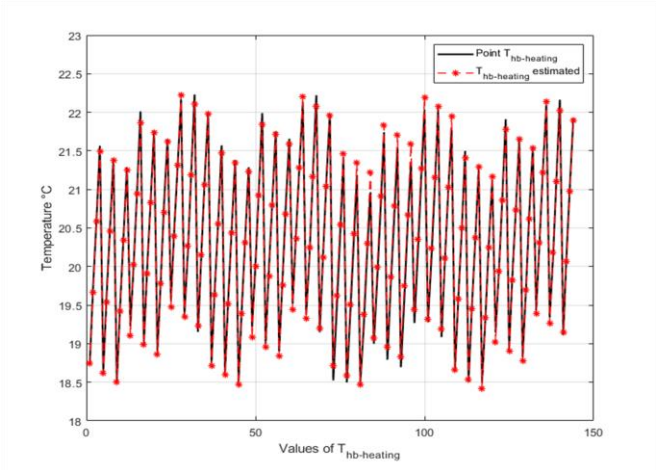

Figure 52 : The value of $T_{hb\text{-}heating}$ when changing the values of $P_{heating\text{-}avg}$, $T_{set\text{-}avg}$, $T_{out\text{-}avg}$ and C_{cloud}

Figure 53 provides a visual representation of the initial 36 $T_{hb\text{-}heating}$ values, specifically derived from the unit model simulations for the case of 3,000 houses. Each group of 12 points within the figure

corresponds to $T_{hb\text{-}heating}$ values associated with varying average outdoor temperatures $T_{out\text{-}avg}$, which range across 0.6°C, 5.6°C, and 10.6°C. Indeed, an ascending trend is apparent within each cluster of 12 data points. This trend can be attributed to the incremental elevation of the average outdoor temperature ($T_{out\text{-}avg}$). As $T_{out\text{-}avg}$ rises, it contributes to a slight but noticeable augmentation in the $T_{hb\text{-}heating}$ values.

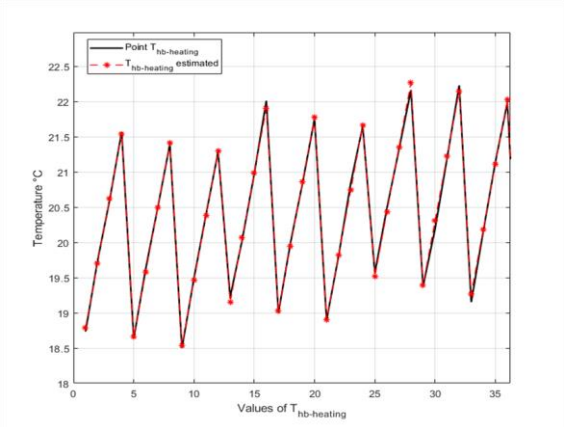

Figure 53: The value of $T_{hb\text{-}heating}$ in the case of 5,000 houses

Notably, within each set of 12 points, an apparent pattern emerges, with temperature evolution evident across every 4 points. This pattern corresponds to the alteration in the average setting temperature $T_{set\text{-}avg}$, which spans 4 different values ranging from 18°C to 21°C, with increments of 1°C. Besides, a trend is observable within each subset of 4 points: an insignificant decrease in $T_{hb\text{-}heating}$ values as the cloud cover coefficient C_{cloud} increases. This behavior aligns with the impact of increasing cloud cover: a reduction in solar irradiance reaching the houses, resulting in a decline in $T_{hb\text{-}heating}$ values.

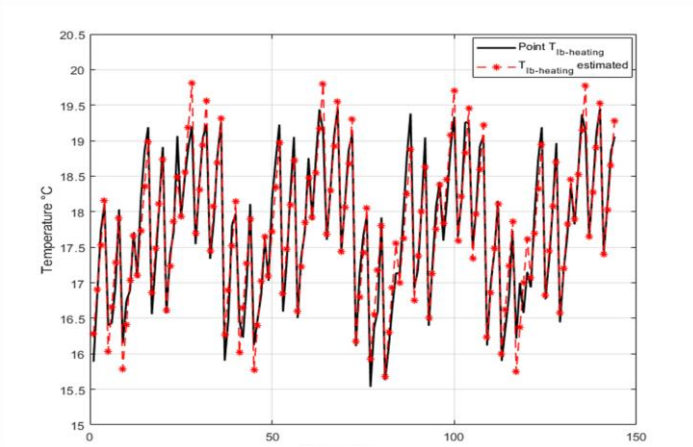

Figure 54 : The value of $T_{lb\text{-}heating}$ when changing the values of $P_{heating\text{-}avg}$, $T_{set\text{-}avg}$, $T_{out\text{-}avg}$ and C_{cloud}

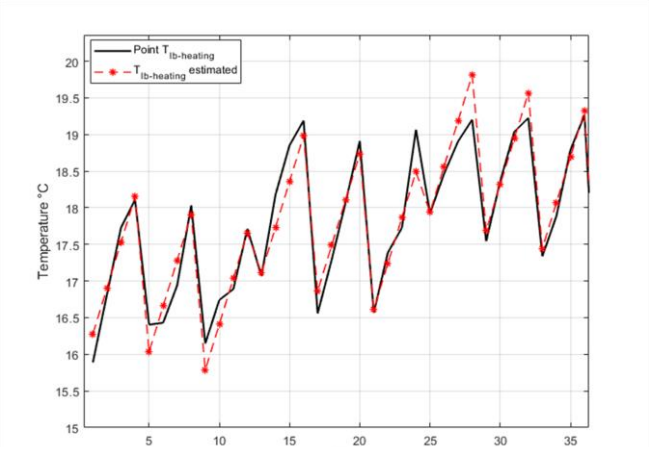

Figure 55 : The value of $T_{lb\text{-}heating}$ for the case of 5,000 houses

Figure 55 exhibits a similar arrangement and parameter variance structure as Figure 53. It also displays the initial 36 data points of $T_{lb\text{-}heating}$. Similarly, each cluster of 12 points corresponds to a different range of average outdoor temperature ($T_{out\text{-}avg}$) values. Within each of these clusters, every set of 4 points represents variations in cloud cover coefficient (C_{cloud}). And in each set of 4 points corresponds to the variance of average setting temperature ($T_{set\text{-}avg}$). While the trends observed when varying $T_{set\text{-}avg}$ and $T_{out\text{-}avg}$ are analogous to those of $T_{hb\text{-}heating}$, the influence of C_{cloud} on $T_{lb\text{-}heating}$ is not as evident. In the second cluster of 12 points, specifically, the differences between the 16th, 20th, and 24th points appear negligible and do not follow any trend. Indeed, it can be attributed to the manner in which $T_{lb\text{-}heating}$ is determined during the unit simulation. The manner in selecting $T_{lb\text{-}heating}$ values is outlined in ANNEX N.

However, it is worth noting that these minor differences in the selection process is negligible. It has minimal impact on the accurate determination of the coefficients for the $T_{lb\text{-}heating}$ function when utilizing the linear regression technique.

Hence, the coefficients for $P_{heating\text{-}avg}$, $T_{set\text{-}avg,}$ $T_{out\text{-}avg}$ and C_{cloud} are found and the final equation of $T_{hb\text{-}heating}$ and $T_{lb\text{-}heating}$ are then shown as follows:

$$T_{hb\text{-}heating} = 1.2124 + 6.608.10^{-5}\, P_{heating\text{-}avg} + 0.9185\, T_{set\text{-}avg} + 0.0729\, T_{out\text{-}avg} - 0.2440 C_{cloud}$$

$$T_{lb\text{-}heating} = 4.3676 + 3.304.10^{-5}\, P_{heating\text{-}avg} + 0.6247\, T_{set\text{-}avg} + 0.1659\, T_{out\text{-}avg} - 0.4933 C_{cloud}$$

As outlined earlier, we have established the relationships between $P_{avg\text{-}agg}$, $T_{hb\text{-}heating}$ and $T_{lb\text{-}heating}$ based on the parameters $P_{heating\text{-}avg}$, $T_{set\text{-}avg,}$ $T_{out\text{-}avg}$ and C_{cloud}. In addition, we propose the following hypothesis: "The point H depicted in Figure 51 represents the apex of the quadratic function."

In summary, armed with the definitions of $P_{avg\text{-}agg}$, $T_{hb\text{-}heating}$ and $T_{lb\text{-}heating}$, along with the assumption of point H as the apex of the quadratic curve, we can now formulate the connection between the aggregated model's thermal power $P_{heating}$ for heating and the internal temperature using the following equation:

$$P_{heating} = h_1 T_{int}^{\ 2} + h_2 T_{int} + h_3$$

With the following conditions:

- The point H is the maximum of the quadratic equation.
- If $T_{int} <= T_{lb\text{-}heating}$ then $P_{heating} = P_{avg\text{-}agg}$
- If $T_{int} >= T_{hb\text{-}heating}$ then $P_{heating} = 0$
- h_1, h_2, h_3 are the coefficients, which are calculated by using 3 values of $P_{avg\text{-}agg}$, $T_{hb\text{-}heating}$ and $T_{lb\text{-}heating}$:

$$h_1 = \frac{-P_{avg-agg}}{(T_{lb-heating} - T_{hb-heating})^2}$$

$$h_2 = \frac{-2\,P_{avg-agg} T_{lb-heating}}{(T_{lb-heating} - T_{hb-heating})^2}$$

$$h_3 = \frac{P_{avg-agg}(T_{hb-heating}^{\ 2} - 2T_{lb-heating}T_{hb-heating})}{(T_{lb-heating} - T_{hb-heating})^2}$$

Coefficients h_1, h_2 and h_3 are calculated in detail through ANNEX O.

With all the elements defined, the control logic of the aggregated heating system model is then designed as follows:

If $T_{lb\text{-}heating} < T_{int} < T_{set}$ then $P_{heating} = h_1 T_{int}^{\ 2} + h_2 T_{int} + h_3$ under the mentioned conditions

If $T_{int} >= T_{hb\text{-}heating}$ then $P_{heating} = 0$

If $T_{int} <= T_{lb\text{-}heating}$ then $P_{heating} = P_{avg\text{-}agg}$

Up to this point, we have successfully defined the quadratic function that describes the relationship between average thermal power and internal temperature. However, there are additional coefficients related to the thermal characteristics of the house used for the aggregated model that require definition. As previously mentioned, every house has its own unique set of coefficients represented by matrix A (A1 to A4) and matrix B (B1 to B12), which characterize the thermal properties of that house. The calculation of these coefficients involves parameters related to the thermal characteristics of each house, including C_{int}, C_m, R_{fi}, R_{si}, R_{m12}, R_{m22}, R_{se} and R_{sky} . A detailed explanation of how these coefficients are calculated using these parameters is provided in ANNEX I.

Now, for our aggregated heating model, which mimics a standard heating system but differ in thermal power calculation, we also require sets of coefficients. These are denoted as matrix A_{agg} with 4 values ($A1_{agg}$, $A2_{agg}$, $A3_{agg}$, $A4_{agg}$) and matrix B_{agg} with 12 values from $B1_{agg}$ to $B12_{agg}$). To represent the

thermal characteristics needed for the aggregated model, we compute average values for these coefficients. These average values are obtained by calculating the mean of each corresponding element in the set (C_{int}, C_m, R_{fi}, R_{si}, R_{m12}, R_{m22}, R_{se}, R_{sky}) across all households. These average values are then represented as ($C_{int-avg}$, C_{m-avg}, R_{fi-avg}, R_{si-avg}, $R_{m12-avg}$, $R_{m22-avg}$, R_{se-avg}, $R_{sky-avg}$). We have done ANNEX K and ANNEX L with deeper research to describe how to we calculate these coefficients and how we can obtain these average values by using the available information and sources of data.

Finally, after having the thermal power consumption curve obtained from the aggregated model for heating, the electrical power consumption is then calculated by taking the thermal power consumption each time step divide by the coefficient of performance COP. The COP for each time step for each heating system is modelled as a linear function of the difference of temperature between outdoor temperature and internal temperature [100] (ΔT) .

$$COP = c_0 + c_1 \Delta T$$

Which mean that each heating system corresponds to a set of c_0 and c_1

In order to find the COP for the aggregated model COP_{agg}, we take average value of all c_0 (defined as c_{0-agg}) and average value of all c_1 (defined as c_{1-agg})

Hence, COP_{agg} is determined by:

$$COP_{agg} = c_{0-agg} + c_{1-agg} \Delta T$$

As a result, the electrical power consumption of the aggregated power is defined as follow:

$$P_{heat-residential} = P_{heat} / COP_{agg} \quad \text{(Watt)}$$

12.Simulation settings of the aggregated heating model

The inputs of the model are shown as follow:

- The number of heating system chosen for simulation
- The outdoor temperature in time series T_{out} (°C)
- The solar irradiation in time series (W/m^2)
- The average thermal power $P_{heating-avg}$ of all households (W)
- The average setting temperature $T_{set-avg}$ (°C)
- The average outdoor temperature $T_{out-avg}$ (°C)
- The cloud coverage coefficient C_{cloud}

The output of the model is the average thermal power consumption of all heating systems in time series with 10-minute time step.

The model is implemented in MATLAB version 2019b and has a ten-minute sampling time. To evaluate the accuracy of the aggregated model, we aim to ascertain its ability to provide thermal power consumption estimations compares to those derived from the unit model. Our testing involves two distinct spatial scales: simulations for 5,000 and 10,000 houses. Furthermore, we seek to gauge the model's performance across varying weather conditions. To this end, we select two distinct periods: one spanning from 13th Jan 2016 to 19th Jan 2016 characterized by an average outdoor temperature of 1.7°C, and another from 24th January 2016 to 30th January 2016, with an average outdoor temperature of 5.1°C.

For solar radiation data, as delineated in Section 7, we employ a clear-sky model developed by Rigollier et al. [99]. This model enables us to generate solar radiation data within the specified time frames. The temperature settings for the simulations are fixed at 19°C and 18°C, designed to represent varying user behaviors. Our simulations of the aggregated model span seven days, allowing us to observe its performance over an extended time horizon. However, the model exhibits consistent behavior across different days. Given this, we present results for a three-day period in this chapter.

Having gathered the requisite data for different numbers of heating systems, Table 32 provides an overview of the values for $P_{heating\text{-}avg}$, $T_{out\text{-}avg}$, $T_{set\text{-}avg}$ and C_{cloud} for two distinct scenarios with different spatial scales the simulation of the aggregated model. The scenario 1 is for 5,000 households and the scenario 2 is for 10,000 households.

	Scenario 1	Scenario 2
Number of heating systems	5000	10000
$P_{heating\text{-}avg}$(W)	10099	9367
$T_{set\text{-}avg}$ (°C)	19	18
$T_{out\text{-}avg}$(°C)	1.7	5.1
C_{cloud}	0.5	0

Table 32: The values of $P_{heating\text{-}avg}$, $T_{set\text{-}avg}$, $T_{out\text{-}avg}$ and C_{cloud} for 5,000 and 10,000 heating systems, respectively

The determination of $P_{heating\text{-}avg}$ values for 2 scenarios comes from the generation of characteristic data for each heating system. In order to validate the outcomes of the aggregated model, we reconstruct the dataset for both scales: 5,000 and 10,000 households. This dataset encompasses the thermal power for each heating system, as well as the set of coefficients that represent the unique characteristics of

each house. For the $P_{heating\text{-}avg}$ values, we calculate the average thermal power of all heating systems. In the case of $T_{set\text{-}avg}$, our goal is to observe the behavior of the aggregated model under varied real-world scenarios. Consequently, we select values of 19°C and 18°C for $T_{set\text{-}avg}$ for scenario 1 and scenario 2, respectively. This differentiation in $T_{set\text{-}avg}$ values allows us to simulate diverse user behaviors. The inclusion of C_{cloud}, representing weather-related factors, involves the selection of two distinct cloud coverage coefficients. These coefficients reflect the reaction of the aggregated model to varying weather conditions. Lastly, for $T_{out\text{-}avg}$, we calculate its value based on the average outdoor temperature during the periods from 13th January 2016 to 19th January 2016, and from 24th January 2016 to 30th January 2016.

13. Simulation results of the aggregated heating model

In this section, we delve into the simulation of the aggregated model both with and without control signals, aiming to estimate thermal power consumption for residential heating across varying numbers of heating systems. The outcomes of the aggregated model are subsequently compared to those of the unit model. Initially, we conducted a 7-day simulation to comprehensively explore the aggregated model's behavior compared to the unit model in terms of performance and computation time. However, in this chapter, we present the results over a 3-day period (4,320 minutes) as it effectively demonstrates the aggregated model's behavior.

We execute the simulation for different numbers of heating systems (5,000 and 10,000 heating systems) in scenario 1 and scenario 2 using two distinct control methods. One simulation employs only thermostat control (referred to as the aggregated model without control signals), while the other incorporates an additional control signal in conjunction with the thermostat control (referred to as the aggregated model with control signals). The details of the control signal are outlined in Chapter 1, where it is highlighted, that peak hours occur from 10 AM to 12 PM and from 6 PM to 10 PM. The simulation follows a straightforward approach: during peak hours, all heating systems are turned off, and they are operated exclusively during off-peak hours.

The simulation outcomes are graphically represented in Figure 56. The figures provide a visual demonstration of the average thermal power consumption for heating across different numbers of heating systems over the course of 3 days, with a time interval of 10 minutes. The plotted curves illustrate the thermal power consumption profiles generated by both the unit model (blue curve) and the aggregated model (red curve). More specifically, Figure 56 [a, b] correspond to the aggregated model applied to 5,000 heating systems in scenario 1 with and without control signals, respectively. Meanwhile, Figure 56 [c, d] portray the analogous scenarios for 10,000 heating systems of scenario 2.

It's worth highlighting that the presentation of aggregated model results serves two primary objectives: firstly, to showcase its applicability across various spatial scales, ranging from a district to a city, region, or even a country; and secondly, to emphasize the agility of the aggregated model in delivering results in contrast to the unit model. This aspect underscores the robustness and efficiency of the aggregated model in practical applications.

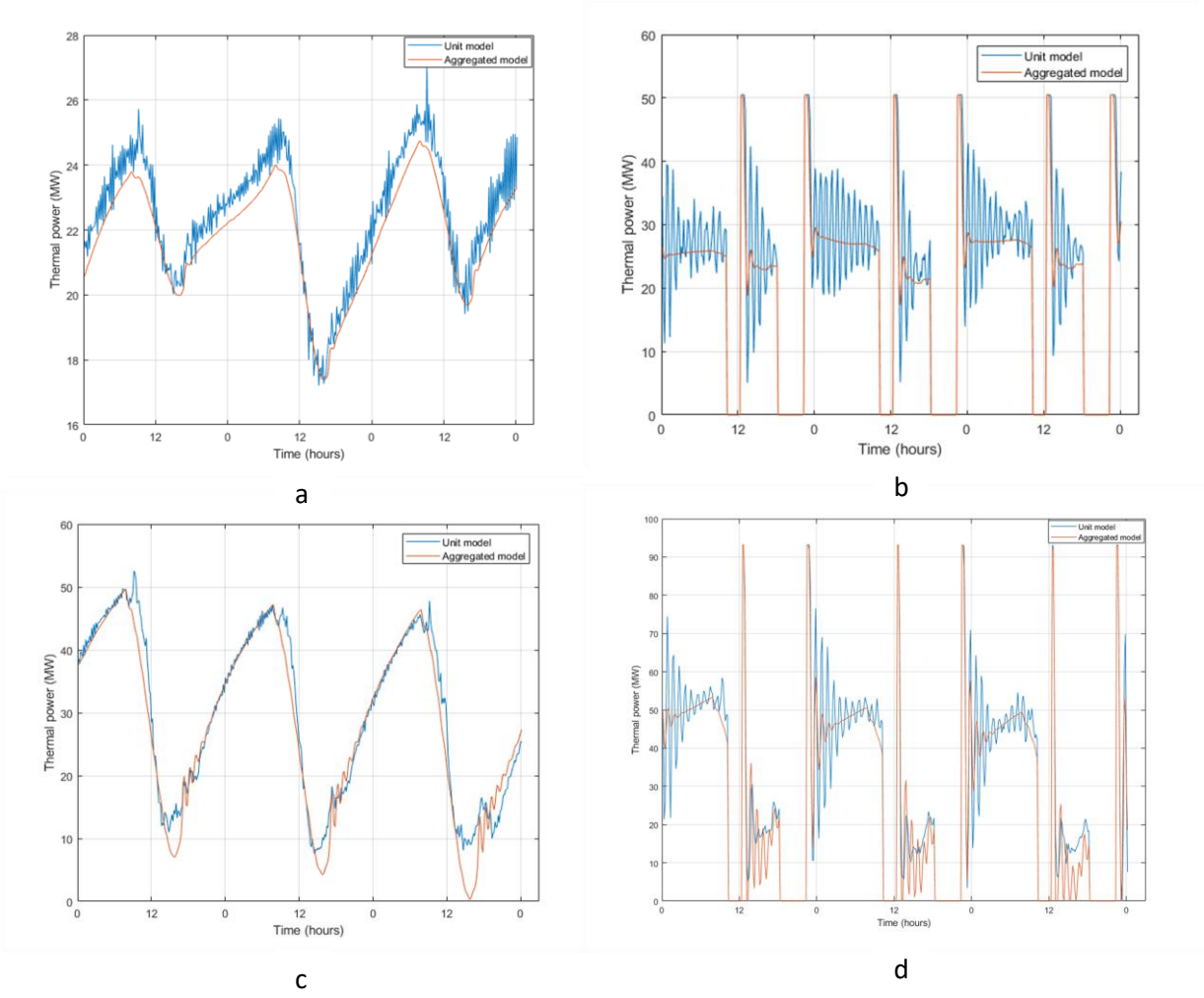

Figure 56: The thermal power consumption for heating in 3 days (W). [a] and [b] describe the simulation of the aggregated models without and with the electricity price control signal applied for scenario 1, respectively while [c] and [d] present those for scenario 2.

Look at the Figure 56 [a, c], it becomes evident that the aggregated model without control signals can capture the behavior of thermal power usage for residential heating. The simulation time for this aggregated model is a mere 0.2 seconds, a staggering 2150 times faster compared to the unit model's simulation time of 430 seconds for scenario 1 with 5,000 households. These computation times were

recorded using MATLAB R2019b on a Dell PC with an Intel(R) Core(TM) i5-8265U CPU running at 1.60GHz

Turning to Figure 56 [b, d], we observe the thermal power consumption patterns of both the unit model and the aggregated model with control signals applied. A noticeable feature post-power cut is the fluctuation in thermal power consumption. This behavior arises from the foundational dataset utilized in [77], which originates from the high-inertia building INCAS. Consequently, the housing characteristics data generated based on this reference lead to a prevalence of high thermal inertia houses. In Figure 56 [b, d], the beginning of the day 1, we witness these fluctuations. This is a result of conducting a 7-day simulation and subsequently selecting a 3-day window for presentation. Further exploration of Figure 56 [b, d] reveals that following a power cut, there appears a rapid decline in thermal power consumption and then followed by an increase. This is due to the close thermal characteristics of all the houses, which results in the similar reaction. When there is the signal again, all the heating system will turn on at the same time.

In contrast, the outcome of the aggregated model is obtained with less fluctuation and flatter. This is due to the hypothesis about the quadratic relation curve between the average thermal power and the internal temperature inside the houses. Therefore, look at Figure 56 [b, d], it is observable that the aggregated model does not present precisely the behavior of the thermal power consumption curve obtained from unit model but it can illustrate the average value of thermal power consumption.

To quantify the accuracy of the aggregated model against the unit model, Table 8 presents the Normalized Absolute Mean Error (NMAE), which normalizes the absolute mean error over the average thermal power consumption of the unit model. This NMAE assessment provides insight into the effectiveness of the aggregated model's predictive capability.

Model type	**Scenario 1 (%)**	**Scenario 2 (%)**
The aggregated model without control signals	5.7	12.05
The aggregated model with control signals	14.39	16.88

Table 33: Normalized Absolute Mean Error (NMEA) (percentage) of the aggregated model, compared to the unit model for scenario 1 and scenario 2, respectively.

Table 33 provides a view of the Normalized Absolute Mean Error (NMAE) values for the aggregated model compared to the unit model across different spatial scales, specifically scenario 1 with 5,000 houses and scenario 2 with 10,000 houses. The NMAE values for the aggregated model without

control signals are 5.7% for scenario 1 and 12.05% for scenario 2. Conversely, for the aggregated model with control signals, the NMAE values are 14.39% for scenario 1 and 16.88% for scenario 2. A notable difference in NMAE values is evident between the aggregated model with and without control signals, particularly for the case of scenario 1. The NMAE value for the aggregated model with control signals in scenario 1 is nearly 2.5 times that of the aggregated model without control signals. This discrepancy is reasonable to expect, given that the aggregated model with control signals aims to provide an average estimation of thermal power consumption rather than precisely mirroring the intricate trends exhibited by the unit model's thermal power consumption curve. Nevertheless, it is observable that the aggregated model's performance is stronger when control signals are not applied.

Subsequent to Table 33, Figure 35 (a, b, c, d) delves into the sensitivity of NMAE concerning average power consumption by varying one parameter ($P_{heating\text{-}avg}$, $T_{set\text{-}avg}$, $T_{out\text{-}avg}$ and C_{cloud}) while maintaining

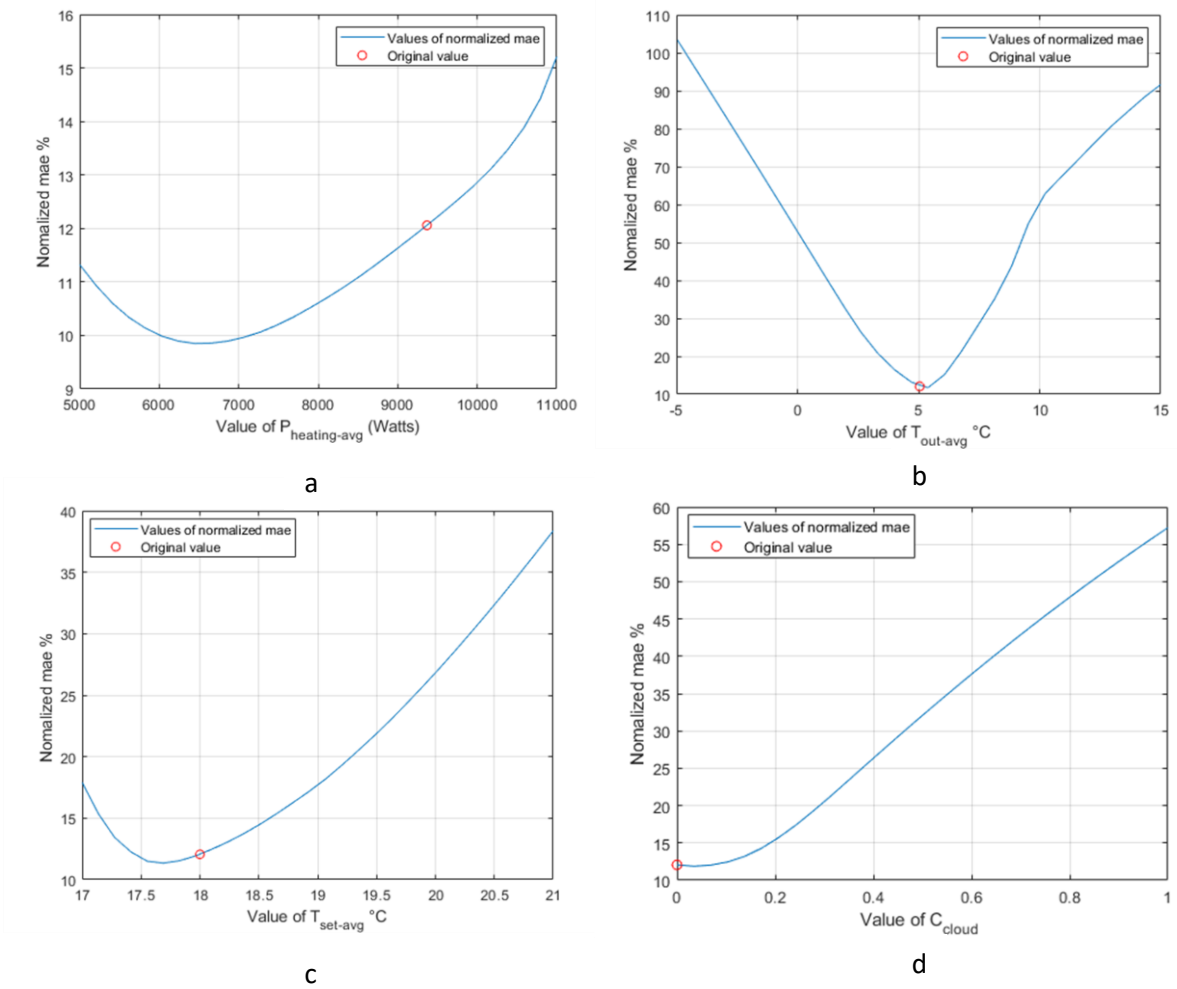

Figure 57: The sensibility of NMAE when we vary the value of 1 value in $P_{avg\text{-}heating}$, $T_{out\text{-}avg}$, $T_{set\text{-}heating}$ and C_{cloud} and keep the values of the other three for 10,000 heating systems.

the other three parameters constant for 10,000 heating systems. These figures illustrate how altering a specific parameter impacts the accuracy of the aggregated model, as reflected by the NMAE.

The primary objective of this sensitivity analysis is to quantitatively assess the impact of uncertain or imprecise knowledge about the average characteristics of the heating system stock on the performance of the aggregated model. To achieve this, a systematic approach is employed where the aggregated model is simulated while varying each parameter within a specified range. The output of this varied aggregated model is then compared with the output of the unit model, which maintains a consistent set of initial parameters ($P_{heating\text{-}avg}$, $T_{set\text{-}avg,}$ $T_{out\text{-}avg}$ and C_{cloud}). consider the scenario involving 10,000 heating systems. The initial parameter values ($P_{heating\text{-}avg}$, $T_{set\text{-}avg,}$ $T_{out\text{-}avg}$ and C_{cloud}) are set to (9367, 18, 5.1, 0). Therefore, to test the sensitivity of parameter C_{cloud} on the aggregated model, we vary values of C_{cloud} in range between 0 and 1 while we keep values of $P_{heating\text{-}avg}$, $T_{set\text{-}avg}$ and $T_{out\text{-}avg}$. For each value of C_{cloud}, we run simulation and compare the output of the aggregated model to that of the unit model. The NMAE and of the aggregated model using the initial set of parameter chosen will play a role in defining if the aggregated model is sensitive to the parameter C_{cloud}. Similarity, we execute the same process for other parameters.

The sensitivity analysis performed in Figure 35 (a, b, c, d) serves to quantify the impact of variations in parameter values on the accuracy of the aggregated model's predictions. By systematically altering one parameter at a time while keeping the other parameters constant, we gain insights into how changes in these parameters influence the output of the aggregated model.
In the case of parameter $T_{out\text{-}avg}$, which represents the setting temperature (Figure 35 b), the NMAE values form a curve. Through a variation of Tout-avg across a range from -5°C to 15°C, the corresponding NMAE values exhibit a distinct curve-like pattern. This curve reaches its minimum point at approximately 5.1°C, resulting in an NMAE value of 12% for a scenario involving 10,000 households. However, as $T_{out\text{-}avg}$ diverges from this optimal point, the NMAE values gradually increase. Particularly, at an extreme value of -5°C, the NMAE value escalates to 135%.This observation underscores the sensitivity of the aggregated model to changes in the $T_{out\text{-}avg}$ parameter. This analysis highlights the need for an appropriate value of $T_{out\text{-}avg}$ to ensure the highest level of predictive accuracy in the aggregated model's outcomes. $T_{out\text{-}avg}$ is the average outdoor temperature over the period under consideration, hence, for the operational use of this model, this variable will be linked to the weather forecast.

Additionally, a same trend is observed when analyzing the sensitivity of the aggregated model to the parameter $T_{set\text{-}avg}$ (Figure 35 c). By varying $T_{set\text{-}avg}$ is varied from 17°C to 21°C. The NMAE values also form a curve, with the minimum NMAE occurring at approximately 17.6°C. This indicates that

the aggregated model is sensitive to changes in the $T_{set\text{-}avg}$ parameter. This parameter is linked to the habit of the users. We would expect an error in choosing the value of $T_{set\text{-}avg}$ is not greater than 1°C.

For the parameter C_{cloud} (Figure 35 d), it is necessary to note that the value of C_{cloud} is always larger or equals 0 and never excess 1. We can see that if value chosen for C_{cloud} is far away from the initial value (representing a good value as the input for the aggregated model), the NMAE rises significantly. Again, this parameter is dependent on weather condition. Hence, the uncertainty of C_{cloud} is related to the accuracy of the weather forecasts.

Conversely, the parameter $P_{heating\text{-}avg}$ (average thermal power) exhibits a relatively less sensitive trend (Figure 35 a). The NMAE values increase only slightly as $P_{heating\text{-}avg}$ deviates from the optimal point, which is around 6500W. This shows that the aggregated model is relatively less sensitive to changes in the $P_{heating\text{-}avg}$ parameter compared to $T_{set\text{-}avg}$, $T_{out\text{-}avg}$ and C_{cloud}. Nevertheless, we can draw the conclusion that the aggregated model still demonstrates consistent and acceptable performance in estimating thermal power consumption. The value of $P_{heating\text{-}avg}$ can be obtained in [102]

As mention earlier, using heat pump data from manufacturers [28], [29], each type of heating system is corresponding to a set of c_0 and c_1. The values of $c_{0\text{-}agg}$ and $c_{1\text{-}agg}$ is calculated by taking the average of all values of c_0 and c_1, respectively. Therefore, the COP_{agg} for each time step is defined (see section 11).
As a result, the electrical power consumption of the aggregated power is defined as follow:
$P_{heat-residential}(i) = P_{heat(i)} / COP_{agg}(i)$ with i is the i^{th} time step.

14. Conclusion

The aggregated model featuring heating systems can describe the behavior of power usage for heating in residential without applying control signal options. The aggregated model with control signal is still needed to be improved but still can be helpful since it creates a premise for the next step in research. The generated aggregated model allows to access the power consumption for heating in residential for a large scale with saving computation time. The simulation time of the aggregated model is only 0.2 seconds, 2150 times faster than the simulation of the unit model, which takes 430 seconds for 10,000 houses. Computation time reported here are the times taken by MATLAB R2019b in running a simulation for 7 days with time step of 10 minutes in a Dell PC with an Intel(R) Core(TM) i5-8265U CPU at 1.60GHz. Besides, we can quantify flexibility for the aggregation of multiple heating systems by testing different control strategies with it. In addition, like aggregated model for domestic hot water, this aggregated model can contribute to reinforcing the development of smart buildings and smart cities, in which demand-side flexibility plays a role in optimizing the implementation of multiple energy sources. Since the dynamics of flexibilities of heating in

residential are very different from those of storage tanks, the combination of these two models gives a better estimate of flexibilities for a wider range of times during the day.

15. Limitation of the aggregated model

The aggregated model nevertheless has a few limitations:

- The data about characteristics of the house is based on the data of 18 houses in reference, which lead to the fact that the proposed aggregated model is only able to describe the power consumption of a specific region. To apply this model to represent the power consumption for heating systems in other regions across France, further extensive studies and adaptations would be necessary. Unfortunately, due to the constraints of the thesis timeframe, we are concluding our investigation here. However, this opens up opportunities for future research and perspectives in this area, where more comprehensive models could be developed to address power consumption variations in different regions of France.
- The presence of errors in the aggregated power consumption with control signals compared to the unit model is attributable to the simplifying assumption concerning the quadratic relationship between average thermal power and internal temperature.
- Additionally, beyond the average parameters considered in this chapter, there might be other influential factors that contribute to the construction and accuracy of the aggregated model, such as thermal capacity of the internal air and thermal capacity of the wall. The complexity of residential heating systems and their interactions with various external factors could introduce additional variables that affect thermal power consumption

16. Perspective

In future research, the proposed aggregated model can be studied to have better representation of heating in residential, which is more presentative the power consumption is various region. Besides, minimize the errors for aggregated models could be a possible way of research to enhance the accuracy of the model.

ANNEX I : Model 6R2C in detail

As described in the section 2, the energy balance of the model 6R2C can be presented as follow:

$$C_{int}\frac{dT_{int}}{dt} = \frac{T_{ext} - T_{int}}{R_{fi}} + \frac{T_{si} - T_{int}}{R_{si}} + \Phi_{int}$$

$$0 = \frac{T_{int} - T_{si}}{R_{si}} + \frac{T_m - T_{si}}{R_{m12}} + \Phi_{si}$$

$$C_m\frac{dT_m}{dt} = \frac{T_{si} - T_m}{R_{m12}} + \frac{T_{se} - T_m}{R_{m22}} + \Phi_m$$

$$0 = \frac{T_m - T_{se}}{R_{m22}} + \frac{T_{ext} - T_{se}}{R_{se}} + \frac{T_{sky} - T_{se}}{R_{sky}} + \Phi_{se}$$

These above differential equations can be represented in a matrix form as:

$$\begin{vmatrix} T_{int}(t) \\ T_m(t) \end{vmatrix} = \begin{vmatrix} A_1 & A_2 \\ A_3 & A_4 \end{vmatrix} \cdot \begin{vmatrix} T_{int}(t-1) \\ T_m(t-1) \end{vmatrix} + \begin{vmatrix} B_1 & B_2 & B_3 & B_4 & B_5 & B_6 \\ B_7 & B_8 & B_9 & B_{10} & B_{11} & B_{12} \end{vmatrix} \cdot \begin{vmatrix} T_{ext}(t-1) \\ T_{sky}(t-1) \\ \Phi_{int}(t-1) \\ \Phi_{si}(t-1) \\ \Phi_m(t-1) \\ \Phi_{se}(t-1) \end{vmatrix}$$

Here

$$A_1 = \frac{1}{C_{int}}\left(\frac{\frac{1}{R_{si}^2}}{\frac{1}{R_{si}}+\frac{1}{R_{m12}}} - \frac{1}{R_{fi}} - \frac{1}{R_{si}}\right)\Delta t + 1$$

$$A_2 = \frac{1}{C_{int}}\left(\frac{\frac{1}{R_{si}}\cdot\frac{1}{R_{m12}}}{\frac{1}{R_{si}}+\frac{1}{R_{m12}}}\right)\Delta t$$

$$A_3 = \frac{1}{C_m}\frac{\frac{1}{R_{si}}\cdot\frac{1}{R_{m12}}}{\frac{1}{R_{si}}+\frac{1}{R_{m12}}}\Delta t$$

$$A_4 = \frac{1}{C_m}\left(\frac{\frac{1}{R_{m12}^2}}{\frac{1}{R_{si}}+\frac{1}{R_{m12}}} - \frac{1}{R_{m12}} - \frac{1}{R_{m22}} + \frac{\frac{1}{R_{m22}^2}}{\frac{1}{R_{se}}+\frac{1}{R_{m22}}+\frac{1}{R_{sky}}}\right)\Delta t + 1$$

$$B_1 = \frac{1}{C_{int}}\frac{1}{R_{fi}}\Delta t$$

$$B_2 = 0$$

$$B_3 = \frac{1}{C_{int}}\Delta t$$

$$B_4 = \frac{1}{C_{int}}\frac{\frac{1}{R_{si}}}{\frac{1}{R_{si}}+\frac{1}{R_{m12}}}\Delta t$$

$$B_5 = 0$$

$$B_6 = 0$$

$$B_7 = \frac{1}{C_m} \frac{\frac{1}{R_{m22}} \cdot \frac{1}{R_{se}}}{\frac{1}{R_{se}} + \frac{1}{R_{m22}} + \frac{1}{R_{sky}}} \Delta t$$

$$B_8 = \frac{1}{C_m} \frac{\frac{1}{R_{m22}} \cdot \frac{1}{R_{sky}}}{\frac{1}{R_{se}} + \frac{1}{R_{m22}} + \frac{1}{R_{sky}}} \Delta t$$

$$B_9 = 0$$

$$B_{10} = \frac{1}{C_m} \frac{\frac{1}{R_{m12}}}{\frac{1}{R_{si}} + \frac{1}{R_{m12}}} \Delta t$$

$$B_{11} = \frac{1}{C_m} \Delta t$$

$$B_{12} = \frac{1}{C_m} \frac{\frac{1}{R_{m22}}}{\frac{1}{R_{se}} + \frac{1}{R_{m22}} + \frac{1}{R_{sky}}} \Delta t$$

ANNEX J : The specific adjustments made to 18 coefficient sets

$$\begin{vmatrix} T_{int}(t) \\ T_m(t) \end{vmatrix} = \begin{vmatrix} A_1 & A_2 \\ A_3 & A_4 \end{vmatrix} \cdot \begin{vmatrix} T_{int}(t-1) \\ T_m(t-1) \end{vmatrix} + \begin{vmatrix} B_1 & B_2 & B_3 & B_4 & B_5 & B_6 \\ B_7 & B_8 & B_9 & B_{10} & B_{11} & B_{12} \end{vmatrix} \cdot \begin{vmatrix} T_{ext}(t-1) \\ T_{sky}(t-1) \\ \Phi_{int}(t-1) \\ \Phi_{si}(t-1) \\ \Phi_m(t-1) \\ \Phi_{se}(t-1) \end{vmatrix}$$

Look at the equation,

For the inter temperature T_{int}, which is calculated by

$$T_{int}(t) = A_1 * T_{int}(t-1) + A_2 * T_m(t-1) + B_1 * T_{ext}(t-1) + B_2 * T_{sky}(t-1) + B_3 * \Phi_{int}(t-1) + B_4 * \Phi_{si}(t-1) + B_5 * \Phi_m(t-1) + B_6 * \Phi_{se}(t-1)$$

For the wall temperature T_m, which is calculated by

$$T_m(t) = A_3 * T_{int}(t-1) + A_4 * T_m(t-1) + B_7 * T_{ext}(t-1) + B_8 * T_{sky}(t-1) + B_9 * \Phi_{int}(t-1) + B_{10} * \Phi_{si}(t-1) + B_{11} * \Phi_m(t-1) + B_{12} * \Phi_{se}(t-1)$$

Look at the Table 34, there are some values of A_4 having their values equals 1, which causes the problem that T_m will continue increasing. And the fact that the wall temperature keep increase plus to the value of A_1 are also close to 1, which also cause internal temperature increase as well and it can make the internal temperature rises up to 30°C when the outdoor temperature is lower than 5°C, which is far away from the reality. In order to address this problem, we do some modification.

If we consider the wall have thermal resistance is R_m, then the thermal balance equation is represented as follows

$$C_{int}\frac{dT_{int}}{dt} = \frac{T_{ext} - T_{int}}{R_{fi}} + \frac{T_m - T_{int}}{R_m} + \Phi_{int}$$

We then have:

$$C_{int}.\frac{\Delta T_{int}}{\Delta t} = \frac{T_{ext} - T_{int}}{R_{fi}} + \frac{T_m - T_{int}}{R_m} + \Phi_{int}$$

$$T_{int}(t) - T_{int}(t-1) = \frac{\Delta t}{C_{int}}\left(\frac{T_{ext}(t-1) - T_{int}(t-1)}{R_{fi}} + \frac{T_m(t-1) - T_{int}(t-1)}{R_m} + \Phi_{int}(t-1)\right)$$

$$T_{int}(t) = T_{int}(t-1)\left(1 - \frac{\Delta t}{C_{int}R_{fi}} - \frac{\Delta t}{C_{int}R_m}\right) + \frac{\Delta t}{C_{int}R_{fi}}T_{ext}(t-1) + \frac{\Delta t}{C_{int}R_m}T_m(t-1)$$

Look at this equation transformation,

The coefficient for $T_{int}(t-1)$ is $\left(1 - \frac{\Delta t}{C_{int}R_{fi}} - \frac{\Delta t}{C_{int}R_{si}}\right)$ which is associated to A_1

The coefficient for $T_m(t-1)$ is $\left(\frac{\Delta t}{C_{int}R_m}\right)$ which is associated to A_2

The coefficient for $T_{ext}(t-1)$ is $\left(\frac{\Delta t}{C_{int}R_{fi}}\right)$ which is associated to B_1

We can see that $A_1+A_2+B_1 = 1$

Hence, for the set of coefficients A_1 in Table 34 is replaced by $1- A_2- B_1$

We did the same approach for the coefficient A_4 for the equation used for calculating the wall temperature. The modification that we did is recalculate $A_4 =1- A_3- B_7$

House	Matrix A	Matrix B
1	$\begin{vmatrix} 0.835 & 0.165 \\ 2.98.10^{-5} & 1 \end{vmatrix}$	$\begin{vmatrix} 2.17.10^{-4} & 1.31.10^{-8} & 1.05.10^{-4} & -2.90.10^{-5} & 0 & 1.80.10^{-11} \\ 6.31.10^{-6} & 1.54.10^{-7} & 1.76.10^{-9} & 2.60.10^{-8} & 0 & 2.15.10^{-10} \end{vmatrix}$
2	$\begin{vmatrix} 0.835 & 0.165 \\ 3.87.10^{-5} & 1 \end{vmatrix}$	$\begin{vmatrix} 1.55.10^{-4} & 2.08.10^{-8} & 1.00.10^{-4} & 9.05.10^{-6} & 0 & 1.85.10^{-11} \\ 1.05.10^{-5} & 2.45.10^{-7} & 2.18.10^{-9} & 2.36.10^{-8} & 0 & 2.18.10^{-10} \end{vmatrix}$
3	$\begin{vmatrix} 0.831 & 0.169 \\ 5.69.10^{-5} & 1 \end{vmatrix}$	$\begin{vmatrix} 2.06.10^{-4} & 6.80.10^{-8} & 1.22.10^{-4} & 5.85.10^{-6} & 0 & 3.88.10^{-11} \\ 1.48.10^{-5} & 7.81.10^{-7} & 3.91.10^{-9} & 4.30.10^{-8} & 0 & 4.46.10^{-10} \end{vmatrix}$
4	$\begin{vmatrix} 0.828 & 0.171 \\ 3.09.10^{-5} & 1 \end{vmatrix}$	$\begin{vmatrix} 2.50.10^{-4} & 5.48.10^{-8} & 1.05.10^{-4} & 2.80.10^{-5} & 0 & 2.37.10^{-11} \\ 7.07.10^{-6} & 6.20.10^{-7} & 1.85.10^{-9} & 1.59.10^{-8} & 0 & 2.68.10^{-10} \end{vmatrix}$
5	$\begin{vmatrix} 0.816 & 0.184 \\ 4.53.10^{-5} & 1 \end{vmatrix}$	$\begin{vmatrix} 2.73.10^{-4} & 5.69.10^{-8} & 1.30.10^{-4} & 2.69.10^{-6} & 0 & 3.30.10^{-11} \\ 1.02.10^{-5} & 5.99.10^{-7} & 3.36.10^{-9} & 3.47.10^{-8} & 0 & 3.47.10^{-10} \end{vmatrix}$
6	$\begin{vmatrix} 0.823 & 0.176 \\ 5.51.10^{-5} & 1 \end{vmatrix}$	$\begin{vmatrix} 1.34.10^{-4} & 2.89.10^{-8} & 9.16.10^{-5} & 7.39.10^{-6} & 0 & 2.14.10^{-11} \\ 1.15.10^{-5} & 3.17.10^{-7} & 2.87.10^{-9} & 2.92.10^{-8} & 0 & 2.35.10^{-10} \end{vmatrix}$
7	$\begin{vmatrix} 0.841 & 0.159 \\ 7.79.10^{-5} & 1 \end{vmatrix}$	$\begin{vmatrix} 1.12.10^{-4} & 3.24.10^{-9} & 7.07.10^{-5} & 7.40.10^{-6} & 0 & 7.63.10^{-13} \\ 1.76.10^{-6} & 3.97.10^{-8} & 3.09.10^{-10} & 3.42.10^{-9} & 0 & 9.35.10^{-12} \end{vmatrix}$
8	$\begin{vmatrix} 0.901 & 0.099 \\ 1.20.10^{-5} & 1 \end{vmatrix}$	$\begin{vmatrix} 2.05.10^{-4} & 4.34.10^{-9} & 9.09.10^{-5} & 5.80.10^{-6} & 0 & 3.09.10^{-12} \\ 4.97.10^{-6} & 8.66.10^{-8} & 5.82.10^{-10} & 1.09.10^{-8} & 0 & 6.16.10^{-11} \end{vmatrix}$
9	$\begin{vmatrix} 0.822 & 0.177 \\ 4.16.10^{-5} & 1 \end{vmatrix}$	$\begin{vmatrix} 2.76.10^{-4} & 2.53.10^{-8} & 1.03.10^{-4} & 1.51.10^{-6} & 0 & 1.53.10^{-11} \\ 8.67.10^{-6} & 2.76.10^{-7} & 2.44.10^{-9} & 2.63.10^{-8} & 0 & 1.67.10^{-10} \end{vmatrix}$
10	$\begin{vmatrix} 0.831 & 0.169 \\ 2.98.10^{-5} & 1 \end{vmatrix}$	$\begin{vmatrix} 1.37.10^{-4} & 1.55.10^{-8} & 7.70.10^{-5} & 1.24.10^{-5} & 0 & 8.34.10^{-12} \\ 6.45.10^{-6} & 1.78.10^{-7} & 1.29.10^{-9} & 1.26.10^{-8} & 0 & 9.58.10^{-11} \end{vmatrix}$
11	$\begin{vmatrix} 0.827 & 0.173 \\ 2.98.10^{-5} & 1 \end{vmatrix}$	$\begin{vmatrix} 2.84.10^{-4} & 4.50.10^{-8} & 1.16.10^{-4} & -4.65.10^{-6} & 0 & 1.26.10^{-11} \\ 8.33.10^{-6} & 5.06.10^{-7} & 2.57.10^{-9} & 2.99.10^{-8} & 0 & 1.41.10^{-10} \end{vmatrix}$
12	$\begin{vmatrix} 0.829 & 0.170 \\ 2.98.10^{-5} & 1 \end{vmatrix}$	$\begin{vmatrix} 2.22.10^{-4} & 1.31.10^{-8} & 1.02.10^{-4} & 7.55.10^{-6} & 0 & 2.82.10^{-11} \\ 8.16.10^{-6} & 1.50.10^{-7} & 1.81.10^{-9} & 1.93.10^{-8} & 0 & 3.21.10^{-10} \end{vmatrix}$
13	$\begin{vmatrix} 0.861 & 0.139 \\ 2.98.10^{-5} & 1 \end{vmatrix}$	$\begin{vmatrix} 1.77.10^{-4} & 3.46.10^{-8} & 8.08.10^{-5} & 1.46.10^{-5} & 0 & 1.80.10^{-11} \\ 1.29.10^{-5} & 4.84.10^{-7} & 2.26.10^{-9} & 2.64.10^{-8} & 0 & 2.53.10^{-10} \end{vmatrix}$
14	$\begin{vmatrix} 0.842 & 0.158 \\ 2.98.10^{-5} & 1 \end{vmatrix}$	$\begin{vmatrix} 1.77.10^{-4} & 4.58.10^{-9} & 1.04.10^{-4} & 1.11.10^{-5} & 0 & 1.69.10^{-11} \\ 8.27.10^{-6} & 5.63.10^{-8} & 1.93.10^{-9} & 2.14.10^{-8} & 0 & 2.08.10^{-10} \end{vmatrix}$
15	$\begin{vmatrix} 0.828 & 0.172 \\ 2.98.10^{-5} & 1 \end{vmatrix}$	$\begin{vmatrix} 2.72.10^{-4} & 3.31.10^{-8} & 1.07.10^{-4} & 9.46.10^{-6} & 0 & 2.49.10^{-11} \\ 9.80.10^{-6} & 3.74.10^{-7} & 2.68.10^{-9} & 2.79.10^{-8} & 0 & 2.82.10^{-10} \end{vmatrix}$
16	$\begin{vmatrix} 0.825 & 0.174 \\ 2.98.10^{-5} & 1 \end{vmatrix}$	$\begin{vmatrix} 1.56.10^{-4} & 6.50.10^{-9} & 1.24.10^{-4} & 1.46.10^{-5} & 0 & 5.65.10^{-12} \\ 3.36.10^{-6} & 7.22.10^{-8} & 1.02.10^{-9} & 1.01.10^{-8} & 0 & 6.27.10^{-11} \end{vmatrix}$
17	$\begin{vmatrix} 0.839 & 0.161 \\ 2.98.10^{-5} & 1 \end{vmatrix}$	$\begin{vmatrix} 9.11.10^{-4} & 7.41.10^{-9} & 6.38.10^{-5} & -1.30.10^{-5} & 0 & 4.35.10^{-12} \\ 5.25.10^{-6} & 8.92.10^{-8} & 8.08.10^{-10} & 1.15.10^{-8} & 0 & 5.23.10^{-11} \end{vmatrix}$
18	$\begin{vmatrix} 0.832 & 0.168 \\ 2.98.10^{-5} & 1 \end{vmatrix}$	$\begin{vmatrix} 2.67.10^{-4} & 8.83.10^{-9} & 1.05.10^{-4} & 1.35.10^{-5} & 0 & 6.15.10^{-12} \\ 5.14.10^{-6} & 1.02.10^{-7} & 1.06.10^{-9} & 1.08.10^{-8} & 0 & 7.11.10^{-11} \end{vmatrix}$

Table 34: 18 sets of coefficients of A1 to A4 and B1 to B12 before the adjustment of A1 and A4

ANNEX K : Sets of matrixes A_{agg} and matrix B_{agg} for the aggregated model

We have18 sets of coefficients for matrix A with 4 values A1 to A4 and matrix B with 12 values B1 to B12 with their calculation methods detailed in ANNEX I. However, we encounter a limitation stemming from our references; we lack values for the parameters (C_{int}, C_m, R_{fi}, R_{si}, R_{m12}, R_{m22}, R_{se}, R_{sky}) for each house. H To address this and derive average values representing thermal properties for our aggregated model; we need to recalculate these parameters for each house

This can be achieved by substituting the values of matrix A and matrix B into the equations provided in ANNEX I. This process yields parameter values (C_{int}, C_m, R_{fi}, R_{si}, R_{m12}, R_{m22}, R_{se}, R_{sky}) for each house.

The average values for the aggregated model parameters ($C_{int-avg}$, C_{m-avg}, R_{fi-avg}, R_{si-avg}, $R_{m12-avg}$, $R_{m22-avg}$, R_{se-avg}, $R_{sky-avg}$) are then defined by calculating the mean of their respective elements across all houses

For example:

$$C_{int-avg} = mean\left(\sum_{1}^{H} C_{int}\right)$$

Where H represents the total number of houses considered. Similar calculations are performed for the other parameters. Consequently, we have values of set ($C_{int-avg}$, C_{m-avg}, R_{fi-avg}, R_{si-avg}, $R_{m12-avg}$, $R_{m22-avg}$, R_{se-avg}, $R_{sky-avg}$) for the aggregated model and by using the equations in ANNEX I, we have all values for matrix A_{agg} and matrix B_{agg}.

ANNEX L: Find $C_{int-avg}$, C_{m-avg}, R_{fi-avg}, R_{si-avg}, $R_{m12-avg}$, $R_{m22-avg}$, R_{se-avg}, $R_{sky-avg}$ from the available source of data

- R_{si-avg} represents thermal resistance associated to the convective heat transfer between internal air and inner side of the wall. The value of R_{si} can be obtained from the report of Ministry of Ecological Transition [103]
- R_{se-avg} represents thermal resistance associated to the convective heat transfer between external air and outer side of the wall. The value of R_{se} can be also obtained from the same report of Ministry of Ecological Transition [103]
- $R_{m12-avg}$ and $R_{m22-avg}$ represents the conduction heat transfer between both sides of the wall capacity. These two values can be achieved from references [104], [105]. In these references, it is mentioned that, according to "Réglementation Thermique (RT) 2012", thermal resistance R_{m12-}

$_{avg}$ should be around 4 m^2K/W while thermal resistance $R_{m22\text{-}avg}$ should achieve a value higher or equal to 2.9 m^2K/W

- $R_{sky\text{-}avg}$ presents infrared radiation between outer wall and environment. This value can be obtain using approach in reference [106].
- For $C_{int\text{-}avg}$, $C_{m\text{-}avg}$, $R_{fi\text{-}avg}$
  - $R_{fi\text{-}avg}$ represents the heat transfer through low inertia elements (glazing and doors).
  - $C_{m\text{-}avg}$ represent thermal capacitance of the wall.
  - $C_{int\text{-}avg}$ represents thermal capacitance of the internal air.

These three parameters require a more detailed investigation. To gather the necessary data, we have compiled information from various sources, providing us with a comprehensive list of different house typologies in France, along with their distribution across different regions. Reference [107] has furnished us with data on distinct house typologies in the Auvergne – Rhone – Alpes region, including the percentage of each typology. Additionally, reference [108] has provided detailed characteristics for each typology, encompassing area, wall materials, heat transfer coefficients for walls and glazing, and door specifications.

We have constructed an Excel file to consolidate all this information, covering various regions in France such as Auvergne – Rhone – Alpes, Bourgogne-Franche-Comté, Bretagne, Centre-Val-de-Loire, Corse, Grand-Est, Hauts de France, Ile de France, Normandie, Nouvelle Aquitaine, Occitanie, Pays de la Loire, Provence-Alpes-Côte d'Azur. This file comprehensively lists each typology, including all associated characteristics.

With the percentage distribution of each typology within a region and knowledge of the wall material for each typology, we can determine the thermal capacitance of the walls for each typology, leveraging information from reference [109]. This calculation yields the value of $C_{m\text{-}avg}$.

Utilizing information about the heat transfer coefficients of glazing and doors for each typology, we can establish the value of $R_{fi\text{-}avg}$.

To calculate the value of $C_{int\text{-}avg}$, we employ data pertaining to the wall, roof, and floor areas. These values are used to compute the volume of each house. $C_{int\text{-}avg}$ is then defined by $V * \rho * c_p$, where V represents the house's volume in cubic meters (m^3), ρ denotes the density of air in kilograms per cubic meter (kg/m^3), and c_p signifies the specific heat capacity of air in joules per kilogram per degree Kelvin (J/kgK).

ANNEX M : Finding the relation between average thermal power consumption and internal temperature

To find the relationship between the average thermal power consumption and internal temperature, the unit model is obtained by repeating the simulation of the heating system for different houses without and with control signals, which includes the peak hours from 10 to 12 o'clock and from 18 to 22 o'clock, the other hours are considered as off-peak hours. Which means that during the peak hours, we will turn of all the heating system and only turn them on during the off-peak hours. Figure 58 presents the simulation for 3 days with the time step of 10 minute is done for 5000 households.

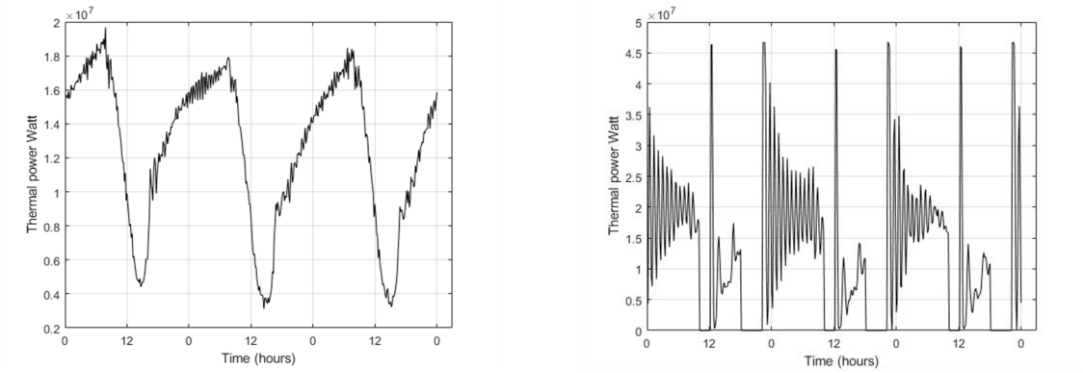

a *b*

Figure 58: (a,b), describe the thermal power consumption for heating of 5,000 households without and with control signals, respectively

Within the unit model with and without off-peak hours control signal, each household has its own thermal power consumption. Hence, for each heating system at each time step, we have one value of thermal power along with one value of internal temperature. Figure 59 illustrates the relation between the average thermal power and internal temperature of 5,000 heating systems at each time step, combining both result from simulation of the unit model without and with control signals. The black dots represent the average thermal power and average internal temperature obtained from the simulation of the unit model.

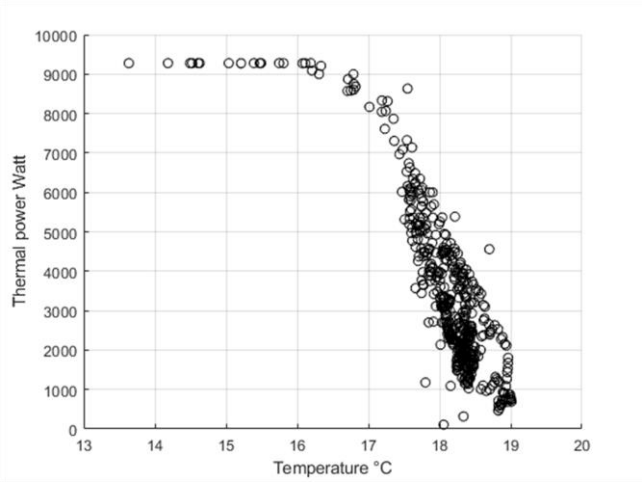

Figure 59: The relation between the average thermal power consumed (kW) and average internal temperature of 5000 heating systems in each time step

Figure 59 shows that the total power and average internal temperature has a relation that follows a form of a quadratic equation.

ANNEX N: Finding the functions for $P_{avg\text{-}agg}$, $T_{lb\text{-}heating}$ and $T_{hb\text{-}heating}$

As mentioned, the idea for generating the aggregated model for heating is to define the relationship curve between average thermal power consumption and average internal temperature as a quadratic function (Figure 60). Now, we want to define $P_{avg\text{-}agg}$, $T_{lb\text{-}heating}$ and $T_{hb\text{-}heating}$ as function of some average parameters regarding heating system characteristics and weather, including average outdoor temperature $T_{out\text{-}avg}$, average setting temperature $T_{set\text{-}avg}$, cloud cover coefficient C_{cloud} and average heating system thermal power $P_{heating\text{-}avg}$.

Following this idea, $P_{avg\text{-}agg}$ is chosen as the average heating system thermal power $P_{heat\text{-}avg}$

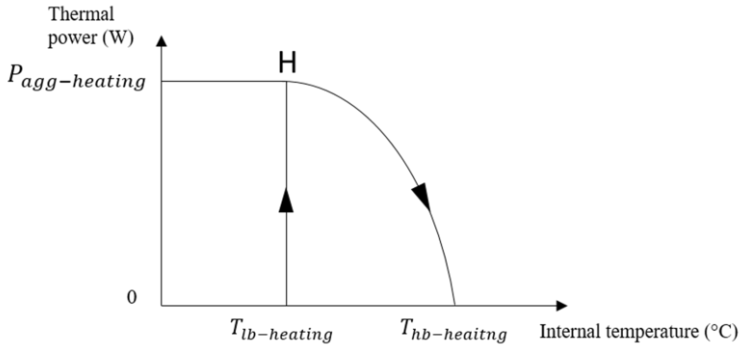

Figure 60 : The relation curve between the average thermal power (W) and the internal temperature for the aggregated model

$$P_{avg\text{-}agg} = P_{heat\text{-}avg}$$

$T_{hb\text{-}heating}$ is defined by the linear function of $P_{heating\text{-}avg}$, $T_{set\text{-}avg,}$ $T_{out\text{-}avg}$,C_{cloud}

$$T_{hb\text{-}heating} = function(P_{heating\text{-}avg}, T_{set\text{-}avg,} T_{out\text{-}avg},C_{cloud})$$

$T_{lb\text{-}heating}$ is given by the linear function of $P_{heating\text{-}avg}$, $T_{set\text{-}avg,}$ $T_{out\text{-}avg}$,C_{cloud}

$$T_{lb\text{-}heating} = function(P_{heating\text{-}avg}, T_{set\text{-}avg,} T_{out\text{-}avg},C_{cloud})$$

In order to find the coefficients for the function of $T_{hb\text{-}heating}$ and $T_{lb\text{-}heating}$, simulation of the unit model is done for different numbers of heating systems and different values of $P_{avg\text{-}heating}$, $T_{set\text{-}heating,}$ $T_{avg\text{-}out}$, C_{cloud} so as to obtain the different values of $T_{lb\text{-}heating}$. We investigate 4 cases corresponding to different numbers of heating systems (see Table 35).

Number of heating systems	$P_{heating\text{-}avg}$ (W)	$T_{out\text{-}avg}$ (°C)	$T_{set\text{-}avg}$ (°C)	C_{cloud}
3,000	14,500	[0.6, 5.6, 10.6]	[18,19,20,21]	[0, 0.5, 1]
5,000	14,149			
7,000	11,321			
10,000	13,292			

Table 35: The value of $P_{avg\text{-}heating}$, $T_{avg\text{-}out}$, $T_{set\text{-}heating}$ and C_{cloud} for different numbers of heating systems

The choice of $T_{hb\text{-}heating}$ is defined as the point which have the maximum internal temperature.
The choice of $T_{lb\text{-}heating}$ is determined as follows (Figure 61): For each point representing the relationship between total thermal power consumption and average internal temperature, we take the average of all points, which are inside the range (T_w-ΔT, T_w+ΔT). In this study, we set ΔT equals 0.2. After having modified curve, the value of $T_{lb\text{-}heating}$ takes the value of the point, which have the second largest power consumption and the lowest average internal temperature. Thes values of $T_{lb\text{-}heating}$ and $T_{hb\text{-}heating}$ are obtained following a simulation with the unit model for 1 given scenario. It is not the $T_{lb\text{-}heating}$ and $T_{hb\text{-}heating}$ of the aggregate model. Then, via the numerous scenarios simulated with the unit model and linear regression, we have an equation for the $T_{lb\text{-}heating}$ and $T_{hb\text{-}heating}$ of the aggregate model, expressed as a function of average parameters ($P_{heating\text{-}avg}$, $T_{set\text{-}avg,}$ $T_{out\text{-}avg}$,C_{cloud}).

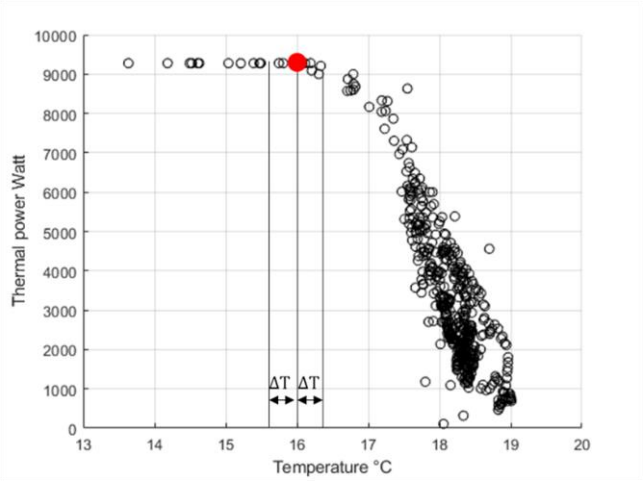

Figure 61: The relation between the average thermal power consumed (kW) and average internal temperature of 5000 heating systems in each time step

From the simulations of 4 cases, along with the variation of $P_{avg\text{-}heating}$ (4 values), $T_{set\text{-}heating}$ (4 values), $T_{avg\text{-}out}$ (3 values) and C_{cloud} (3 values), 144 values of $T_{hb\text{-}heating}$ and $T_{lb\text{-}heating}$ are obtained. A fitted linear regression model is used to identify the coefficients for the functions of $T_{hb\text{-}heating}$ and $T_{lb\text{-}heating}$. Figure 63 and Figure 62 demonstrate 144 values of $T_{hb\text{-}heating}$ and $T_{lb\text{-}heating}$, respectively. The black line shows values obtained from simulations of the unit model, while the red line represents the results obtained from a fitted linear regression model.

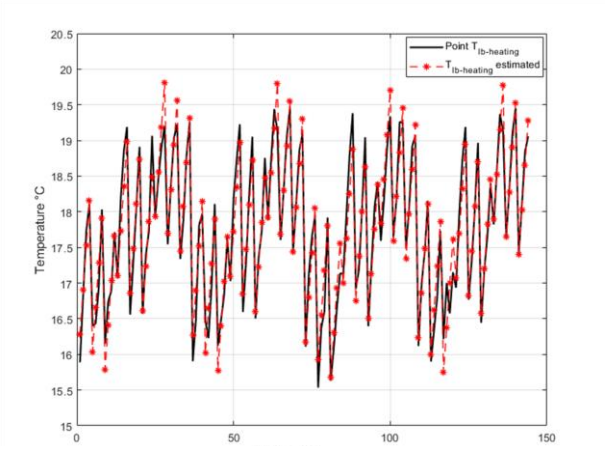

Figure 62: The value of $T_{lb\text{-}heating}$ when changing the values of $P_{avg\text{-}heating}$, $T_{set\text{-}heating}$, $T_{avg\text{-}out}$ and C_{cloud}

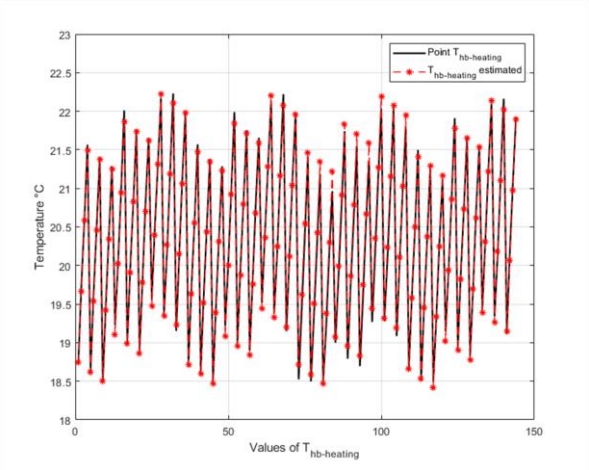

Figure 63 : The value of $T_{hb\text{-}heating}$ when changing the values of $P_{avg\text{-}heating}$, $T_{set\text{-}heating,}$ $T_{avg\text{-}out}$ and C_{cloud}

Hence, the coefficients for $P_{heating\text{-}avg}$, $T_{set\text{-}avg,}$ $T_{out\text{-}avg}$ and C_{cloud} are found and the final equation of $T_{hb\text{-}heating}$ and $T_{lb\text{-}heating}$ are then shown as follows:

$$T_{hb\text{-}heating} = 1.2124 + 6.608.10^{-5} P_{heating\text{-}avg} + 0.9185 T_{set\text{-}avg} + 0.0729 T_{out\text{-}avg} - 0.2440 C_{cloud}$$

$$T_{lb\text{-}heating} = 4.3676 + 3.304.10^{-5} P_{heating\text{-}avg} + 0.6247 T_{set\text{-}avg} + 0.1659 T_{out\text{-}avg} - 0.4933 C_{cloud}$$

ANNEX O : Finding coefficient for h_1, h_2, h_3 for the function to calculate thermal power consumption

As outlined earlier, with the definitions of $P_{avg\text{-}agg}$, $T_{hb\text{-}heating}$ and $T_{lb\text{-}heating}$, along with the assumption of point H as the apex of the quadratic curve, we can formulate the connection between the aggregated model's thermal power $P_{heating}$ for heating and the internal temperature using the following equation:

$$P_{heating} = h_1 T_{int}^{\ 2} + h_2 T_{int} + h_3$$

With the following conditions:

- The point H is the maximum of the quadratic equation.
- If $T_{int} <= T_{lb\text{-}heating}$ then $P_{heating} = P_{avg\text{-}agg}$
- If $T_{int} >= T_{hb\text{-}heating}$ then $P_{heating} = 0$
- h_1, h_2, h_3 are the coefficients, which are calculated by using 3 values of $P_{avg\text{-}agg}$, $T_{hb\text{-}heating}$ and $T_{lb\text{-}}$

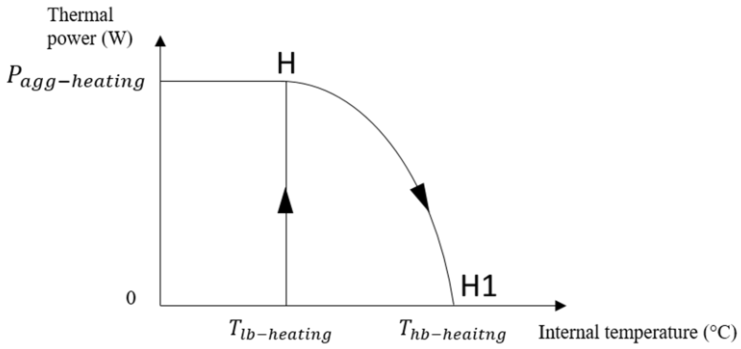

Figure 64 : The relation curve between the average thermal power (W) and the internal temperature for the aggregated model

h_1, h_2, h_3 are the coefficients, which are calculated by using 3 values of $P_{avg\text{-}agg}$, $T_{hb\text{-}heating}$ and $T_{lb\text{-}heating}$ (Figure 64):

We have:

At the point H: $\begin{cases} P_{\text{heating}} = P_{\text{avg-agg}} \\ T_{int} = T_{\text{lb-heating}} \end{cases}$ => $P_{\text{avg-agg}} = h_1 T_{\text{lb-heating}}^{\ 2} + h_2 T_{\text{lb-heating}} + h_3$

At the point H1: $\begin{cases} P_{\text{heating}} = 0 \\ T_{int} = T_{\text{hb-heating}} \end{cases}$ => $0 = h_1 T_{\text{hb-heating}}^{\ 2} + h_2 T_{\text{hb-heating}} + h_3$

Solve this 2 equations, we obtain:

$$h_1 = \frac{-P_{avg-agg}}{(T_{lb-heating} - T_{hb-heating})^2}$$

V. Chapter 4: Applications of the aggregated models in minimizing the electricity cost

Dans ce chapitre, nous avons intégré trois modèles agrégés différents pour traiter la flexibilité énergétique dans les domaines de l'eau chaude sanitaire (ECS), de la recharge des véhicules électriques (EVC) et du chauffage résidentiel (HR). En englobant le comportement combiné des charges résidentielles, ces modèles facilitent l'évaluation de l'impact global de la flexibilité du côté de la demande, contribuant ainsi à l'optimisation de l'utilisation de l'énergie et à la progression d'environnements urbains intelligents et durables. Nous nous concentrons ainsi sur l'exploration de la mise en œuvre pratique des modèles agrégés, proposés dans le but de minimiser les coûts d'électricité dans un délai donné.

In this chapter, we have integrated three different aggregated models to address the energy flexibility within the domains of domestic hot water (DHW), electric vehicle charging (EVC), and heating in residential (HR). These aggregated models, which encapsulate multiple units of electric water heaters (EWHs), electric vehicles (EVs), and heating systems, prove to be versatile and effective tools for analyzing power consumption behaviors in residential settings, regardless of the application of control signals.

The adaptability of these aggregated models allows for their utilization in diverse scenarios and contexts. One application of these models is their ability to quantify and assess the degree of flexibility achievable through the aggregation of multiple units. By testing with various control strategies within the model, the influence of these strategies on residential power consumption can be evaluated. This facilitates a thorough understanding of the efficiency and efficacy of different control approaches across various spatial scales, from smaller districts to extensive cities or even entire regions. Moreover, these aggregated models offer a significant reduction in computation time, resulting in thousands of times faster and more efficient analyses compared to traditional unit-based simulations, especially when dealing with large numbers of households.

Furthermore, the application of these aggregated models extends to the advancement of smart buildings and smart cities. As demand-side flexibility emerges as a pivotal factor in optimal energy management, these aggregated models are tools for integrating and harmonizing multiple energy sources within a smart grid framework. By encompassing the combined behavior of residential loads, these models facilitate an assessment of the holistic impact of demand-side flexibility, contributing to the optimization of energy utilization and the progression of intelligent and sustainable urban environments. In this chapter, our focus shifts towards exploring the practical implementation of the proposed aggregated model with the aim of minimizing electricity costs within a designated timeframe.

1. The case study

Financial factor always play an important role in all the events. When talk about the context of managing electricity consumption, the goal often revolves around curtailing expenses associated with it. In the paradigm of energy aggregation, where intermediaries act as conduits between end-users and the power system, the issue concern becomes minimizing costs while maintaining operational efficiency.

These intermediaries, known as aggregators, operate by offering services to system operators. They respond to orders or signals from the electricity market, essentially acting as mediators in optimizing energy consumption. In this framework, we delve into a case study where the aggregators need a prediction in the power consumption of the residential to respond to the order of the Distributed System Operator. They will provide optimal demand side management (DSM) services to DSOs and consider load shifting schemes aimed at maximizing cost savings to the DSO. They undertake the task of testing different control strategies to minimize electricity costs by treating the electricity price on the SPOT market as a driving factor.

2. Optimization problem formulation

The optimization problem is about minimizing electricity costs. The approach involves strategically cutting off power during specific time intervals in order to reduce costs. However, these actions must satisfy a constraint that ensure the total duration of power-off periods remains within defined limits. The objective lies in an optimization problem where the aggregator seeks to minimize electricity costs through the selection of power-off signals.

The optimization problem is formulated to determine the most effective control signal strategy that achieves the objective of minimizing electricity costs, considering a cut-off duration decided by users. The optimization variable, denoted as S_i, represents the control signal for the i^{th} time step of the chosen period. If S_i equals 1, the power is turned off, and it is turned on only when S_i equals 0. The mathematical representation of the problem is as follows:

Objective: Minimize the total electricity cost during one day

$$\sum_{i=1}^{N} (1 - S_i) * (P_{DHW-i} + P_{EVC-i} + P_{HR-i}) * C_i$$

Where S_i is the control signal at i^{th} time step, $P_{DHW\text{-}i}$ is domestic hot water power consumption at i^{th} time step, $P_{EVC\text{-}i}$ is electric vehicle charging power consumption at i^{th} time step, $P_{HR\text{-}i}$ is heating in residential power consumption at i^{th} time step. P_{DHW}, P_{EVC} and P_{HR} is the power consumption as the output from the aggregated models for DHW, EVC and HR. C_i is the electricity price at i^{th} time step. N is total of time steps in the chosen period.

To tackle this problem, Genetic Algorithm Approach is employed as a heuristic optimization method to search for the optimal control signal strategy, which can give a minimum electricity cost. The utilization of genetic algorithms for consumer planning to curtail electricity expenses has been a topic explored in recent research [9], [110]. GA is particularly advantageous for tackling nonlinear optimization problems due to its capacity for random exploration across multiple potential solutions simultaneously. This approach proves effective, as it relies solely on a fitness function, allowing GA to address complex issues.

In this chapter, the GA is harnessed to discover for the optimal control signal strategy that results in the lowest electricity cost while adhering to predefined constraints. The GA procedure commences with an initial population of potential individuals, each represented as a binary vector. These vectors signify potential control strategies for the aggregated models of DHW, EVC, and HR. The binary values within the vector indicate the scheduling of cut-offs for each time step.

Subsequently, each individual's fitness within the population is evaluated. Fitness measures an individual's effectiveness in achieving the optimization objective. In this context, the fitness metric involves calculating the total electricity cost for the day based on the control strategy proposed by the individual. The GA selects individuals that exhibit superior performance to act as the foundation for generating the next generation, functioning as parents. Over successive generations, the GA method finds the optimal control signal strategy that minimizes overall costs throughout the day.

It is important to note that, in this chapter, the analysis is for a single-day timeframe. Which means that we find the optimal control strategy during one-day only. However, during the processing of the GA method, the objective function of minimizing the electricity cost is under the period of 2 days but the optimal control strategy is only defined during the 1^{st} day. The reason for this choice is that if we consider the temporal limitation of only 1 day, this can lead to an issue where the optimal control signal strategy tends to cut off power towards the end of the day, potentially causing a rebound effect that would carry over to the following day. This scenario could yield unrealistic solutions that do not comprehensively reflect power consumption behaviors, particularly in the period following the power cut-off. The choice of finding the optimal control strategy for 2 days can address this concern. This strategic adjustment enables the consideration of rebound periods that might arise throughout the day when control signals are applied. This approach ensures a more holistic representation of power consumption behaviors and mitigates the impact of the temporal constraint.

In this section, we synergize the three proposed aggregated models for DHW, EVC and HR to find the optimal control strategy in order to minimize the electricity cost for a given number of households within the designated region. This integration of models is referred to as the "**Integrated Aggregated Model**" representing a comprehensive framework that considers the interplay of these three significant residential energy consumption components.

To comprehensively assess the response of the integrated aggregated models and to describe varied outcomes resulting from the optimization problem, in this case study, we investigate different scenarios:

- Scenario 1: The integrated aggregated model tested by using price electricity of 3 different days
- Scenario 2: Change number of cut-off power hours
- Scenario 3: Change the values of input for the integrated aggregated model

Each scenario is discussed further below.

3. The parameters for GA

As mentioned above, the benefit of the Genetic Algorithm in solving optimization problems relies on various parameters, such as population size, the number of generations, mutation rate, and crossover rate. An analysis is done to determine which values of the parameter for GA could be preferable to find the optimal solution while compromising the computational time and GA efficiency.

Consequently, the performance of the GA method is tested by varying with different values for the parameters of population size and number of generations. The crossover rate is set at 75% and the mutation rate is defined at 1%. We vary the value of population size in the range of [50 100 200 250] while the value of the number of the generation is chosen from the set [50 100 200 300], as described in Table 36.

To execute these tests, we use the electricity price of the day 17th Jan 2023, which is mentioned in the Figure 66b. The optimization tests in this chapter is done by using MATLAB R2019b, running on a Dell PC featuring an Intel(R) Core(TM) i5-8265U CPU operating at 1.60GHz.

Parameters de GA	
Population size	[50 100 200 250]
Number of generations	[50 100 200 250]

Table 36 : Values of parameters for GA

Each combination of population size and the number of generations employed in the GA results in a unique optimal control strategy. The evaluation of these parameter choices is primarily based on the reduction in electricity costs achieved over the course of a day, as indicated in Table 37. It needs to note that the optimal control signals derived from GA are sensitive to both the quality of the population and the number of generations. A large population with low quality individuals does not guarantee optimal solutions, just as a high-quality population with a small number of generations may not lead to optimal outcomes.

Number of generations	Population size	Cost reduction (%)
50	50	0.125
100	50	5.44
200	50	6.56
250	50	6.56
50	100	15.06
100	100	15.15
200	100	15.15
250	100	15.72
50	200	6.56
100	200	15.72
200	200	15.72
250	200	15.72
50	250	15.15
100	250	15.15
200	250	15.72
250	250	15.72

Table 37 : Different values of electricity cost reduction corresponding to each set of parameters for GA

The relationship between the values of electricity cost reduction and the variations in the number of generations and population size is graphically depicted in Figure 65. This visualization provides insights into how different combinations of these parameters influence the cost reduction achieved.

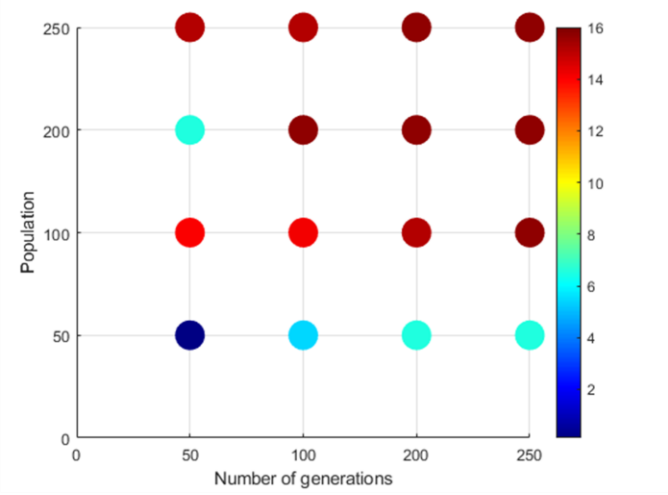

Figure 65: Values of electricity cost reduction in percentage when changing values of parameters for GA

It is observable that both population size and the number of generations have a significant impact on the effectiveness of GA in finding optimal control strategies. When the number of generations is increased, control strategies that result in higher reductions in electricity costs tend to be found. Similarly, the population size plays a crucial role in the search for optimal solutions. As shown in Figure 65, with 50 generations, the GA optimization method has difficulty in finding the best control signals; this is proved by the low electricity cost reduction. For the cases with the number of generations is 50, the case with the size of the population is 100 shows a better performance than the case with the population size is 200. This can be explained by the quality of the population at the 1st generation.

In general, cases with more than 200 generations and population sizes larger than 200 tend to exhibit better overall performance. In order to compromise between the computational time and the effectiveness of the GA, the population size of 200 and 200 generations are chosen for the GA optimization method to find the optimal control strategy, which gives the higher electricity cost reduction in this chapter.

4. Scenarios and results

4.1. Scenario 1: The integrated aggregated model tested by using price electricity of 3 different days

In this scenario, we select three distinct days with varying electricity price trends to evaluate the performance of the "Integrated Aggregated Model". The electricity price control signal utilized in this study is derived from data recorded on January 3rd , January 17th, 2023, and January 21st, 2023 [41]. This dataset provides hourly electricity price information from the SPOT market, measured in €/MWh (Euros per megawatt-hour). Figure 66 (a, b, c) display the electricity price data for on January 3rd, January 17th, 2023, and January 21st, 2023, respectively, obtained from the SPOT market. Upon analysis of the data, it is apparent that on January 21st, 2023, specific time periods, notably from 9 h to 11 h and 17 h to 22 h, exhibit higher electricity prices. Consequently, the price control signal is chosen to be activated during these time periods. This signifies that energy usage reduction or constraint for the integrated aggregated model will be implemented between 9 h to 11 h and 17 h to 22 h, as indicated by the red rectangles in Figure 66c. Nevertheless, for January 3rd, 2023, a different electricity price trend is observed throughout the day. Notably, prices remain high from 7 h until 20h. For this day, the price control signal is selected for the period from 8 h to 12 h and from 17h to 19h, as depicted by the red rectangle in Figure 66. Besides, the price control signal chosen for January 17th, 2023 is between 7 h to 12 h and 18 h to 19 h, as indicated by the red rectangles in Figure 66b

For reference:

- January 3rd , 2023 is denoted as "D1"

- January 17th, 2023 is denoted as "D2"

- January 21st, 2023 is denoted as "D3"

Our investigation involves the analysis of 3 distinct days characterized by diverse trends in electricity prices on the market. The primary aim is to comprehensively assess the response of the integrated aggregated models and to describe varied outcomes resulting from the optimization problem. By examining these 3 days with differing price trends, we aim to gain an understanding of how the integrated models perform under different market conditions and how they optimize energy consumption in response to fluctuating electricity prices. This approach allows to capture a broader spectrum of scenarios and better evaluate the effectiveness of our proposed aggregated models in minimizing electricity costs and enhancing demand-side flexibility.

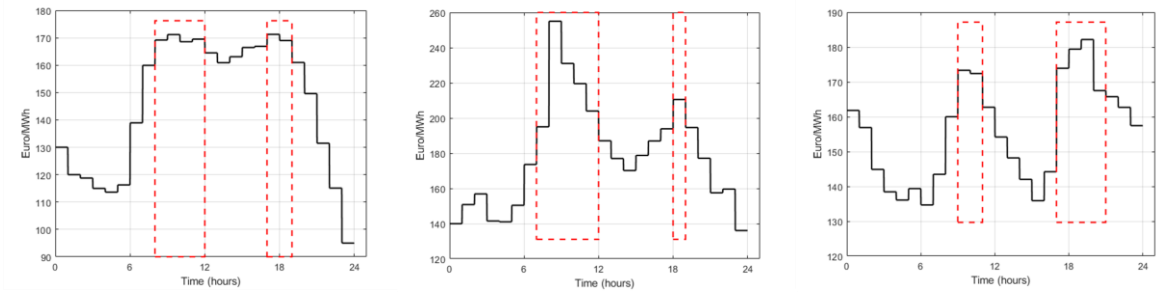

Figure 66: (a, b, c) The electricity price in the spot market on 3rd January 2023 (D1), 17st January 2023 (D2) and 21st January 2023 (D3), respectively

The minimization problem is subject to specific constraints to ensure the total power-off time is confined by a set duration of 6 hours for the power-off period (this duration can be adjusted based on user preferences or requirements).

In this chapter, we tackle the economic challenge of minimizing electricity costs through the integration of three aggregated models: DHW, EVC and HR. The optimization process employs a genetic algorithm over the 2-day period.

The initial step involves incorporating all pertinent data and variables associated with the DHW, EVC, and HR. This encompasses factors like the electricity price trajectory throughout the day, outdoor temperature, the number of households under consideration, geographical coordinates of the location, and the set of average parameter values for each aggregated model. The value of input for the integrated aggregated model is shown in **ANNEX P**

To provide a clear perspective of the strengths of the aggregated models, we establish a reference scenario where no control signal is implemented. Additionally, various other scenarios are examined, involving the application of a price control signal with a 6-hour power cut-off. This facilitates a comparison with the outcomes derived from the optimization problem mentioned earlier. The determination of the cut-off periods is simply based on the observed trend of electricity prices for each respective hour, as illustrated in the accompanying Figure 66.

Case	Description
D0	The aggregated model without control signal
D1-PS ; D2-PS ; D3-PS	The aggregated model with price control signal applied (using price of day D1, D2 and D3)
D1-GA ; D2-GA ; D3-GA	The aggregated model with the optimal control signal (using price of day D1, D2 and D3)

Table 38 : Three different cases, in which the integrated aggregated model is applied with different control signals using the electricity price of D1, D2 and D3

Table 38 describes the different cases using the electricity of 3 different days D1, D2 and D3, respectively. The case use the price control signal strategy D1, D2 and D3 are noted as D1-PS, D2-PS and D3-PS, respectively. The other case concerning the optimal control signal found by using GA, which give the minimum electricity cost over the day, they are denoted as D1-GA, D2-GA and D3-GA, respectively.

When the electricity price control signal is applied to the integrated aggregated model, the control logic is as follows: during periods of high electricity prices, the power is cut off and it is only activated during periods of low electricity prices. Upon implementing the optimal control signal, the model adheres to the cut-off signal's directives, turning off during such periods and operating during others. Throughout this chapter, the assumption is made that when a signal to cut off power is given, all households are simultaneously switched off.

Furthermore, our investigation encompasses several indicators to comprehensively evaluate the behavior of the integrated aggregated model across three distinct cases.

- **Indicator 1**: Percentage of energy shifted during peak hours. This indicator quantifies the proportion of energy that is shifted from cut-off power hours. The total energy shifted from cut-off power periods is divided by the overall energy consumption during the simulation period.

- **Indicator 2**: Reduction in electricity cost. This indicator quantifies the reduction in electricity costs achieved through the application of control signals during the 1st day and a period at the

beginning of the following day, where experience the rebound power consumption caused by cut-off power duration.

- **Indicator 3**: Simulation time. This indicator measures the time required for the simulation process, reflecting the computational efficiency of the integrated aggregated model.

By analyzing these indicators across the different cases, we gain a comprehensive understanding of the performance and benefits of the integrated aggregated model under various conditions.
On Figure 67, we first illustrate the power consumption for DHW, EVC and heating for 5,000 households.

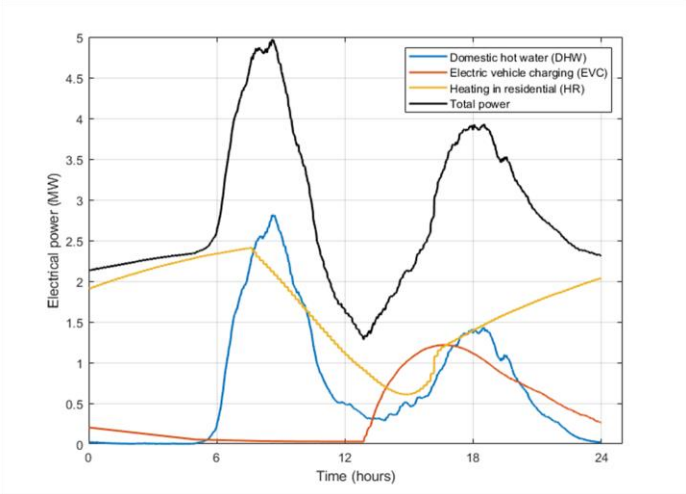

Figure 67: Power consumption of DWH, EVC and HR of 5,000 households

By leveraging the proposed aggregated model designed for three distinct types of loads, we can rapidly generate the entire power consumption profile in less than two second. The resulting visualization encapsulates the essential characteristics of the power usage patterns. This graphical representation serves as an initial impression, granting a snapshot of the power consumption behaviors across 5,000 households.

In the scenario employing the electricity price data from D1, the optimized price control signal using the genetic algorithm (GA) spans from 16h to 22h. Meanwhile, the initial price control signal covers the timeframe of 7 h to 12 h and from 17h to 18h (Figure 68a1). Upon analysis, it is observable that both D1-PS and D1-GA exhibit a post-cut-off rebound in power consumption.

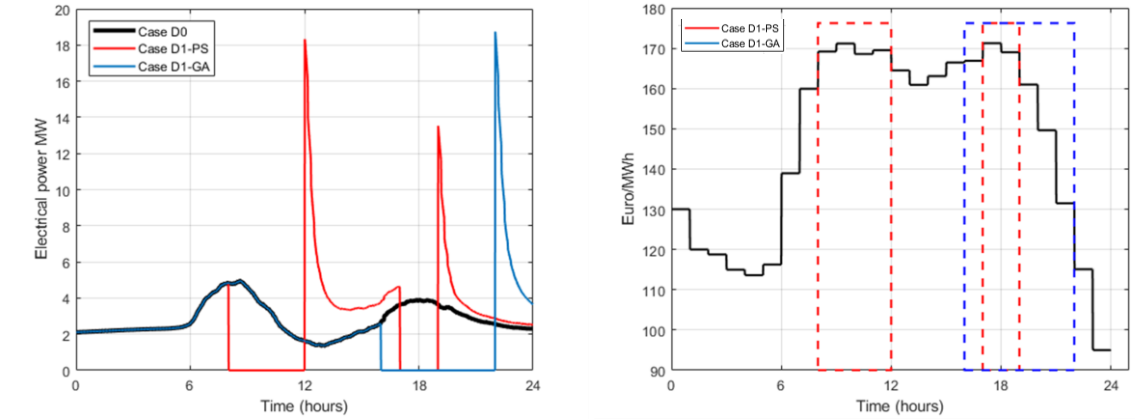

a1 b1

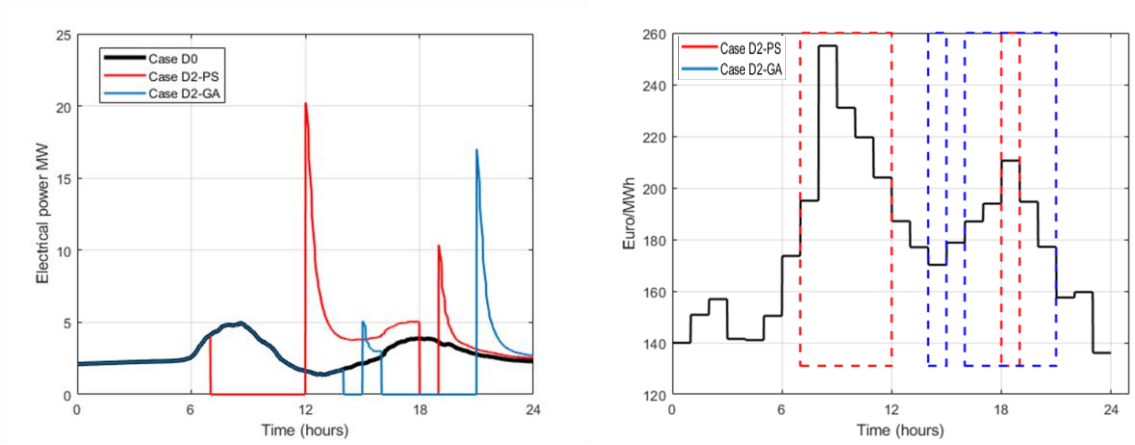

a2 b2

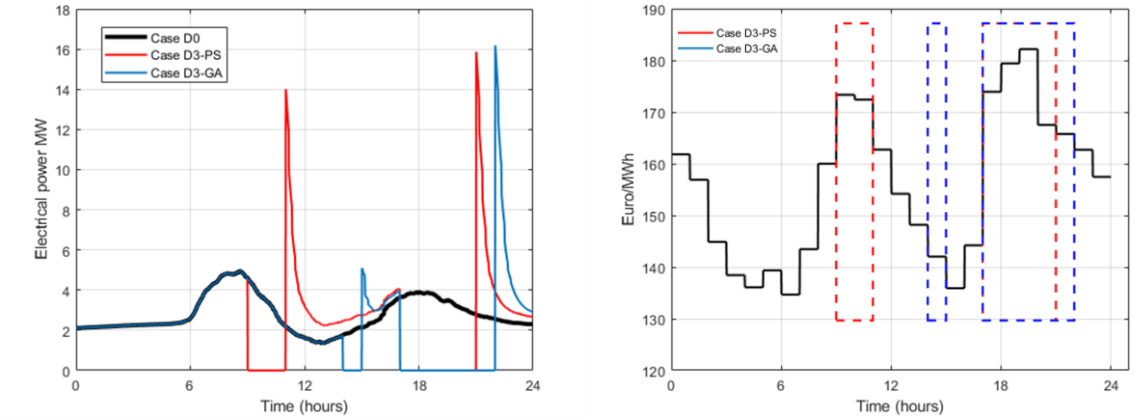

a3 b3

Figure 68: (a1, a2, a3) The power consumption of the integrated aggregated model for 5,000 households of the cases using the price of D1, D2 and D3, respectively. (b1, b2, b3) Electricity price of D1, D2 and D3, respectively

It is noticeable that the difference in shifted energy of the case D1-PS is slightly higher than D1-GA (Table 39). Nonetheless, the case D1-GA, leveraging the optimal control strategy facilitated by GA, displays a superior performance with the reduction in electricity cost of 16.27%, 8 times higher than the case using price control signal. This can be explained by a reason that due to the electricity price of D1 is witnessed a high trend from 6h to 22h, the rebound in the case D1-PS transpires at a time when electricity prices are higher than the time corresponding to the rebound in the D1-GA case. The outcomes are summarized in Table 39, providing the results for the aforementioned indicators.

Notably, the simulation times for both the cases D0 and D1-PS are impressively short, standing at just 1.59 and 1.64 seconds, respectively. This serves to underscore the efficiency of the integrated DHW, EVC, and HR model in rapidly computing power consumption and aiding in the identification of optimal control signal strategies. It is also important to acknowledge that the computation time for the D1-GA case, determined through GA optimization, extends to 3786 seconds (approximately 64 minutes). This considerable time is due to the GA-based approach. In other words, this highlights that if using the unit models instead of the integrated aggregated model could demand several days to achieve the same outcome.

For the case of involving **unit models** for DHW, EVC, and HR, to obtain a total power consumption curve for 5,000 households can take up to 2 hours. When employing GA for optimization with 200 generations, the computational time for finding optimal control strategies can reach up to 400 hours. Due to the limitation of the time, we cannot give the exact number; however, the predicted time of 400 hours emphasizes the effectiveness of utilizing the integrated aggregated model. Using the proposed integrated aggregated model, with using a GA method for optimization can save up to 99.7% computational time compared to the usage of the unit model.

For the scenario employing the electricity price data of the day D2, the price control signal encompasses the hours from 7 h to 12 h and from 18 h to 19 h. With the GA optimization used, the resultant optimal control signal pertains to the interval from 14 h to 15 h and from 16h to 21h. And for the case using the electricity price of the day D3, the optimal control strategy is found with the interval from 14 h to 15 h and from 17h to 22h. For these two cases, the similar trend is witnessed compared to the case employing D1. The control strategies found by using GA show a better performance compared to the price control signal.

Indicators	Case D0	Case D1-PS	Case D1-GA	Case D2-PS	Case D2-GA	Case D3-PS	Case D3-GA
Shifted energy (%)	0	32.52	29.75	32.57	28.11	31.07	27.85
The reduction in electricity cost (%)	0	2.01	16.27	9.76	16.67	9.53	15.15
Simulation time (Second)	1.59	1.64	3786	1.57	3905	1.57	3914

Table 39 : Results of two mentioned indicators for three cases using electricity price of D1

One thing needs to mention is that in both 3 cases, the shifted energy from the cases employing GA control strategy is less than the cases using price control signal, however the reduction in electricity cost of the cases employing GA is higher. This highlights the role of the integrated model combined to GA optimization method in assisting the decision of the aggregator. This allows aggregator not only understands the behavior of the power consumption in a large scale rapidly but also finding the best control signal strategy to participate to different activities in the energy market.

By employing the three proposed aggregated models for distinct loads DHW, EVC, and HR, the power consumption of a substantial number of households can be promptly estimated within a mere 2 seconds. Moreover, harnessing the potential of the genetic algorithm-based optimization technique, an optimal control signal strategy can be identified to achieve about 16% reduction in total electricity cost and about 28% energy shifted. The aggregator can implement load shifting strategies to reduce energy consumption as following instructions from DSO to ensure the grid stability. Additionally, in a scenario encompassing 5,000 households and utilizing the GA, the optimal control signal strategy materializes within an approximate span of 1 hour, which can help to save up to 99.7% computational time compared to the usage of the unit model, underscoring the efficacy of the integrated aggregated models.

4.2. Scenario 2: Varying the duration of cut-off power hours

In this scenario, we explore different durations of power cut-off periods throughout the day, ranging from 1 hours to 10 hours. We apply these variations to the integrated aggregated model, and the input data for the model can be found in ANNEX P.

The electricity price data used is from day D2, as previously mentioned in scenario 1. Our objective here is to examine how the integrated aggregated model react and observe the different outcomes

resulting from the optimization problem under various cut-off power durations. By assessing these different durations, this can be added feature to our proposed model.

The primary goal remains finding the most optimal control signal strategy to minimize electricity costs over the course of 2 days while considering different cut-off durations. The control strategy only applied to the 1st day. As mentioned above, we keep employing GA for the optimization process, while ensuring the power cut-offs. For the case using the optimal control strategies with the cut-off duration from 1 to 10 hours, they are denoted as H1-GA to H10-GA, respectively (Table 40). In addition, we establish a reference scenario where no control signals are applied, denoted as the case H0. Beside the optimal control strategies found by using GA, we also use price control signal for the comparison and denoted as H1-PS to H10-PS, respectively. The time slots, in which the electricity price is high during the day, are also selected for each case, representing in Table 40.

Case	**Slots (Price control signal)**	**Case**	**Slots (GA control signal)**
H1-PS	8h -9h	H1-GA	18h -19h
H2-PS	8h -10h	H2-GA	16h -17h 18h - 19h
H3-PS	8h -11h	H3-GA	15h -16h 17h - 19h
H4-PS	8h -11h 18h - 19h	H4-GA	15h -16h 17h - 20h
H5-PS	8h -12h 18h - 19h	H5-GA	15h -16h 17h - 21h
H6-PS	7h -12h 18h - 19h	H6-GA	14h -15h 16h - 21h
H7-PS	7h -12h 18h - 20h	H7-GA	13h -14h 15h - 21h
H8-PS	7h -12h 17h - 20h	H8-GA	12h -13h 15h - 22h
H9-PS	7h -12h 16h - 20h	H9-GA	8h -10h 14h - 21h
H10-PS	7h -13h 16h - 20h	H10-GA	8h -11h 14h - 21h

Table 40 : Price control signal slots for different power cut-off duration

In order to have a better visualization about the cut-off power control strategies found by using GA, compared to the price control signal, the power consumption of the 1st day for the cases H7-PS, H7-GA, H10-PS and H10-GA are demonstrated in Figure 69. The control strategy found by using GA for the case H7-GA is from 14h to 15h and from 15h to 21h. It is observable that the cut-off power periods is followed by the time with low electricity price. Hence, with the rebound effect occurs right after these periods, the electricity cost can be reduced.

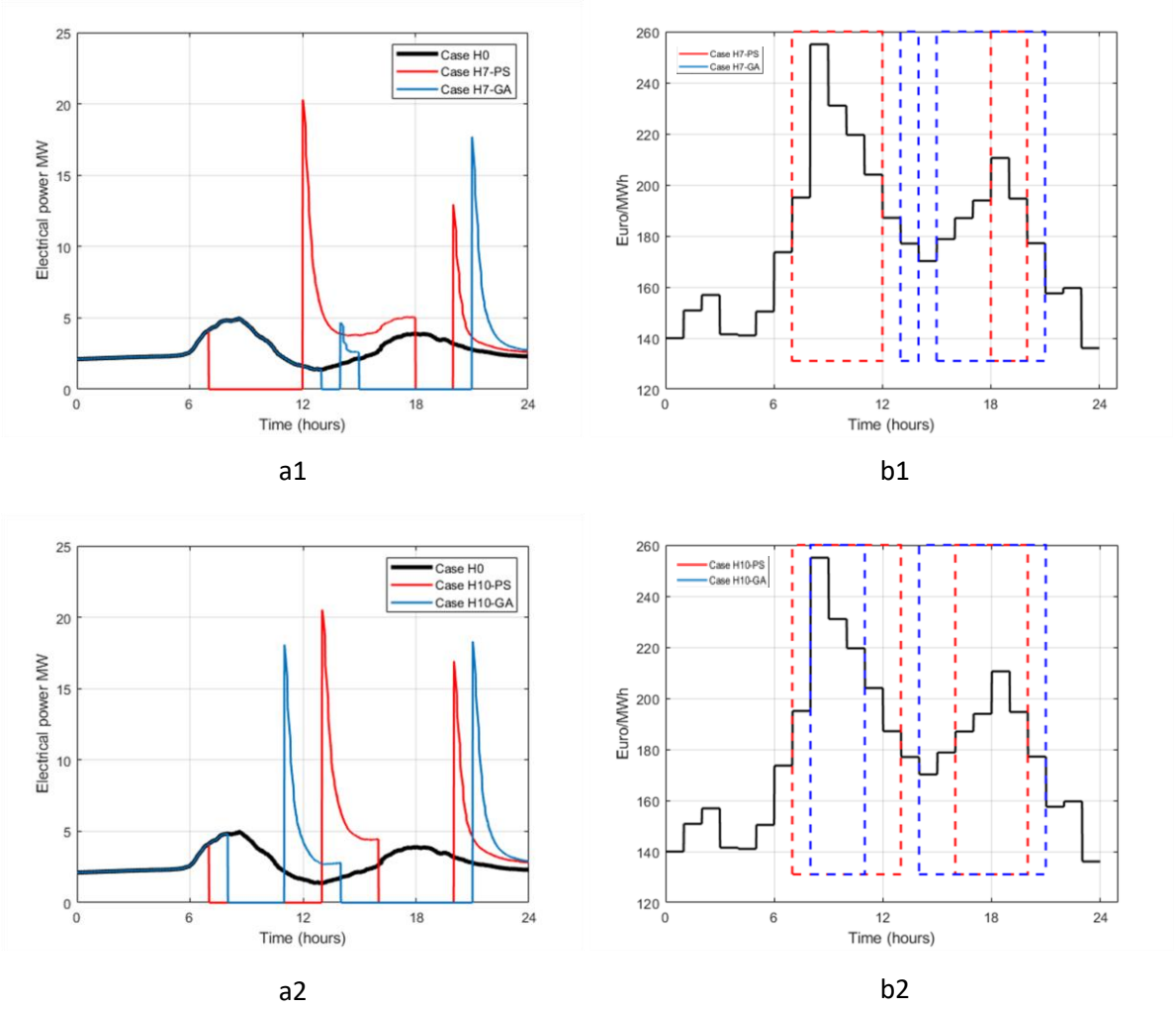

Figure 69: (a1, a2) The power consumption of the integrated aggregated model for 5,000 households of the cases with 7-hour and 10- hour cut-off duration, respectively. (b1, b2) Electricity price of D2

For the case H10-GA, the first cut-off power period is from 8h-11h, which is followed by the high electricity price. However, it can be observed that the rebound power consumption after the 1st cut-off power period of the price control signal strategy is much higher than that cause by GA control

strategy. This can explain for why the control strategy obtained from GA can have 25.23% electricity cost reduction, more than 3% higher than that of the case H10-PS.

Case	Shifted energy (%)	Reduction in electricity cost (%)	Case	Shifted energy (%)	Reduction in electricity cost (%)
H1-PS	7.18	1.09	H1-GA	5.7	1.75
H2-PS	13.12	1.78	H2-GA	10.54	4.81
H3-PS	17.32	2.34	H3-GA	14.87	6.86
H4-PS	23.02	3.23	H4-GA	19.99	10.44
H5-PS	25.79	5.09	H5-GA	24.44	13.83
H6-PS	32.57	9.76	H6-GA	28.11	16.67
H7-PS	37.69	13.17	H7-GA	31.61	18.71
H8-PS	43.34	16.24	H8-GA	35.46	20.08
H9-PS	48.19	18.14	H9-GA	45.35	22.39
H10-PS	50.38	22.01	H10-GA	49.55	25.23

Table 41: Shifted energy and electricity cost reduction of all cases with different cut-off duration (%)

Table 41 reveals the shifted energy and the electricity cost reduction in percentage, which are obtained from all cases, both with price control signals and GA control signals. Figure 70 depicts the shifted energy and the electricity cost reduction in percentage with respect to the cut-off power duration.

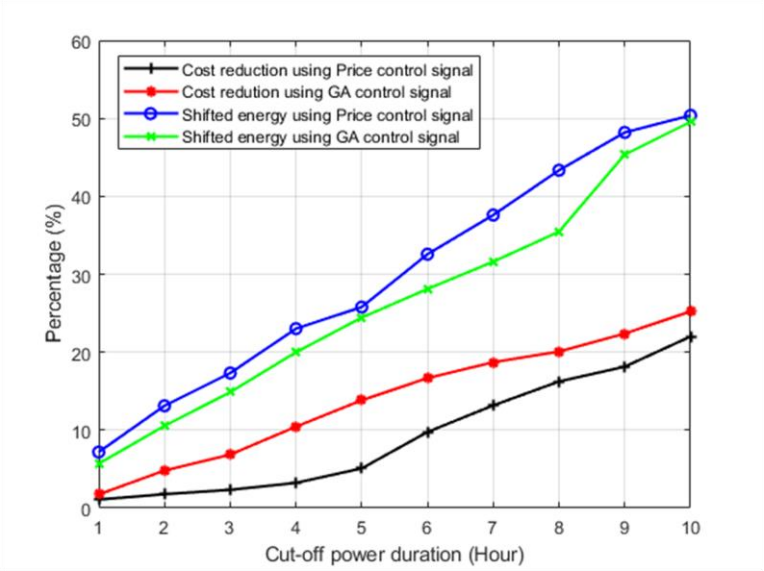

Figure 70: Shifted energy and electricity cost reduction with different cut-off duration from 1 hour to 10 hours (%)

The utilization of GA to optimize control strategies consistently demonstrates its effectiveness in terms of reducing electricity costs Figure 70. Compared to cases employing price control signals, the GA-driven scenarios achieve higher cost reductions. However, it needs to mention that the shifted energy obtained in the cases using GA is lower than in those using price control signals. The relationship between the duration of power cut-offs, electricity cost reduction, and shifted energy is evident. Longer cut-off durations lead to increased reductions in electricity costs and greater amounts of shifted energy. This relationship makes sense as cutting power for longer periods results in more significant savings in electricity costs.

While testing the integrated aggregated models with various cut-off power durations may not perfectly mirror real-world scenarios, as it is rare to cut off power in a winter day for 10 hours, it serves to evaluate the models' functionality and robustness under different conditions. From an aggregator's perspective, these models, coupled with optimization methods, enable quicker and more informed decisions regarding the optimal cut-off durations for cost reduction. Nevertheless, those cut-off durations need to remain within acceptable limits and do not affect too much user comfort.

Especially, the decision can be made quickly thanks to the rapidness of the integrated aggregated model in computational times, which is obviously difficult to obtain when using the unit model.

4.3. Scenario 3: Change the values of input for the integrated aggregated model

In this particular scenario, we conduct an evaluation of the integrated aggregated model by modifying the input parameters. We introduce variations in the parameter sets concerning the capacity and power rating for each of the aggregated models, encompassing DHW, EVC, and HR. The fact that when varying the sets of parameters, this demonstrate the different characteristics of the group of households that the aggregators manage. Additionally, this scenario allows comprehensively investigating various situation in which the aggregated can still have a prediction of the power consumption consumed by different groups of households that they manage.

We vary the input of the model with 2 cases.

- Case 1: Vary the global capacity the system concerning the parameter average volume of all water heaters $V_{avg}$and the parameter average battery capacity of all EVs B_{avg}.
- Case 2: Vary the global power rating of the system concerning the parameter average power rating of all water heaters P_{avg} and the parameter average thermal power rating of all heating systems $P_{heating\text{-}avg}$.

The optimization problem subjects to specific constraints to ensure that the total power-off time does not exceed a predefined duration of 8 hours for the power-off period. The electricity price data used for this optimization problem is sourced from D3, as established in Scenario 1.

4.3.1. Case 1: Vary the global capacity the system

For this case, the parameter average volume of all water heaters V_{avg} and the parameter average battery capacity of all EVs B_{avg} are varied at the same time while keeping original value other parameters. We maintain the original values of all other parameters and utilize the set of parameters in **ANNEX P** as a reference for this evaluation. The values of parameters V_{avg} and B_{avg} are adjusted both upwards and downwards 30%, 20% and 10% compared to their respective reference values.

Table 42 provides a summary of all the cases in which these parameters V_{avg} and B_{avg} are varied. Within this table, the cases C10, C10-PS, and C10-GA are the cases use the reference values, which mentioned in **ANNEX P**.

To identify optimal control strategies for each case, ranging from C07-GA to C13-GA, the GA method is employed. Since we are considering the electricity price data from the day D3, the price control signal extends from 9 h to 12 h and from 17 h to 22 h. This approach allows us to assess how changes in these parameters influence electricity cost savings and control strategies in residential energy management.

Case	Description
C07; C08; C09; C10; C11; C12; C13	The aggregated model without control signal (with the capacity parameter values = 0.7; 0.8; 0.9; 1.0; 1.1; 1.2; 1.3 the reference value)
C07-PS ; C08-PS ; C09-PS ; C10-PS ; C11-PS ; C12-PS ; C13-PS ;	The aggregated model with price control signal applied (with the capacity parameter values = 0.7; 0.8; 0.9; 1.0; 1.1; 1.2; 1.3 the reference value)
C07-GA ; C08-GA ; C09-GA ; C10-GA ; C11-GA; C12-GA ; C13-GA ;	The aggregated model with the optimal control (with the capacity parameter values = 0.7; 0.8; 0.9; 1.0; 1.1; 1.2; 1.3 the reference value)

Table 42 : Different cases, in which the parameters concerning the capacity of the model are varied

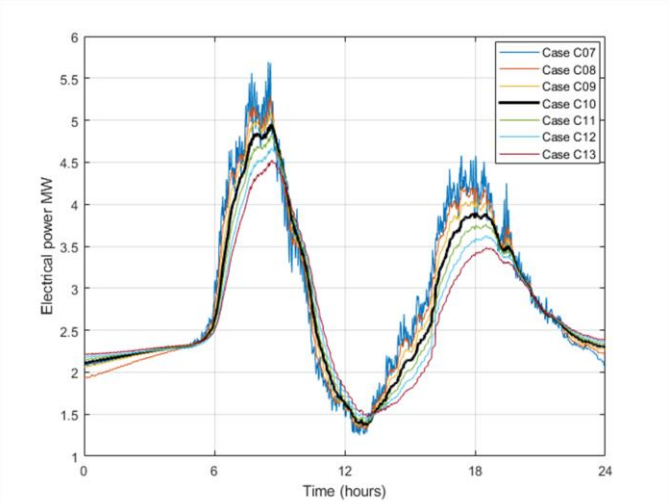

Figure 71: Total power consumption of DWH, EVC and HR of 5,000 households of the cases C07 to C13

Figure 71 compares the total power consumption of the integrated aggregated model for all 7 cases C07 to C13. Among these cases, C10 serves as the reference, employing the input values from **ANNEX P**. This comparison gives a better idea about the impact of varying the values of parameter sets concerning the capacity of the system.

Case C07 exhibits the highest total power consumption compared to the other cases. This outcome can be attributed to the decrease in the average volume of the water heater population. With the same hot water demand from users and consistent power ratings for water heaters, the reduced water heater

volume may result in an inadequate supply of hot water to users. This, in turn, prompts water heaters to heat water more frequently, leading to higher power consumption for water heating. Same for electric vehicles, we reduce the average battery capacity of the population of EVs but the distance travelled per day do not change. This also causes an increase in power consumption for charging EVs.

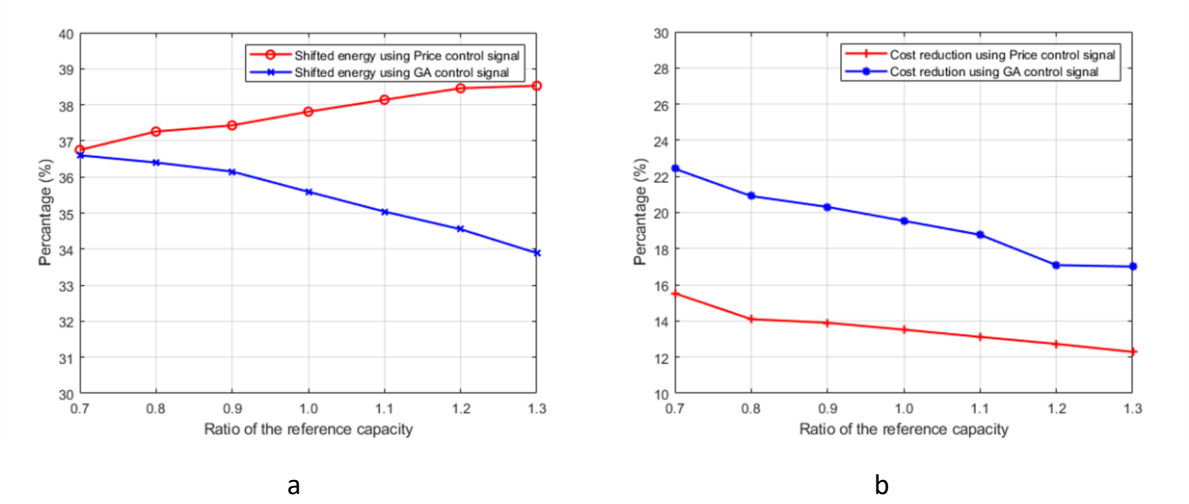

a b

Figure 72: (a, b) Shifted energy and electricity cost reduction for different cases when varying the parameters concerning capacity of the system (%)

Figure 72 illustrates the shifted energy and electricity cost reduction when varying the ratio of the parameters concerning the capacity of the systems.

As can be seen from the figures that the shifted energy percentage of the cases using GA control signals exhibit a decreasing trend. However, this decrease is relatively modest, typically around 0.3% for each increment in the reference capacity ratio. This can be attribute for the decreasing in the total power consumption as the ratio increases. In contrast, the shifted energy percentage of the cases using price control signal experiences a rising trend. For this case, the reason lies in the cut-off power period of the price control signal, from 9h to 12h and from 17h to 22h. Look at Figure 72, during the period 9h to 12 h, the power consumption is rising as increasing the ratio of the reference capacity instead of decreasing trend.

The cases employing GA control strategies consistently achieve a more favorable reduction in electricity costs compared to those utilizing price control signals. The electricity cost reduction percentage for the GA cases decreases as the reference capacity ratio increases, reflecting the corresponding reduction in power consumption. Moreover, as the capacity ratio rising, the electricity cost reduction decreases, from 16% to 12%.

This scenario serves to highlight the integrated aggregated model's capacity for optimizing control strategies effectively through the application of the GA method. By conducting sensitivity tests involving variations in parameter values, the model highlights its potential to manage power consumption under diverse real-world conditions.

4.3.2. Case 2: Vary the global power rating of the system

For this case, the average power rating of all water heaters P_{avg} and the parameter average thermal power ratings of all heating systems $P_{heating\text{-}avg}$ are varied at the same time while keeping original value other parameters. We choose the set of parameters in **ANNEX P** for the integrated aggregated model as a reference. The values of parameters P_{avg} and $P_{heating\text{-}avg}$ are then decreased and increased 30%, 20% and 10% compared to the their reference values.

Table 43 lists all the cases where the value of the parameters P_{avg} and $P_{heating\text{-}avg}$ are varied. In Table 43, the cases P10-PS and P10-GA are the cases use the reference values, which mentioned in **ANNEX P**.

Case	Description
P07 ; P08 ; P09 ; P10 ; P11 ; P12 ; P13	The aggregated model without control signal (with the power rating parameter values = 0.7; 0.8; 0.9; 1.0; 1.1; 1.2; 1.3 the reference value)
P07-PS ; P08-PS ; P 09-PS ; P10-PS ; P11-PS ; P12-PS ; P13-PS ;	The aggregated model with price control signal applied (with the power rating parameter values = 0.7; 0.8; 0.9; 1.0; 1.1; 1.2; 1.3 the reference value)
P07-GA ; P08- GA ; P09-GA ; P10-GA ; P11-GA; P12-GA ; P 13-GA ;	The aggregated model with the optimal control (with the power rating parameter values = 0.7; 0.8; 0.9; 1.0; 1.1; 1.2; 1.3 the reference value)

Table 43 : Different cases, in which the parameters concerning the power rating of the model are varied

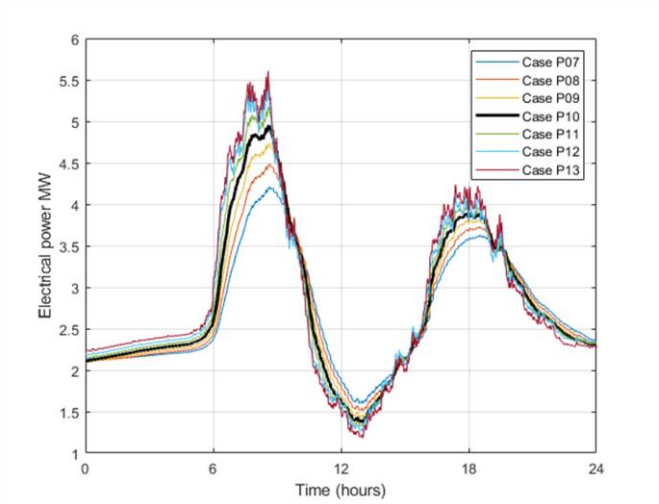

Figure 73: Total power consumption of DWH, EVC and HR of 5,000 households of the cases P07 to P13

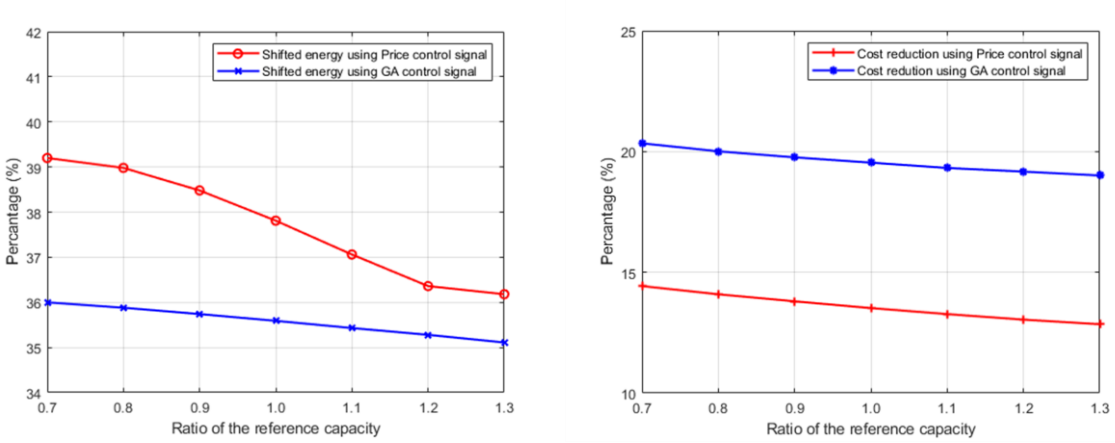

a b

Figure 74: (a, b) Shifted energy and electricity cost reduction for different cases when varying the parameters concerning power rating of the system (%)

Figure 73 illustrates the total power consumption of the integrated aggregated model for all 7 cases P07 to P13. The case P10 is the case use the input reference from **ANNEX P**. This comparison allows for a comprehensive assessment of how varying parameter values related to system power ratings impacts overall power consumption.

The observations indicate that the total power consumption is highest in case P13, wherein the average power rating of the water heaters and heating systems is increased. This is due to when increasing the average power rating of the population of water heaters, with the same demand of hot water from users, the power consumption increases correspondingly. Same for heating in residential, we increase the average thermal power rating of the population of heating systems, but the users do not change. This also causes an increase in power consumption for heating.

Figure 74 it depicts the shifted energy and electricity cost reduction when parameters related to system power ratings are modified. As can be seen from the figures that shifted energy percentage with the case using both price control signal and GA control signal exhibit a declining trend as parameter values change. For the case using price control signal, this is primarily because during cut-off slot from 9h to 12h and from 17h to 22h, when parameter values are varied increasingly, in majority of time, the total energy shifted during the power cut-off period decrease while total energy consumed throughout the day also rises in general. This results in a decrease in shifted energy percentage.

GA control strategies continue to outperform price control signals in terms of reducing electricity costs. As with the first case, the electricity cost reduction is significantly better in GA cases.

The same as the case 1, the sensibility test on the model proves its potential in controlling the power consumption under different conditions in reality.

By leveraging the integrated aggregated model in testing various scenarios, we can assess its response under real-world conditions, encompassing differences in household characteristics, user behaviors, and varying weather conditions. Rapidly obtaining power consumption estimations on a large scale without requiring detailed information is a significant advantage. From an aggregator's perspective, having a quick understanding of power consumption behaviors among the groups of households they manage enables faster decision-making when responding to orders from the DSO. This includes making decisions on shifting power consumption to specific time slots, which can be determined using optimization methods to achieve cost reductions in electricity consumption.

5. Conclusion

The integrated aggregated model combining the aggregated models of domestic hot water, electric vehicle charging and heating in residential exhibits their potential in empowering aggregators to swiftly comprehend the power consumption patterns of the households they manage. It can provide the aggregator with insights into the expected power demand from a particular area which is crucial for energy planning. The proposed integrated aggregated model allows testing different scenarios in

order to determine the control strategies with the assistance of the GA optimization method, which helps aggregator implement demand response programs, encouraging residential consumers to shift their power consumption to the off-peak hours. Furthermore, their quick computational time adds to their value, facilitating the assessment and quantification of energy flexibility on a substantial scale, such as city-wide or country-wide applications.

ANNEX P: Parameters and inputs for each model

Domestic hot water aggregated model

The input of the EWH aggregated model is the total domestic hot water demand in time series. We use the tool "Load Profile Generator" to generate the total hot water profile for 5,000 households. (Figure 75)

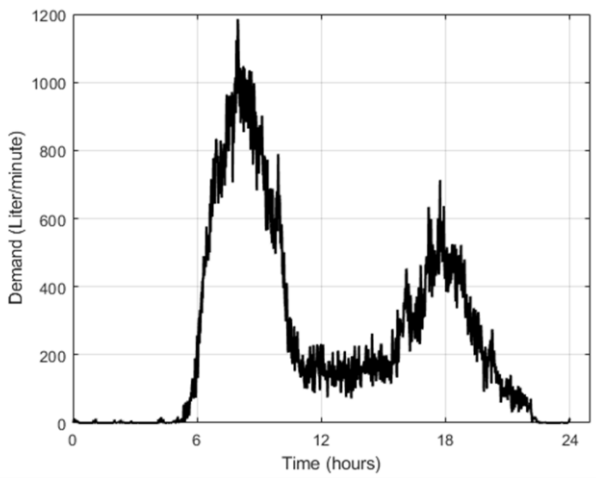

Figure 75: Hot water demand for 5,000 households

Table 44 and Table 45 present the parameter used for the aggregated model for DHW.

Parameter	Value	Unit	Parameter	Value	Unit
T_{amb}	20	°C	C_p	4186	J/kgK
T_{in}	15	°C	ρ	997	kg/m^3
η	1		k	0.6	W/mK
N	4	_	U	0.5265	W/m^2K

Table 44: The parameters for simulation of the aggregated model

Number of households	5000
P_{avg} (W)	2803
V_{avg}(liter)	250
H_{avg}(m)	1.61
T_{set}(°C)	60

Table 45: The values of P_{avg}, V_{avg} , H_{avg} and T_{set} for 5,000 households

Electric vehicle charging aggregated model

For the aggregated model for EVC, the parameters needed are the average for:

- Average battery capacity B_{avg} (kWh),
- Average range anxiety factor R_{avg},
- Average driving energy consumption per kilometer D_{avg} (kWh/km),
- Average behavior coefficient U_{avg}
- Average distance travelled per day K_{avg} (km)

Number of EVs	5,000
B_{avg} (kWh)	45
D_{avg} (kWh/km)	0.15
R_{avg}	1.5
U_{avg}	1.25
K_{avg} (km)	15

Table 46: Values of average for: battery capacity B_{avg} (kWh), range anxiety factor R_{avg}, driving energy consumption per kilometer D_{avg} (kWh/km), behavior coefficient U_{avg} and distance travelled per day K_{avg} (km) 5,000 EVs.

The input of the aggregated model is the number of vehicles at home in time series. This input is generated using EV profile charging load model. This model allows to build the schedule of a vehicle during a day and gives us the exact location of the vehicle at each time step. The Figure 76 describes the number of electric vehicles, which are present at home at each time step during the day.

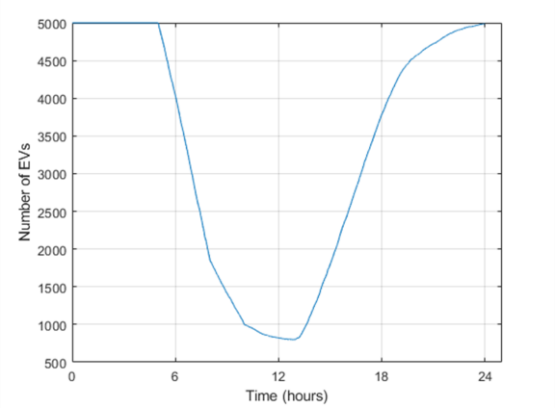

Figure 76: Number of EV at home for 5,000 households

1.1.1. Heating

The parameters required for the aggregated model for heating in residential are shown in Table 47, including the average thermal power rating $P_{heating\text{-}avg}$(W), the average setting temperature $T_{set\text{-}avg}$ (°C), the average outdoor temperature $T_{out\text{-}avg}$(°C) and the coefficient of cloud coverage C_{cloud} .

Number of heating systems	5000
$P_{heating\text{-}avg}$(W)	9350
$T_{set\text{-}avg}$ (°C)	19
$T_{out\text{-}avg}$(°C)	5
C_{cloud}	0

Table 47: The values of $P_{heating\text{-}avg}$, $T_{set\text{-}avg}$, $T_{out\text{-}avg}$ and C_{cloud} for 5,000 heating systems, respectively

The input of the aggregated model is the outdoor temperature, sky temperature and solar radiation (in time series). The outdoor temperature is chosen in 1st January 2016 in Grenoble, sky temperature is recalculated from outdoor temperature. Solar radiation under clear sky conditions at specific locations and times using a clear-sky model, which is developed by Rigollier et al. [99]. Especially, for the aggregated model for heating in residential, we also need the information regarding the heat pump used for heating systems. As mentioned in the chapter 1, we use the methodology from (reference) to find the COP for each time step. The COP is defined as the quadratic function of the difference between internal temperature and air temperature. We use data from [28], [29].

VI. Conclusion

In this thesis, we aim to build different aggregated models, which can represent the power consumption for different types of residential loads. We start the research with the chapter 1 with the generation of the aggregated model for domestic hot water, chapter 2 is about the aggregated model for electric vehicle charging, chapter 3 presents the model for residential heating and chapter 4 emphasizes utilization of three mentioned models in a case study.

The first chapter describes the research process involved in developing an aggregated model for domestic hot water demand. The chapter begins with an introduction that highlights the significance of DHW in demand-side flexibility and the roles of electric water heaters and thermodynamic water heaters in meeting DHW requirements in France. A literature review of existing aggregated models for DHW is presented, mentioning the unique contributions and advantages of the proposed aggregated model compared to previous models.

The proposed aggregated model is not overly dependent on intricate details about the characteristics of each water heater or user behavior. It primarily necessitates two types of input: the total hot water demand in a time series format and average parameters. These average parameters encompass the mean power rating of all houses, the average volume of all houses, and the mean thermostat setting temperature across all houses. These parameter values can readily be sourced from existing data, such as data provided by organizations like Ademe or Insée. By relying solely on this information, the aggregated model excels in estimating the power consumption of thousands of water heaters within seconds, rendering it thousands of times faster than the unit model, while still delivering highly accurate results. Additionally, this aggregated model can react under different type of control signals and give the power consumption in time series. Consequently, it can predict power consumption when subjected to external control signals like price signals or off-peak signals.

The second chapter of the thesis is about the generation of an aggregated model for electric vehicle charging (EVC) at residential. The chapter starts with the construction of an EV usage profile for each electric vehicle. A comprehensive EV profile model is developed, incorporating user charging behavior. This model not only tracks the location of the electric vehicle at each defined time step but also calculates the state of charge of the electric vehicle during these intervals. Two distinct aggregated models are introduced in this chapter: one without control signals and another with control signals.

The aggregated model without control signals is established using the relationship between the average power consumption of all electric vehicles at home and the number of electric vehicles present at home. This relationship is modeled as half of an ellipse, with parameters derived from the results obtained from the unit model. To define this curve, average parameters related to the average

battery capacity of all electric vehicles, average power consumption of all cars, average anxiety factor, average daily travel distance, and charging behavior coefficient are utilized. These average values can be sourced from literature and available government data. Besides, the aggregated model with control signals is constructed by considering the power difference between the unit model without applied control signals and the unit model with control signals. This power difference is defined as a linear function and serves as the foundation for building the aggregated model with control signals.

The standout feature of these aggregated models is their efficiency, enabling swift and efficient computations that facilitate scalable analyses of electric vehicle charging. Furthermore, the model only needs an input presenting the number of EVs at home in time series and is capable of functioning effectively with minimal information about household characteristics and EV specifications is a significant advantage. This ease of access allows users of the model to proactively predict and quantify energy flexibility, making it a valuable tool in the realm of EVC analysis.

Chapter 3 outlines the process of developing an aggregated model for residential heating. Like in previous chapters, the main objective remains is to create an aggregated model capable of estimating power consumption for residential heating. The chapter begins with a description of a reduced thermal model 6R2C. This model simplifies complexity to a single thermal zone and a single interface with the external environment. The experimental house "INCAS" at the INES site in Le Bourget du Lac, France, is used as the basis for data generation. Parameters for the 6R2C model specific to the INCAS house, as well as 17 other houses, are obtained. These 18 parameter sets serve as the foundation for creating a group of houses, and power consumption for heating is calculated for each house, referred to as the unit model. Using the average power consumption from the unit model, a relationship is established between average power consumption and average internal temperature at each time step. This relationship takes the form of a quadratic function parameterized by average parameters, including the average thermal power rating, average outdoor temperature, average setting temperature, and cloud coverage of the sky. The group of houses is then represented by a single representative house with average characteristics of all houses. The proposed aggregated model calculates the average power consumption of all houses by determining the average thermal power consumption as a defined function of the internal temperature.

This aggregated model is capable of operating with or without control signals applied. A comparison between the power consumption results obtained from the unit model and the aggregated model demonstrates the effectiveness of the aggregated model. Additionally, a sensitivity analysis is conducted to evaluate the aggregated model's responsiveness to variations in the average parameters.

The generated aggregated model offers rapid access to power consumption data for residential heating on a large scale, significantly reducing computation time. However, the data used in this chapter is

limited to one group of houses. Hence a compliment research is needed to have an aggregated model more representative and comprehensive.

In the chapter 4, three distinct aggregated models are integrated to address energy flexibility in the domains of domestic hot water (DHW), electric vehicle charging (EVC), and residential heating (HR). These aggregated models, encompassing multiple units of electric water heaters (EWHs), electric vehicles (EVs), and heating systems, prove to be effective tools for analyzing power consumption behaviors in residential settings, also with the application of control signals. The adaptability of these aggregated models allows for their utilization in diverse scenarios and contexts. One key application of these models is their ability to quantify and assess the degree of flexibility achievable through the aggregation of multiple units. By experimenting with various control strategies within the model, the impact of these strategies on residential power consumption can be evaluated.

An optimization problem is constructed in pursuit of minimizing electricity costs within a specified timeframe. Three scenarios are investigated to explore the potential of the integrated aggregated model. The first scenario involves the test of the integrated aggregated model under different electricity price trends on the SPOT market. The second scenario presents the functionality of the integrated aggregated models under different cut-off power duration. Finally, the third scenario illustrate the test of the model when varying the input parameters concerning the capacity : average volume of all water heater and average battery capacity of all EVs; and the input parameters concerning the power rating: average power rating of all water heaters and average thermal power rating of all heating systems. The results underline the integrated aggregated model's potential in aiding aggregators to quickly grasp power consumption patterns in the households they manage. These considered scenarios emphasize the robustness of aggregated models in representing the power usage behavior of various loads across a large spatial scale.

In conclude, we have successfully in generating methodologies in building the aggregated models for different type of power consumption, encompassing domestic hot water, electric vehicle charging and heating in residential. These aggregated models have different applications to different energy market actors. These models can be a tool for the aggregators in load management. They can provide the insights into the expected power consumption in a large spatial scale with in a second. This have an essential role in promoting the demand response program with the peak load shifting. Additionally, these models can also estimate the power consumption when introducing the different control strategies in time series. This allows aggregators to make data-driven decisions in optimizing electricity cost reduction with the assistant of the GA optimization method. The fact that aggregator can better control the residential energy consumption, which directly contribute to the stability of the grid and indirectly facilitates the integration of renewable energy sources like wind or solar into the power system. As mention in « Bilan Prévisionnel 2023-2035 de RTE », the power system is evolving

requirements include the imperative for "flexibilities," with the primary focus on the development of demand modulation and energy storage solutions with the potential of adding approximately 5 GW of operational margin. In this context, demand side flexibility is playing a crucial role and the proposed aggregated models can give a contribution in the long-time research in achieving the objective about the energy flexibility in 2035 of RTE.

VII. Perspective

Following on from this work, several avenues could be explored. It is understandable that the models are not yet perfect but we can still keep improving. Due to lack of time, we were unable to simulate the power consumption of the unit model in different regions to improve the representativeness of the unit model data for residential heating. This regional specificity could make the aggregated model for residential heating even more accurate and reflective of the current context in France. Additionally, while genetic algorithms have been used effectively in our research, exploring other optimization methods could be valuable. Different algorithms might offer advantages in terms of finding optimal control strategies for increased reliability.

The integrated aggregated model for DHW, EVC, and HR has significant potential in assisting different market participants like TSO, DSO, aggregators, and researchers..., these models can be studied regarding various objectives, which depends on the users. For instance, in the future, the flexibility to the power system will play an important role and this is where the proposed aggregated models proves its advantages in aiding the long term research, facilitating the decision as well as the long term objective of the RTE. Another direction would be investigating how the integrated aggregated model can contribute to the robustness and resilience of energy systems. This might involve scenarios related to grid stability during extreme weather events or other emergencies.

Reference

[1] S. Koch, “Demand response methods for ancillary services and renewable energy integration in electric power systems,” ETH Zurich, 2012. doi: 10.3929/ETHZ-A-009756530.

[2] European Council, “Conclusions on 2030 Climate and Energy Policy Framework.” 2014.

[3] Agora Energiewende, “The European Power Sector in 2020: Up-to-Date Analysis on the Electricity Transition,” p. 18, 2021.

[4] RTE, “Téléchargez les données publiées par RTE.” [Online]. Available: https://www.services-rte.com/fr/telechargez-les-donnees-publiees-par-rte.html

[5] Choisir.com, “Bilan Électrique 2022 En France : Tendances Et Chiffres Clés,” Mar. 2023, [Online]. Available: https://www.choisir.com/energie/actualites/192164/bilan-electrique-2022-en-france-tendances-et-chiffres-cles

[6] U.S. Energy Information Administration, “Nuclear power plants generated 68% of France’s electricity in 2021,” 2023. [Online]. Available: https://www.eia.gov/todayinenergy/detail.php?id=55259

[7] International Energy Agency and Réseau de Transport d’Electricité, Conditions and Requirements for the Technical Feasibility of a Power System with a High Share of Renewables in France Towards 2050. OECD, 2021. doi: 10.1787/6be9f3ac-en.

[8] M. Afzalan and F. Jazizadeh, “Residential loads flexibility potential for demand response using energy consumption patterns and user segments,” Applied Energy, vol. 254, p. 113693, Nov. 2019, doi: 10.1016/j.apenergy.2019.113693.

[9] B. Mota, P. Faria, and Z. Vale, “Residential load shifting in demand response events for bill reduction using a genetic algorithm,” Energy, vol. 260, p. 124978, Dec. 2022, doi: 10.1016/j.energy.2022.124978.

[10] European University Institute, “The economics of explicit demand-side flexibility in distribution grids: the case of mandatory curtailment for a fixed level of compensation,” 2020.

[11] IRENA, “Demand-side flexibility for power sector transformation,” Analytical Brief, 2019. [Online]. Available: https://www.irena.org/-/media/Files/IRENA/Agency/Publication/2019/Dec/IRENA_Demand-side_flexibility_2019.pdf?rev=f2bc0604644e49669e2237b0e98e6eb6

[12] “Demand-side flexibility for power sector transformation,” p. 44.

[13] C. H. Antunes, A. Soares, and Á. Gomes, “An energy management system for residential demand response based on multiobjective optimization,” in 2016 IEEE Smart Energy Grid Engineering (SEGE), Aug. 2016, pp. 90–94. doi: 10.1109/SEGE.2016.7589506.

[14] J. Kondoh, N. Lu, and D. J. Hammerstrom, “An Evaluation of the Water Heater Load Potential for Providing Regulation Service,” IEEE Transactions on Power Systems, vol. 26, no. 3, pp. 1309–1316, Aug. 2011, doi: 10.1109/TPWRS.2010.2090909.

[15] M. H. Nehrir, R. Jia, D. A. Pierre, and D. J. Hammerstrom, “Power Management of Aggregate Electric Water Heater Loads by Voltage Control,” in 2007 IEEE Power Engineering Society General Meeting, Jun. 2007, pp. 1–6. doi: 10.1109/PES.2007.386024.

[16] A. Haider, W. Stark, and T. K. A. Brekken, “Electric Hot Water Heater Primary Frequency Control,” in 2018 IEEE Energy Conversion Congress and Exposition (ECCE), Sep. 2018, pp. 2670–2675. doi: 10.1109/ECCE.2018.8557350.

[17] “Energy consumption in households,” Eurostat Statistics Explained, Jun. 2022. Accessed: Nov. 28, 2022. [Online]. Available: https://ec.europa.eu/eurostat/statistics-explained/index.php?title=Energy_consumption_in_households#Energy_products_used_in_the_residential_sector

[18] “L’eau chaude sanitaire,” Agence de la transition écologique (ADEME Expertises), 2019. Accessed: Nov. 28, 2022. [Online]. Available: https://expertises.ademe.fr/batiment/passer-a-laction/elements-dequipement/leau-chaude-sanitaire

[19] “Heures Pleines/Heures Creuses, comment cela fonctionne-t-il ?,” Enedis, 2022. Accessed: Feb. 10, 2022. [Online]. Available: https://www.enedis.fr/faq/gerer-sa-consommation-delectricite/heures-pleinesheures-creuses-comment-cela-fonctionne-t-il#:~:text=Les%208%20Heures%20Creuses%20%3A,et%208h00%20d'autre%20part.

[20] S. J. Darby, “Smart electric storage heating and potential for residential demand response,” Energy Efficiency, p. 11, 2018.
[21] L. Schibuola, M. Scarpa, and C. Tambani, “Demand response management by means of heat pumps controlled via real time pricing,” Energy and Buildings, vol. 90, pp. 15–28, Mar. 2015, doi: 10.1016/j.enbuild.2014.12.047.
[22] V. Lakshmanan, H. Sæle, and M. Z. Degefa, “Electric water heater flexibility potential and activation impact in system operator perspective – Norwegian scenario case study,” Energy, vol. 236, p. 121490, Dec. 2021, doi: 10.1016/j.energy.2021.121490.
[23] E. Georges, S. Quoilin, S. Mathieu, and V. Lemort, “Aggregation of flexible domestic heat pumps for the provision of reserve in power systems.,” San Diego, p. 12, 2017.
[24] D. Fischer, T. Wolf, J. Scherer, and B. Wille-Haussmann, “A stochastic bottom-up model for space heating and domestic hot water load profiles for German households,” Energy and Buildings, vol. 124, pp. 120–128, Jul. 2016, doi: 10.1016/j.enbuild.2016.04.069.
[25] J. Hu, H. Zhou, Y. Zhou, H. Zhang, L. Nordströmd, and G. Yang, “Flexibility Prediction of Aggregated Electric Vehicles and Domestic Hot Water Systems in Smart Grids,” Engineering, vol. 7, no. 8, pp. 1101–1114, Aug. 2021, doi: 10.1016/j.eng.2021.06.008.
[26] M. T. Ahmed, P. Faria, O. Abrishambaf, and Z. Vale, “Electric Water Heater Modelling for Direct Load Control Demand Response,” in 2018 IEEE 16th International Conference on Industrial Informatics (INDIN), Jul. 2018, pp. 490–495. doi: 10.1109/INDIN.2018.8472102.
[27] U. Çakır, K. Çomaklı, Ö. Çomaklı, and S. Karslı, “An experimental exergetic comparison of four different heat pump systems working at same conditions: As air to air, air to water, water to water and water to air,” Energy, vol. 58, pp. 210–219, Sep. 2013, doi: 10.1016/j.energy.2013.06.014.
[28] Weldom, “Chauffe-Eau Electrique.” [Online]. Available: https://www.weldom.fr/media/catalog/product/doc_qualite/doc_qualite/mi/MI_5618198.pdf
[29] Stiebel-eltron, “Chauffe-eau électriques.” [Online]. Available: https://www.stiebel-eltron.fr/content/dam/ste/fr/telechargements/Brochure%20chauffe-eau%20%C3%A9lectriques_VF.pdf
[30] Airwell, “Tdf Eleo Chauffe-Eau Thermodynamique.” [Online]. Available: https://www.airwell-pro.fr/wp-content/import/fiches/fr/TDF-Eleo.pdf
[31] Stiebel-eltron, “Fiche technique.” [Online]. Available: https://www.stiebel-eltron.fr/fr/produits-et-solutions/eau_chaude_sanitaire/chauffe-eau_thermodynamiques/shp-a-220-300--x--plus/shp-a-300-plus/caracteristiques-techniques.product.pdf
[32] VIESMANN, “Feuille technique.” [Online]. Available: https://www.viessmann.fr/content/dam/public-brands/fr/produits/pompes-chaleur/vitocal-060-a/FT_Vitocal-060-a.pdf/_jcr_content/renditions/original./FT_Vitocal-060-a.pdf
[33] Y. P. Chandra and T. Matuska, “Stratification analysis of domestic hot water storage tanks: A comprehensive review,” Energy and Buildings, vol. 187, pp. 110–131, Mar. 2019, doi: 10.1016/j.enbuild.2019.01.052.
[34] Y. M. Han, R. Z. Wang, and Y. J. Dai, “Thermal stratification within the water tank,” Renewable and Sustainable Energy Reviews, vol. 13, no. 5, pp. 1014–1026, Jun. 2009, doi: 10.1016/j.rser.2008.03.001.
[35] E. Saloux and J. A. Candanedo, “Modelling stratified thermal energy storage tanks using an advanced flowrate distribution of the received flow,” Applied Energy, vol. 241, pp. 34–45, May 2019, doi: 10.1016/j.apenergy.2019.02.075.
[36] J. Lago, F. De Ridder, W. Mazairac, and B. De Schutter, “A 1-dimensional continuous and smooth model for thermally stratified storage tanks including mixing and buoyancy,” Applied Energy, vol. 248, pp. 640–655, Aug. 2019, doi: 10.1016/j.apenergy.2019.04.139.
[37] C. Kizilors and D. Aydin, “Effect of thermostat position and its set-point temperature on the performance of a domestic electric water heater,” International Journal of Low-Carbon Technologies, vol. 15, no. 3, pp. 373–381, Aug. 2020, doi: 10.1093/ijlct/ctaa007.
[38] Institut national de la statistique et des études économique, “Comparateur de territoires.” [Online]. Available: https://www.insee.fr/
[39] IZI by EDF, “Bien choisir la capacité de son chauffe-eau.” [Online]. Available: https://www.izi-by-edf-renov.fr/blog/comment-choisir-capacite-chauffe-eau

[40] Noah Pflugradt, Load Profile Generator. 2015. [Online]. Available: https://www.loadprofilegenerator.de/
[41] Réseau de transport d'électricité (RTE), "éCO2mix - Les données de marché." [Online]. Available: https://www.rte-france.com/eco2mix/les-donnees-de-marche
[42] Stiebel-eltron, "Stiebel-eltron Fiche technique." Accessed: Nov. 28, 2022. [Online]. Available: https://www.stiebel-eltron.fr/fr/produits-et-solutions/eau_chaude_sanitaire/petits_chauffe-eauchauffe-eaumurauxetsursocle/chauffe-eau_muraux30a150l/esh-w-plus------/esh-200-w-plus/caracteristiques-techniques.product.pdf
[43] R. Yokoyama, T. Shimizu, K. Ito, and K. Takemura, "Influence of ambient temperatures on performance of a CO2 heat pump water heating system," Energy, vol. 32, no. 4, pp. 388–398, Apr. 2007, doi: 10.1016/j.energy.2006.06.020.
[44] L. Yang, X. Qin, L. Zhao, S. Ye, X. Wei, and D. Zhang, "Analysis and comparison of influence factors of hot water temperature in transcritical CO2 heat pump water heater: An experimental study," Energy Conversion and Management, vol. 198, p. 111836, Oct. 2019, doi: 10.1016/j.enconman.2019.111836.
[45] S. A. Pourmousavi, S. N. Patrick, and M. H. Nehrir, "Real-Time Demand Response Through Aggregate Electric Water Heaters for Load Shifting and Balancing Wind Generation," IEEE Transactions on Smart Grid, vol. 5, no. 2, pp. 769–778, Mar. 2014, doi: 10.1109/TSG.2013.2290084.
[46] K. Ahmed, P. Pylsy, and J. Kurnitski, "Hourly consumption profiles of domestic hot water for different occupant groups in dwellings," Solar Energy, vol. 137, pp. 516–530, Nov. 2016, doi: 10.1016/j.solener.2016.08.033.
[47] D. George, N. S. Pearre, and L. G. Swan, "High resolution measured domestic hot water consumption of Canadian homes," Energy and Buildings, vol. 109, pp. 304–315, Dec. 2015, doi: 10.1016/j.enbuild.2015.09.067.
[48] INTERNATIONAL ENERGY AGENCY, "Global EV Outlook 2022- Securing supplies for an electric future," p. 4, 2022.
[49] International Renewable Energy Agency, "Renewable Energy Prospects for the European Union," Feb. 2018.
[50] J. Zhong et al., "Coordinated control for large-scale EV charging facilities and energy storage devices participating in frequency regulation," Applied Energy, vol. 123, pp. 253–262, Jun. 2014, doi: 10.1016/j.apenergy.2014.02.074.
[51] O. Borne, "Vehicle-to-grid and flexibility for electricity systems: from technical solutions to design of business models," p. 146, 2019.
[52] S. Izadkhast, P. Garcia-Gonzalez, and P. Frías, "An Aggregate Model of Plug-In Electric Vehicles for Primary Frequency Control," IEEE Transactions on Power Systems, vol. 30, no. 3, pp. 1475–1482, May 2015, doi: 10.1109/TPWRS.2014.2337373.
[53] H. Zhang, Z. Hu, Z. Xu, and Y. Song, "Evaluation of Achievable Vehicle-to-Grid Capacity Using Aggregate PEV Model," IEEE Transactions on Power Systems, vol. 32, no. 1, pp. 784–794, Jan. 2017, doi: 10.1109/TPWRS.2016.2561296.
[54] A. Jamali Jahromi, M. Mohammadi, S. Afrasiabi, M. Afrasiabi, and J. Aghaei, "Probability density function forecasting of residential electric vehicles charging profile," Applied Energy, vol. 323, p. 119616, Oct. 2022, doi: 10.1016/j.apenergy.2022.119616.
[55] M. R. Sarker, Y. Dvorkin, and M. A. Ortega-Vazquez, "Optimal Participation of an Electric Vehicle Aggregator in Day-Ahead Energy and Reserve Markets," IEEE Transactions on Power Systems, vol. 31, no. 5, pp. 3506–3515, Sep. 2016, doi: 10.1109/TPWRS.2015.2496551.
[56] A. Schuller, C. M. Flath, and S. Gottwalt, "Quantifying load flexibility of electric vehicles for renewable energy integration," Applied Energy, vol. 151, pp. 335–344, Aug. 2015, doi: 10.1016/j.apenergy.2015.04.004.
[57] E. Sortomme and M. A. El-Sharkawi, "Optimal Scheduling of Vehicle-to-Grid Energy and Ancillary Services," IEEE Transactions on Smart Grid, vol. 3, no. 1, pp. 351–359, Mar. 2012, doi: 10.1109/TSG.2011.2164099.
[58] P. L. Bonate, "A Brief Introduction to Monte Carlo Simulation," Clin Pharmacokinet, vol. 40, no. 1, pp. 15–22, Jan. 2001, doi: 10.2165/00003088-200140010-00002.

[59] C. Gaete-Morales, H. Kramer, W.-P. Schill, and A. Zerrahn, “An open tool for creating battery-electric vehicle time series from empirical data, emobpy,” Sci Data, vol. 8, no. 1, p. 152, Dec. 2021, doi: 10.1038/s41597-021-00932-9.
[60] Federal Ministry dor Digital and Transport, “Mobility in Germany 2017“ - German NTS Mobilität in Deutschland (MiD).” 2017.
[61] F. G. Venegas, M. Petit, and Y. Perez, “Impact of Non-Systematic Electric Vehicle Charging Behaviour on a Distribution Substation,” in 2019 IEEE PES Innovative Smart Grid Technologies Europe (ISGT-Europe), Sep. 2019, pp. 1–5. doi: 10.1109/ISGTEurope.2019.8905710.
[62] M. C. Falvo, D. Sbordone, I. S. Bayram, and M. Devetsikiotis, “EV charging stations and modes: International standards,” in Automation and Motion 2014 International Symposium on Power Electronics, Electrical Drives, Jun. 2014, pp. 1134–1139. doi: 10.1109/SPEEDAM.2014.6872107.
[63] M. Pappalardo et al., “La mobilité des Français Panorama issu de l’enquête nationale transports et déplacements 2008,” 2010.
[64] J. H. Lee, D. Chakraborty, S. J. Hardman, and G. Tal, “Exploring electric vehicle charging patterns: Mixed usage of charging infrastructure,” Transportation Research Part D: Transport and Environment, vol. 79, p. 102249, Feb. 2020, doi: 10.1016/j.trd.2020.102249.
[65] F. Gonzalez Venegas, M. Petit, and Y. Perez, “Plug-in behavior of electric vehicles users: Insights from a large-scale trial and impacts for grid integration studies,” eTransportation, vol. 10, p. 100131, Nov. 2021, doi: 10.1016/j.etran.2021.100131.
[66] M. Mohammadi-Landi, M. Rastegar, M. Mohammadi, and S. Afrasiabi, “Stochastic Optimal Sizing of Plug-in Electric Vehicle Parking Lots in Reconfigurable Power Distribution Systems,” IEEE Transactions on Intelligent Transportation Systems, vol. 23, no. 10, pp. 17003–17014, Oct. 2022, doi: 10.1109/TITS.2022.3166781.
[67] “Quelle est l’autonomie d’une voiture électrique ? - EDF.” Accessed: Jun. 06, 2023. [Online]. Available: https://particulier.edf.fr/fr/accueil/guide-energie/electricite/autonomie-voiture-electrique.html
[68] European Commission. Joint Research Centre. Institute for Energy and Transport. and TRT Trasporti e Territorio Srl., Projections for electric vehicle load profiles in Europe based on travel survey data. LU: Publications Office, 2013. Accessed: Jun. 06, 2023. [Online]. Available: https://data.europa.eu/doi/10.2790/24108
[69] Y. Ess, “Evolution Du Parc Roulant Automobile Depuis Janvier 2010”.
[70] “Fiches techniques voitures électriques / Fiches techniques des voitures électriques.” Accessed: Jul. 03, 2023. [Online]. Available: https://www.fiches-auto.fr/articles-auto/voiture-electrique/s-2531-fiches-techniques-voitures-electriques.php#haut_menu_2018
[71] “Se déplacer en voiture : seul, à plusieurs ou en covoiturage ?” Accessed: Jul. 03, 2023. [Online]. Available: https://www.ecologie.gouv.fr/sites/default/files/DE_4p_covoiturage-v4-050722_SH_OK.pdf
[72] Eurostat, “Energy consumption in households,” 2023, [Online]. Available: https://ec.europa.eu/eurostat/statistics-explained/index.php?title=Energy_consumption_in_households#Energy_products_used_in_the_residential_sector
[73] H. Zhao and F. Magoulès, “A review on the prediction of building energy consumption,” Renewable and Sustainable Energy Reviews, vol. 16, no. 6, pp. 3586–3592, Aug. 2012, doi: 10.1016/j.rser.2012.02.049.
[74] J. Cai and J. Braun, A practical and scalable inverse modeling approach for multi-zone buildings. 2014.
[75] Ghjuvan Antone Faggianelli1, , Adrien Brun2, , Etienne Wurtz2, and and Marc Muselli1, “GREY-BOX MODELLING FOR NATURALLY VENTILATED BUILDINGS,” presented at the 14th Conference of International Building Performance Simulation Association, India, Dec. 2015.
[76] A. Boodi, K. Beddiar, Y. Amirat, and M. Benbouzid, “Simplified Building Thermal Model Development and Parameters Evaluation Using a Stochastic Approach,” Energies, vol. 13, no. 11, p. 2899, Jun. 2020, doi: 10.3390/en13112899.

[77] Chloé LUCAS, “Flexibilité pour le réseau électrique à forte pénétration de systèmes photovoltaïques par l’optimisation du pilotage des consommations,” Université de Grenoble, July 2021.
[78] T. Berthou, P. Stabat, R. Salvazet, and D. Marchio, “Comparaison de modèles linéaires inverses pour la mise en place de stratégies d’effacement,” pp. 1–11, Jun. 2012.
[79] Clara SPITZ, “Analyse de la fiabilité des outils de simulation et des incertitudes de métrologie appliquée à l’efficacité énergétique des bâtiments,” Université de Grenoble, 2012.
[80] Clara SPITZ and Thomas RECHT, “Validation expérimentale sur les maisons INCAS.,” Energétique Des Bâtiments et Simulation Thermique, p. pages 199–224, Eyrolles 2016.
[81] U.S. Department of ENERGY, EnergyPlus. [Online]. Available: https://energyplus. net/
[82] J. KENNEDY et R. EBERHART, “Particle swarm optimization,” presented at the International Conference on Neural Networks, Nov. 1995, p. pages 1942–1948.
[83] S. Truchet, A. Jay, E. Wurtz, J. Anger, A. Brun, and P. Bernaud, “Impact of thermal inertia coupled to natural night ventilation. A case study for a high performance building in continental climate,” International Journal of Ventilation, vol. 0, no. 0, pp. 1–14, Mar. 2023, doi: 10.1080/14733315.2023.2188346.
[84] M. Robillart, P. Schalbart, F. Chaplais, and B. Peuportier, “Model reduction and model predictive control of energy-efficient buildings for electrical heating load shifting,” Journal of Process Control, vol. 74, pp. 23–34, Feb. 2019, doi: 10.1016/j.jprocont.2018.03.007.
[85] M. Kabore, G. Michaux, J. Ledreau, P. Salagnac, and R. Greffet, “Parametric Study Of The Thermal Performance Of A Single-family House Equipped With An Airflow Window Integrating A Heated Glazing,” presented at the Building Simulation 2019, Rome, Italy, pp. 2019–2025. doi: 10.26868/25222708.2019.211049.
[86] H. Yoshino, T. Hong, and N. Nord, “IEA EBC annex 53: Total energy use in buildings—Analysis and evaluation methods,” Energy Build, pp. 124–136, 2017.
[87] Éric Vorger, “Étude de l’influence du comportement des habitants sur la performance énergétique du bâtiment,” Mines ParisTech, 2014.
[88] R. Missaoui, H. Joumaa, S. Ploix, and S. Bacha, “Managing energy Smart Homes according to energy prices: Analysis of a Building Energy Management System,” Energy and Buildings, vol. 71, pp. 155–167, Mar. 2014, doi: 10.1016/j.enbuild.2013.12.018.
[89] Météo-France Centre-Est and Division Développements-Etudes-Climatologie, “Climat de la région Rhône-Alpee.” 2010. [Online]. Available: https://www.auvergne-rhone-alpes.developpement-durable.gouv.fr/IMG/pdf/Climat_actuel_en_Rhone-Alpes_septembre_2010_cle0b2cd1.pdf
[90] Météo France, “Bilan climatique de l’année 2016.” 2017. [Online]. Available: https://meteofrance.fr/sites/meteofrance.fr/files/files/editorial/Bilan%20annuel%20complet%202016.pdf
[91] Météo France, “Bilan climatique de l’année 2015.” 2016. [Online]. Available: https://meteofrance.fr/sites/meteofrance.fr/files/files/editorial/Bilan_ann%C3%A9e-2015-definitif_defma_0.pdf
[92] Météo France, “Bilan climatique de l’année 2018.” 2019. [Online]. Available: https://meteofrance.fr/sites/meteofrance.fr/files/files/editorial/Bilan-climatique-annee2018.pdf
[93] Météo France, “Bilan climatique de l’hiver 2018-2019.” 2020.
[94] Météo France, “Bilan climatique de l’année 2017.” 2018. [Online]. Available: https://meteofrance.fr/sites/meteofrance.fr/files/files/editorial/Bilan-climatique-definitif-annee2017-V2.pdf
[95] National Centers for Environment Information, Integrated Surface Dataset (Global). [Online]. Available: https://www.ncei.noaa.gov/
[96] Swinbank, W. C., “Long-wave radiation from clear skies,” Quarterly Journal of the Royal Meteorological Society, pp. 339–348, 1963.
[97] S. Pandiaraj, A. Abdul Jaffar, S. Muthusamy, H. Panchal, and S. Pandiyan, “A study of solar heat gain variation in building applied photovoltaic buildings and its impact on environment and indoor air quality,” Energy Sources, Part A: Recovery, Utilization, and Environmental Effects, vol. 44, no. 3, pp. 6192–6212, Sep. 2022, doi: 10.1080/15567036.2022.2096725.

[98] G. Oliveti, N. Arcuri, R. Bruno, and M. De Simone, “An accurate calculation model of solar heat gain through glazed surfaces,” Energy and Buildings, vol. 43, no. 2, pp. 269–274, Feb. 2011, doi: 10.1016/j.enbuild.2010.11.009.
[99] C. Rigollier, O. Bauer, and L. Wald, “On the clear sky model of the ESRA — European Solar Radiation Atlas — with respect to the heliosat method,” Solar Energy, vol. 68, no. 1, pp. 33–48, Jan. 2000, doi: 10.1016/S0038-092X(99)00055-9.
[100] D. Fischer, T. Wolf, J. Wapler, R. Hollinger, and H. Madani, “Model-based flexibility assessment of a residential heat pump pool,” Energy, vol. 118, pp. 853–864, Jan. 2017, doi: 10.1016/j.energy.2016.10.111.
[101] Météo France, “L’hiver,” 2022, [Online]. Available: https://meteofrance.com/comprendre-la-meteo/saisons/hiver#:~:text=Petit%20tour%20d'horizon%20des,7%20degr%C3%A9s%20sous%20la%20normale.
[102] Engie, “Quelle puissance de chauffage par m^2 ?,” 2021. [Online]. Available: https://www.engie-homeservices.fr/dossiers/aide-et-financement/quelle-puissance-de-chauffage-par-m2#:~:text=La%20puissance%20de%20chauffage%20au%20m%C2%B2%20d'un%20radiateur%20%C3%A9lectrique,entre%2070%20et%20100%20W.
[103] Ministère de la transition écologique, “Règles Th-bat – Parois opaques.” Sep. 2017. [Online]. Available: https://rt-re-batiment.developpement-durable.gouv.fr/IMG/pdf/4-fascicule_parois_opaques_methodes.pdf
[104] IZI by EDF, “L’Isolation Thermique par l’Intérieur (ITI), comment ça marche ?,” 2023. [Online]. Available: https://www.izi-by-edf-renov.fr/blog/isolation-murs-interieur-iti
[105] IZI by EDF, “L’Isolation Thermique des murs par l’Extérieur (ITE), comment ça marche ?,” 2023. [Online]. Available: https://www.izi-by-edf-renov.fr/blog/isolation-murs-exterieur-ite
[106] Bigladder, “Outside Surface Heat Balance.” [Online]. Available: https://bigladdersoftware.com/epx/docs/8-6/engineering-reference/outside-surface-heat-balance.html
[107] Agence qualité construction, “Typologies & Consommation: Région AUVERGNE-RHÔNE-ALPES.” 2015.
[108] ADEME, “Bâtiments résidentiels: Typologie du parc existant et solutions exemplaires pour la rénovation énergétique en France.” 2015.
[109] ADEME, “Guide Des Matériaux Isolants pour une isolation efficace et durable.” [Online]. Available: http://www.aldeau.com/ouvrages_libres/15.pdf
[110] L.-M. Ionescu, N. Bizon, A.-G. Mazare, and N. Belu, “Reducing the Cost of Electricity by Optimizing Real-Time Consumer Planning Using a New Genetic Algorithm-Based Strategy,” Mathematics, vol. 8, no. 7, Art. no. 7, Jul. 2020, doi: 10.3390/math8071144.

RÉSUMÉ

Dans un contexte caractérisé par l'intégration généralisée de sources d'énergie renouvelables non pilotables, le concept de "production égale consommation" devient de plus en plus central. Ce scénario renforce l'importance du potentiel réel de flexibilité de la consommation résidentielle dans le futur. L'exploitation efficace de cette flexibilité énergétique nécessite l'utilisation de divers modèles. Ainsi, la thèse propose le développement de modèles agrégés conçus pour différents types de charges résidentielles : l'eau chaude domestique, le chargement de véhicules électriques et le chauffage résidentiel. Ces modèles fonctionnent efficacement sous différents types de signaux de contrôle et servent des objectifs distincts dans la gestion de la consommation d'énergie, facilitant l'évaluation et la quantification de la flexibilité énergétique à des échelles spatiales spécifiques. Dans cette thèse, nous avons réussi à dégager des méthodologies pour construire des modèles agrégés pour différents types de consommation d'énergie dans le secteur résidentiel. Une étude de cas a été réalisée pour explorer le potentiel et les avantages des modèles proposés pour aider les agrégateurs dans la gestion de la charge.

MOTS CLÉS

Flexibilité énergétique ; Réponse à la demande ; Modèles agrégés ; Déplacement de la charge ; Consommations énergétiques

ABSTRACT

In a context characterized by the widespread integration of uncontrollable renewable energy sources, the concept of "production equals consumption" is becoming increasingly pivotal. This scenario elevates the significance of the actual potential for residential consumption flexibility in the future energy domain. Effectively harnessing this energy flexibility necessitates the utilization of diverse models. Thus, the thesis endeavors to delve into the development of aggregated models designed for various types of residential loads, including domestic hot water, electric vehicle charging, and heating in residential. These models works effectively under different type of control signals and serve distinct purposes in the management of energy consumption, facilitating the assessment and quantification of energy flexibility within specific spatial scales. In this thesis, we have successfully in generating methodologies in building the aggregated models for different type of power consumption in residential. A case study has been done to explore the potential and advantages of the proposed models in assisting the aggregators in load management.

KEYWORDS

Energy flexibility; Demand response; Aggregated models; Load shifting; Energy consumption